

Understanding nano-stabiliser and nano-bio interactions of nanocrystals

DOCTORAL THESIS
SUBMITTED IN FULFILMENT OF THE REQUIREMENTS
FOR THE DEGREE OF
DOCTOR OF NATURAL SCIENCES
AT KIEL UNIVERSITY, KIEL, GERMANY

BY

Friederike Gütter

KIEL 2018

Reviewer: Prof. Dr. Regina Scherließ

Co-Reviewer: Prof. Dr. Hartwig Steckel

Date of exam: 06.04.2018

Accepted for publication: 06.04.2018

sgd. Prof. Dr. N. Oppelt

Research articles contributing to this thesis

Conference contributions:

Gütter F., Peltonen L., Strachan C. J, Scherließ R. (2017) Nanocrystal production- Understanding stabiliser-drug-interaction. 9th Polish-German Symposium on Pharmaceutical Sciences

Gütter F., Saarinen J., Scherließ R., Steckel H., Santos H. A., Peltonen L., Strachan C. J. (2016) Production of auto-fluorescent nanocrystals and uptake studies in Caco-2 cells. 10th World Meeting on Pharmaceutics, Biopharmaceutics and Pharmaceutical

Gütter F., Scherließ R., Steckel H. (2015) Stabilisers in nanocrystal production: Concentration dependency and cell toxicity. 8th Polish-German Symposium on Pharmaceutical Sciences

*Ein jegliches hat seine Zeit, und alles Vorhaben unter dem Himmel hat seine Stunde:
Geboren werden hat seine Zeit, sterben hat seine Zeit;
weinen hat seine Zeit, lachen hat seine Zeit;
pflanzen hat seine Zeit, ausreißen, was gepflanzt ist, hat seine Zeit
klagen hat seine Zeit, tanzen hat seine Zeit;
suchen hat seine Zeit, verirren hat seine Zeit;
behalten hat seine Zeit, wegwerfen hat seine Zeit;
zerreißen hat seine Zeit, zunähen hat seine Zeit;
schweigen hat seine Zeit, reden hat seine Zeit;
lieben hat seine Zeit, hassen hat seine Zeit;
Streit hat seine Zeit, Friede hat seine Zeit*

Lutherbibel 2017 Prediger 3 1-2, 4, 6-9

Für meine Eltern

Lack of a specific mark or a reference to a trademark does not imply that this work or parts of it can be used or copied without copyright permission.

Table of contents

1	Introduction and Objectives	1
1.1	Introduction.....	1
1.2	Objectives.....	2
2	Theoretical Background.....	4
2.1	Types of nano-objects	4
2.2	Production of nanocrystals	5
2.2.1	Production methods.....	5
2.2.2	Importance of stabilisation in nanocrystal production.....	7
2.3	Effects of nanoisation	9
2.4	Fate of (nano)objects in biological environments	11
2.5	Tools for the assessment of transport of substances in and through cells ...	15
3	Materials and Methods	19
3.1	Materials.....	19
3.1.1	Model drugs	19
3.1.2	Stabilisers	23
3.1.3	Cell culture	28
3.2	Methods.....	30
3.2.1	Media milling.....	30
3.2.2	Stabiliser characterisation.....	31
3.2.3	Particle characterisation.....	33
3.2.4	Physico-chemical drug characterisation.....	36
3.2.5	Determination of drug-stabiliser interaction.....	40
3.2.6	Dissolution	44
3.2.7	General cell culture and toxicity testing.....	46
3.2.8	Determination of drug transport through cells	47
3.2.9	Visualisation of drug transport in cells.....	50

4	Results and Discussion	58
4.1	Production of nanocrystals	58
4.1.1	Influence of stabiliser	59
4.1.2	Influence of bead size	61
4.2	Stabiliser influences on nanosuspension properties.....	64
4.2.1	Minimal stabilisation concentration	64
4.2.2	Stability of nanosuspensions with various stabilisers.....	67
4.2.3	Cell toxicity of stabilisers in Caco-2 cells	68
4.2.4	Concluding remarks of stabiliser characteristics for the selection of two stabilisers for further studies	70
4.3	Characterisation of selected nanosuspensions	71
4.3.1	Particle size of suspension before milling	71
4.3.2	Stability of nanosuspensions	74
4.3.3	Solid state before and after milling.....	77
4.3.4	Cell toxicity of selected stabilisers and nanosuspensions.....	83
4.3.5	Concluding remarks of the characterisation of selected nanosuspensions.....	85
4.4	Characterisation of drug-stabiliser interaction	85
4.4.1	Stabiliser - particle interaction studies in literature.....	85
4.4.2	Contact angle measurements	87
4.4.3	Isothermal titration calorimetry.....	91
4.4.4	Comparison of contact angle measurements and isothermal titration calorimetry	99
4.4.5	Concluding remarks of stabiliser-drug interaction studies.....	100
4.5	In-vitro dissolution of suspensions.....	101
4.5.1	Solubility in dissolution media.....	101
4.5.2	Dissolution of coarse suspension	103
4.5.3	Dissolution of nanosuspensions	107

4.5.4	Concluding remarks of dissolution studies.....	110
4.6	Transport of drugs through epithelial cells.....	111
4.6.1	Validation of the Caco-2 transwell model.....	111
4.6.2	Experimental approach for method set-up.....	114
4.6.3	Permeation comparison of coarse drug suspensions and nanosuspensions.....	117
4.6.4	Dissolution rate of drugs at transport study conditions and inclusion in permeation results	122
4.6.5	Concluding remarks of transport studies.....	126
4.7	Uptake of nanocrystals in cells	129
4.7.1	Uptake studies with CARS microscopy.....	129
4.7.2	Uptake studies with fluorescence microscopy	140
4.7.3	Concluding remarks of fluorescence microscopy and CARS microscopy	143
5	Concluding Remarks and Overall Discussion	146
6	Summary	152
7	Summary (German)	154
8	References	157
9	Appendix	181
9.1	List of abbreviations.....	181
9.2	Materials.....	184
9.2.1	APIs, stabilisers and dispersion medium	184
9.2.2	Surface area measurements.....	185
9.2.3	Buffer in dissolution studies	186
9.2.4	Cell culture.....	187
9.3	Methods.....	189
9.3.1	HPLC	189

9.3.2	Fluorimetry	191
9.4	Additions to results	191
9.4.1	Particle sizes and conductivity of zeta-potential measurements .	191
9.4.2	Particle size distributions	192
9.4.3	Solid state of nanosuspensions	192
9.4.4	Isothermal titration calorimetry	193
9.4.5	Quantification of particle uptake in cells with Imaris.....	194
9.4.6	Calculation of dose per macrophage	195

1 Introduction and Objectives

1.1 Introduction

The development of an optimal formulation approach is one of the key activities of formulators in the pharmaceutical industry. Next to the pharmacodynamic performance of the pharmaceutical product, sufficient aqueous solubility of an active pharmaceutical ingredient (API) can be seen as an important criterion in the galenic development of pharmaceutical dosage forms. Especially for poorly water soluble drugs an appropriate formulation is necessary to establish the product in the market [Fahr and Liu, 2007]. Beneath low aqueous solubility, a low dissolution rate and permeability of the drug can lead to poor bioavailability, which can hinder a potentially effective drug entering the market as well. For an improvement of bioavailability, the drug itself can be altered like creating a pro-drug or a salt of the drug. However, this change is very complex from a regulator's perspective. When changing the dosage form of a poorly water soluble drug an improvement in drug uptake can be achieved without the need for creating new drug substances.

Poorly water soluble drugs pose a challenge not only in formulation technology but also more and more in preclinical studies, as 90 % of the drugs in the drug development pipelines are poorly water soluble [Loftsson and Brewsterb, 2010]. There is a high chance for an optimal formulation approach if the physico-chemical properties of the drugs, regarding solubility in biorelevant media and permeability through cellular barriers, are understood, leading to minimised risk of late failure in human clinical trials [Möschwitzer, 2013]. The biopharmaceutical classification system (BCS) is one way to characterise drugs regarding their solubility and permeability. Currently, all new drugs approved by the U. S. Food and Drug Administration (FDA) and the European Medicines Agency (EMA) need to have information relating BCS classification. Four different classes can be distinguished, with BCS IV class drugs having low solubility and permeability while BCS II class drugs share the low solubility with the benefit of being good permeable.

The BCS classification can be used for formulation optimisation. Butler and Dressman summarised the conceptualisation regarding the four different classes. For application

purposes, permeation enhancer addition can increase bioavailability of class III and IV drugs [Butler and Dressman, 2010]. To overcome the solubility problem in class II and IV, lipid based delivery systems, polymer based nanocarriers, crystal engineering (nanocrystals and co-crystals), self-emulsifying solid dispersions and miscellaneous techniques can be used. BCS class IV drugs are furthermore often efflux protein substrates, meaning that an inhibition of these transporters, like Pgp, can improve bioavailability [Ghadi and Dand, 2017]. Nanosuspensions (a suspension of nano-objects in a non-solvent) can be advantageous in formulating class II drugs because even without co-solvents, the solubility rate can increase so that pharmacokinetic studies can be performed.

Researching nanomaterials in medicine is currently of high interest. Many associations have formed to investigate and advance activities in the area of nanotechnology. The financial potentials in the nanomedicine market are important as well. According to the Business Communications Company Research Healthcare Report 2015 the global nanomedicine market was valued at 248.3 billion US dollar in 2014 and should reach 528 billion US dollar by 2019 (Report ID: HLC069C). In 2013, 247 nanomedicine products were in clinical trials. However, only 38 products have received FDA regulatory approval for patient use in 60 years of investigational research in the field of nanomedicines [Etheridge et al., 2013]. Until today, the number of nanotherapeutics, that entered clinical practice, raised approximately to 50 [Caster et al., 2017]. Nanocrystals held the second largest market share with 29 % of all nano-formulations in the United States in the years 2010 - 2015 [D'Mello et al., 2017].

In August 2017 Hassan et al. published a review about 'Evolution and clinical translation of drug delivery nanomaterials' and stated that even though materials in the field of nanomedicines have therapeutically improved, there are still problems with regard to bio-distribution and degradation rate that pose a challenge for the successful translation to clinical application [Hassan et al., 2017].

Better understanding of nano-object production and fate in biological environments could increase the amount of products succeeding in clinical trials [Wang et al., 2017b].

1.2 Objectives

This thesis has two main aims:

One goal is to create a better understanding of the fate of nanocrystals in biological environments. Gao et al. stated in 2012 that no research on the evidence of direct uptake of drug nanocrystals has been conducted. They suggested that for drug nanocrystals, much work should be done to investigate the evidence of direct uptake pathways and some potential influencing factors, such as surface properties and particle size [Gao et al., 2012]. Many previous works have used labelled nanoparticles or artificial metal particles [Nativo et al., 2008; Awaad et al., 2012; Munger et al., 2012] to investigate the behaviour of nano-objects in-vitro. The challenging detection of drug nanocrystals could be the main obstacle, as to why former studies focused on non-therapeutically used formulations. This explains the need for techniques in nanotechnology for the detection of nanocrystal formulations in tissues. Coherent anti-Stokes Raman spectroscopic microscopy and fluorescence microscopy were therefore chosen to be applied in this work as tools for nanocrystal imaging and uptake in cells. The uptake and transport of nanocrystals in and through cells should be determined with regard to the influence of particle size, type of stabiliser, incubation time and type of drug (BCS II and IV).

In addition to in-vitro experiments, the detailed investigation of the influence of milling parameters, type of stabiliser, stabiliser concentration and type of drug on the particle size was the second aim in this thesis. Selecting milling parameters for nanocrystal production is until today done by trial and error principles [Merisko-Liversidge and Liversidge, 2011]. The choice of stabilisers and their adequate concentration can be crucial for the creation of a stable nanosuspension. There is a need for fast methods, which are able to forecast the stabilisation efficacy of a stabiliser for a newly discovered API in research processes of industrial companies or in academia. Therefore, the feasibility of isothermal titration calorimetry and contact angle measurement was tested as characterisation methods for stabiliser-drug interactions.

2 Theoretical Background

2.1 Types of nano-objects

Defining the size range of nano-objects is somewhat contentious. On the one hand, an official definition of nanocrystals can be found in the ISO norm ISO/TS 80004. In this norm, a nanocrystal is a “nano-object with a crystalline structure” whereas a nano-object is defined as a “discrete piece of material with one, two or three external dimensions in the nanoscale (length range approximately from 1 nm to 100 nm)”. Figure 1 plots different kinds of nano-objects.

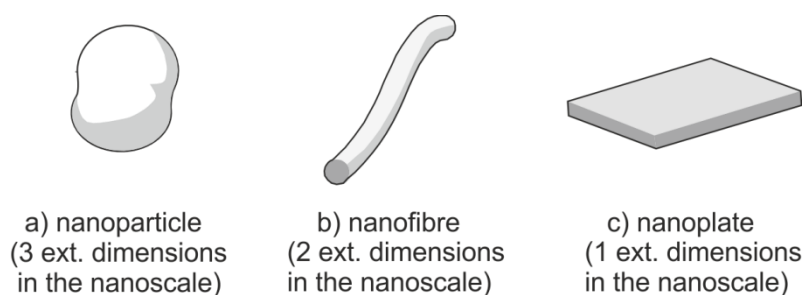


Figure 1: Shapes of nano-objects described and adapted from ISO/TS 80004:2010,2.2.

On the other hand, the FDA was involved in the publication of a 'draft' guidance, which defines engineered nano-products or products that employ nanotechnology as objects that:

- (i) Have at least one dimension in the 1 nm - 100 nm range or
- (ii) Are of a size range up to 1000 nm, providing the unique properties (including physical/chemical properties or biological effects) attributable to the dimensions up to 100 nm [McCarty, 2011].

Nevertheless, a typical size range that can be found in various literature is between 200 nm and 600 nm [Rabinow, 2006; Keck and Müller, 2006; Chin et al., 2014]. It is for this specific reason that in this thesis, the term 'nanocrystal' refers to all particles with a size below 600 nm.

In the majority of cases, the term 'nanocrystal' in publications refers to a nano-object composed of 100 % drug (with stabilisers adhered), mostly produced by crushing or precipitation. In contrast, a 'nanoparticle' is created from different substances which

form the particle by some kind of reaction. This reaction can be exemplary an ionic gelation or coacervation which lead to assembly of polymers, proteins or lipid-based structures with a particle size mostly between 1 nm and 200 nm [Uchegbu et al., 2013]. Advantages of these nanoparticles are a controlled creation and thereby a variety of surface modifications for drug targeting or inclusion of toxic drugs for minimisation of side effects. Disadvantages are often a low drug load and complicated manufacturing steps, including several reactions that have to be controlled. Another form of a nano-object can be liposomal formulations. AmBisome[®] is one of the popular representatives of this group which is an amphotericin B formulation against generalised fungi infections. The liposomal formulation leads to less nephrotoxicity but the treatment costs are approximately 1000 US dollars per day, while the costs for a treatment with amphotericin B solution are in the range of about 10 US dollars per day [Müller and Keck, 2012]. Müller et al. state that the production of nanocrystals may lower costs and reduce physical stability problems compared to liposomal formulations [Müller and Keck, 2012].

2.2 Production of nanocrystals

2.2.1 Production methods

One way to produce nanocrystals is the comminution of coarse powders. In most of the cases, the drug has to be suspended in a non-solvent which can be water for BCS class II and IV drugs.

Almost all nanocrystal products on the market are produced by bead/pearl milling [Hafner et al., 2014] whereby small beads (often 0.2 mm - 0.6 mm) out of steel, glass, ceramics, special polymers or zirconium oxide are transferred into a milling chamber together with a drug suspension comprising a stabiliser. The milling chamber can have various geometries and sizes. By applying energy to the system, mostly by some kind of stirring, larger particles are broken down to smaller structures. The power consumption, that is responsible for grinding, is made up of the stress energy and the number of bead-bead, bead-wall and bead-rotor contacts [Beinert et al., 2015]. Many different contact principles between the milling beads can be differentiated. Some examples are: impact, torsion, shearing and rolling (Figure 2), which comminute the particles between the milling beads.

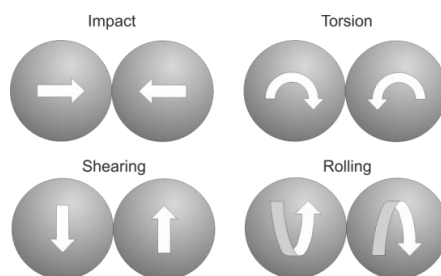


Figure 2: Scheme of contact principles of milling beads during milling.

Newly formed surfaces have to be stabilised to avoid agglomeration or aggregation and therefore insufficient milling which will be explained in more detail in section 2.2.2. Many parameters can potentially influence the particle size outcome. Some of the most important are milling time, bead size, amount of beads, stirring speed and the type and amount of stabiliser(s) [Peltonen and Hirvonen, 2010].

Media milling is a ‘top-down’ production method, as larger particles are the point of origin. Another well known ‘top-down’ production method for nanocrystal creation is high pressure homogenisation [Verma et al., 2009b]. High pressure homogenisation can be categorised into two principles: the jet stream and the piston-gap principle. For the jet stream principle, two fluid streams collide in an Y-type or Z-type chamber under pressure up to 1700 bar whereby the fluids carry the particles which should be grinded. The comminution principle is based on shear and cavitation forces. The piston gap principle usually works with pressures from 1500 to 2000 bar whereby a drug suspension is forced through a small gap (e.g. 5 μm - 20 μm). The particles are reduced in size due to the high power of the shockwaves caused by cavitation.

With ‘bottom-up’ methods, the initial starting point is a solution of the drug. Nano-objects are formed from this drug solution which is mixed with a non-solvent. This can be done by, for example, using supercritical fluid technology, evaporative precipitation into aqueous solution or controlled crystallisation during freeze drying [de Waard et al., 2008]. Precipitation often leads to small, uniform particles with a narrow particle size distribution [Li et al., 2007] but the process needs to be strictly monitored to avoid uncontrolled particle growth. With this technique, nanocrystals or nanoparticles can be produced. The drawbacks of productions with bottom-up techniques are that the drug, to be formulated, needs to fulfil certain prerequisites, like sufficient ability to dissolve in one of the solvents which can be exemplary ethanol, methanol or dimethyl sulfoxide. In addition, the process needs to be evaluated

regarding miscibility of the solvent in a non-solvent and proper elimination of the solvent after precipitation [Gao and Chen, 2008]. 'Top-down' methods, like media milling, have other challenges to face than 'bottom-up' techniques such as erosion of the milling material during the milling process [Flach et al., 2016], high energy costs, and it is more time consuming compared to precipitation methods. Furthermore, the high energy input can lead to partially amorphisation of the drug. The knowledge of the solid state is important for the prediction of the drugs' behaviour after administration and in storage. A crystalline drug has to overcome the energy of the crystal lattice before dissolving, whereas the amorphous form is unordered and therefore, in most of the cases, easier to dissolve. One disadvantage of the amorphous state, however, is its instability which mostly results in recrystallisation over time. Especially for drugs with polymorphic forms, this recrystallisation can lead to the formation of an undesirable polymorph. Polymorphs of one drug can cause significant differences in the bioavailability, solubility and dissolution rate of the drug. Nevertheless, the majority of the nano-object products on the US and EU market for oral administration are nanocrystalline formulations like Rapamune[®] (sirolimus), Tricor[®] (fenofibrate) or Emend[®] (aprepitant) produced by media milling [Hafner et al., 2014] as the large scale production with media milling is well understood and controllable.

2.2.2 Importance of stabilisation in nanocrystal production

Stabilisation is fundamental to avoid particle growth over time: not only for nanocrystals created by bead milling but nano-suspensions in general. Because of the high specific surface area, particles are more likely to agglomerate or even aggregate to achieve a lower energy level compared to micronised suspensions. In order to avoid aggregation, stabilisers from different categories can be used. Steric stabilisers can be polymers or non-ionic surfactants, which attach to the particle surfaces and hinder the approach of the particles with their long chains. Another principle is the use of ionic surfactants which can diffuse to the surface of a particle and impart charge on it. This prevents aggregation by similar charging which leads to an electrostatic potential barrier. A new approach for better stabilisation is to protect stabilisers on nano-crystalline surfaces from desorption. This can be performed by, for example, cross-linking of the adsorbed stabilisers resulting in immobilised stabiliser layer(s) [Kim and Lee, 2011].

Interactions between particles can be described by the DLVO theory, named after the scientists Derjaguin, Landau, Verwey and Overbeek. Both principles for stabilisation of

nanoparticles, physical and ionic, lead to hindrance of aggregation because they increase the energy barrier, the particles have to overcome for aggregation and therefore minimise the risk of potential well which can be seen in Figure 3.

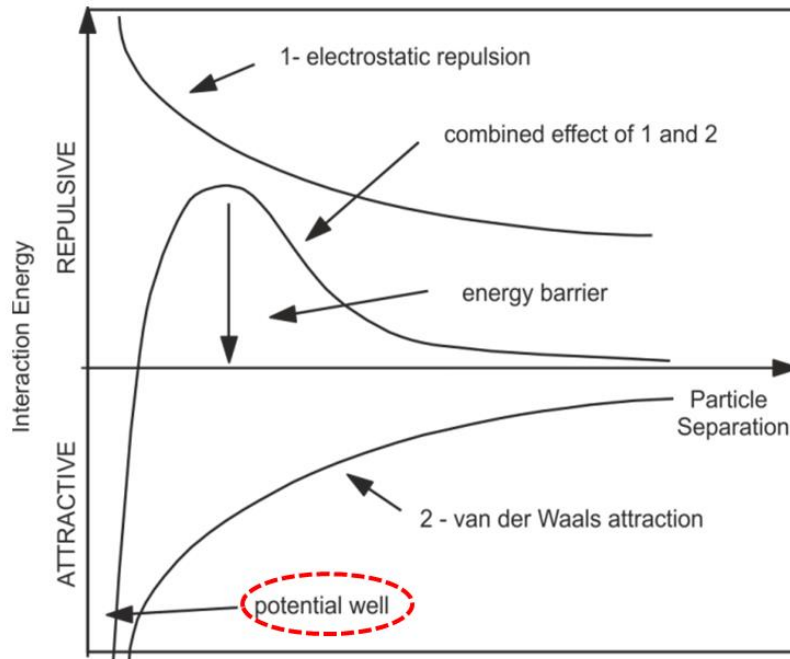


Figure 3: DLVO-theory energy diagram adapted from Lyklema et al. (1999).

For steric stabilisation, the adsorbed molecules have a loss of free movement. The reduction of conformational freedom causes negative entropy change and therefore, the free energy system increases, leading to repulsion. Efficient steric stabilisation depends on the chain-solvent interactions, the chain number and the chain length of the adsorbed molecules [Costas, 2016]. Furthermore, the attachment ability of the stabilisers to the newly formed surfaces is of importance [Verma et al., 2009a]. Investigating the interaction of API and stabiliser in nanosuspensions is highly important to understand milling processes, storage stability of the suspension and the behaviour of the crystals in biological environments, especially regarding solubility, surface interactions and toxicity. An understanding of the interaction can be used to estimate the required type and amount of stabiliser for new APIs in pharmaceutical industry or academic research so that costs can be reduced as well as the time for the preparation of nanosuspensions. Wu et al. concluded that the formulation of nanosuspension is challenging because of two major aspects:

- i) A lack of fundamental understanding of interactions within nanosuspensions and
- ii) A lack of an efficient and high throughput stabiliser screening techniques [Wu et al., 2011]

Many stabilisers have proven to have a high efficacy in stabilising nanosuspensions, regardless of drug specification. Indeed, every company has its own gold standard but this does not change the fact that the trial and error principle increases costs and is time consuming. Furthermore, this lack in an efficient screening method for suitable stabilisers may result in drugs, not reaching the market despite their proven therapeutic benefit.

Concentration of stabiliser solutions should be chosen wisely. Too low concentrations can lead to insufficient stabilisation while too high concentrations can cause toxicity or Ostwald ripening. In literature, the mass ratio of stabiliser and drug, which is mostly used, ranges from 1:20 to 1:1 [Merisko-Liversidge and Liversidge, 2011].

2.3 Effects of nanoisation

Orally administered poorly water-soluble drugs often show problems in bioavailability, like varying bioavailability in the fed or fasted state, a retarded onset of action and/or low bioavailability due to low dissolution rates [Junyaprasert and Morakul 2015]. All these problems can be addressed with the choice of a nano-particulate containing formulation. A minimisation of bioavailability fluctuation in the fasted or fed state as well as the increase in dissolution rate is based on the understanding that the total surface area for nano-formulations is further increased than for micronised powders, which are often used when formulating poor aqueous soluble drugs to tablets in the pharmaceutical industry nowadays. The dissolution rate is directly proportional to the surface area of a particle, so that an increase in surface area leads to an increase in dissolution rate. This relationship is illustrated in the extended Noyes-Whitney-equation (Equation 1).

$$\frac{dC}{dt} = k_1 S (C_s - C)$$

Equation 1: Extended Noyes-Whitney-equation. C standing for the concentration at time point t, C_s for saturation solubility, S for surface area and k₁ as a constant.

It shows that the rate of dissolution is proportional to the difference between the concentration C at time t , the saturation solubility C_s and the surface area S . k_1 is a constant which includes the diffusion coefficient and the thickness of the concentration layer [Bruner and Tolloczko, 1900].

By comparing nanocrystals and micro-particles, not only the dissolution rate can be increased but also the saturation solubility, dissolution velocity and adhesiveness to surfaces/cell membranes [Müller et al., 2001; Rabinow, 2005; Gao et al., 2012]. All these effects can lead to a better bioavailability, especially when a drug from BCS class II is utilised, as the solubility is the most influencing factor here [Loebenberga and Amidon, 2000]. Below particle sizes of 1,000 nm, also the saturation solubility of the formulated drug can be increased [Junyaprasert and Morakul 2015; Müller, R. H. and Peters, K. 1998]. The adhesion to cell membranes can lead to an increased concentration gradient at the surface of the cell and therefore allow faster permeation. Also the retention time can be increased so that the nano-objects have more time to dissolve.

Nanoisation also has an influence on the distribution of an API in-vitro and in-vivo. Nano-objects are more likely to cross membranes and be taken up by cells compared to micro-objects. Hence, a higher concentration of drug can be maintained inside cells, so that even the bioavailability can be enhanced in comparison to a solution of the drug [Junghanns and Müller, 2008]. Furthermore, the stability of nanosuspensions can be enhanced compared to solutions [Möschwitzer et al., 2004].

All in all, drug nanocrystals can dramatically improve the bioavailability of orally administered poorly soluble drugs as shown by changes in pharmacokinetic parameters of blood profiles like rising area under the blood concentration–time curve (AUC) and an increase in maximum plasma concentration (C_{max}). This can exemplarily be shown with the study of Jinno et al. as they detected an increase in C_{max} from 582 ng/mL (hammer-milled; 13 μ m) to 5,371 ng/mL (nano-milled; 0.22 μ m) for orally administered cilostazol suspensions to dogs (under fasted conditions). Both suspensions were administered with the same concentration (100 mg/body). Furthermore, the AUC increased 6.6 fold, from 2,722 ng/h/mL to 17,832 ng/h/mL [Jinno et al., 2006].

2.4 Fate of (nano)objects in biological environments

Oral uptake of particles from the gastrointestinal tract is generally, with less than 5 %, low [Florence and Attwood, 2016]. The uptake can involve transcellular and paracellular permeation as transport routes (Figure 4), as well as lymphatic transport.

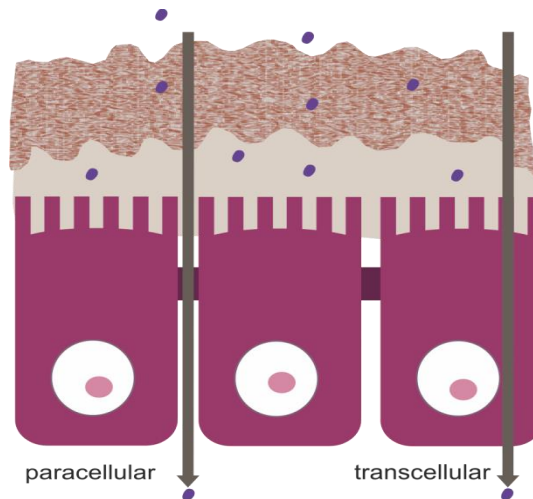


Figure 4: Scheme of enterocytes (light purple) with their glycocalyx (brown) and mucus (patterned red) and nano-object (dark purple) transport.

Transcellular transport of particles requires some kind of endocytosis. Endocytosis is an energy dependent process which can be categorised in caveolae- and clathrin-mediated endocytosis, phagocytosis, pinocytosis and micropinocytosis. Caveolae- and clathrin-mediated endocytosis are receptor-mediated and two of the most important pathways for nano-objects between 10 nm and 500 nm. Below 10 nm, pinocytosis (uptake of fluids) is the most prominent uptake pathway, while above 500 nm actin-dependent phagocytosis of macrophages, dendritic cells and neutrophils is known to be the dominant process [Nuri and Park, 2014]. Nevertheless, it has to be said that in biological environments a strict separation and categorisation of interaction pathways, in general, is not possible as all processes happen next to each other and often also in relation to one another.

Recently it was found that the human body produces nanoparticles itself. Calcium is excreted in the intestinal lumen and forms amorphous magnesium-substituted calcium phosphate nanoparticles, which trap soluble macromolecules, such as bacterial peptidoglycan and orally fed protein antigens, in the lumen and transport them via Peyer's patches to immune cells of the intestinal tissue [Powell et al., 2015]. Peyer's Patches are accumulations of lymphoid follicles containing, amongst others

lymphocytes, macrophages and connective tissue cells. The surface of Peyer's Patches is covered with M cells. Compared to other parts of the gastrointestinal tract, where enterocytes and goblet cells are present, which produce mucus and a thicker glycocalyx, the structure of the M cells facilitates the approach of microorganisms and particles (Figure 5).

Compared to enterocytes, M cells are small in number. In the human gastrointestinal tract the ratio of enterocytes to M cells is 1,000,000 to 1 [Tyrrer et al., 2007]. The mechanisms that control the transport route within M cells remain largely unknown [Söderholm, 2015]. Also, mechanisms of how nanoparticles penetrate the intestinal barrier are poorly characterised.

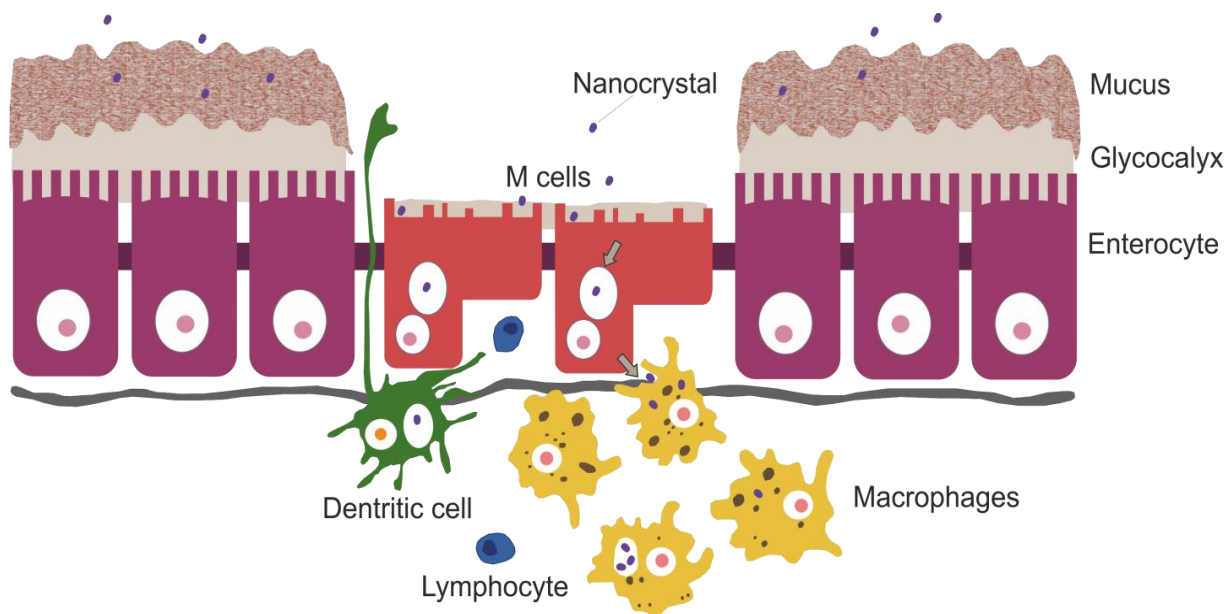


Figure 5: Scheme of a Peyer's Patch surrounded by enterocytes.

Even though already in the 1980s and 1990s different pathways of particles in and through tissues were discussed, like Peyer's Patches lympho-epithelial M cells uptake [Eldridge et al., 1990], paracellular transport [Aprahamian et al., 1987] and endocytosis by intestinal enterocytes [Kreuter et al., 1989; Mathiowitz et al., 1997], the detailed pathways are not characterised to a full extent. In 1990, O'Hagan related size ranges of nano-objects to their site uptake and fate in the intestine (Table 1).

Table 1: Influence of the size of nano-objects and the fate in various tissues adapted from O'Hagan (1990).

Site/mechanism	Size range	Fate after uptake
Enterocyte/endocytosis	< 220 nm	Reticuloendothelial system uptake
Paracellular transport	100 - 200 nm	Unknown
Intestinal macrophages	1 μ m	Mesenteric lymph nodes (MLN)
'Persorption'	5 - 150 μ m	Blood and excretory fluids
Peyer's patches	20 nm - 10 μ m	Peyer's Patches and MLN

Later on, it became clear that this strict size ranges do not display reality but give a rough estimation of where the nano-objects might end up.

The importance of stabilisers, surrounding the nano-object, on the uptake in cells, has also been studied. Hillery et al. found that an adsorption of poloxamers on polystyrene particles appeared to inhibit particle uptake in the small intestine of rats [Hillery. and Florence, 1996]. Contrariwise, Nadai et al. showed that poloxamers can enhance oral uptake of particles due to gastric mucosa damage [Nadai et al., 1972]. This contrary information indicates that a definitive answer cannot be given yet. All parameters must be investigated, such as stabiliser concentration, cell type, type of stabiliser, type of drug, surrounding conditions and many more. Ionic stabilisers, for example, do response differently when pH and ionic strength in gastrointestinal fluids changes [Peltonen and Hirvonen, 2010].

Uptake data in literature show that different cell types take up nano-objects of different sizes and to a different extent. Rejman et al. explored that a murine melanoma cell line took up particles of up to 500 nm [Rejman et al., 2004]. Depending on the role of the cell type, the uptake in cells is variable. Caco-2 cells, which mimic the intestinal epithelial cells, have a barrier function, while macrophages should take up foreign particles to present them to the immune system [Des Rieux et al., 2006; Cartiera et al., 2009]. Apart from the oral route, intravenous administration of nano-objects is also possible. Gustafson et al. state that macrophages tend to be a problem when nano-objects are administered intravenously, due to their ability to rapidly clear the nano-objects from circulation and therefore, hinder their potent medicinal effects

[Gustafson et al., 2015]. They summarised various publications, showing the influence of particle geometry, surface charge and functionalisation on macrophage uptake and in-vivo fate as well as toxicity. Depending on their shape, whether short rods or longer rods, the nano-objects accumulated in the liver or spleen. Spherical particles were taken up more rapidly than rods. The influence of the size and surface charge is plotted in Table 2.

Table 2: Influence of size and surface charge on the elimination of insoluble nano-objects, adapted from Gustafson et al. (2015).

Size	< 15 nm	Removed quickly (under 24 hours)
		Renal elimination
	15 nm - 40 nm	Removed less quickly (2 weeks)
		Biliary clearance
	> 40 nm	May reside in the body indefinitely
		Reside in liver and spleen
Surface charge	Neutral and zwitter-ionic	Longer circulation time than charged counterparts
		Different adsorption of proteins on more hydrophobic surfaces (more albumin, IgG) than hydrophilic
	Positively charged	Generally taken up to a greater extent than neutral or negative counterparts

The extent of nano-object absorption reported in the literature, is dependent on the intestinal model, selected material, type of species and time. The absorption of nano-objects ranges from 0.5 % - 10 % in just three of the many examples available [Kukan et al., 1989; Le Ray et al., 1994; McClean et al., 1998].

Hofmann-Antenbrink et al. blamed the non-easy detection in the biological milieu or tissue as one reason for the poor knowledge and inconsistent results in the field of short- and long-term toxicities, bio-distributions and clearance of nano-objects in

humans. Especially magnetic iron oxide particles were investigated, regarding the influence of particle size, surface charge and morphology on the interactions with tissues but yet, no consent has been reached regarding the impact of these parameters [Hofmann-Antenbrink et al., 2015].

As soon as nano-objects circulate in-vivo, they adapt a protein corona which has an influence on the fate of the objects [Tenzer et al., 2013; Lesniak et al., 2012; Ruge et al., 2012]. Depending on the type of stabiliser, which is situated on the surface of nanoparticles, the adsorption pattern of proteins can be different [Blunk et al., 1993].

To conclude, it can be said that uptake of nano-objects via the oral or intra-venous route is proven but the details of the uptake mechanisms remain controversial. One main challenge is that many studies investigate artificial particles which are easy to detect but do not display the properties of marketed products.

2.5 Tools for the assessment of transport of substances in and through cells

One of the simplest ways to study transport of substances across a barrier is the usage of an artificial membrane test, the so called Parallel Artificial Membrane Permeability Assay. A liquid membrane, consisting of an inert organic solvent like dodecane or hexadecane on a filter is used as a barrier between an apical and basolateral compartment. Two advantages of this method are the possibilities for high-throughput and cost effective experiments. One disadvantage can be the non-detection of drug interactions with transporters in the intestinal barrier. Therefore, pharmaceutical industry nowadays often uses the Caco-2 model [Shah et al., 2006]. Investigations of oral drug uptake can be done by this simplified model of the barrier of epithelial cells. Caco-2 cells are a colon carcinoma cell line from human colon cells. Even though they are derived from the colon, their enzymatic behaviour and barrier function are comparable to healthy small intestine epithelial cells. Still, there is a difference between Caco-2 cells and intestinal enterocytes, such as less brush border peptidase and mucins [Lundquist and Artursson, 2016]. Furthermore, an under-prediction of paracellular absorption more often occurs with this cell line compared to in-vivo studies. In addition, an overexpression of efflux transporters like Pgp has been described for Caco-2 cells compared to intestinal enterocytes [DiMarco et al., 2017]. As the Caco-2 model is a well distributed model, the permeation of nano-objects was already tested

for several drugs and nano-object formulations. Again, a large number of publications deal with artificial particles [Imai et al., 2017; He et al., 2013].

The transport of particles in comparison to solutions is interesting to investigate. Most approaches of nano-object formulations intend to use the advantage of faster dissolution rates because the nano-objects dissolve faster than their micro- or macro-pendants, so that the concentration gradient between the intestinal lumen and the blood vessels is higher which also leads to an increase in permeation. Some publications show that the permeation of nano-objects can be even higher than their solution formulation, so that there has to be an additional effect of nano-objects apart from their dissolution rate enhancement. The EMA stated in their scientific discussion about Rapamune[®], which is a sirolimus nanocrystal containing tablet, that the tablet and a solution of sirolimus were not bioequivalent after a single dose of 1 mg administered to healthy volunteers. The AUC was increased by 82 % for the tablet compared to the solution. The bioavailability of the tablet and the solution were approximately 17 % and 14 %, respectively [Procedure No. EMEA/H/273/X/21]. Lamprecht et al. investigated, whether tacrolimus containing polymeric nanoparticles were favourable regarding penetration of ulcerated tissues over dissolved drug. Due to the accumulation of nanoparticles in the inflamed tissue, and therefore, high local drug concentration, the Pgp capacity was saturated at this local site and the metabolism and transport of the drug were minimised [Lamprecht et al., 2005].

Next to the transport of particles through cellular barriers also the particulate uptake in cells can be of interest. As mentioned in section 2.4, the uptake of nano-objects in macrophages can lead to limited bioavailability due to fast clearance of the nano-objects. When administered systemically, approximately 95 % of the nanomaterial never reaches its target, because it is sequestered by filtration organs [Florence, 2012]. Nevertheless, there are some areas where an uptake in immune competent cells is desirable. The complexity of signals regulating the immune system leads to major challenges for therapies in the field of immunisation based on traditional single-agent bolus drug treatment. Vaccination over mucosae like the intestinal, nasal or lung mucosa often benefit from particulate formulations. These particles can stimulate immune cells directly through their physical and chemical properties and lead also to a local immune response [Trows and Scherließ, 2016]. Furthermore, the research on particle-laden immune cells as living targeting carriers for drugs continues

to progress, leading to new approaches for immunotherapy [Moon et al., 2012]. Macrophages play an important role in physiological mechanisms like inflammation, homeostasis and immune response but also in pathophysiological processes such as chronic inflammation in diseases like rheumatoid arthritis or diabetes [Wynn et al., 2013]. Their primary role is to create an early response to foreign material contamination and its clearance. The uptake of nano-objects in macrophages could be useful in certain diseases as a targeted therapeutic approach, for example, in virus infections [Dou et al., 2006; Dutta et al., 2008], bacterial infections [Clemens et al., 2012] or as tumour-associated macrophages in cancer [Zhu et al., 2013]. In these cases, macrophages can be used as cell based delivery systems, loaded with drugs or other therapeutics. They can be loaded ex-vivo and then be administered to the host. Loading the drug into carrier cells can increase the circulation time from several hours for the free drug to 10 days for the nanocrystalline drug, loaded into cells [Staedtke et al., 2010; Dou et al., 2006]. Loading of the nano-objects in these living platforms is a crucial step. Methods need to be explored that can exactly determine the amount of particles which are taken up, to increase efficacy of the formulation and reduce side effects. Particles, taken up, need to be separated from particles that have merely been adsorbed on the surface of the cells which could be washed away.

Imaging methods can be used to quantify the uptake but they often require labelling of the particles which can alter the in-vitro or in-vivo behaviour of the nano-object. Therefore, techniques are favoured that can localise unlabelled organic particles. Fluorescent probes are the most common way to study cell uptake. Live cell imaging, nanoparticle tracking, enzyme degradation of endocytic load and many more analyses are possible with fluorescence microscopy [Duncan and Richardson, 2012]. Another, quite new, imaging technique is coherent anti-Stokes Raman microscopy. The rising interest in this technique, which can be seen in an increase in publications, led to the first commercial available microscope in the year 2011 (from Leica). It is a fast and label-free imaging technique. Therefore, the influencing factor of labelling on distribution and uptake can be excluded, so that the characteristics of the formulation as is are in focus. Brandenberger et al. titled in a paper from 2010: "Intracellular imaging of nanoparticles: Is it an elemental mistake to believe what you see?" They investigated the uptake of quantum dots (sulphur and cadmium containing) in macrophages by choosing six different areas which visually seemed to show quantum dots taken up by macrophages. Interestingly after electron spectroscopic imaging

analysis, just one area was confirmed having quantum dots in macrophages [Brandenberger et al., 2010]. Also Xu et al. saw an uptake of Nile red dye which was loaded in polylactic-co-glycolic acid (PLGA)-nanoparticles by fluorescent imaging but with coherent anti-Stokes Raman microscopy, they detected the non-fluorescent PLGA which revealed that the nanoparticles did not enter the cells but just stayed at the surface of the cell. Nile red must have been dissociated into the cell from there [Xu et al., 2009]. These are just two out of many examples that show, why there is a need in chemically specific microscopic techniques for organic structures like coherent anti-Stokes Raman microscopy.

In conclusion, the knowledge of in-vitro permeation through the Caco-2 model can give hints to bioavailability; not only of the drug but also of the drug formulation, but differences to in-vivo environments should not be neglected. Furthermore, the interest in techniques that can quantify the uptake of nano-objects in cells is rising due to relatively new approaches like cell based delivery systems.

3 Materials and Methods

3.1 Materials

This chapter gives details on the used drugs, stabilisers and cell lines, while chapter 9.2 in the appendix holds details on quality and supplier origin of the used materials.

3.1.1 Model drugs

Curcumin (CUR) and glibenclamide (GLI) were investigated as model substances in this project. In this part, the two drugs will be explained in more detail, regarding their physico-chemical parameters and their therapeutic use.

3.1.1.1 Curcumin

CUR is a well investigated, natural compound that is commonly known as an ingredient of turmeric (*Curcuma longa*). The phenolic, π -electron rich structure of the CUR molecule, which is shown in Figure 6, causes its yellow colour as well as fluorescent behaviour which emits light at 500 nm when excited at 420 nm.

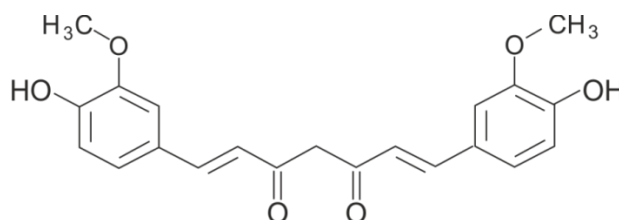


Figure 6: Chemical structure of CUR.

The molecule can exist in its enolate or bis-keto form. When present in the enolate form, the anti-oxidative effect of CUR is pronounced [Metz, 2000]. The bis-keto form is more likely to form in acidic and neutral aqueous solutions as well as in the cell membranes, than the enolate form [Wang et al., 1997]. At pH 3-7, CUR acts as a potent H-atom donor [Jovanovic et al., 1999].

The Raman activity of CUR is based on the functional groups listed in Table 3.

Table 3: Example for Raman activity of the functional groups of CUR from Lestari and Indrayanto (2014).

Raman wavenumber in cm^{-1}	Functional group
--------------------------------------	------------------

1626.2	C=O
1600.4	Aromatic C=C
1430.2	Phenol C-O
1249.3	Enol C-O

CUR can have different polymorphic forms which differ in conformation of the molecule and interaction between the neighbouring CUR molecules. Sanphui et al. findings in 2011 show three types of polymorphs, with one polymorph (polymorph 2) having a higher dissolution rate and solubility than the others (Table 4) [Sanphui et al., 2011].

Table 4: Melting temperatures of CUR polymorphs from Sanphui et al. (2011).

Polymorph	Onset temperature in °C	Peak temperature in °C
1	177.54	181.42
2	171.95	175.12
3	168.29	172.85

The log P value for CUR was found in the database chemspider with 3.29. CUR is poorly soluble in water and weakly permeable as well and therefore belongs to BCS class IV. Hence, CUR belongs to the group of APIs that are most challenging in formulation. Many formulation strategies are employed in research, which are nowadays just realised in the food supplement market. Amongst other products, cyclodextrin (CAVACURMIN[®] by Wacker Chemie AG, Curcumin Extrakt 45 by Dr. Wolz Zell GmbH) and liposomal formulations (Optimal Liposomal Curcumin by Seeking Health) are commercially available. Especially in India, turmeric has a long tradition in treating numerous discomforts of diseases like arthritis, menstrual difficulties, ulcers, hepatic disorders, cold and bruises [Ramawat, 2009].

Many molecular targets for CUR have been investigated, such as transcription factors, inflammatory cytokines, kinases, growth factors and antiapoptotic proteins. This variability of targets could enable a broad range of application but nowadays it is only used in food supplement products. The FDA has approved CUR as “Generally Recognised As Safe” (GRAS), showing that CUR can be used safely as a food additive [Chainani-Wu, 2004]. Also in pharmaceutical application, no toxicity could be seen in a phase I study, for 8 g of CUR per day being administered for 3 months [Sharma, 2005].

Lately, the anticancer effect of CUR has been studied more intensively. CUR is known to inhibit ABC transporter function like Pgp [Limtrakul et al., 2007; Anuchapreeda et al., 2002] which shows that CUR could be a beneficial co-medication against multi-drug-resistant tumours. Nevertheless, it is discussed controversially if CUR is also a Pgp substrate [Chearwae et al., 2004; Wang et al., 2017a]. Wu et al. state that “it is not surprising that CUR has become one of the most exciting natural product modulators in recent years” [Wu et al., 2011]. CUR, in its free form and as nano-formulations, has been under investigation in human clinical trials for many years in the field of colorectal cancer, pancreatic cancer, breast cancer and multiple myeloma and has shown beneficial results [Ornchuma et al., 2014]. The EMA has stated 7 clinical trials with CUR by the year 2010. However, because they were performed with either a very high dose or with combination products, they are of limited value to the EMA [EMA/HMPC/456848/2008]. With improved formulation strategies this could be changed, as lower doses could be applicable.

In summary, it can be said that CUR has been used over decades for various kinds of diseases and therefore, its safety is proven but because of poor solubility and bioavailability its efficacy is limited, so that adequate formulation strategies are needed to fulfil the potential of this drug for pharmaceutical applications.

3.1.1.2 Glibenclamide

GLI is a poorly water soluble drug (solubility < 8 µg/mL in pH 7.4 phosphate buffer [Seedher and Kanojia, 2009]) but has a relatively high permeability through intestinal barriers, which warrants it to be classified under BCS Class II [Lindenberg et al., 2004]. The solubility of GLI increases with higher pH because it serves as a weak acid with a pKa of about 6.5, so that the adsorption of GLI can differ in the gastro-intestinal tract [Brockmeier et al., 1985]. The deprotonation of GLI takes place at the sulphonylurea structure of the molecule which can be seen in Figure 7.

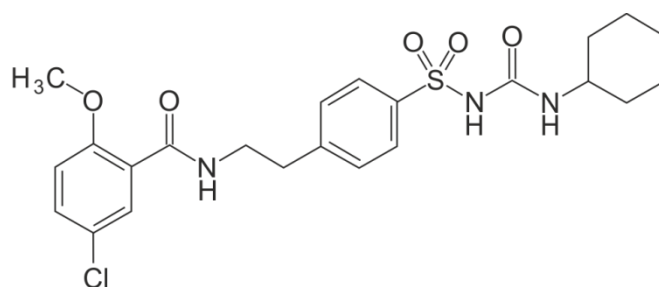


Figure 7: Chemical structure of GLI.

Due to two aromatic ring systems and two carbonyl groups, GLI shows fluorescence at 354 nm after excitation at 302 nm [Khalaf and Perween, 2012].

Log P of GLI was found in chemspider database with 3.754. GLI can show polymorphism (Table 5). This table indicates that the stability and solubility of GLI is dependent on its polymorphic form.

Table 5: Polymorphs of GLI with their melting point.

Literature source	Named polymorphs	Melting conditions	Melting point in °C	comments
Suleiman. et al. (1989)	I (more stable)	The samples were placed on the hot-stage at room temperature and	173.1	At 37 °C 0.66 mg/100 mL solubility in distilled water No significant difference in dissolution to form II
	II (less stable)	heated at a rate of 5 °C per min.	148.7	At 37 °C 1.06 mg/100 mL solubility

The Raman activity of GLI is based on the functional groups listed in Table 6.

Table 6: Example for Raman wavenumbers of functional groups of GLI from Mah et al. (2013).

Raman wavenumber in cm^{-1}	Functional group
1714	C=O
1593	Aromatic C=C
Doublet at 1345 and 1156	SO ₂
1442	Enol C-O

GLI is used as an antidiabetic drug which is applied in the treatment of non-insulin dependent diabetes. It is known to block ATP-dependent potassium channels, which leads to a depolarisation of the beta-cells in the pancreas, therefore, activates calcium channels and leads to secretion of insulin. GLI is a known Pgp inhibitor [Golstein et al., 1999]. Recently, GLI had been identified to minimise posttraumatic secondary injuries by interacting with a non-selective cation channel (transient receptor potential melastatin 4) [Hersh et al., 2017]. Doses administered can be 1.25 mg every 12 hours over one week. The usual starting dose in diabetes treatment is 5 mg for adults. The standard dosage form on the market is the tablet but in neonatal diabetes there is also a need for suspensions with starting doses of 0.2 mg/kg/d, which are commonly produced from tablets. This preparation can easily lead to dosage inconformity [Di Folco et al., 2012]. Nanosuspensions as formulation strategy, which could be dried and re-dispersed before administration, could make the production and application easier.

3.1.2 Stabilisers

It was described earlier that for the creation of nanocrystal suspensions via milling, stabilisers are essential. In this study, five different types of stabiliser were tested for their ability to stabilise CUR and GLI nanosuspensions.

3.1.2.1 Polysorbates

Polysorbates are surface active agents (surfactants). They are formed by the ethoxylation of sorbitan before addition of fatty acids. Depending on fatty acid and ethoxylation type, polysorbates are named differently. In this work, Polysorbate 80 (PS80) was selected, which is mostly created out of 8 = oleic acid and 0 = monoester with 20 polyoxy ethylene units (Figure 8).

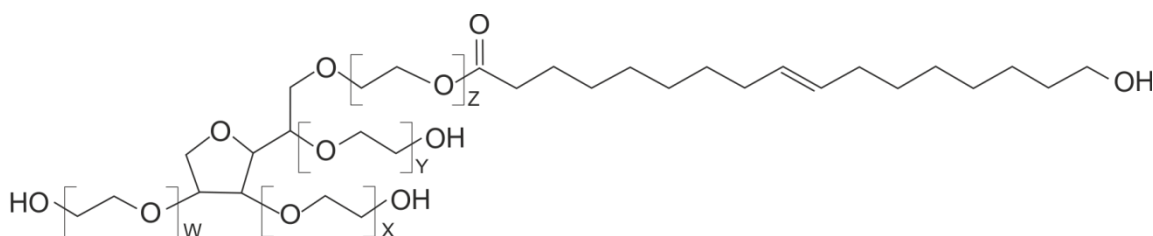


Figure 8: Chemical structure of PS80 ($W + X + Y + Z = 16$).

Polysorbates are a mixture of components. PS80 has, like mentioned above, high percentages of oleic acid ester content ($67.8 \pm 0.7\%$ to $96.6 \pm 1.3\%$) [Braun et al., 2015] along with myristic, palmitic, palmitoleic, stearic, linoleic, and α -linolenic acid

esters. The calculated molecular weight is 1,310 daltons, assuming 20 ethylene oxide units, 1 sorbitan, and 1 oleic acid as the primary fatty acid [Sigma-Aldrich ProductInformation Tween® 80 Sigma Ultra].

Braun et al. tested sixteen batches of PS80, which they selected from different suppliers and demonstrated a had high variability in physical characteristics such as critical micellar concentration (CMC), cloud point, hydrophilic-lipophilic-balance (HLB) and micelle molecular weight [Braun et al., 2015]. Therefore, in this work, just one production batch was used.

PS80 molecules aggregate in solution to different structures, depending on the concentration. The CMC in water ranges from 13.4 ± 0.6 mg/L to 24.7 ± 1.4 mg/L [Braun et al., 2015]. Below these concentrations, the polysorbate molecules are dissolved as monomers. By increasing the concentration above the CMC, different structures can be found. Siqueira et al. found a monomodal intensity distribution near 4 nm, measured with dynamic light scattering, for PS80 [Siqueira et al., 2013].

Polysorbates can be used as stabilisers in nanoemulsions, [Wang, 2014] as stabilisers of nanostructured lipid carriers [How et al., 2011] and in nanocrystalline formulations [Peltonen and Hirvonen, 2010]. PS80 can be utilised as component for oral and parenteral administration [Liang, 2012]. When used as a stabiliser of nano-objects, PS80 can change the nano-bio-interaction of the drug with tissues. Leno et al. found that PS80 coated nanoparticles were favourable to increase organ distribution for a HIV therapeutic drug and therefore, enhance the efficacy of the drug [Leno et al., 2014]. Araujo et al. explored PS80 to be the most effective surfactant for the direction of particles to non-reticuloendothelial system organs with a concentration above 0.5 % [Araujo et al., 1999].

All these literature data suggest that PS80 can have a positive effect on nanosuspension formation and application and therefore, it was included in this work.

3.1.2.2 Hydroxypropyl methylcellulose

Hydroxypropyl methylcellulose (HPMC) is a non-ionic polymer. This chemically changed cellulose ether can be produced with different molecular weights, depending on the number of subunits (n) that can be seen in Figure 9. Parameters, like viscosity of an HPMC solution, are depending on their molecular weight, whereas the degree of substitution leads to changes in hydrophobicity.

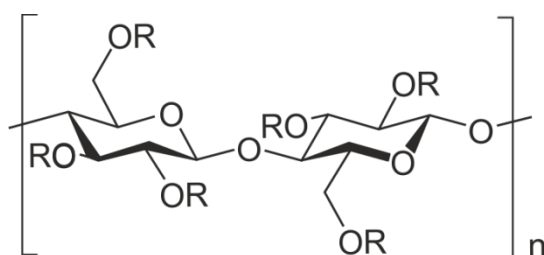


Figure 9: Chemical structure of HPMC; n = number of units; R = hydroxypropyl or methyl groups.

The structure of HPMC in aqueous solution is still not fully explored. Proposed structural behaviour of HPMC in water ranges from individual chains, forming loops at high concentrations with the hydrophobic parts interacting, to the formation of fringed micelles [Müller, 2010; Klemm et al., 2005]. The properties of dissolved HPMC are dependent on the average-, molar- and region-specific degree of substitution, the solvent, temperature, concentration and molar mass [Kulicke et al., 2005]. Sarkar investigated the viscosity ranges and corresponding molecular weights for HPMC, produced by Colorcon GmbH, which is a company of The DOW chemical company (METHOCEL™) [Sarkar, 1979]. The results can be seen in Table 7.

Table 7: Molecular weights and corresponding viscosities of HPMC grades [Sarkar, 1979].

Grade number	2 % viscosity range in mPa x s	M _w range in kDa
5	4 - 6	18 - 22
25	20 - 30	48 - 60
50	40 - 60	65 - 80
100	80 - 120	85 - 100

In this project, METHOCEL E5 Premium LV was used, which has following properties (Table 8).

Table 8: Key figures of Methocel E5 Premium LV taken from *METHOCEL Cellulose Ethers in Aqueous Systems for Tablet Coating*.

Product description	Corresponding values
Methoxyl	28 - 30 %
Hydroxypropyl	7 - 12 %
Viscosity, 2.0 % in water,	4 - 6 mPa x s

HPMC can be used as an excipient for hard capsules [Al-Tabakha, 2010], in retard matrix tablets [Timmins et al., 2014] or as coating material [Roy et al., 2009; Sangalli et al., 2004]. Also, as stabiliser in nanosuspensions as well as nanoemulsions it is widely explored [Kumar et al., 2015; Plakkot et al., 2011; Karashima et al., 2016; Chen et al., 2015]. The use of HPMC products is generally recognised as safe (GRAS).

As HPMC is a widely explored and safe agent it was included in this thesis.

3.1.2.3 Sodium dodecyl sulfate and tetra decyl trimethyl ammonium bromide

Ionic stabilisers can also be called tensides or surfactants. They can be positively or negatively charged. One of the most widely known representatives of the latter group is sodium dodecyl sulfate (SDS), displayed in Figure 10.

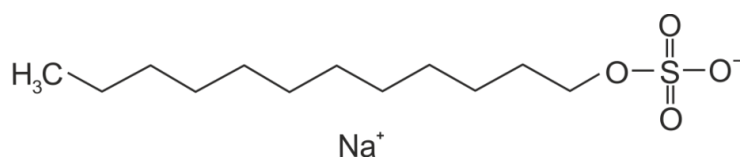


Figure 10: Chemical structure of SDS.

It is used in soaps and washing detergents but also has many applications in pharmaceutical sciences. As a solubility enhancer it can be used in dissolution studies of poorly soluble drugs [Madelung et al., 2014], as a nucleation inhibitor in bottom-up production of nanocrystals [Dalvi and Yadav, 2015] and as a stabiliser for nanocrystals [Toziopoulou et al., 2017; Fu et al., 2017; Liu, 2013].

Depending on the determination method, the CMC can vary so that, amongst other things, CMC in literature were found between 4 mM and 10 mM [Rahman and Brown, 1983; Khan and Shah, 2008]. Its structural behaviour in a buffer solution can differ, as Fuguet et al. found the CMC of SDS in 50 mM phosphate buffer being 1.99 mM [Fuguet et al., 2005].

An example for a positively charged stabiliser is tetra decyl trimethyl ammonium bromide (TTAB). TTAB has a long ethylene chain as well with a positively charged ammonium head group (Figure 11).

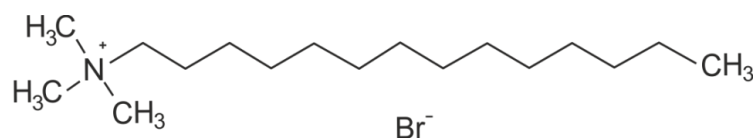


Figure 11: Chemical structure of TTAB.

TTAB is employed in lyotropic liquid crystal formulations [Yavuz et al., 2014], as pore creator in porous silica nano-particles [Xu et al., 2015] and the positive charge allows the application of ionic interaction with negatively charged structures, for example, for stabilisation issues. Dhar et al. found that the stability of nanocrystalline cellulose (NCC) suspension was dependent on the adsorption of TTAB. The interaction was electrostatically driven which was followed by hydrophobically driven polymer-induced micellisation of TTAB on NCC particles [Dhar et al., 2012].

CMC values in water were found at 3.77 mM and 1.93 mM in 20 mM phosphate buffer for TTAB [Fuguet et al., 2005].

These two ionic stabilisers were added to this work, as they show potent stabilisation characteristics and can have a change in behaviour when being applied to biological surroundings, like buffered solutions which was of interest in the cell studies conducted.

3.1.2.4 Poloxamers

Poloxamers are non-ionic poly ethylene oxide-poly propylene oxide copolymers which general structure is given in Figure 12.

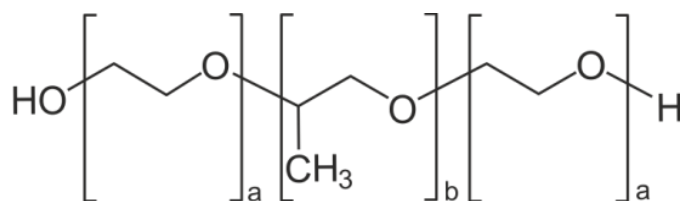


Figure 12: Chemical structure of poloxamers. a = ethylene oxide unit b = propylene oxide unit.

Depending on the number and arrangement of 'a' and 'b' structures, they have different molecular weight, solubility in water and surface activity. One of the most commonly used poloxamer is poloxamer 407 (a = 95 - 105, b = 54 - 60) with molecular weights ranging from 9840 - 14600 Da. Depending on their molecular weight, poloxamers can be of a liquid (poloxamere 124; molecular weight = 2090 - 2360 Da) or solid (poloxamere 407) state. Poloxamers are explored as thermosensitive gelling agents

[Yu et al., 2017], in micelle formation processes [Ćirin et al., 2017; Mendonça et al., 2016] for solubility improvement and in nanosuspension stabilisation. Poloxamers adsorb on lipophilic surfaces with their middle-structure leaving the arms as steric barrier. The hydrodynamic thickness of the adsorbed polymers is proportional to the chain length 'a' (see Figure 12) as well as the molecular weight [Lee et al., 1989]. Anwar et al. utilised poloxamer 407 for the improvement of the aqueous solubility of their tested API and higher systemic circulation time of the created lipid nanocapsules [Anwar et al., 2016]. Hence, poloxamer adsorption on surfaces can have a relevant effect in bio-distribution of particles. Macrophages tend to take up less API particles when poloxamers are adsorbed to the particles, which can lead to a longer circulation time in the bloodstream after intravenous administration [Dunn et al., 1997; Owens and Peppas, 2006]. It has to be kept in mind that desorption can occur, especially in the surrounding of serum proteins [Neal et al., 1998]. A stable adsorption occurs when the proportion and the size of polyethylene oxide and polypropylene oxide segments are chosen wisely for the appropriate drug. Hydrogen bonds between drug and the polyethylene oxide ether groups, hydrophobic van-der-Waals interactions and weak polymer-solvent interactions can lead to quite stable interaction patterns [Moghimi and Hunter, 2000].

In this work, poloxamer 124 (Pol124) (a = 10 - 15; b = 18 - 23) and poloxamer 407 (Pol407) were chosen, as they differ in composition and therefore, the differences in structure might be transferable to the ability and efficacy of producing nanosuspensions.

3.1.3 Cell culture

On the basis of in-vitro experiments, a correlation to in-vivo behaviour of the formulated drug can be aimed. Cell systems, as living structures, can be suitable for the prediction of drug transport through cells or uptake in cells in-vivo [Artursson et al., 2012].

When a drug should be administered orally, the main absorption barrier are the enterocytes in the small intestine as there, most drugs have to pass the cells to appear in the blood stream, if they should be systemically effective. A drug should have sufficient permeability to achieve adequate bioavailability. In drug discovery, the Caco-2 cell model is a successfully used model for permeability screening [Hidalgo, 2001].

Caco-2 cells are a human colon carcinoma cell line. As explained in the theoretical background (chapter 2.5), the barrier functions of this colon cell line are comparable to healthy small intestine epithelial cells. It is an adherent cell line which forms connective monolayers. Hence, this ability can be used for permeability screening as the cells can be grown on a membrane. Under optimal culturing conditions, the monolayer is forming within 21 days and should look like displayed in Figure 13.

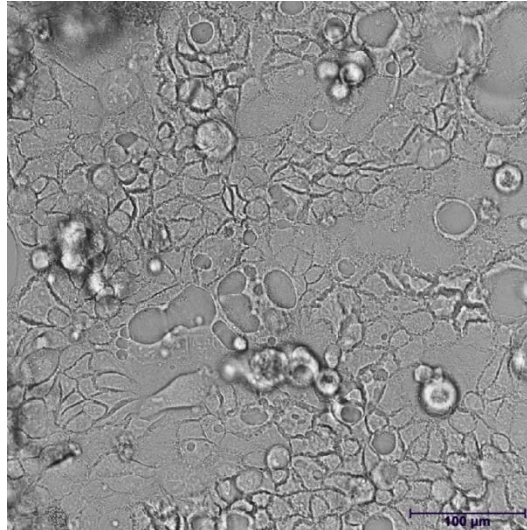


Figure 13: Caco-2 cells. bright field image. cells imaged in cell culture medium.

As the Caco-2 model is a widely explored permeation model for testing permeation of drugs, it was also used in this work to gain better understanding in the permeation of nanosuspensions.

The second cell line, utilised in this work, was the RAW 264.7 cell line. It is an Abelson leukaemia virus-induced tumour cell line from mice. These adherent macrophages can be used for pinocytosis and phagocytosis studies. They have the morphology of monocytes like can be seen in Figure 14.

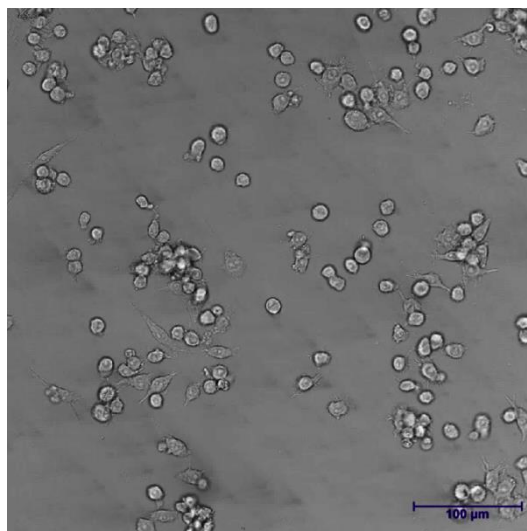


Figure 14: RAW 264.7 cells. bright field image. cells imaged in cell culture medium.

In this work, the cell line was used to test the capability for nano-object uptake with regard to size, time and type of stabiliser.

3.2 Methods

3.2.1 Media milling

Media milling is a standard practise for large scale production of nanocrystals in pharmaceutical industry, using agitated ball mills, like horizontal bead mills in recirculation mode [Möschwitzer, 2013]. Most nanocrystal products on the market are produced with the NanoCrystal[®] technology which is patented by the Perrigo Company PLC [US Patent 5145684]. The core of the patent is a horizontal bead mill with a circulating drug suspension. One example for the construction of an agitated ball mill on laboratory scale is the horizontal bead mill type Dispermat[®] which was utilised in this work (Figure 15).

The suspension, consisting of coarse drug particles and stabiliser solution, is kept in a closed vessel together with the milling beads. The suspension has to be separated from the beads after milling. Therefore, the Dispermat[®] has a dynamic gap between milling vessel and outlet for circulation purposes. Particles in suspension are able to pass this gap while milling beads stay in the milling chamber. Hence, an automated separation of beads and product is achieved more easily when comparing the bead separation process to, for example, a planetary mill, where the beads have to be manually removed.

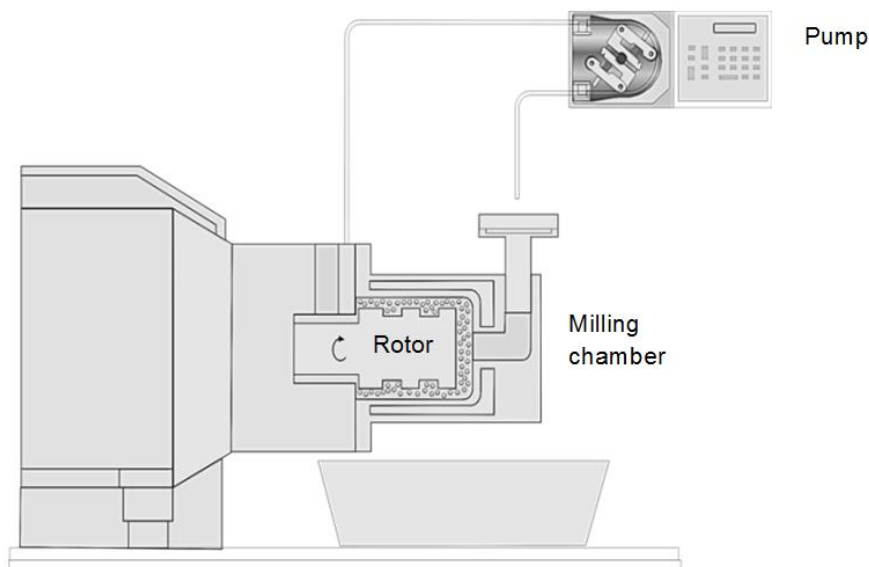


Figure 15: Scheme of a horizontal media mill in circulating mode.

Starting material that gets in between bead–bead, bead-wall and bead-rotor contacts is exposed to a certain force, depending on the nature of the contact, so that depending on the rotor speed, milling time and bead size, different particle sizes can be produced.

Particle size reduction to the nano-scale was accomplished, in this work, with the Dispermat® SL-C 5 (VMA Getzmann GmbH, Germany) in a circulation setup. Pump speed for all experiments was at 69 mL/min (set for double-distilled water). External cooling fluid was cooled down to 8 °C and circulated through the casing of the milling chamber while milling. As sealing liquid, the stabiliser solution for the ongoing milling was used. Rotor speed was set to 4,000 rpm and for every experiment 10 g of drug was used in 100 g of final formulation. Before milling, the drug was added to the stabiliser solution and directly homogenised with an Ultra Turrax® (Ultra Turrax® T25 basic, IKA®-Werke GmbH & Co. KG, Germany, rod of 1.7 cm diameter) for 10 seconds at 11,000 min⁻¹ to minimise floating of the drug on the surface.

3.2.2 Stabiliser characterisation

Different stabiliser characteristics can have an influence on the stability as well as on the production of nanosuspension. Therefore, in this work, the zeta potential of the produced nanosuspensions and the CMC were tested for selected stabiliser solutions.

3.2.2.1 Zeta potential

With zeta potential measurements, the electrostatic or charge repulsion/attraction between particles can be measured. It is the calculated average potential in the surface of shear and can be measured by performing an electrophoresis experiment and simultaneously measuring the velocity of the particles by, for example, Laser Doppler Velocimetry, which can be done by the Zetasizer Nano ZS from Malvern Instrument Ltd (Malvern Instrument Ltd., UK). This was the instrument of choice for this work. Cuvettes from the Zetasizer Nano series (Malvern Instrument Ltd., UK) were used with stoppers. Samples were diluted (1:100 for GLI and 1:1000 for CUR) with double-distilled water before measurement. One measurement contained 3 measurement repetitions with 10 - 100 runs (automatic mode) and a 60 second delay between the measurements. The temperature was set to 23.3 °C.

3.2.2.2 Critical micelle concentration

One of the most used methods to measure the CMC are surface tension measurements. In this work, the Processor Tensiometer K12 (Krüss GmbH, Germany) was utilised to measure the surface tension of the stabiliser solutions. A platinum Wilhelmy plate was used for all measurements. This plate is connected to a force sensor, so that after introduction of the plate to the sample, the plate is pulled out of the sample and this force can be measured. Based on this value, the length of the plate and the contact angle of the solution at the plate, the surface tension can be calculated. The typical pattern of increasing concentrations of surfactants is plotted in Figure 16.

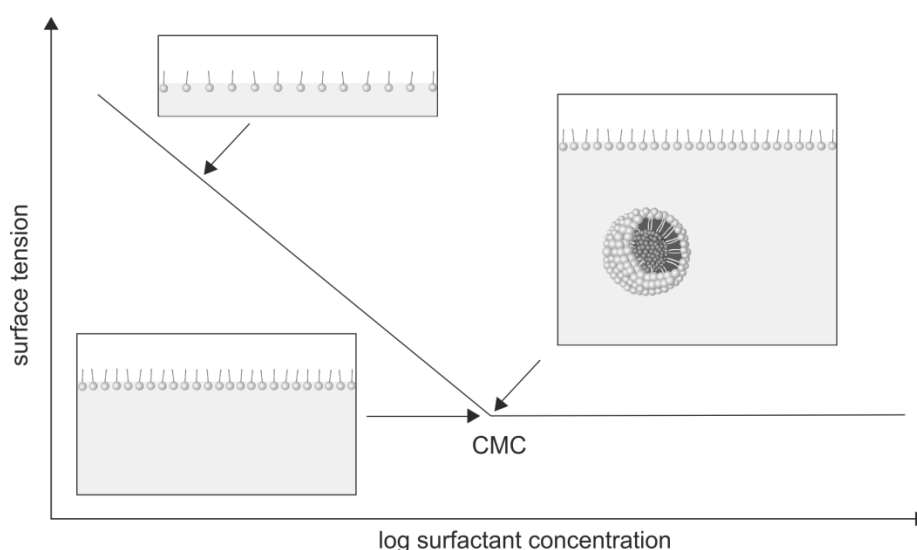


Figure 16: Surface tension plot of a surface active agent with increasing concentrations.

The CMC was taken from the graphs created with increasing concentrations of the stabilisers and was plotted with the same axis than shown above. The graph values were calculated by Microsoft Excel 2010.

3.2.3 Particle characterisation

3.2.3.1 Particle morphology of coarse material

By using a scanning electron microscope, the particle shapes of the coarse powders of GLI and CUR were investigated. In the scanning electron microscope, a beam of electrons is produced by an electron gun. The electrons travel through electromagnetic fields and lenses, which focus the beam down toward the sample. These electrons lead to a removal of secondary electrons that leave the sample, are collected, amplified and analysed [Smith and Oatley, 1955]. Different areas of the sample produce a different amount of secondary energy, so that a picture can be generated by the analyser.

The samples were prepared by fixing the powder on a carbon sticker and coating the sample with gold by a sputter coater (BAL-TEC SCP 050 Sputter Coater, Leica Instruments, Germany) to avoid charging of the samples. Images within this work were visualised with a Zeiss Ultra 55 plus (Carl Zeiss NTS GmbH, Germany) combined with a SE2 detector, at a working voltage of 2 kV. A magnification of 500 x was utilised.

3.2.3.2 Particle size measurements

Depending on the particle size, different measurement techniques are applicable. Laser light diffraction (LD) is suitable to measure particles from 0.01 μm to 8750 μm (HELOS[®], Sympatec GmbH, Germany) whereas for particle size ranges from 0.3 nm to 10 μm (Zetasizer Nano ZS, Malvern Instruments Ltd., UK) dynamic light scattering (DLS) is generally the technique of choice. It has to be kept in mind that these size ranges are instrument dependent numbers so that they can differ to instruments from other brands.

Laser diffraction

In laser diffraction, a continuous-wave laser is directed on the sample, followed by the light being inflected from the surface of the particle at an angle which is dependent on the size of the particle. The inflected light is then focused with a lens on a detector array, where a diffraction pattern is collected. When observing the intensity of light inflected at different angles, the relative amounts of particles with different sizes can

be determined by a complex algorithm. The principle behind the algorithm is, that smaller particles deflect light at relatively larger angles compared to larger particles [Skoog et al., 2013].

There are two principles of data analysis for laser diffraction, Fraunhofer and Mie, whereby both describe scattering by homogenous spheres of random size. For particles much larger than the wavelength of the emitted light, the Fraunhofer method can be used. Particles are here seen as round and impervious to light. Amongst other things, the inflection intensity and the intensity at the maximum of the inflection pattern are taken to calculate the size of the particle(s). The LD method requires the particles to be in a dispersed state, either in liquid or in air.

Consideration of the particles size alone is not enough to describe a population of particles. Equally important is the interpretation of the particle size distribution. For LD, the Span can be used as a particle size distribution value. It is calculated like shown below (Equation 2).

$$Span = \frac{x_{90} - x_{10}}{x_{50}}$$

Equation 2: Particle size distribution calculation. X-values stand for a particle size. X₉₀, for example, means that 90 % of the particles are smaller than the size value for X₉₀.

Analysis, in this project, was accomplished with the CUVETTE® (suspensions) or RODOS® (powder) module of a Helium-Neon Laser Optical System (HELOS®, Sympatec GmbH, Germany). For the CUVETTE® measurements one drop of suspension was dispersed in double-distilled water and measured with a R2 lens (focal length: 50 mm and measuring range: 0.25 µm up to 87.50 µm) directly after stirring. The powder was dispersed with the RODOS® module into the measuring zone by compressed air (3 bar) and measured with appropriate lenses. The calculation of the volumetric particle diameter was accomplished with Windox 5 software, based on Fraunhofer enhanced evaluation. From the cumulative volume-based distribution (Q3), the values of X₁₀, X₅₀ and X₉₀ were determined in quadruplicate. Reported values are given as mean ± standard deviation.

Dynamic light scattering

In dynamic light scattering (DLS) the particles are not seen as static elements because they are measured in suspension and therefore, can undergo Brownian motion which is a random motion caused by thermal density fluctuations of the solvent.

Again, a continuous-wave laser is used as a light source, which is shown through a lens on the probe, which is placed in a cuvette. The scattered light is mostly detected at an angle of 173° from a photomultiplier.

When the laser light meets a particle in suspension it can be scattered as shown in Figure 17.

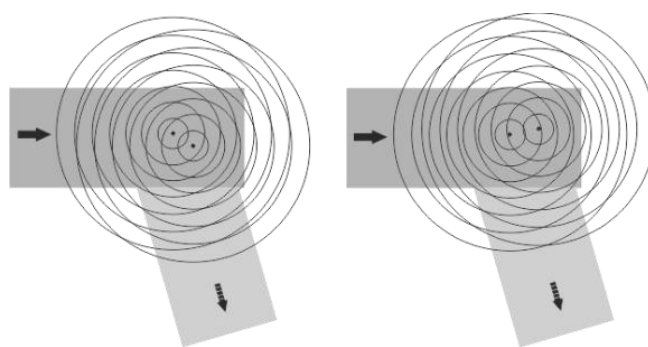


Figure 17: Sketch of the change in the interference pattern of scattered intensity in DLS over time, caused by Brownian motion adapted from Schärfl et al. (2007).

Hence, DLS measures the Doppler-broadening of the light that creates Rayleigh scattering when interacting with the particle(s). The time dependent intensity fluctuation is then used to obtain particle size information. Smaller particles move faster compared to larger particles and have therefore, faster intensity fluctuations. With the Stokes-Einstein-relationship (Equation 3), different intensity fluctuations can be analysed with respect to the velocity of the Brownian motion. Because the particle size is calculated during movement of the particle, the diameter that is measured equals the hydrodynamic diameter (d_H) of a spherical particle.

$$d_H = \frac{kT}{3\pi\eta D_T}$$

Equation 3: Stokes-Einstein-relationship for the determination of the hydrodynamic diameter (d_H) out of the Boltzmann's constant (k), sample temperature (T), solvent viscosity (η) and the translational diffusion coefficient (D_T).

Sample temperature, T and solvent viscosity, η must be known and the translational diffusion coefficient (D_T) is calculated from the intensity fluctuations. k is the

Boltzmann's constant. Often, the hydrodynamic diameter of a sample is plotted as z-average. The z-average is an intensity-based overall average size.

For dynamic light scattering, the particle size distribution is characterised by the polydispersity index (PDI). This is a value ranging from 0 to 1 with 0 being a 100 % monomodal distributed sample.

In this work, the size of the nanocrystals was determined, using DLS (Zetasizer Nano ZS, Malvern Instruments Ltd., Malvern, UK). Samples were diluted (1:100 for GLI and 1:1000 for CUR) with transport buffer (for composition see chapter 9.2.4.2) or double-distilled water. If not mentioned otherwise, the dilution medium was transport buffer. The suspension was transferred to 3 mL acrylic cuvettes, mixed with a pipette and measured (3 x 10 runs). Particle size results are given as z-average and particle size distribution as PDI.

3.2.4 Physico-chemical drug characterisation

The physico-chemical characteristics of the drug are of major interest for the stability of the drug itself and the produced nanosuspension. For nanosuspensions, the solubility of the drug in the non-solvent is influencing particle growth while the solid state of the drug could also lead to stability issues. The surface area of the coarse drug suspension was of interest with regard to stabiliser-drug interactions and drug quantification was, amongst other things, necessary for dissolution and permeation studies.

3.2.4.1 Drug quantification

Drug quantification for solubility, transport and dissolution studies was performed by reversed phase high performance liquid chromatography (RP-HPLC). High performance liquid chromatography is a type of liquid chromatography where the solubilised drug sample (mobile phase) is directed over a stationary phase with pressure. The drug molecules are interacting with this highly porous solid phase, packed inside a cylindrical column. Depending on the distribution coefficient of the drug between mobile and stationary phase, the drug is leaving the column at a certain time point. With this technique, various chemical compounds can be separated and quantified in a mixture. Due to different hydrophobic and lipophilic characteristics of drugs, the separation is accomplished. The eluted drug can be detected with various detectors of which the most common one is an ultraviolet (UV) detector.

In this work a Waters HPLC system (Waters Materials and Methods Corporation, USA) was utilised, together with a LiChroCart® 125-4, LiChrospher® 100 RP18-5 column (Merck KGaA, Germany). For more information, details can be found in the appendix (chapter 9.3.1).

Content stability was analysed with UV spectroscopy. In this widely applied method, a light is shown on the solubilised probe, which is situated in a cuvette of a defined width. The light interacts with the sample, which absorbs light, so that the transmitted light has different energies compared to the incoming light.

In this thesis, the UV spectrophotometer Thermo Scientific™ Evolution 201 (Thermo Scientific Inc., USA) was utilised with a quartz cuvette (SUPRASIL®, Hellma GmbH & Co. KG, Germany) that had a light pass way of 10 mm. The solvent for both drugs was ethanol and the detection wavelength for CUR was set to 420 nm and 300 nm for GLI. A calibration was done in ethanol and the correlation coefficient had to be above 0.99.

3.2.4.2 Saturation solubility

The saturation solubility in different media was measured by production of a 1 millimole (mM) suspension of drug and dispersion media in centrifugation tubes out of poly propylene. The tubes were shaken over 24 hours on a laboratory shaker (Model SM from Edmund Bühler GmbH, Germany, shaking speed of 5), centrifuged at 7,197 relative centrifugal force (rcf) for 5 min (Centrifuge 5430 R, Eppendorf AG, Germany), filtered with an Omnifix® 5 mL syringe (B. Braun Melsungen AG, Germany) through a disposable polyethylene terephthalate filter with a pore size of 0.20 µm (CHROMAFIL® Xtra PET-20/25, Macherey-Nagel GmbH & Co. KG, Germany) and analysed with HPLC (see chapter 3.2.4.1). The saturation solubility was determined for the coarse drugs as well as selected nanosuspensions in dissolution buffers (see chapter 4.5.1 and appendix chapter 9.2.3).

3.2.4.3 Solid state characterisation

Two methods for solid state characterisation were utilised in this thesis: differential scanning calorimetry (DSC) and X-ray powder diffraction (XRPD).

Differential scanning calorimetry

In DSC, the difference in the heat flow between a sample and a reference cell is precisely controlled by a temperature program. The energy changes in the sample can

be endothermic or exothermic, depending on the sample absorbing (endothermic) or releasing (exothermic) energy during the thermal treatment. DSC can be used for qualitative and quantitative measurements but in the pharmaceutical science it is usually applied to characterise polymorphism, hydrates and amorphous systems.

DSC analysis was performed using Pyris™ Diamond DSC (PerkinElmer Inc., USA) with 1 mg to 3 mg sample amount. Samples were heated in sealed aluminium pans with a pinhole at a rate of 10 K/min from 20 °C to 250 °C under nitrogen flow of 20 mL/min using an empty sealed pan (with a pinhole) as a reference. Data evaluation was accomplished with Pyris™ Software Version 9.0.2.0193 (PerkinElmer Inc, USA).

X-ray powder diffraction

Every crystalline substance has its unique X-ray diffraction pattern. Therefore, qualitative analyses can be done with XRPD. In this thesis, XRPD was utilised to detect the solid state of the sample. When a sample is in a crystalline state, the X-ray beam, that is shown on the probe, gets diffracted in a, for the crystal typical, way. This diffraction angle is dependent on the distance between certain crystal levels, while the diffraction intensity is related to the number and nature of atomic reflection centres [Skoog et al., 2013]. An amorphous sample gives a low frequent halo which displays as a diffuse, wide background.

The solid state of coarse GLI powder was determined with the Stadi P X-ray diffractometer of Stoe & Cie GmbH, Germany) in transmission mode using Cu-K α 1-radiation (40 kV, 30 mA). The samples were measured in the range of 2°- 35° at a step rate of 2Theta = 0.05° with 2 seconds measuring time per step. Due to technical issues, all other XRPD measurements were accomplished with the Stoe Stadi-Ps diffractometer (Stoe & Cie GmbH, Germany), together with the MYTHEN 1K-detector (Dectris AG, Switzerland) with Cu-K α 1-radiation (40 kV, 30 mA) in transmission geometry. The measurement range was set to 2° - 80° 2Theta at a step rate of 2Theta = 2° with 60 seconds measuring time per step.

For both methods, a solid sample is needed for measurements. Hence, the nanosuspensions had to be dried. Freeze drying was the method of choice. In freeze drying, a liquid sample is frozen and afterwards the water is sublimated under vacuum. Freeze drying was accomplished with the ALPHA 1-4 with the system control LDC1M (Martin Christ Gefriertrocknungsanlagen GmbH, Germany). The samples were frozen

with a thickness of approximately 0.5 cm at -25 °C for 2 hours. Afterwards the primary drying was activated with a shelf temperature of -10 °C and a negative atmosphere pressure of 2 mbar over 24 hours. A secondary drying was appendant with a shelf temperature of 10 °C and vacuum conditions over another 24 hours.

3.2.4.4 Surface area

Surface area measurements were done via BET gas adsorption as described in the European pharmacopoeia (Ph. Eur. 8, 2.9.26). By measuring the adsorption of a gas, usually nitrogen, on the surface of the sample compared to a reference, the monomolecular layer formation of the gas can be calculated. In this work, this was done by the volumetric method combined with a multiple point method. Sample and reference were cooled, so that the nitrogen is forced to adsorb on the surface of the sample. Different increasing relative pressures ($\frac{\text{partial vapour pressure of adsorbed gas } (P)}{\text{saturated pressure of adsorbed gas } (P_0)}$) were applied to the system and each time the adsorbed volume of nitrogen was automatically measured with a manometer. The volume of the monomolecular layer (V_m) of the gas can be calculated via the BET-equation that is given in Equation 4.

$$\frac{1}{[V_{a(\frac{P_0}{P}-1)}]} = \frac{C-1}{V_m C} * \frac{P}{P_0} + \frac{1}{V_m C}$$

Equation 4: BET-equation. Variables are defined as: P = partial vapour pressure of adsorbate gas in equilibrium with the surface, in pascals; P₀ = saturated pressure of adsorbate gas, in pascals; V_a = volume of gas adsorbed at standard temperature and pressure (STP) [273.15 K and atmospheric pressure (1.013 × 10⁵ Pa)], in millilitres; V_m = volume of gas adsorbed at STP to produce an apparent monolayer on the sample surface, in millilitres; C = dimensionless constant that is related to the enthalpy of adsorption of the adsorbate gas on the powder sample.

The calculation of the specific surfaces (S) from adsorption data was done by multiplying V_m with the area which is occupied by one adsorbate molecule (A_m) and the Avogadro's number (Equation 5).

$$S = V_M * A_m * N$$

Equation 5: Calculation of the specific surface (S) out of V_m (volume of a gas monolayer), A_m (area of one adsorbated molecule) and N (Avogadro's number).

In this thesis, samples were kept under vacuum for above 12 hours as a conditioning step (VacPrep 61, Micromeritics Instrument Corporation, USA), to remove adsorbed molecules and to avoid unspecific binding of gas molecules on the surface. The surface area was measured with a Gemini 2360 System (Micromeritics Instrument Corporation, USA). The samples were compared to a reference sample vessel, filled

with the amount of glass beads, which corresponded to the dead space volume of the sample as measured with a helium pycnometer (Pycnomatic ATC, Porotec GmbH, Germany). Both tubes were cooled to 77 K during analysis. The dead space of the sample tube was measured with Helium prior to each measurement. Nitrogen was used as test gas. Information regarding the quality of the utilised gases can be found in the appendix (chapter 9.2.2). The specific surface area was calculated based on a multipoint correlation with eleven different relative pressures between 0.05 p/p₀ and 0.3 p/p₀. Measurements were done in triplicate for each drug.

3.2.5 Determination of drug-stabiliser interaction

3.2.5.1 Isothermal titration calorimetry

Calorimetric techniques are powerful tools for studying interactions at molecular levels. Isothermal titration calorimetry (ITC) is one of many techniques that measures calorimetric changes. It can detect small changes of heat during reactions for the determination of the thermodynamic parameters such as entropy (ΔS), enthalpy (ΔH), Gibbs free energy (ΔG), heat capacity, binding constants and effective number of binding sites in biological reactions [Rowe et al., 1998; Ladbury, 2001]. That is why ITC is used to investigate biomolecular interactions with the advantage of a label-free application. The enthalpy is an indication of changes in hydrogen interaction and van-der-Waals bonding while the entropy is indicating changes in conformational changes of molecules [Dutta et al., 2015].

Figure 18 shows the principle of an ITC experiment. The instrument has two cells, one holding the reference cell and one holding the sample cell. The sample cell is loaded with one component of the investigational interaction reactants while the reference cell is filled with water. Usually, a solution (or suspension) of the component in an organic or inorganic medium is suitable. The other part of the instrument is a syringe. It holds the other reaction partner at the experiment which is injected through a hole in the paddle into the sample cell while the paddle stirs.

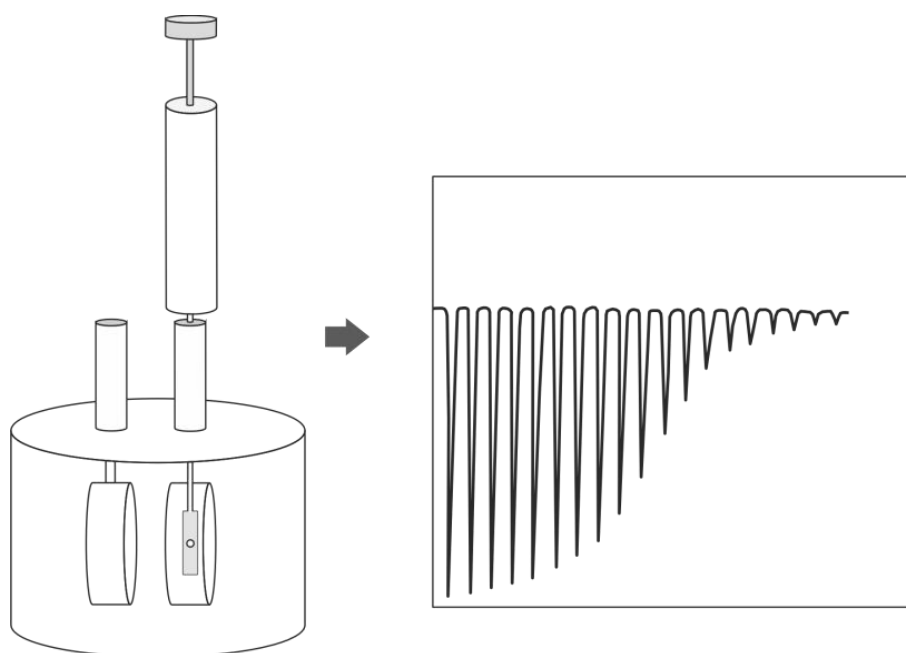


Figure 18: Left: sketch of the used ITC setup with sample cell and syringe next to the reference cell. Right: titration pattern displaying heat amplitude for each titration step.

A constant power is supplied to the reference cell heater. The sample cell has a feedback mechanism between power and temperature which means that if there is a loss/gain in heat in the sample cell, there is more/less power applied to the cell, so that the temperatures between reference cell and sample cell remain constant.

The diagram in Figure 18 displays also the raw data of an ITC experiment. The change in heat is calculated by integrating the heater power over the time required for the control heater power to return to a baseline value. For each injection from the syringe in the sample cell, a power difference to the reference cell is measured. The created peaks hold, as their area/length, the information about the heat absorption or heat creation of one injection. Over time, multiple injections into the sample cell enable the detection of a heat interaction pattern. If the heat interaction stays the same across the time period of administered injections, there is no change in thermal interaction between the reactant in the cell and in the syringe.

Adsorption of stabilisers on drugs can be characterised with ITC. The physico-chemical explanation of this interaction is, that prior to adsorption, the number of degrees of freedom is higher than for the adsorbed species. Adsorption is therefore spontaneously happening when the change in enthalpy (ΔH) has a sufficiently large negative value as the entropy change (ΔS) of the process should be negative, due to greater entropy of the adsorbent in liquid state than in adsorbed state. A spontaneous process is

happening when the Gibbs free energy (ΔG) is negative. The relationship between ΔG , ΔH and ΔS is displayed in Equation 6.

$$\Delta G = \Delta H - T\Delta S$$

Equation 6: Gibbs free energy (ΔG) calculation from enthalpy (ΔH), entropy (ΔS) and temperature (T).

As the adsorption process of polymers on particles is in general entropically unfavourable, due to less variability in conformation change of the polymer, the hydrophobic interactions have to be high enough to destroy the organised water structures near the particle surface and therefore increase entropy of the system [Vaynberg et al., 1998].

The general setup and concentrations of the tested solutions/suspensions as well as appropriate control experiments are of major importance, as are settings such as injection volume, injection rate, spacing between injections, filter period, reference power, stirring speed and temperature. Standard adjustments for the later parameters are dependent on the type of experiment.

In this work, ITC was used to display the interaction of two stabilisers with two drugs to obtain a better understanding of how the stabilisers interact with drug surfaces. Isothermal titration calorimetry experiments were performed with the VP-ITC MicroCalorimeter (MicroCal, USA). A sample cell of 1.8 mL volume was filled with 1 mL coarse drug suspension (10 mg/mL), which was prepared in an Eppendorf tube by mixing the drug powder and Milli Q water (produced with Millipore Milli-Q Integral 15, Merck KGaA, Germany) with a Thermo Scientific™ Finn timer™ F1 pipette (Thermo Scientific Inc., USA). Titration was accomplished with stabiliser solution in a 300 μ L syringe with 10 μ L injection volumes per injection at a reference power of 20 μ Cal/sec, a temperature of 25 °C and a stirring speed of 1000 rpm. The concentration of the stabiliser suspension was calculated to simulate milling conditions, so that the relation of the amount of stabiliser and drug, for the minimal stabilising concentration that was found in media milling, was achieved in the experimental setup.

3.2.5.2 Contact angle measurements

The interaction potential of liquids with solid surfaces can be characterised with contact angle measurements. The Young equation (Equation 7) displays the correlation of

contact angle ($\cos\theta$), surface tension of the liquid (σ_{li}), interfacial tension between liquid and solid (σ_{sl}) and the surface free energy of the solid (σ_s).

$$\sigma_s = \sigma_{sl} + \sigma_{li} * \cos\theta$$

Equation 7: Young equation for the determination of surface free energy of solids (σ_s). $\cos\theta$ = contact angle; σ_{li} = surface tension of the liquid; σ_{sl} = interfacial tension between liquid and solid.

Contact angle measurements can display the interaction of the stabiliser in solution and the interplay of this solution with a drug surface. As stabilisers can interact with surfaces, they can decrease the interfacial tension between liquid and solid and/or the surface tension of the liquid so that the contact angle decreases. Bad/No wetting is seen when the contact angle is over or equally 90° , while good wetting leads to lower contact angles (Ph. Eur. 8, 2.9.45). The contact angle can be measured between a droplet and a solid surface (Figure 19).

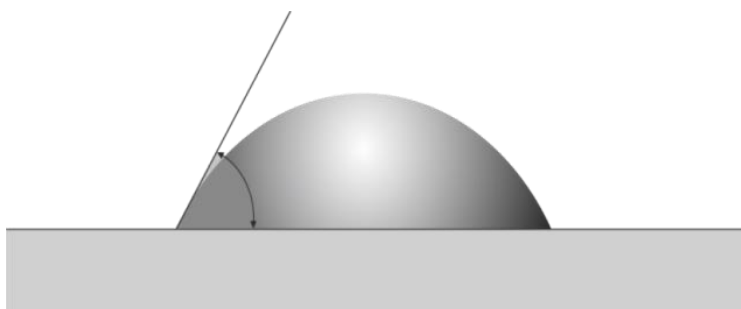


Figure 19: Solid surface with a liquid droplet and applied tangent with contact angle.

For contact angle measurements between drug and stabiliser solution, the drug is normally compressed to a compact so that the angle of one drop stabiliser solution on this compact can be measured.

Contact angles between drug and stabiliser solution were measured with a goniometer (Type G1 from Krüss GmbH, Germany). The drug was processed with a hydraulic press (PW 10 from Paul-Otto Weber GmbH, Germany) to achieve a compressed drug pellet. Diameter of the die (1.3 cm), compaction force (5 kN), holding time (1 min) and amount of drug (0.25 g) were fixed values. A glass syringe was used for the creation of one drop of stabiliser suspension, while simultaneously focusing the surface of the drug pellet. When the drop appeared in the field of view the contact angle was

measured immediately by laying a tangent on the edge of the droplet. The view through the ocular is schematically plotted in Figure 20.

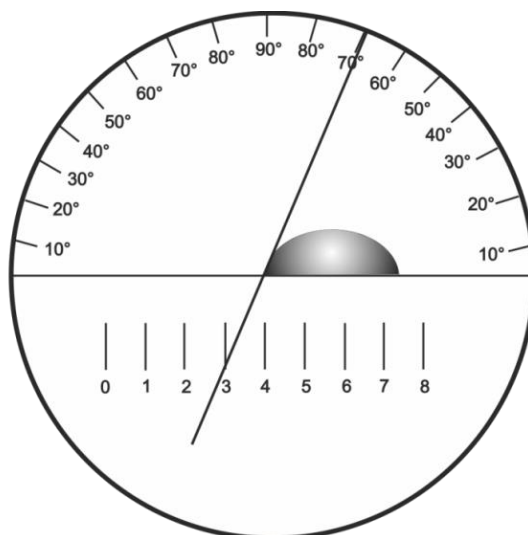


Figure 20: Sketch of the view through the ocular of a goniometer. Lower scale displaying length measurement of the droplet and upper scale for contact angle measurements.

Because of temperature differences between experiments, all values were related to double-distilled water contact angle that was measured at the experiment day in quadruplicate. Concentrations of stabiliser solutions were selected from milling data, to cover a concentration area around the minimal stabilisation concentration, which was found in milling experiments for each drug.

3.2.6 Dissolution

Dissolution is a standard method in pharmaceutical technology to compare different formulations. Dissolution can serve as a tool in drug development, in providing control of the manufacturing process and to assess the need for further bioequivalence studies. The standard method is to test solid dosage forms such as tablets and capsules but also transdermal therapeutic systems or nanosuspensions can be tested for molecular drug release from the dosage form.

For all dissolution studies a paddle apparatus, described as apparatus 2 in the European Pharmacopoeia 8, 2.9.3 (Erweka DT6, Erweka GmbH, Germany), was used with a stirring speed of 50 rpm at 37 °C. When taking the sample, approximately 2 mL sample were filtered through a polyethylene terephthalate filter with a pore size of 0.20 µm (CHROMAFIL® Xtra PET-20/25, Macherey-Nagel GmbH & Co. KG,

Germany), while the filter was attached to a cannula with a diameter of 0.9 mm and a length of 70 mm (Sterican[®], B. Braun Melsungen AG, Germany) which always remained at the same height. After taking the sample, 2 mL pre-warmed (37 °C) dissolution medium was filtered through the filter to push possible adsorbed drug back to the dissolution vessel. All used buffer compositions are described in detail in chapter 9.2.3.

3.2.6.1 Conditions for glibenclamide

Conditions used were inspired by FDA recommendations for glibenclamide (glyburide) tablet products [U.S. Food and Drug Administration. Drug Database] as well as pre-tests on solubilisation. 500 mL borate buffer pH 9.4 (USP 36 under Buffer Solutions) was used as the first dissolution medium. The content of GLI was determined with UV spectroscopy (for details see chapter 3.2.4.1).

The second dissolution medium was 900 mL phosphate buffer pH 8 (USP 36 under Buffer Solutions). Due to lower solubility of GLI in this medium, the concentrations measured were below the detection limit of UV measurements, so that the content was determined with HPLC and UV detection (method see chapter 9.3.1). Sampling time points were 1, 2, 3, 4, 5, 10, 15, 20, 25, 30, 40, 50, 60, 80, 100, 120, 180, 240, 1220 and 1440 minutes. Perfect sink conditions were used. Therefore, suspensions with an amount of drug, corresponding to approximately 10 % of the determined saturation concentrations were applied to the dissolution vessels, which were 26.5 - 27 mg for boric acid buffer and 5.8 - 6.7 mg for phosphate buffer.

3.2.6.2 Conditions for curcumin

Pre-tests indicated that the solubility in acetic acid buffer was the highest (data not shown). Thus, 900 mL of acetic acid pH 4 were taken as dissolution medium. Sampling time points for CUR needed to be decreased as CUR solutions were degrading over time, so that HPLC analysis had to be close to sampling time point. Therefore, sampling time points were reduced to 1, 5, 10, 15, 30, 45, 60, 80, 120, 180, 240, 1220 and 1440 minutes. Sink conditions could not be applied as CUR was not detectable at such low concentrations, so 5 times saturation concentration had to be used (1.3 - 1.7 mg).

3.2.7 General cell culture and toxicity testing

Caco-2 cells with a passage number of 62 - 69 were cultured in Duplecco's modified medium (DMEM) containing 50,000 U/566 mL penicillin and 50 mg/566 mL streptomycin as antibiotics, sodium pyruvate (60.5 g/566 mL), non-essential amino acids (4.9 mg/566 mL L-alanine, 8.25 mg/566 mL L-asparagine x H₂O, 7.3 mg/566 mL L-aspartic acid, 8.1 mg/566 mL L-glutamic acid, 4.1 mg/566 mL glycine, 6.3 mg/566 mL L-proline, 5.8 mg/566 mL L-serine) and 9 % fetal bovine serum (FBS). The culturing conditions were 5 % CO₂ and 37 °C, with feeding every 2 - 3 days. For passaging, which was done when the confluence reached 80 % - 90 %, the cells were rinsed with PBS buffer, incubated with trypsin/EDTA solution (0.25 %/0.02 %) for 6 - 7 minutes, counted, and approximate 1,000,000 cells were transferred to a new flask (75 cm² growth area) containing pre-warmed medium. The counting was done with a counting chamber under a light microscope with the cells being stained with trypan blue (0.5 % from Biochrom GmbH, Germany) (dark blue cells were not counted as they are dead). Storage of the cells was accomplished in 5 % dimethyl sulfoxide (DMSO) - medium solutions in liquid nitrogen until used, while the DMSO was disposed after centrifugation when the cells were cultured.

For toxicity tests 30,000 cells were seeded per well on a 96-well plate (TPP[®] Zellkulturplatten 96F, TPP Techno Plastic Products AG, Switzerland) three days prior experiment. Until experiment day, the cells were incubated at 5 % CO₂ and 37 °C. At the day of the experiment the medium was sucked off and was replaced by 200 µL sample volume. Incubation time of the sample was 4, 5, 6 or 24 hours, respectively. The sample volume was replaced by a 25 µL of a 5 mg/mL 3-(4,5-dimethylthiazol-2-yl)-2,5-diphenyltetrazolium bromide (MTT) reagent in HBSS solution and incubated over 2 hours. Afterwards 100 µL of a 5 % SDS in dimethyl formamide/double-distilled water (50:50, adjusted to pH 4.7) solution was added. Subsequently, the plate was placed on a shaker (IKA[®] Vortex 4 basic, IKA[®]-Werke GmbH & Co. KG, Germany) for 1 min at 400 rpm and measured afterwards, utilising a plate reader (TECAN SPECTRA, Tecan Trading AG, Switzerland) at 570 nm. Data processing software was easy WIN fitting (32 bit). Samples were determined in quadruplicate and for each plate a positive control (5 mM SDS solution in water) and a negative control (DMEM or transport buffer) were run. The achieved absorption values were related to both controls (positive = 0 % cells alive; negative = 100 % cells alive). Most cell culture

liquids were purchased from Biochrom AG (Germany). For further compositions please see chapter 9.2.4.

3.2.8 Determination of drug transport through cells

For the so called 'transwell model', Caco-2 cells are grown on a filter for approximately 21 days, to form a monolayer of tightly bound cells which serve as a barrier for transport of drugs. Figure 21 shows the transwell setup with the possibility of investigating the transport of substances from A (apical) to B (basolateral) or from B to A.

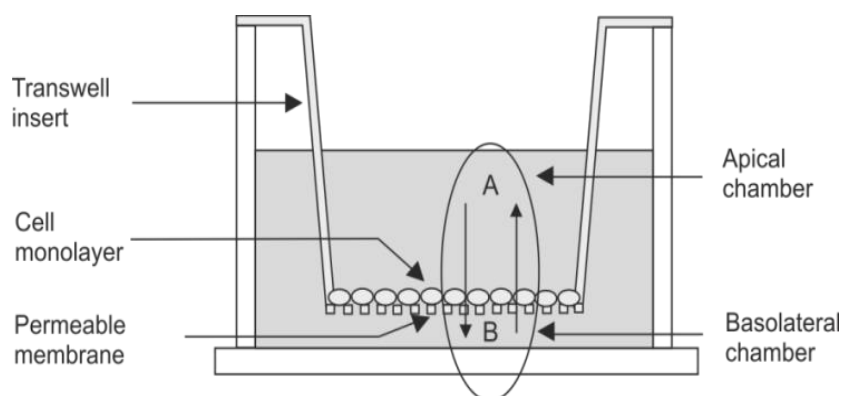


Figure 21: Transwell setup for transport studies with Caco-2 cells.

The apparent permeability coefficient (P_{app}) can be calculated from the initial concentration, the permeation time and the permeated concentration. With the P_{app} , estimations regarding bioavailability of the substance can be done (see Table 9):

Table 9: Relation of apparent permeability coefficient and bioavailability adapted from Zhen et al. (2017).

P_{app} (cm x sec ⁻¹)	Bioavailability (%)
$> 1 \times 10^{-6}$	100
$0.1 \times 10^{-6} - 1 \times 10^{-6}$	1 – 100
$< 1 \times 10^{-7}$	< 1

This general correlation is a simple model which does not reflect all drugs and formulations but gives a rough estimation for some drugs. Exceptions are, for example, drugs that permeate paracellular, as in this case, they show lower permeation in the Caco-2 cell model than in humans [Artursson et al. 2012].

The P_{app} for transport studies in this thesis was calculated as displayed in Equation 8.

$$P_{app} = \frac{dQ}{dt \times C_0 \times A}$$

Equation 8: Calculation of P_{app} with dQ/dt as the steady-state flux in $\mu\text{M}/\text{sec}$, A as the surface area of the filter (cm^2) and C_0 as the initial concentration in the donor chamber in μM .

The reduction in donor concentration was taken into account after every sampling so that the donor concentration was recalculated by subtracting the cumulative amount transported to the receiver chamber for each time interval.

3.2.8.1 Transport studies

Standardisation of cell culture is of major importance for the comparison of different data sets. For transport studies in transwells, the device itself and the cells should not vary too much from experiment to experiment. The transwell should be of the same material for all experiments. Pore size, pore density and growth area should be the same as well. As cells are not easy to standardise, a few parameters should be investigated and kept constant to achieve a tight monolayer with comparable characteristics each time, such as:

- Reproducible transepithelial electrical resistance (TEER) values and permeation of a marker substance through tight junctions
- Defined seeding density
- Characteristic morphology

A reproducible cell number per area in the stationary growth phase, which forms a connective monolayer, is the aim [Wunderli-Allenspach et al., 2000]. Similar seeding density and growing times with comparable feeding cycles should lead to a reproducible cell number in the stationary growth phase with characteristic morphology, while the connectivity of these cells should be controlled by TEER measurements and permeation studies with substances that only pass the cells via tight junctions [Braun et al., 2000]. The latter can be substances such as lucifer yellow or mannitol, while the former TEER values can be measured with voltohmmeters.

Transport studies were performed with the transwell system from Greiner Bio-One International GmbH (Germany). As inserts for 12 well plates, Thincerts[®] with an area of 1.131 cm^2 , pore sizes of $1 \mu\text{m}$ and $3 \mu\text{m}$ and pore densities of $2 \times 10^6 \text{ cm}^{-2}$ for the $1 \mu\text{m}$ pore size and $0.6 \times 10^6 \text{ cm}^{-2}$ for the $3 \mu\text{m}$ pore size transwells were used. Prior

to transport experiments the transwell system with the cell monolayer was validated. Caco-2 cells with passage numbers ranging from 65 to 70 were seeded with a density of 100,000 cells per cm² culture area 16 - 23 days before the transport experiment. The upper compartments and the lower compartments were filled with 0.7 mL and 1.5 mL of medium, respectively. At every feeding or rinsing, the upper compartment was sucked off last and fed first to avoid pressure under the cells which could lead to monolayer disruption. Every 2 - 3 days, the medium was replaced (the cells were fed) and kept in culture conditions of 37 °C and 5 % CO₂ with constant humidity.

As transport medium either the culture DMEM medium or transport buffer was used. One day before the experiment the cells were fed. At the day of the experiment the TEER was measured with the EVOM voltohmmeter connected to the STX2 electrode (World Precision Instruments, Inc., USA), directly after the cells were removed from the incubator, to ensure that the validation parameters were achieved. When buffer was used as transport medium, the cells were washed twice and incubated over 30 min with transport buffer. The pre-experiment TEER was afterwards compared to the post-experiment TEER, to prove monolayer integrity during the experiment. After determining the TEER values, the suspension, which permeation should be tested, was placed in the apical compartment (0.7 mL) while cell culture medium or transport buffer was put in the basolateral compartment (1.5 mL) for A-B studies and contrariwise for B-A studies. Sampling time points were 1 hour, 3 hours, 5 hours and 24 hours. At these time points 0.3 mL of sample for A-B studies and 0.1 mL for B-A studies were withdrawn from the basolateral or apical compartment, respectively and were replaced by fresh transport buffer or medium. In between, the cells were kept in the incubator at 37 °C and 5 % CO₂.

In addition to the suspensions, a marker substance was tested on each plate. The permeation rate of the suspension was always calculated in relation to atenolol to control for day to day cell variability. After the experiment, the cells were washed twice with buffer or medium and incubated for 30 minutes. Afterwards the post-experiment TEER value was measured and a second test for monolayer integrity was done. For this, a 0.1 µg/µL lucifer yellow solution in PBS buffer was applied. When the transport medium was cell culture medium, the cells were washed three times with PBS buffer. When the transport medium was buffer, the cells were washed once with PBS buffer. Then, 0.7 mL lucifer yellow solution was pipetted in the apical compartment and 1.5 mL

PBS buffer were applied to the basolateral compartment. The cells were incubated for 1 hour at 37 °C with 5 % CO₂. Finally, 0.5 mL of sample were withdrawn from the basolateral compartment and analysed for lucifer yellow content fluorometrically (LS 55 Fluorescence Spectrometer, PerkinElmer Inc., USA) (measurement details can be seen in the chapter 9.3.2). For measurements, the cuvette module was utilised together with a quartz cuvette (SUPRASIL[®], Hellma GmbH & Co. KG, Germany). Data processing was done with FL WinLab[™] software. Fluorescence spectrometric measurements are similar to UV spectrometry (see chapter 3.2.4.1) with some difference like that fluorescence is measured (more details are also find in chapter 3.2.9.3).

3.2.8.2 Dissolution rate with regard to permeation studies

The dissolution rate was tested to compare it to the permeation studies. To ensure this comparison, not a standard dissolution set-up was chosen but a setting that was similar to the environment in permeation studies. The aim was, to investigate how much of the amount of drug, that was situated in the apical compartment, did dissolve over time without changing concentration conditions in the actual permeation study, but still compare these two methods. In the permeation studies, three different kinds of dilution media (DMEM, transport buffer pH 7.4 and transport buffer pH 6.5) and four sampling time points (1 hour, 3 hours, 5 hours and 24 hours) were used. All suspensions used in the transport study were also tested for dissolution rate. For this, 10 mL of 1 mM drug suspensions were created in 15 mL centrifuge tubes. These tubes were stored in a heating oven (Heraeus[®] function line, Heraeus Holding GmbH, Germany) at a temperature of 37 °C. At sampling time points, the samples were centrifuged at 7,197 relative centrifugal force (rcf) for 5 min (Centrifuge 5430 R, Eppendorf AG, Germany), filtered with an Omnifix[®] 5 mL syringe (B. Braun Melsungen AG, Germany) through a disposable polyethylene terephthalate filter with a pore size of 0.20 µm (CHROMAFIL[®] Xtra PET-20/25, Macherey-Nagel GmbH & Co. KG, Germany) and analysed with HPLC (for details see chapter 9.3.1).

3.2.9 Visualisation of drug transport in cells

3.2.9.1 Cell culture and general preparation methods

CARS studies

Due to the use of a different cell laboratory, for CARS studies, the passaging method changed slightly from the description in chapter 3.2.7. The cells (Caco-2 or RAW 264.7) were washed with Hanks' Salt solution buffer, which included 0.5 mM EDTA and were incubated at room temperature for 3 min. Then, 1.5 mL of a 0.25 % (w/v) EDTA-trypsin solution was added and incubated for 5 min in the incubator (37 °C and 5 % CO₂). Around 10 mL of media was added to the flask. A cell counting was done while the cells were centrifuged at 1,500 rcf for 5 min. The supernatant was removed and the cells were dispersed in the needed amount of media.

Fluorescence microscopic studies

Caco-2 cells were cultured like described in chapter 3.2.7. RAW 264.7 cells for fluorescence microscopy studies had similar culturing conditions, with the difference being that the cells were passaged by cell scraping with a cell scraper (length 16 cm, blade length 1.35 cm, Sarstedt, Inc. USA). Therefore, the growth medium was replaced by fresh medium and a cell scraper was used to detach the cells from the bottom of the flask. The cells were dispersed and placed into a new flask. The passage numbers used for experiments ranged from 4 - 10.

3.2.9.2 Coherent anti-Stokes Raman microscopy

Raman based microscopy is a useful tool for the chemical characterisation of many applications. The Raman technique is a vibrational spectroscopy method that essentially detects molecular vibrations. In spontaneous Raman scattering the sample is illuminated with a laser and light is scattered. Laser with a single wavelengths of ,for example, 532 nm, 785 nm and 1064 nm can be used. Scattered light is collected with lenses and filtered by a filter, like a notch filter. Raman scattered light is then dispersed onto a detector in a spectrograph, using typically a diffraction grating or a prism. In general, the laser light that is scattered with the exact same energy as the laser, is called Rayleigh scattering. However, approximately one in a million times, the light will be scattered at a different wavelength to the incoming light because it interacts with the molecule and causes vibration. The wavelengths scattered at a different wavelength than the incoming light are characteristic for each molecule. This scattering can be measured at a shorter wavelength (Stokes) or at a longer wavelength (Anti-Stokes). Raman is a two photon scattering technique, where the first photon strikes the sample and a second photon is scattered. In Raman spectroscopy, the sample does not receive enough energy to transit the molecules into an excited electronic

state, but instead the molecule goes to a virtual energy state from where it quickly relaxes to an excited vibrational state. Raman detects change in polarisability in a molecule, which can be seen as the distortion of the electron cloud around the nuclei [Skoog et al. 2013].

Coherent anti-Stokes Raman scattering microscopy is a variation of Raman imaging. It is a four-wave mixing process, where three laser beams are coherently driven into the sample through high NA objective. The beams are spatially and temporally mixed in a small focus so that from the sample a fourth, anti-Stokes photon is created that is then detected [Camp et al., 2014]. The Jablonski diagram, provided below in Figure 22, shows the energetic steps of these three laser beams that work simultaneously to create the CARS signals.

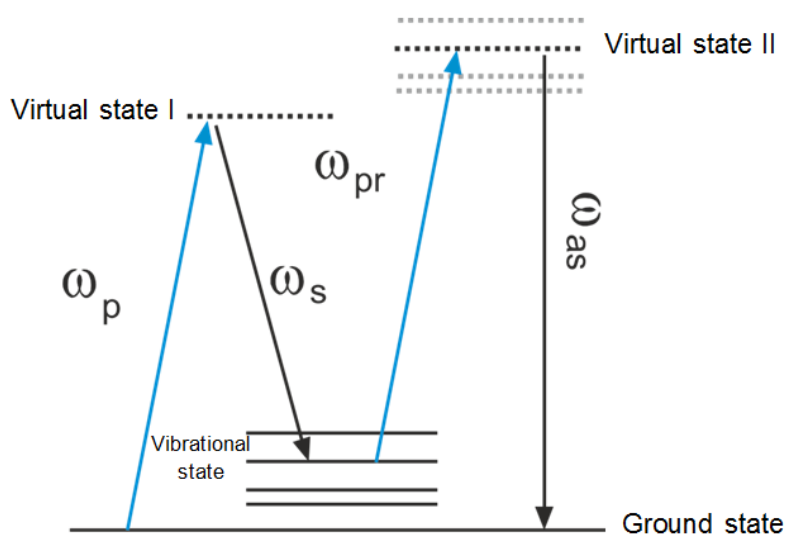


Figure 22: Jablonski diagram in CARS microscopy adapted from Strachan et al. (2011).

At the beginning, all molecules of the measured sample are in the ground state. When the pump beam is applied with the frequency ω_p , some molecules move to a virtual state and a simultaneous addition of the Stokes beam, with the same frequency as the Stokes shifted light (ω_s), puts the molecules into a vibrational state. At this point in time, the electron cloud surrounding the chemical bonds is vigorously oscillating with the frequency $\omega_p - \omega_s$. This indicates, that a certain structure in the molecule has to be addressed to achieve this vibrational state. By changing the wavenumbers of the laser, diverse differences of ω_p and ω_s can be produced until the desired vibration is achieved. Simultaneously, the probe beam with the frequency ω_{pr} is shone onto the

probe. The molecules transit from the vibrational state to another virtual state, from which they spontaneously emit the CARS signal with a frequency of ω_{CARS} . After interaction with a bond/a molecule, the incoming photon from the laser is emitted with a shift depending on the interplay. Consequently, a shift in wavenumber or nanometer of the applied laser light is used to describe CARS scattering [Krafft et al., 2009; Evans and Xie 2008].

The generated vibrational state described above is similar to that of Raman spectroscopy but the difference between CARS and Raman spectroscopy is important to understand. Raman scattering happens spontaneously when a laser beam of one wavelength is used. With CARS, the vibrational state can be tuned to, so that the signal is much faster and stronger than with Raman. The minimal sample volume that is measurable in confocal Raman microscopy is diffraction limited. The minimum sample spot diameter will change with varying illumination wavelength so that with higher wavenumbers the spot will decrease. In addition, the refractive index plays a role when looking at the depth of field. For coherent Raman mapping, no pinhole is required because it is inherently confocal. The spatial resolution is with 1 μm axially and 200 - 400 nm laterally, slightly higher than in conventional Raman microscopy and fluorescence interference is not that high [Müllertz et al., 2016]. One of the drawbacks of Raman spectroscopy is the low signal intensity so that, for example, fluorescent impurities can easily disturb and overlap the signal. To avoid this problem excitation lasers in the far UV or near infrared part of the spectrum are used. Also pulsed lasers with gated detections can be used to ensure that the fast, femtosecond Raman signal is filtered from the slower picosecond fluorescent emission. Raman scattering is linear to concentration while CARS signals are quadratically increasing with concentration. Both techniques can be used for quantitative analysis [Müllertz et al., 2016] but Raman is easier to apply for quantitative studies as CARS signals have resonant and non-resonant parts and therefore the extraction of quantitative data is challenging.

CARS is especially suitable for detecting lipid structures with their strong signal giving of C-H stretching, so that solid lipid extrudates, lipid based matrix tablets [Windbergs et al., 2009] and lipid droplets in cells [Jurna et al., 2009] were already investigated with CARS. Live cell and tissue imaging is another application field of CARS [Darville et al., 2015; Saarinen et al., 2017]. The first commercially available CARS microscope has been on the market since 2011 (Leica TCS SP8 CARS) and this was used in this

work. This CARS microscope can detect structures that have wavenumber shift from approximately $1,250\text{ cm}^{-1}$ - $3,400\text{ cm}^{-1}$ and has two other non-linear imaging methods included: second harmonic generation (SHG) and two-photon fluorescence excitation (TPFE). All three methods can be very useful in pharmaceutical applications [Fussel et al., 2013].

Visualisation of cell lines was performed with a TCS SP8 CARS microscope (Leica Microsystems, Germany). The system consists of an inverted microscope equipped with a laser-scanning confocal scan-head and photomultiplier tube (PMT) and GaAsP hybrid (HyD) photodetectors. The CARS signal was detected in forward direction using non-descanned PMT detectors. A water-immersion 25 x objective with an NA of 0.95 (Leica HCX IR APO L 25 x /0.95 W) was used in all experiments. The CARS excitation source was a Nd:YVO₄ solid-state-laser (APE GmbH, Germany) with an optical parametric oscillator (OPO). The Stokes beam (ω_s) had a fixed wavelength of 1064.5 nm and a pulse duration of 7 ps. The pump and probe beams (ω_p and ω_{pr}) at 781 – 827 nm were generated from the OPO with the pulse duration of 5 – 6 ps. 325,000 cells were seeded one day prior the day of experiment per well (growth area: 1.9 cm²) and covered with 1 mL of cell culture medium. At the day of experiment the cells were washed. The cells were incubated with a 250 µg/mL GLI nanosuspension in 10 mM HBSS+HEPES buffer. The cell membrane was stained with CellMask® Orange (Thermo Fisher Scientific Inc., USA) and cells were fixed with 1 mL of a 2.5 % glutaraldehyde solution on 24-well glass-bottom plates (MatTek Corporation, USA). Two-photon excited fluorescence (TPEF) was used to probe the cell membranes. Z-stacks covering the whole height of cells were recorded using a step size of 500 nm. Caco-2 cell had an incubation time of 2, 6 or 24 hours while RAW cells were incubated for 2 or 6 hours. GLI nanocrystals used had a particle size of $300\text{ nm} \pm 50\text{ nm}$ or $500\text{ nm} \pm 80\text{ nm}$. Quantitative analysis of the particle uptake in the cells was accomplished with Imaris 9.0 Demo that was kindly provided from Bitplane (Northern Ireland, UK). As no standard set-up was used, the analysis will be explained in the results part (chapter 4.7.1.3).

3.2.9.3 Fluorescence microscopy

Fluorescence happens when a molecule absorbs light at ultraviolet wavelengths and emits it after a time delay of 10^{-8} seconds or less. Depending on the number of energy levels for the electronic state and the energy sub-states, the absorption spectra vary

for different molecules. Fluorescent molecules are highly conjugated molecules, so that internal conversion of the absorbed light may carry the excited molecule only back to the lowest vibrational level of the excited state and not directly to the ground state by radiation-less electronic transition (Figure 23). The energy of the emitted photon is usually lower than the energy of the excited photon due to the mentioned internal conversion. This phenomenon is called the 'Stokes shift'. The shift allows the separation of exciting and emitting light with just leaving the fluorescent object of interest to detect [Swarbrick, 2007].

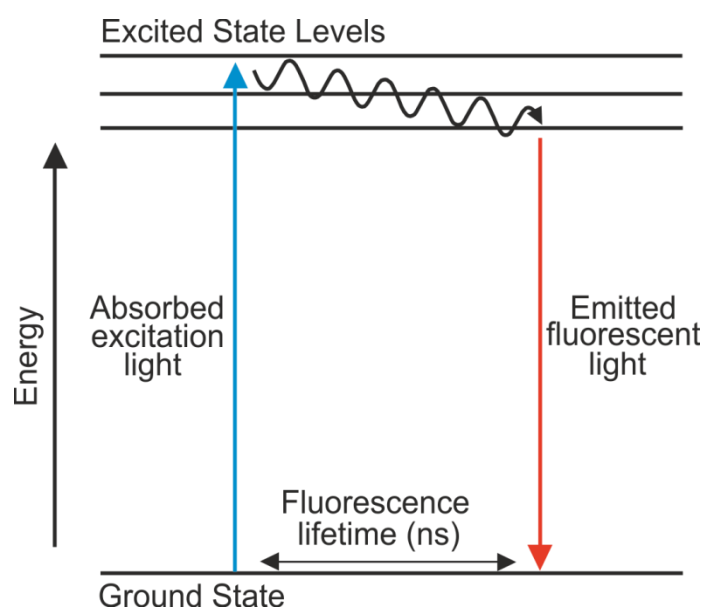


Figure 23: Jablonski diagram in fluorescence microscopy.

Just a few of the excited molecules in a probe will return to the ground state, emitting fluorescence. This fraction is called the quantum yield. Fluorescence emission spectra as well as the quantum yield can be dependent on many things, like type of dispersion medium, pH of dispersion medium, ion concentration and presence of other fluorophores. But under given conditions, the quantum yield is a physical constant [Wang and Taylor, 1990]. Fluorescence microscopy is a sensitive method because one fluorophore can emit many detectable photons so that often low laser powers lead to usable imaging while preserving the sample from degrading or biological tissue from being destroyed.

Dependent on this physical background, a fluorescence microscope in its basic form is composed of an excitation source, often a laser, with a subsequent excitation

monochromator, the sample holder, an emission monochromator and a detector. For confocal scanning, a resonant or slit scanner can be of good use. One way to improve transmission of emitted light is to use a beam splitter.

Many different kinds of special fluorescence microscopy imaging techniques have been developed over the years. Two-photon fluorescence excitation (TPFE) is one of them. It addresses the problem of spectral separation of background fluorescence and excitation light which is most prominent when the excitation and emission wavelength are near to each other. It separates the emitted fluorescence and the excitation light by a large energy gap by promoting simultaneous absorption of two photons into an excited state [Duveneck et al., 2003]. TPFE is a nonlinear, optical imaging method which has been used in many fields, like tracking the fate of drugs in cells [Mouras et al., 2010] or visualisation of lipids in transdermal transport [Yu et al., 2003]. It is a good method to use, when dealing with biological tissue. There are thousands of dyes on the market to label cell structures with fluorophores for discrimination and detection of cell targets. This has enabled progress over several decades in understanding the mechanistic of cell-cell and drug-cell interactions as well as internal cell metabolism. Particle tracking via fluorescent labeling has been done to a high extent but chemical change of surfaces can alter the behaviour of particles in biological environments dramatically [Gupta and Curtis, 2004].

In this project, a Leica TCS SP5 broadband confocal fluorescence microscope (Leica Microsystems, Germany) was used to image the particles and the cells. Z-stacks of the whole height of the cells were created with steps of 100 nm. The detection of the membrane stain was done with the 543 nm excitation helium-neon laser with emission collection at 550 - 600 nm. CUR visualisation, on the other side, was done by the cells excitation with a 488 nm argon laser and detection at 500 - 550 nm. A 96x immersion objective with immersion oil (Leica Microsystems™ Immersion Oil, Leica Microsystems, Germany) was utilised. 200,000 cells were seeded in one well of a 24-well glass f-bottom sensoplates (polystyrene) from Greiner Bio-One International GmbH (Germany) three days prior the day of experiment per well (growth area: 1.9 cm²) and covered with 1 mL of cell culture medium. At the day of experiment the cells were washed gently with PBS buffer. The cells were incubated with a 250 µg/mL CUR nanosuspension in PBS buffer for 2 or 6 hours. CUR nanocrystals used, had a particle size of 300 ± 50 nm or 500 ± 80 nm. Afterwards, the cells were washed with PBS

buffer. Then, the buffer was removed and replaced by the staining solution (5 µg/mL CellMask™ Orange, Thermo Fisher Scientific Inc., USA). The cells were incubated in the dark for 6 minutes. The staining was removed and 1 mL of fixation liquid (2.5 % glutaraldehyde in PBS buffer) was added. The cells were incubated over 10 minutes. After incubation the cells were washed with PBS buffer and 1 mL of PBS buffer was added for the transport to the microscope and imaging. Quantitative analysis of the particle uptake in the cells was accomplished with Imaris 9.0 Demo that was kindly provided from Bitplane (Northern Ireland, UK). As no standard set-up was used, the analysis will be explained in the results part (chapter 4.7.1.3).

3.2.9.4 Statistical evaluation

Statistical evaluation was accomplished with the SigmaPlot 11.0 software (Systat Software GmbH, Germany). The differences of the mean values of two groups were compared regarding significance with a t-test. Therefore, the software utilised a normality test (Shapiro-Wilk), which had to be passed, followed by an equal variance test. When this test was also passed, the t-test was applied with a 95 % confidence interval. For some comparisons, the normality or equal variance test failed. Here, the Mann-Whitney Rank Sum Test was applied. A difference was referred to significant when the p-value was between 0.01 and 0.05 while it was highly significant when the p-value dropped below 0.01.

4 Results and Discussion

As described in chapter 1.2, the aims of this thesis were the investigation of stabiliser drug interferences with regard to an improved milling parameter selection as well as the research of stabiliser-drug-cell interactions, to generate a better understanding of nanocrystal fate in biological tissues. Accordingly, the following chapter explains and discusses the findings in processing of drugs and stabilisers followed by application of the produced nanosuspensions in biological relevant setups.

4.1 Production of nanocrystals

For a successful milling process, various parameters must be considered. Initial screening experiments with several drugs included following factors for choosing the best candidates for the purpose of this thesis:

- i. Grindable
- ii. Low toxicity (non-carcinogen and non-mutagen substances)
- iii. Ease of detection (fluorescent and/or Raman active)
- iv. Cost effective (less than 250 Euro per 100 g)

Both, curcumin (CUR) and glibenclamide (GLI) did fulfil these criteria so that they were chosen as model drugs for this work.

The choice of stabilisers was based on their physico-chemical variation. Therefore, two charged stabilisers (tetra decyl trimethyl ammonium bromide (TTAB) and sodium dodecyl sulfate (SDS)), a neutral surfactant (polysorbate 80 (PS80)) and three polymers (hydroxypropyl methylcellulose (HPMC), poloxamer 124 (Pol124) and poloxamer 407 (Pol407)) were selected.

As the influence of the size of the nanocrystals on uptake and transport in and through different kind of cells was of interest, milling parameters had to be found for the production of different nanocrystal sizes. Like described in the introduction, various parameters have an influence on the outcome of the nanocrystal production. For the mill used in this work, Scherließ already investigated optimal parameter setups for cholesterol as a model drug [Scherließ, 2008]. It was concluded, that a rotor speed of 4,000 rpm and a drug content of 10 % were most suitable. These parameters were also used in this thesis. As every drug needs different stabilisation concentrations,

Scherließ's results regarding stabiliser concentration could not be directly transferred to this work. Accordingly, various experiments had to be performed with CUR and GLI. Scherließ also found, that the longer the milling time and the smaller the milling beads, the smaller the nanocrystals, which is consistent with the common knowledge about milling processes. This tendency could also be seen for CUR and GLI. Rotor speed, drug content, milling time and size of milling beads seem to be transferable in a certain frame from one drug to another, while stabilising concentration needs to be tested for each drug individually. Hence, some milling parameters are more robust when changing type of drug than others. In this work, the influence of the bead size and type of stabiliser on the milling outcome was investigated in more detail.

Concentrations of stabilisers are calculated as percentage of the used amount of drug for all following experiments.

4.1.1 Influence of stabiliser

The effect of different types of stabilisers on the grindability of CUR and GLI was studied. With all used stabilisers (PS80, HPMC, Pol407 and Pol124, SDS and TTAB) nanosuspensions with both drugs could be created. By changing the stabiliser concentrations stepwise, the following concentrations of stabilisers, as detailed in Table 10, were tested.

Table 10: Tested stabiliser concentrations for CUR and GLI. Underlined values are the concentrations that were plotted in Figure 24.

Stabiliser	Concentration in % for CUR	Concentration in % for GLI
HPMC	12.5	10
	20	<u>5</u>
	<u>25</u>	2.5
Pol407	<u>100</u>	70
	50	50
	20	<u>20</u>
	10	10
		5
	2.5	
Pol124	<u>200</u>	<u>100</u>
	180	70
	60	50
		25
PS80	150	
	50	20
	<u>25</u>	<u>7.5</u>
	20	5
	10	
SDS	<u>5</u>	<u>3</u>
	3	1
	1	
TTAB	5	
	3	<u>6</u>
	<u>1</u>	3
	0.5	1

For the following Figure 24, the values of the lowest particle size of each tested stabiliser were chosen.

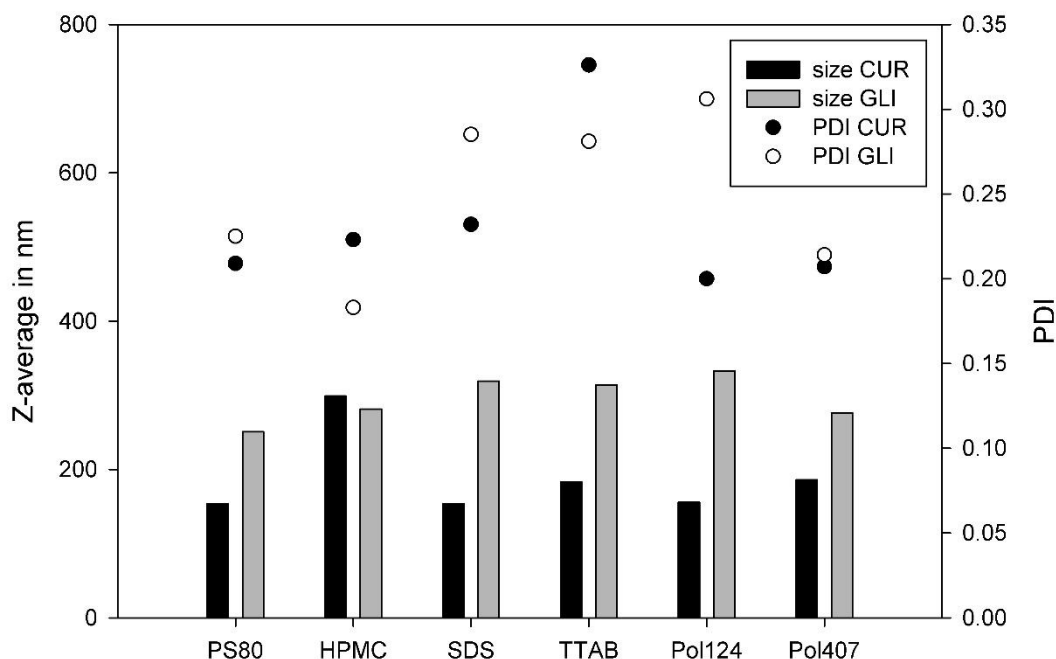


Figure 24: Particle size (bars) and particle size distribution (PDI; dots) of GLI and CUR nanocrystals. Production parameters: rotor speed = 4,000 rpm; drug content = 10 g; pump speed = 69 mL/min; milling time = 240 min. Stabiliser concentration with lowest achieved particle size was selected. Milling bead sizes were 1 - 1.2 mm for GLI and 0.66 - 0.91 mm for CUR. n = 1. Particle size measured in double-distilled water.

With SDS, the smallest particle size, with 154 nm for CUR, could be produced. Lowest particle size for GLI (251 nm) was manufactured with PS80. Particle size distributions were similar for CUR, with the exception of TTAB stabilised nanocrystals, where an increase to 0.33 in PDI could be seen. The PDI values of GLI did vary between 0.18 and 0.31 with Pol124 stabilised nanosuspensions having the highest PDI. GLI nanocrystals were, in average, larger than CUR nanocrystals after 240 minutes of milling which could be due to larger milling bead size. Interestingly, HPMC stabilised nanosuspensions did not show this particle size gap between CUR (299 nm) and GLI (281 nm). Therefore, the smallest achieved size for HPMC stabilised nanosuspensions for both drugs was around 300 nm with the selected conditions.

4.1.2 Influence of bead size

For the production of different nanocrystal sizes, diverse sizes of milling beads, varying milling time or rotor speed can be selected. In this thesis, the variation of milling bead sizes was the method of choice to produce different nanocrystal sizes.

It was described earlier that with all stabilisers, nanosuspensions could be produced. The particle size development of the first millings was monitored every hour until maximum milling time of 4 hours. Longer millings times did just lead to very small changes in particle sizes so that the maximum milling time was set to 4 hours. For the detection of the influence of varying bead sizes, one stabiliser/stabiliser combination was picked for each drug, of which milling result from preliminary test already existed. Therefore, also the milling time was different for CUR and GLI. Data in Figure 25 and Figure 26 show, that larger milling beads lead to a decrease in particle size and PDI reduction.

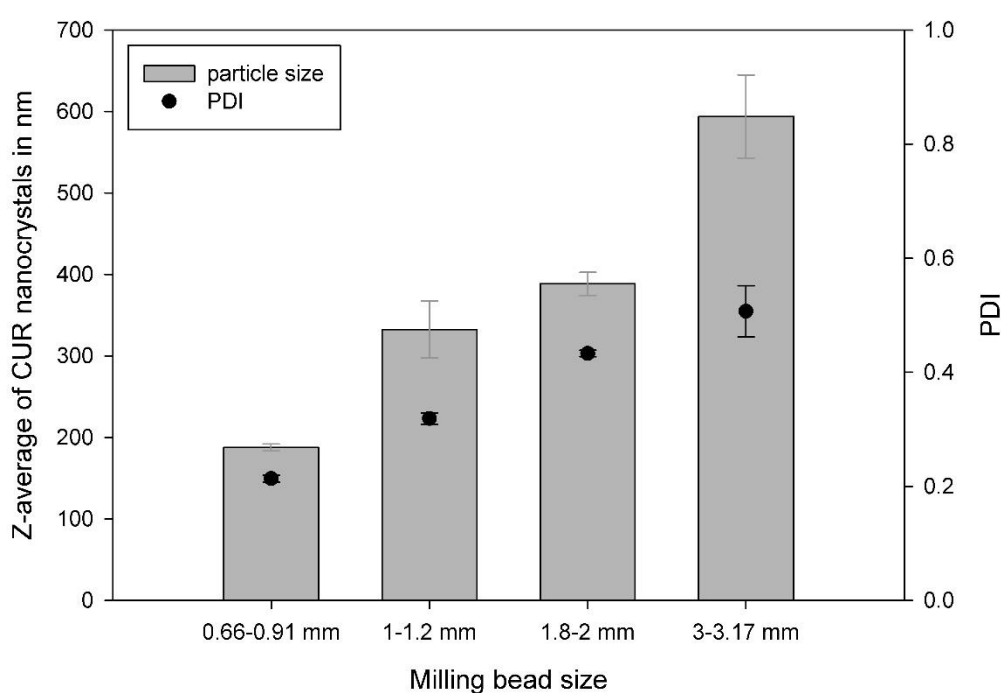


Figure 25: Particle sizes (bars) and particle size distributions (PDI; dots) of CUR nanocrystals stabilised with 25 % PS80. Production parameters: rotor speed = 4,000 rpm; drug content = 10 g; pump speed = 69 mL/min; milling time = 120 min. n = 2. error bars = min/max.

Particle sizes between $188 \text{ nm} \pm 4.3 \text{ nm}$ and $594 \text{ nm} \pm 50.9 \text{ nm}$ could be produced for CUR by varying the milling bead size. A further decrease in particle size would be possible with longer milling times. One experiment with smaller bead sizes (0.4 - 0.6 mm) (data not shown) did not lead to a further decrease in particle size compared to the 0.66 - 0.91 mm sized beads.

For GLI, particle sizes between $231 \text{ nm} \pm 39 \text{ nm}$ and $511 \pm 42.7 \text{ nm}$ could be generated.

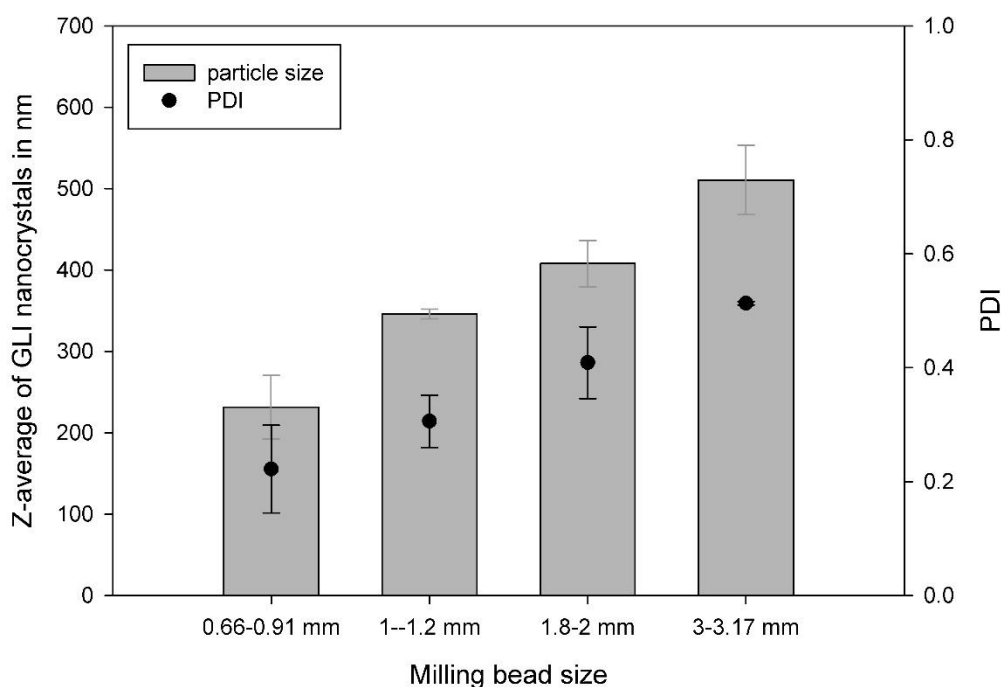


Figure 26: Particle sizes (bars) and particle size distributions (PDI; dots) of GLI nanocrystals stabilised with 2.5 % HPMC + 2.5 % PS80. Production parameters: rotor speed = 4,000 rpm; drug content = 10 g; pump speed = 69 mL/min; milling time = 240 min. n = 2. error bars = min/max.

For CUR, the size of the nanocrystals decreased by a factor of three comparing the smallest and the largest beads used. GLI nanocrystals just had a 2.2 times decrease in size. Hence, a 3.9 times increase in milling bead size at the same milling time (120 min for CUR and 240 min for GLI) lead to 330 % less particle size reduction for CUR and 220 % for GLI nanocrystals.

Some conditions have to be considered when working with large bead sizes. With large beads, the filling volume had to be decreased (from 80 % to 60 %) while otherwise beads were destroyed by high forces in the milling chamber. Possibly, the beads could not roll off in cavities and therefore got crushed between the milling chamber wall and other beads. Due to this phenomenon, which was observed in this thesis, the filling volume had to be decreased when using bead sizes of 2 mm or 3 mm. Furthermore, it was noticed that with large milling beads and long milling times (4 hours) a degradation of GLI took place, which resulted in a smell of sulfonate. In the case of GLI, the stress produced by large milling beads is higher compared to small milling beads which could be due to higher weight forces of the beads. This is in agreement with the modelling of Beinert et al. as they found that with increasing grinding media size, the stress energy increased [Beinert et al., 2015].

Summarised, the common knowledge about influence of milling time and bead size could be confirmed. In this work, nanocrystals of different average particle size and type of stabiliser could be produced. Still, the type of stabiliser and stabiliser concentration is one part of the milling that is not totally understood until today, so that the next chapter will focus on this stabiliser influence.

4.2 Stabiliser influences on nanosuspension properties

Five different stabilisers were used in this thesis. They were chosen due to their different properties as explained in chapter 3.1.2. The final selection of stabilisers for cell studies was done by assessment of minimal stabilisation concentration and cell toxicity.

4.2.1 Minimal stabilisation concentration

Important for a stable nanosuspension is the concentration of the stabilising agents. Too low stabilisation can lead to agglomeration or aggregation of particles while too much stabiliser may cause Ostwald ripening and therefore particle growth as well. For each stabiliser a concentration that just allowed the production of a stable nanosuspension as well as a concentration that led to unstable suspensions were found and are displayed in Table 11 and Table 12.

Table 11: Minimal stabilisation concentrations for GLI to form nanocrystals.

Stabiliser	Concentration that led to a unstable suspension	Concentration that led to a stable nanosuspension
Pol124	$\leq 25 \%$	50 %
Pol407	$\leq 1.25 \%$	2.5 %
HPMC	$\leq 5 \%$	10 %
PS80	$\leq 2.5 \%$	5 %
SDS	$\leq 1 \%$	3 %
TTAB	$\leq 3 \%$	6 %
HPMC+PS80	$\leq 2.5 \% + 1.25 \%$	2.5 % + 2.5 %

Table 12: Minimal stabilisation concentrations for CUR to form nanocrystals.

Stabiliser	Concentration that lead to unstable suspensions	Concentration that led to a stable nanosuspension
Pol124	≤ 180 %	200 %
Pol407	≤ 5 %	10 %
HPMC	≤ 20 %	25 %
PS80	≤ 10 %	20 %
SDS	≤ 1 %	3 %
TTAB	≤ 0.5 %	1 %
HPMC+PS80	≤ 5 % + 5 %	12.5 % + 12.5 %

The order of efficacy in stabilisation could be ranked as Pol124 < HPMC = HPMC + PS80 < PS80 < Pol407 < SDS < TTAB for CUR and Pol124 < HPMC < TTAB < PS80 = HPMC + PS80 < SDS < Pol407 for GLI. Similarities were seen for Pol124 and HPMC as the most ineffective stabilisers and Pol407 as well as SDS as most effective stabilisers for both drugs. The most prominent difference in stabilisation efficacy could be seen for TTAB, having the most effective stabilisation concentration for CUR but just medium efficacy for GLI.

The difference between the two poloxamers can be explained by their structure. It seems that a higher ratio of polyethylene oxide groups and a higher molecular weight leads to a lower minimal stabilisation concentration, which was drug independent in the current study. Liu, P. et al. found that the driving force for adsorption originates from the hydrophobic nature of the polypropylene oxide segment, while the polyethylene oxide segments offer the steric hindrance that is necessary to achieve stable nanosuspensions. Thus, short polyethylene oxide chain length caused a poor physical stability of the nanosuspensions [Liu et al., 2014]. This was also the trend found in this work.

The shift in efficacy for TTAB, comparing CUR und GLI, can be explained by zeta potential measurements. As TTAB is an ionic stabiliser, zeta potential measurements can give a statement about the attachment and localisation of TTAB molecules on the surface of the drugs. Therefore, TTAB and SDS stabilised nanosuspensions were investigated as well as suspensions stabilised with the non-ionic surfactant PS80. The results are plotted in Figure 27 and Figure 28.

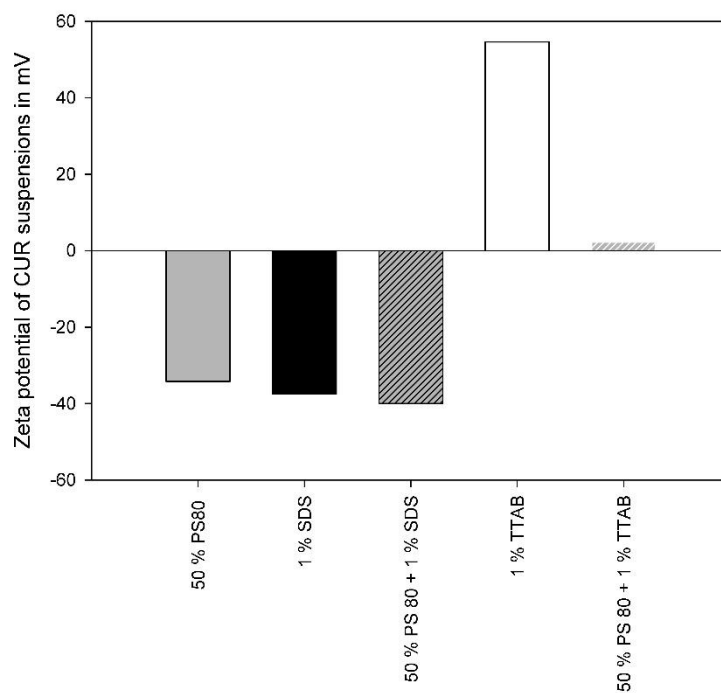


Figure 27: Zeta potential of CUR suspensions (after 240 min of milling). Measured in double-distilled water. Corresponding particle sizes and conductivity can be found in the appendix (chapter 9.4.1). n = 1.

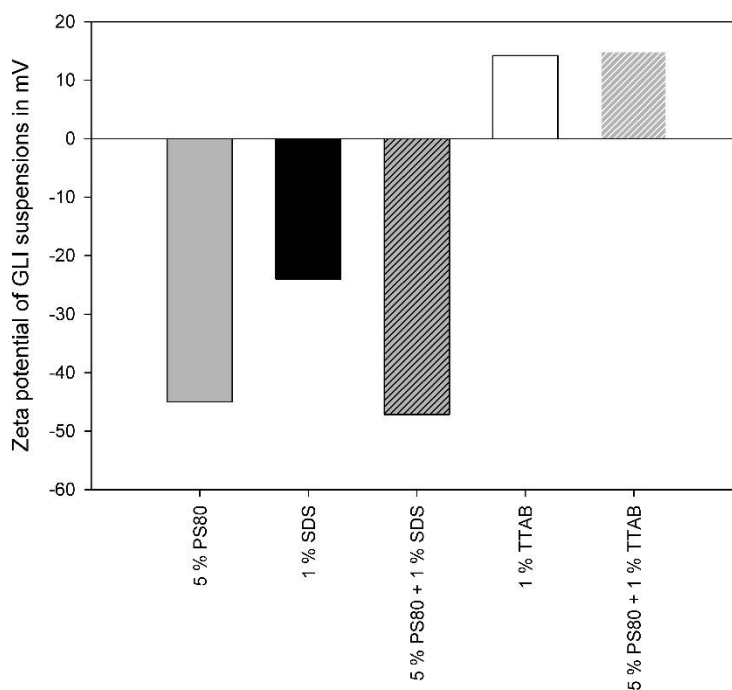


Figure 28: Zeta potential of GLI suspensions (after milling of 240 min). Measured in double-distilled water. Corresponding particle sizes and conductivity can be found in the appendix (chapter 9.4.1). n = 1.

A combination of SDS and PS80 resulted in a slight increase of zeta potential to -40.0 mV, in relation to the two stabilised CUR suspensions (-35.6 mV for PS80 stabilised nanosuspension and -37.5 mV for SDS stabilised nanosuspension). Also for GLI suspensions, the zeta potential increased slightly above the highest PS80 value from -45 mV to -47.2 mV). The combination of TTAB and PS80 led to a similar zeta potential as TTAB alone for GLI suspensions but for CUR suspensions just 4 % of the initial TTAB value were reached with the combination. This indicated that a combination of stabilisers adsorbed to the surface of different drugs individually. As the zeta potential represents charge at the hydrodynamic shear plane, imaginably PS80 could adsorb on GLI first and tightly, followed by TTAB so that only this component is crucial for the resulting zeta potential, while for CUR, TTAB could be equally bound together with PS80 on the surface. For SDS-PS80 combinations a different adsorption pattern can be interpreted. For GLI, PS80 could be more prominent in the outer layer while for CUR it seemed to be a mixture comparably to SDS-PS80 combinations. Possibly, GLI has more positive charges on the surface than CUR, so that the negative charged SDS could bind tightly and the positive charged TTAB was to be found in the shear plane. More detailed interaction measurements of stabilisers and drugs can be found in chapter 4.4.

4.2.2 Stability of nanosuspensions with various stabilisers

Suspensions are metastable systems. Instability can be caused by flocculation or sedimentation as well as agglomeration or even aggregation of particles. Especially in biological environments, stabilisation efficacy can change, as the proteins and ions present can lead to different stabiliser-particle or particle-particle interactions. Therefore, the particle size was also measured in buffer, which mimics biological environments. Pol124, SDS and TTAB stabilised nanosuspensions agglomerated in buffer, so that the particle size exceeded 1000 nm. For the other stabilisers, examples from the suspensions were picked randomly and stored for 6 months at 25 °C in closed screw cap vessels. Corresponding particle sizes can be found in Table 13 and Table 14. Before measurement, the samples were shaken until no deposit on the bottom of the vessel could be seen. All nanosuspensions remained stable (did not exceed more than 1,000 nm).

Table 13: Particle sizes of CUR nanosuspensions.

Type and concentration of stabilisers	Starting particle size in nm	Particle size after 6 months in nm
50 % PS80	172	187
80 % Pol407	277	191
25 % HPMC	449	380

Table 14: Particle sizes of GLI nanosuspensions.

Type and concentration of stabilisers	Starting particle size in nm	Particle size after 6 months in nm
20 % PS80	312	327
50 % Pol407	313	328
10 % HPMC	347	363

4.2.3 Cell toxicity of stabilisers in Caco-2 cells

The measurement of cell toxicity is crucial for the cell culture studies in chapter 4.6 and chapter 4.7, as toxic substances lead to biases in results and misinterpretation can occur. Therefore, the effect of different stabiliser concentrations on epithelial cells was measured and is illustrated in Figure 29.

SDS and TTAB needed the lowest amount of stabiliser in milling experiments and were therefore tested in low concentrations while for HPMC, PS80 and Pol124 higher concentrations were needed, so that the tested amount was increased according to preliminary milling studies.

It could be seen that TTAB showed very high toxicity at all tested concentrations. Also, incubation with SDS led to low cell viability, even though low concentrations were tolerated better by the cells than the same concentrations of TTAB. HPMC did not show a toxic potential with all tested concentrations and was therefore ranked as the stabiliser with the lowest toxicity of all used stabilisers. PS80 showed the most linear relationship between toxicity and concentration. Therefore, the choice of the appropriate concentration in cell studies should be uncomplicated, as concentrations can be titrated. Nevertheless, all tested concentrations for this experimental set-up were toxic.

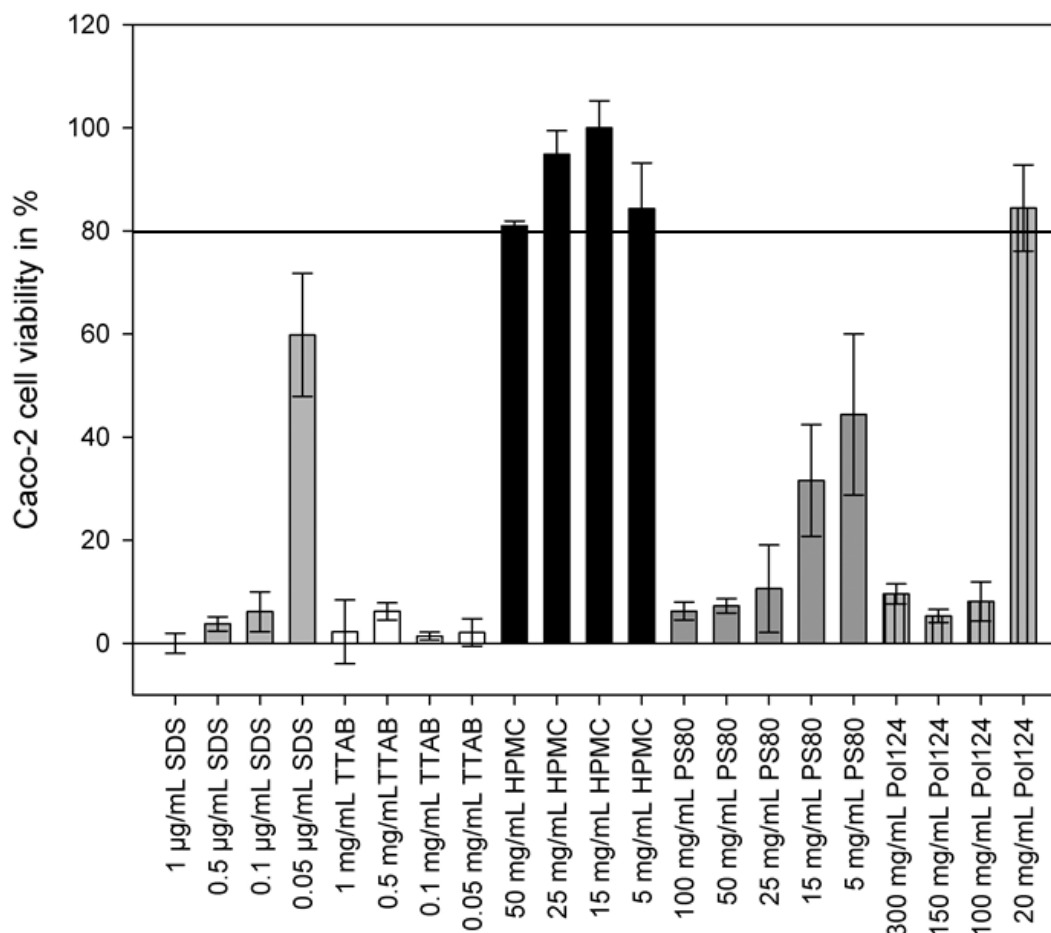


Figure 29: Cell tolerability of various stabilisers and stabiliser concentrations in Caco-2 cells. The line at 80 % cell viability represents the limit for non-toxic solutions. Stabilisers were solubilised in buffer and incubated for 4 h. n = 4. error bars = SD.

Pol124 had a high toxicity at high concentrations but at the lowest tested concentration it was non-toxic. Still, PS80 was ranked together with Pol124 on the second place regarding cell viability as less concentrations of PS80 were needed to stabilise CUR and GLI nanocrystals compared to Pol124. It became obvious that the MTT toxicity test was not suitable for Pol407 as the absorption of light was higher than for the control (data not shown). Hence, it is likely that Pol407 did react during the assay or created high absorption by itself. Pol407 and Pol124 have similar structures so that it could not be excluded that also Pol124 somehow interacted with the MTT test.

4.2.4 Concluding remarks of stabiliser characteristics for the selection of two stabilisers for further studies

One of the first selection parameters was the stability of the nanosuspension in buffer. SDS, TTAB and Pol124 did not form stable nanosuspensions in buffer and could therefore not be used for further studies.

Cell viability measurements showed, that HPMC was not toxic for the used cell line. Pol407 did interfere with the toxicity test, so that no results could be created. Therefore, Pol407 was excluded from further studies. Consequently, the only remaining stabiliser, PS80, was selected for further studies as it was stable in buffer. Still, the toxicity of PS80 was quite high so that a combination of HPMC and PS80 was chosen together with HPMC alone.

In conclusion, HPMC, with its minimal stabilising concentration for each drug and a 1:1 combination of PS80 and HPMC were taken for all following experiments. That is why all following experiments were planned with regard to the stabilising concentrations for HPMC and HPMC + PS80 displayed in Table 15.

The influence of the particle size on transport through and uptake in cells was of further interest for all following studies. Chapter 4.1.1 revealed that the lowest achievable particle size for HPMC stabilised particles was 300 nm with the selected conditions. Therefore, the small particle size was set to 300 nm (CUR and GLI small). As the PDI increased with increasing particle sizes, the larger particle size was set to 500 nm (CUR und GLI large) so that the PDI could be kept below 0.5.

Table 15: Selected stabilisation concentrations for CUR and GLI.

Samples	Stabiliser(s) in wt% of drug	
	HPMC	HPMC + PS80
CUR small	25	12.5 + 12.5
CUR large	25	12.5 + 12.5
GLI small	10	2.5 + 2.5
GLI large	10	2.5 + 2.5

4.3 Characterisation of selected nanosuspensions

The influences of three different properties of the nanocrystals - namely particle size, type of stabiliser and type of drug - were investigated in dissolution, cell uptake and transport studies. As the stabiliser properties were already discussed in the previous chapter, this chapter will highlight the properties of the selected nanosuspensions for further dissolution and cell studies.

To be able to interpret any further results, first an understanding of how and why nanocrystals are forming under the above mentioned conditions has to be created. Therefore, also the knowledge of particle size before milling and stability of the nanosuspension are of interest.

As the solid state can have an influence on the solubility of the drugs and therefore on the rate and extent of dissolution and absorption, XRPD and DSC measurements were carried out. The melting point was of further interest as Li et al. found that beneath the log P value, also the melting point of the drugs is one important criterion influencing adsorption. Low melting points and log P values at approximately 5 can be favourable for rapid absorption [Li et al., 2014].

Finally, the stabilisers should not be toxic in the selected concentration range so that toxicity tests were repeated more detailed at longest cell experiment time.

4.3.1 Particle size of suspension before milling

The suspension for milling purposes was prepared with stabiliser solution, the addition of drug and a homogenisation step like described in chapter 3.2.1. This passage shows the influence of the wetting and homogenisation of the drugs before milling. Table 16 demonstrates the change in particle size from the coarse powder to pre-processed suspension measured by laser diffraction.

GLI seems to be crushable to small particles more easily. Preparation with the Ultra Turrax® for 10 seconds already led to 4.5 times reduction in particle size, while for CUR, agglomeration of coarse particles could be seen. CUR tended to agglomerate when surrounded by aqueous stabiliser solution. This could be one reason why CUR needs more than the double concentration of stabilisers to be stabilised compared to GLI. If the microcrystal suspension already agglomerated, the nanocrystalline formulation could be even more likely to agglomerate further.

Table 16: Particle sizes measured by laser diffraction. n = 4. ± = SD. Coarse powder was measured with the RODOS module (particle size distributions displayed in chapter 9.4.2) while for the suspension the CUVETTE module was utilised.

Sample	X ₁₀ in µm	X ₅₀ in µm	X ₉₀ in µm
Coarse powder GLI	8.35 ± 0.35	52.47 ± 4.60	135.21 ± 15.33
GLI suspension 2.5 % HPMC + 2.5 % PS80	1.62 ± 0.22	11.62 ± 3.01	44.16 ± 11.6
GLI suspension 10 % HPMC	2.68 ± 0.79	19.21 ± 6.12	51.51 ± 14.45
Coarse powder CUR	1.84 ± 0.04	8.70 ± 0.19	29.64 ± 0.83
CUR suspension 12.5 % HPMC + 12.5 % PS80	3.64 ± 0.73	19.99 ± 2.81	48.44 ± 11.58
CUR suspension 25 % HPMC	3.95 ± 0.33	13.11 ± 3.01	42.91 ± 15.01

Two examples for particle size distributions of the pre-processed suspensions are shown below in Figure 30 and Figure 31. CUR suspensions with HPMC could be interpreted to have less agglomeration than with HPMC and PS80 combined but the high standard deviation makes interpretation challenging. Sedimentation of particles could be seen during measurements which also reflect the relatively high standard deviation. It seems that, after homogenisation, the two drugs were on a similar starting level in the mean of particle size and particle size distribution compared to the coarse powder.

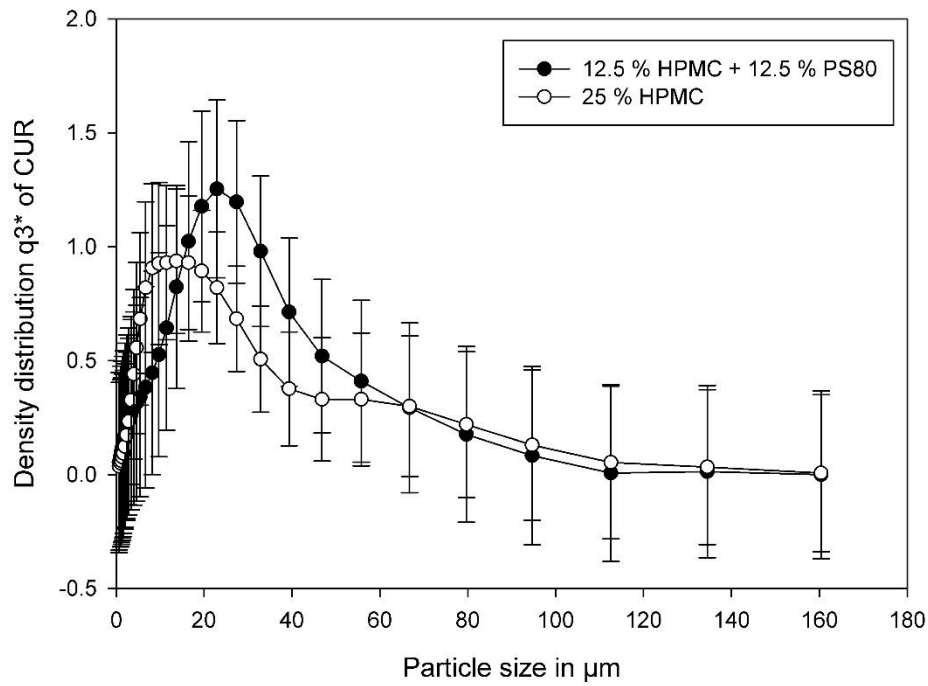


Figure 30: Particle size distributions of CUR coarse suspension after homogenisation. n = 3. error bars = SD.

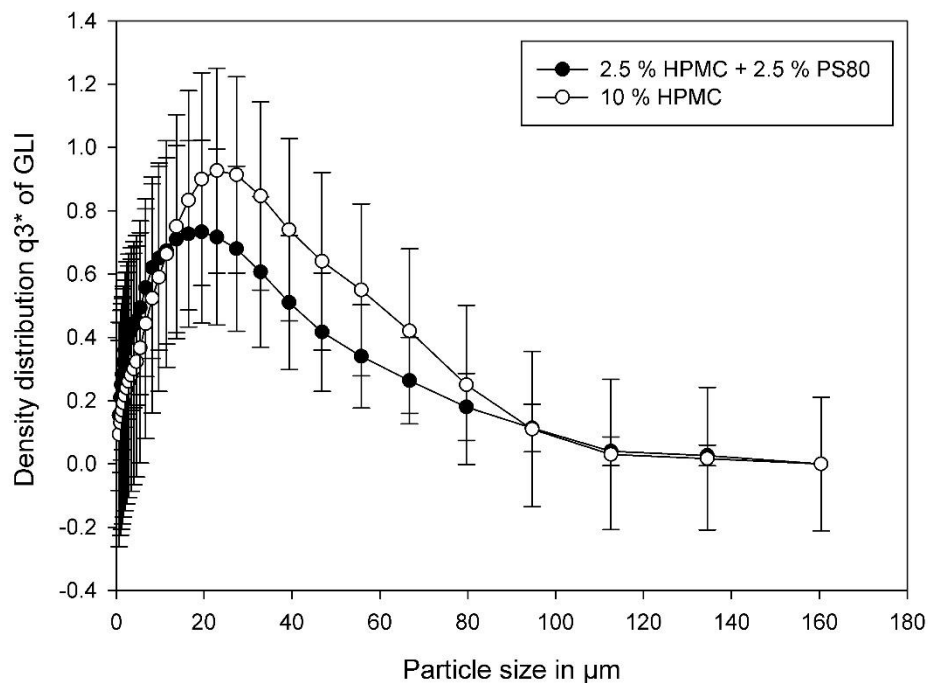


Figure 31: Particle size distributions of GLI coarse suspension after homogenisation. n = 3. error bars = SD.

Span values are ranging from 2.24 for GLI, stabilised with HPMC and PS80 to 3.66 for CUR, stabilised with HPMC.

4.3.2 Stability of nanosuspensions

Nanosuspensions were used for dissolution, transport and uptake studies until one month after production to have comparable batches. This chapter will show stability data of the selected nanosuspensions regarding API content and particle size. Furthermore, the solubility can have an influence on the stability of a nanosuspension so that it was also investigated in this chapter.

4.3.2.1 Solubility of drugs in stabiliser solutions

The solubility of a drug in the (stabiliser-)non-solvent is detrimental in nanosuspensions, as a high solubility could induce Ostwald ripening and therefore, particle growth. Solubility data of the selected nanosuspensions are listed in Table 17.

Table 17: Solubilities of CUR and GLI suspensions after 24 hours of shaking of an over-saturated (1 mM) suspension in double-distilled water.

Drug suspension	Stabiliser	Solubility in $\mu\text{g/mL}$
CUR coarse powder	25 % HPMC	0.54 ± 0.02
	12.5 % HPMC + 12.5 % PS80	10.66 ± 0.51
CUR small	25 % HPMC	21.39 ± 6.21
	12.5 % HPMC + 12.5 % PS80	23.77 ± 8.06
GLI coarse powder	10 % HPMC	Not detectable
	2.5 % HPMC + 2.5 % PS80	Not detectable
GLI small	10 % HPMC	18.76 ± 3.38
	2.5 % HPMC + 2.5 % PS80	10.71 ± 0.78

CUR showed higher solubility, when a mixture of HPMC and PS80 was present, compared to just HPMC. For GLI the HPMC stabilised nanosuspension exhibited an increase in solubility compared to the HPMC + PS80 stabilised nanosuspension.

It was not expected that the nanosuspensions did lead to this high increase in solubility as the saturation solubility should not be increased this much at particles sizes of 300 nm. Hence, it could be concluded that nanoisation could have led to a nanosuspension composed of nanocrystal in a supersaturated drug solution. Another reason could be that the shaking time of 24 hours was too short to achieve saturation solubility.

4.3.2.2 Particle size and content stability

All nanosuspensions stabilised with HPMC and HPMC + PS80 were stable in size and particle size distribution over one year, which can be seen in Figure 32. Stability was in this case defined as no increase in particle sizes above 1000 nm as well as PDI below 0.8.

A slight increase could be seen for all nanosuspension but, over 12 months, the increase in particle size did not exceed 200 nm. Nevertheless, the nanosuspensions should not be used for experiments after 12 months of storage. Maximal storage over 1 month seems more reasonable as already after 3 month the particle sizes of the small and large nanosuspensions did grow more similar to one another.

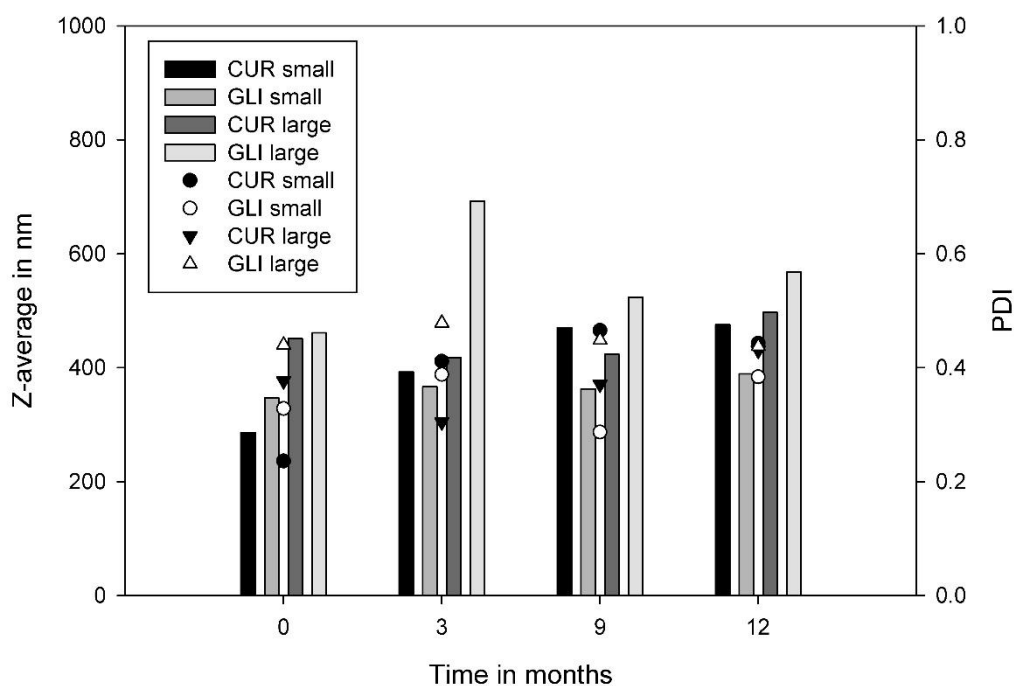


Figure 32: Particle sizes (bars) and PDI (dots) of CUR and GLI nanosuspensions measured over 12 month. n = 1.

Furthermore, the content of CUR and GLI in nanosuspension was determined with UV spectroscopy every 1 - 4 month(s). Especially for CUR, it is known from literature that degradation in solution happens over time. Figure 33 shows the results of the content stability over 12 month for CUR. Fortunately, no degradation could be detected. At the beginning of the stability study, the CUR nanosuspension, stabilised with HPMC, showed a concentration of $6.33 \text{ g}/100 \text{ mL} \pm 0.16 \text{ g}/100 \text{ mL}$ which decreased by 7.6 % to $5.85 \text{ g}/100 \text{ mL} \pm 2.81 \text{ g}/100 \text{ mL}$ after 12 month. For the HPMC+PS80 stabilised

nanosuspension even an increase in content could be seen (from 5.87 g/100 mL \pm 0.10 g/100 mL to 6.24 g/100 mL \pm 0.37 g/100 mL) which is possibly due to measurements uncertainties.

This stability should not be confused with the (in)stability of CUR in solution. When conducting HPLC analysis for dissolution studies, a decrease of solubilised CUR in buffer was rapid. After 2 hours the concentration was reduced by half.

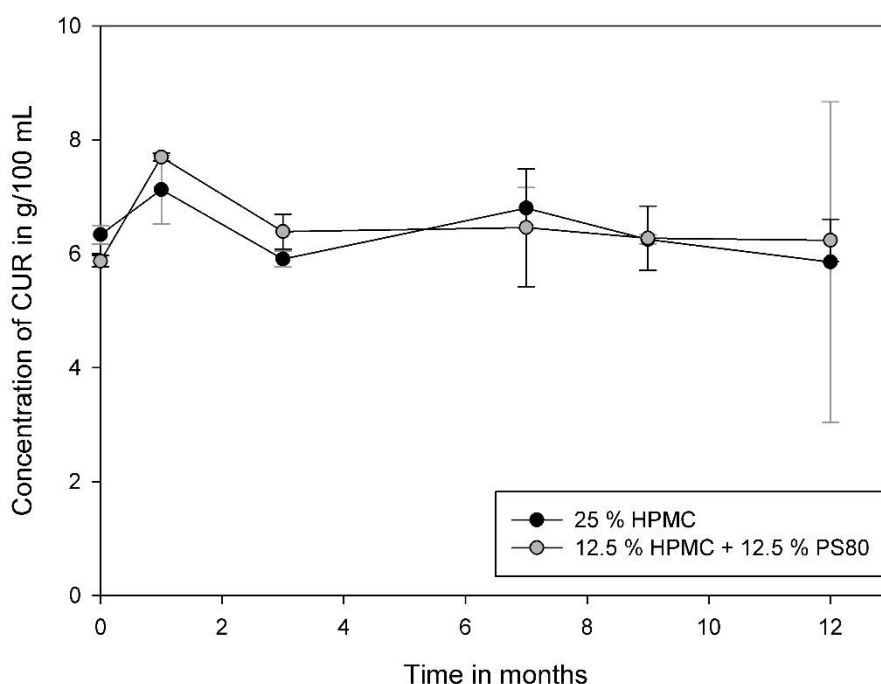


Figure 33: Concentration of CUR in nanosuspensions measured over 12 month. Nanocrystals were dissolved in ethanol for measurements. n = 3. error bars = SD.

It has to be mentioned that with UV spectroscopy no separation of CUR and CUR degradation products is possible. Therefore, if the degradation products also interact with the same wavelength, they are included in the measured values. Tønnesen et al. investigated the degradation of CUR in isopropanol by measuring the spectrum from 200 nm to 600 nm. During degradation, the absorption maximum at 420 nm, which was also measured in this work, dropped and new signals increased around 200 – 250 nm, so that the degradation would be detectable in the set-up of this work [Tønnesen et al., 1986].

GLI stability is plotted in Figure 34. GLI nanosuspension content showed minimal degradation tendencies over 12 months. The HPMC stabilised nanosuspension

exhibited a 10.6 % decrease from $7.43 \text{ g/100 mL} \pm 0.12 \text{ g/100 mL}$ to $6.64 \text{ g/100 mL} \pm 0.99 \text{ g/100 mL}$ while the HPMC + PS80 stabilised nanosuspension showed a 14.2 % decrease from $7.98 \text{ g/100 mL} \pm 1.15 \text{ g/100 mL}$ to $6.85 \text{ g/100 mL} \pm 0.14 \text{ g/100 mL}$.

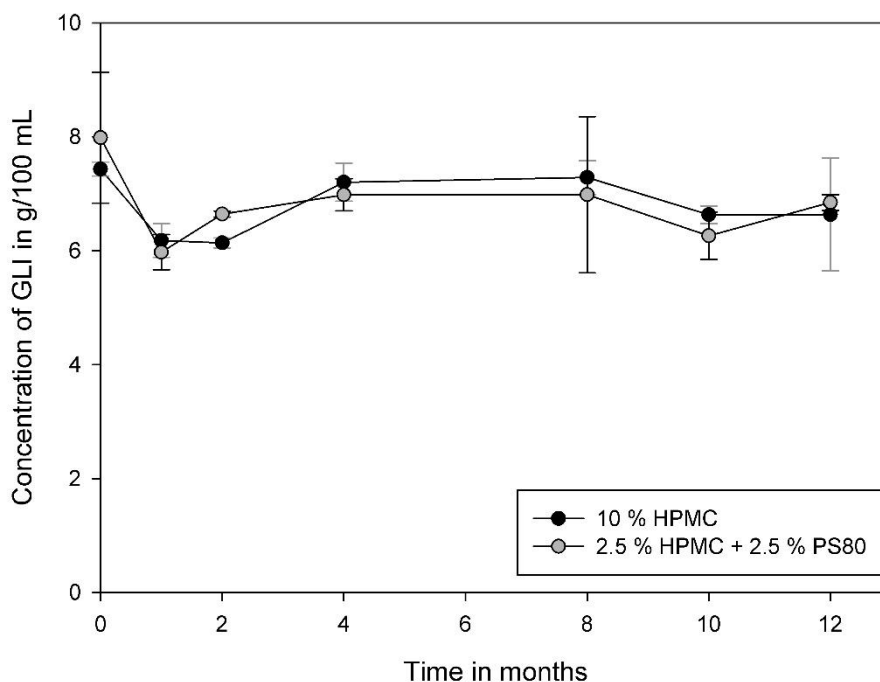


Figure 34: Concentration of GLL in nanosuspensions measured over 12 month. Nanocrystals were dissolved in ethanol for measurements. n = 3; error bars = SD.

These two figures also revealed that approximately 2 - 4 g of 10 g initial powder, which was applied to the mill, remained in the milling system and accordingly got lost for further processing.

Summarised, stable nanosuspensions with the two selected stabilisers could be produced. They were relatively stable in size and content over 12 month.

4.3.3 Solid state before and after milling

To establish a stable and successful milling process and to receive stable nanosuspensions, the crystalline state is favourable. Determination of the solid state faces a challenge for nanocrystals. First of all, most available standard methods for the determination of the solid state are based on the measurement of a dry powder. Drying of the nanosuspensions can lead to a change in molecular order of the drug depending on the drying technique but to which extent is unclear. Furthermore, when nanocrystals

are dried, the signals in DSC and XRPD can be less defined than for macrocrystalline samples and a misinterpretation can be made more easily [Hao et al., 2012]. Physically, it is doubtful that a crystalline drug shows amorphous content after wet-milling because water acts as a plasticiser and therefore triggers recrystallisation, so that it is more likely that polymorphs are forming with an intermediate amorphous state than amorphous parts alone. Hao et al. stated that it is more plausible that if amorphous parts are detected, they come from interplay between drug and stabiliser after drying [Hao et al., 2012].

The complicated nature of the solid state determination proves that at least two methods should be used to try to determine the solid state of nanocrystals. Some researchers found that DSC did not show a sign of glass transition but X-ray experiments indicated an amorphous state with a total absence of Bragg peaks [Descamps and Willart, 2016]. Therefore, two methods were used for combinational interpretation in this thesis.

Coarse powder structure of CUR (Figure 35) and GLI (Figure 36) was measured to be crystalline. In XRPD measurements defined Bragg peaks stand for a crystalline sample, while an undefined halo represents an amorphous state.

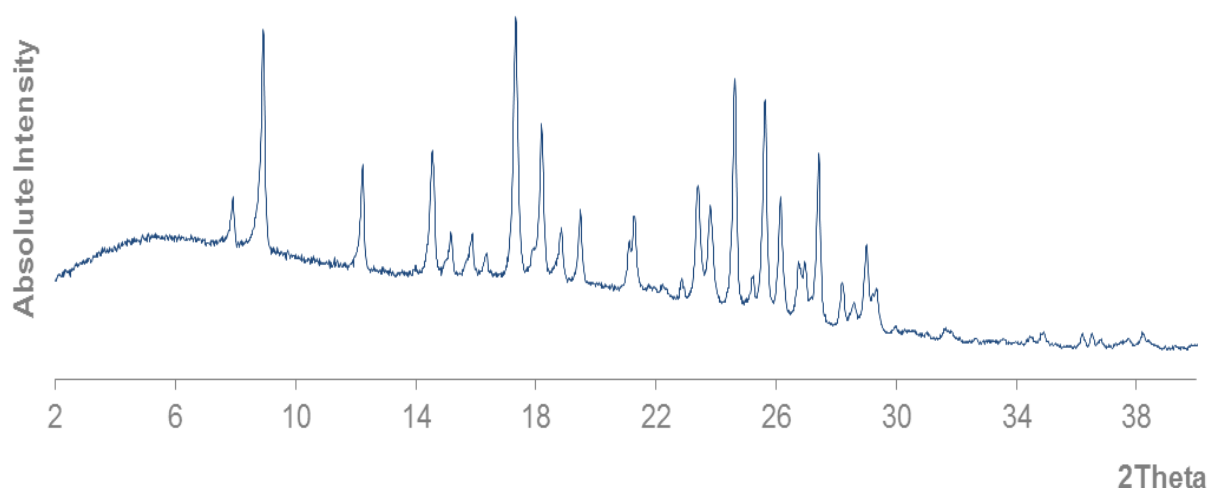


Figure 35: XRPD diffractogram of CUR as received from supplier.

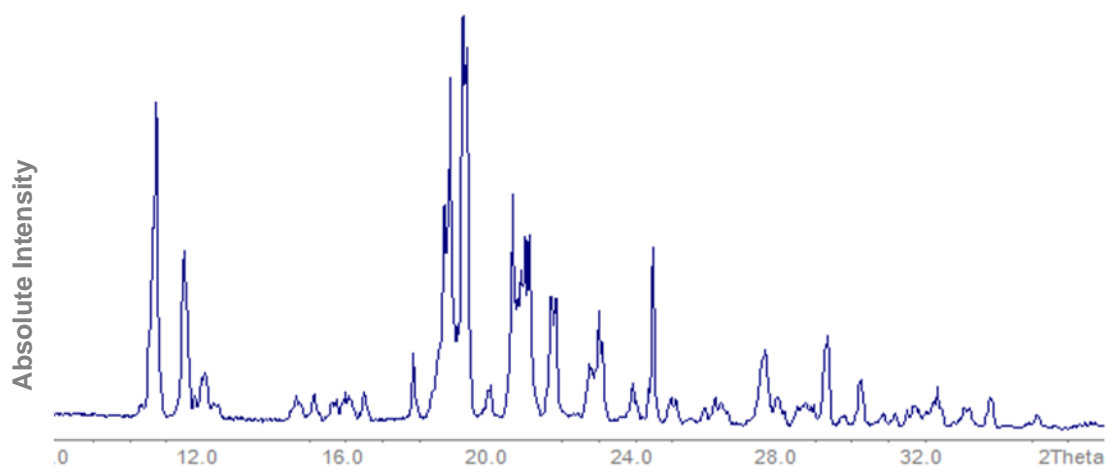


Figure 36: XRPD diffractogram of GLI as received from supplier.

DSC curves of the coarse drugs can be observed in Figure 37 and Figure 38. An endothermic melting point in DSC diagrams is related to a crystalline state, while a glass transition and possible exothermic recrystallisation are typical for amorphous states.

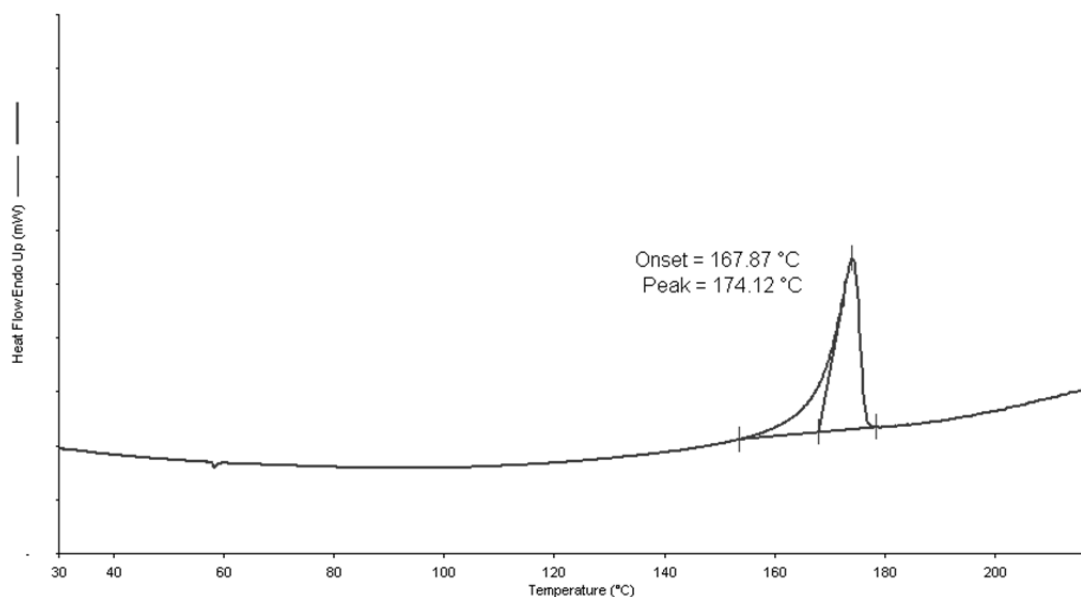


Figure 37: DSC curve of coarse CUR as received from supplier. Area of the peak was 94.77 J/g. Y-axis length corresponds to 20 mV.

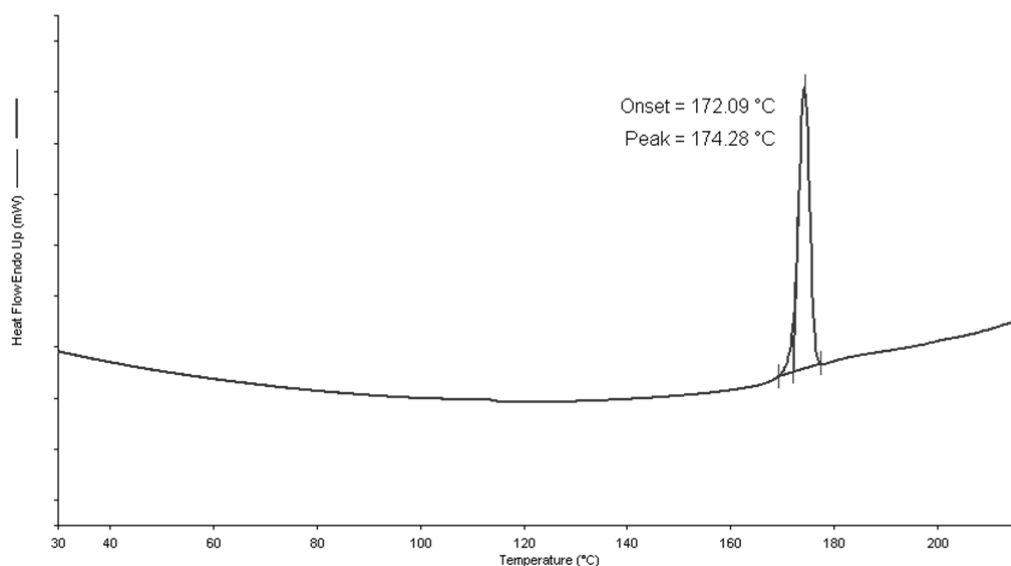


Figure 38: DSC curve of coarse GLI as received from supplier. Area of the peak was 85.31 J/g. Y-axis length corresponds to 20 mV.

The defined melting peaks for each drug show a crystalline structure of the coarse powders as well. For CUR, a slightly exothermic signal was found at 58.24 °C with an area of -0.875 mJ. XRPD diffractograms are indicating a fully crystalline sample but it has to be mentioned that XRPD has a detection limit of around 10 % for amorphous content [Saleki-Gerhardt et al.1994], so that CUR coarse powder could be partially amorphous as received from the supplier.

An XRPD of a selected freeze dried CUR nanosuspension was not as defined as the coarse substances as can be seen in Figure 39. A high background signal that resulted in a shift of the baseline and low intensities could indicate a partially amorphous material but the difference in intensity can also be related to sample preparation. Furthermore, stabilisers were present in this sample so that the signal could be changed by them.

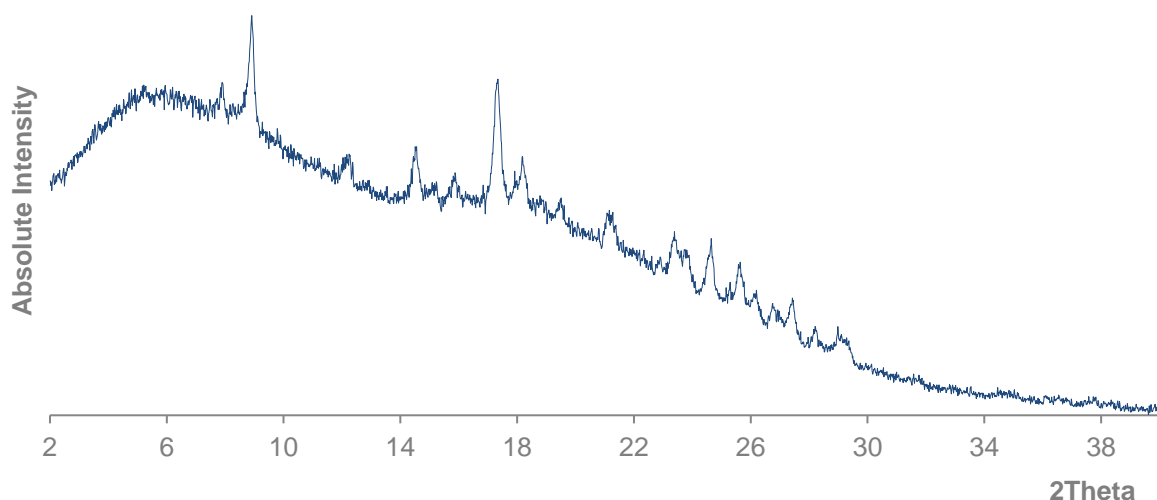


Figure 39: XRPD diffractogram of 500 nm CUR freeze dried nanosuspension. Stabilisers present: 12.5 % HPMC and 12.5 % PS80.

For a dried GLI nanosuspension with the same size and stabiliser combination, still defined Bragg peaks could be detected like plotted in Figure 40. Also in this sample stabilisers were present but in lower concentrations compared to the CUR nanosuspensions, so that no signal could be seen of them.

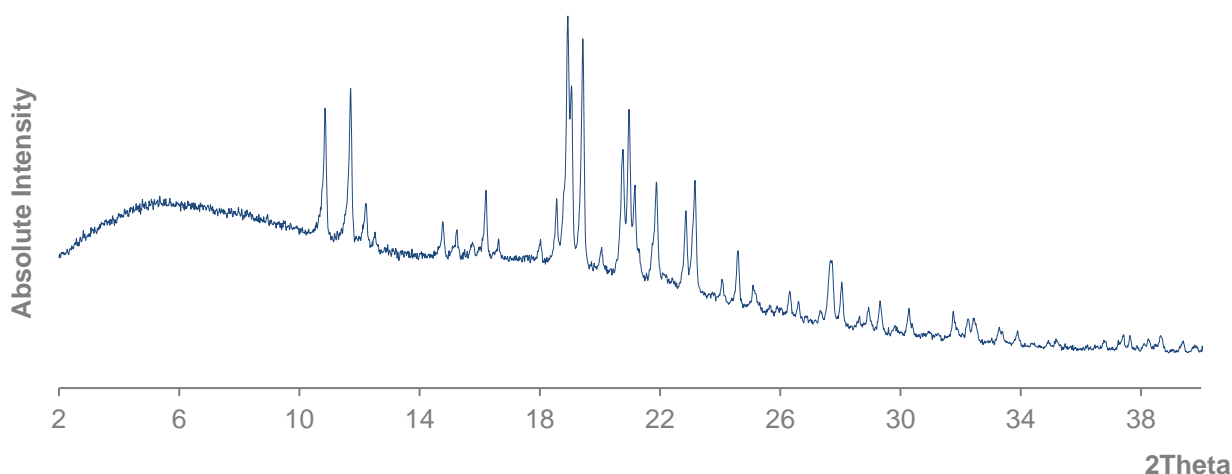


Figure 40: XRPD diffractogram of 500 nm GLI freeze dried nanosuspensions. Stabilisers present: 2.5 % HPMC and 2.5 % PS80.

The example for CUR and GLI nanosuspensions, which were measured by XRPD, were also investigated by DSC and results are given in Figure 41 and Figure 42. The DSC curves showed a melting peak, indicating crystalline state of the drug after milling

and freeze drying. All other values of onset and peak temperature of the selected nanosuspensions can be found in the appendix at chapter 9.4.3.

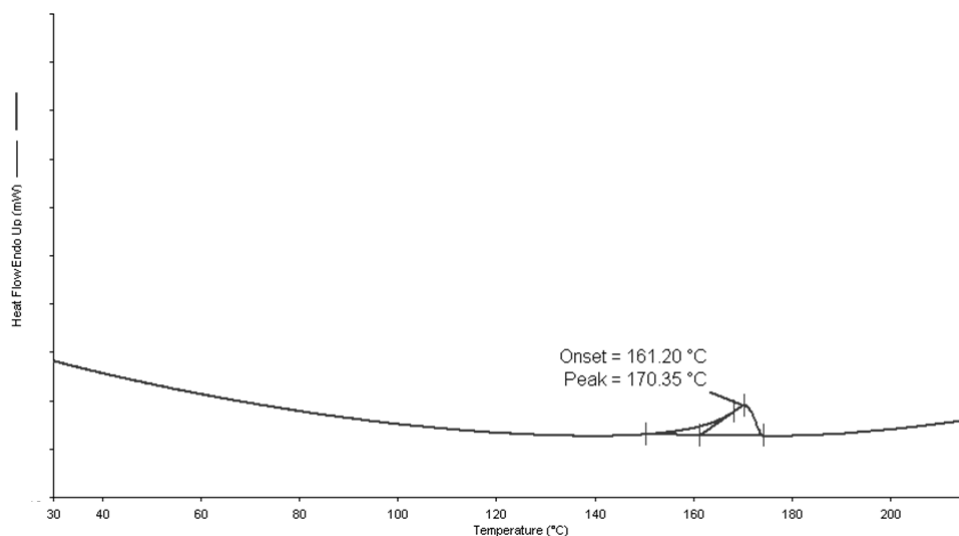


Figure 41: DSC curve of 500 nm CUR freeze dried nanosuspension. Stabilisers present: 12.5 % HPMC and 12.5 % PS80. Peak area of 51.14 J/g. Y-axis lengths corresponds to 20 mV.

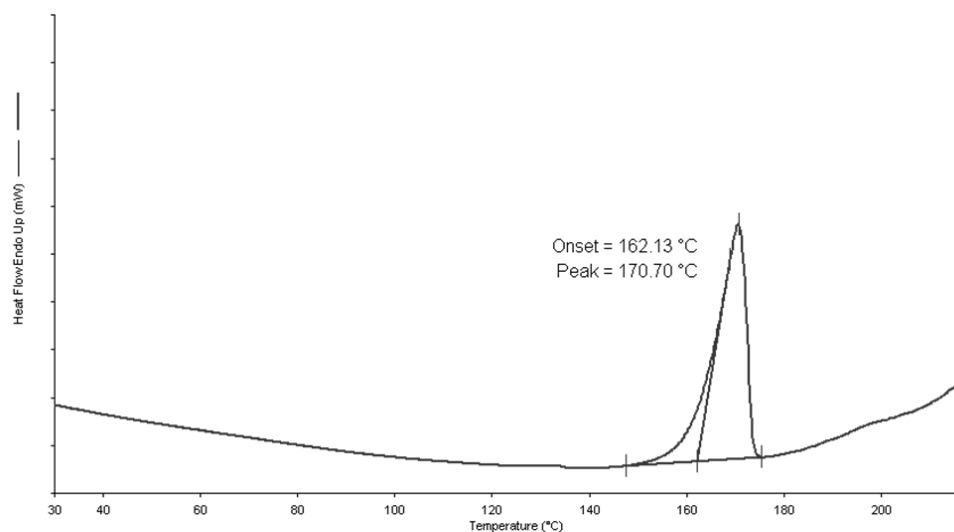


Figure 42: DSC curve of 500 nm GLI freeze dried nanosuspensions. Stabilisers present: 2.5 % HPMC and 2.5 % PS80. Peak area of 73.31 J/g. Y-axis lengths corresponds to 20 mV.

For both drugs a shift in melting point and also a decrease in peak area related to sample amount (J/g) was detected. Both phenomena can be possibly related to the stabilisers present. Polymorph formation for GLI was excluded, as the value for the melting peak of the polymorph, in literature, was with 148.7 °C significantly lower. For CUR, the drop in peak area and also broadening of the peak led to difficulties in manually integration and setting the peak temperature. Still, the formation of

polymorphs could not be excluded as one known polymorph showed a melting peak at 172 °C (polymorph 3; see chapter 3.1.1.1) and also the decrease in area compared to the coarse powder could be related to a change in crystalline state.

Most results indicated that CUR and GLI were still in the crystalline state after milling. For CUR nanosuspensions, one XRPD measurement indicated a potential change in solid state but as DSC measurements did not confirm this finding, the solid state should be crystalline. It cannot be excluded that CUR was forming another polymorph during milling or drying. XRPD and DSC measurements clearly showed a crystalline state for GLI. Still, the freeze drying step of the nanosuspensions could have altered the solid state of the APIs, so that no definite answer can be given to the question if milling induced (partial) amorphisation of the drugs.

4.3.4 Cell toxicity of selected stabilisers and nanosuspensions

Incubation with small GLI nanosuspensions, stabilised with 10 % HPMC or 2.5 % HPMC and 2.5 % PS80, did not show a change in Caco-2 cell viability compared to the control when incubated over 24 hours. They were not toxic. CUR, in contrast, interfered with the MTT test setup used in this work, as the absorbance measured was extraordinary high. Hence, for CUR just the stabilisers themselves were investigated as it is stated in literature that CUR has a low toxicity potential for Caco-2 cells [Zhen et al., 2017]. CUR needed highest stabiliser concentrations and therefore the area around minimal stabilisation concentration of CUR (25 % HPMC and 12.5 % HPMC + 12.5 % PS80) was investigated.

HPMC showed high cell viability over a wide range of concentrations. Concentrations from 16,279 % related to 1 mM of CUR, used in transwell studies, showed less than 80 % of cell viability which represents 60 mg/mL as plotted in Figure 43. Below this value, every concentration can be used. Also the combination of HPMC and PS80 was not toxic in the used concentrations (data not shown). For toxicity tests, the amount of HPMC was fixed with approximately 400 % (1.5 mg/mL) and at a concentration of PS80 of 70 % (0.25 mg/mL), the cells had a viability of 82 % while an increase to 140 % PS80 (0.5 mg/mL) lead to a cell viability of 78 %. Nevertheless, this concentration is far away from the used 12.5 % HPMC + 12.5 % PS80 stabilising concentrations for CUR in transport and uptake studies.

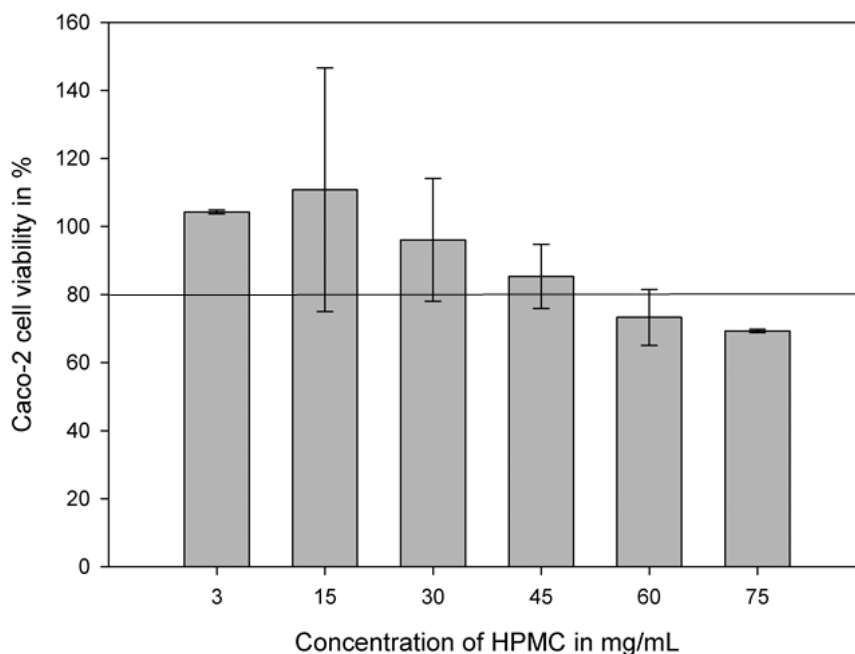


Figure 43: Cell tolerability of HPMC. Cell viability above 80 % indicates non-toxic solutions. Stabilisers were solubilised in transport buffer and incubated for 24 h. n = 4. error bars = SD.

Results for PS80 are plotted in Figure 44. A concentration of 27 % (0.1 mg/mL) was not toxic, while the next tested concentration of 68 % (0.25 mg/mL) showed cell viability below 80 %. So, the minimal stabilisation concentration of 20 % PS80 for CUR is still in the non-toxic range.

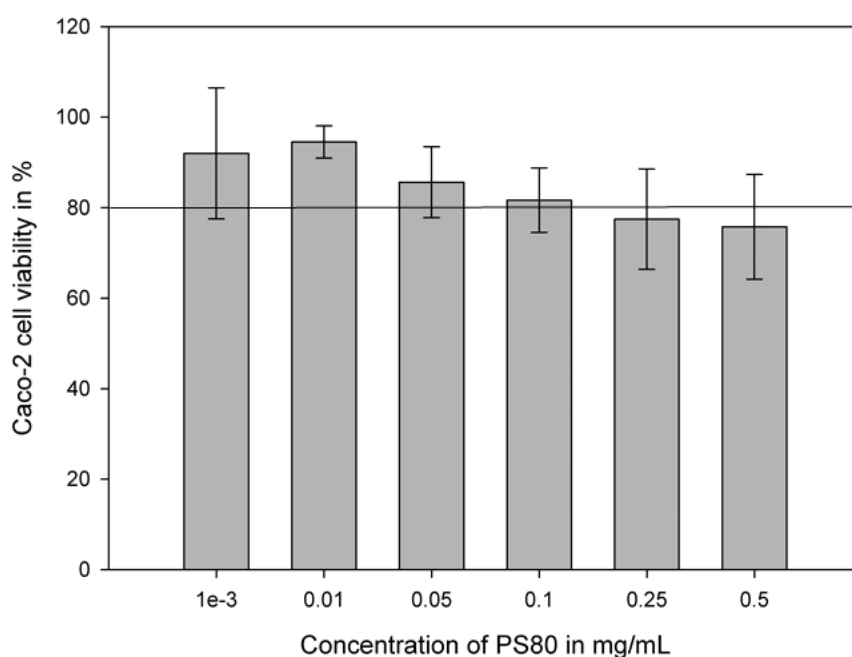


Figure 44: Cell tolerability of PS80. Cell viability above 80 % indicating non-toxic solutions. Stabilisers were solubilised in transport buffer and incubated for 24 h. n = 4. error bars = SD.

Cell viability was most important for transport studies as the monolayer needs to be intact over the time of the experiment, so that the results can be comparable. In uptake studies, the cell viability could be seen visually. When the cells detached from the bottom of the plate or the cells changed morphologically the experiment was repeated.

4.3.5 Concluding remarks of the characterisation of selected nanosuspensions

Stable nano-objects of a most probable crystalline state could be produced. Cell toxicity studies showed that all selected nanosuspensions should be non-toxic for the transport studies. This could be directly tested for GLI nanosuspensions. CUR nanosuspensions showed interferences with the selected toxicity test, so that the probable toxicity of the nanosuspension was assessed from testing various stabiliser concentrations and combinations. No concentration that was used for the cell studies (25 % for HPMC and 12.5 % HPMC + 12.5 % PS80) demonstrated cell toxicity. The selected nanosuspensions proved to be predestined for further cell studies.

4.4 Characterisation of drug-stabiliser interaction

Until today, it is not completely understood how stabilisers hinder nanosuspensions from agglomeration [Wang, Y. et al. 2013]. Within this chapter, three different methods were tested for the predictability of minimal stabilisation concentration for CUR and GLI and their interaction potential with each other. The choice of methods was based on a literature review, which is summarised in the section below.

4.4.1 Stabiliser - particle interaction studies in literature

One part of the literature tested several APIs with different kind of stabilisers, regarding the stability of the achieved nanosuspension and milling performances but this short review will focus on the influence of the stabiliser characteristics. One of the main factors for successful stabilisation is the hydrophobicity of the stabiliser. It seems that the higher the hydrophobicity, the better the attachment to the hydrophobic surface of the drug [Lee et al., 2005]. The molecular weight of the stabiliser can have an influence, too. The work of Choi et al. indicated that lower molecular weight polymers are more suitable for nano-comminution than larger polymers [Choi et al., 2008].

Nakach et al. addressed the lack of methods for stabiliser screening in industry and academic research and measured the surface tension and zeta potential for the selection of the appropriate stabiliser concentration. They tested 19 stabilisers and

investigated the ability of the stabilisers to create a stable nanosuspension (with a model hydrophobic and non-ionisable highly insoluble API) in small milling setups. If the resulting particle size was too high (over 500 nm), the stabiliser was excluded. With different techniques they selected, with PVP and SDS, the best stabilisers for their drug and looked at the surface tension of the mixture of PVP and SDS at different ratios and found a minimum value at 60 % of PVP suggesting a maximum of surface activity of PVP/SDS mixtures. Utilising zeta potential measurements, this combination was suggested as well because with the increase of SDS concentration to 40 % from lower ratios, the zeta potential decreased down to -54 mV and remained almost constant. They concluded that their approach of stabiliser (concentration) selection was intended to support formulators to select a suitable wetting/dispersant system for any API to achieve an up-scalable industrial process leading to stable nanosuspensions [Nakach et al., 2014].

One of the promising publications, studying the mechanistic molecular interaction of stabiliser molecules with a drug surface, used atomic force microscopy (AFM). The specific adsorption geometry for the polymers could be seen. A smooth and regularly branched adhesion resulted in a better stabilisation compared to clustered polymers, which did not stabilise the API suspension [Verma et al., 2009a]. Unfortunately, AFM has, until now, not proven an efficient screening technique, which would be used in industry, as the equipment is expensive and the analysis is time consuming. Lately, also Fourier transform infrared spectroscopy was used by Abhayrai et al. to get insights into PLGA-polysorbate 80 interaction. During adsorption of polysorbate 80 on PLGA nanoparticles, the acyl chain of polysorbate 80 acts as a flexible structure and changes conformation, while the ester group was less hydrated, which increased hydrophobic interactions [Abhayraj et al., 2016].

Regarding stabiliser interaction, there is a literature pool of critical micellisation concentration investigations done with isothermal titration calorimetry (ITC) [Schicke, 2010]. Furthermore, nano-objects and their interaction with different substances have already been measured [Rixiang and Lau, 2016; Kolakovic et al., 2013], but there are just a few publications that deal with the interaction of stabilisers with nano-objects. A lot of publications have chosen contact angle measurements (CAM) to predict the feasibility of a drug-stabiliser system to form nanosuspensions. Cerdeira et al. found ineffective stabilisers for miconazole to have a high contact angle (CA) and therefore

less wetting than the other effective stabilisers [Cerqueira et al., 2010], whereas with ineffective stabilisers a nanosuspension could not be created. In nanosuspension production, usually the stabiliser with the lowest CA is chosen [Pardeike and Müller, 2010; Pardeike et al., 2011] but this does not automatically lead to the best stabilisation. Pardeike et al. tested with CAM, which stabiliser they should choose prior to milling experiments. Liu et al. investigated the hydrophobicity and geometry of stabilisers [Liu et al., 2014]. However, the question, whether CAM are also able to display concentration dependencies and indicate the lowest stabilising concentration, is still left without an answer. Hence, to contribute to this question, CAM is assessed in this thesis to predict stabilising concentrations in nanocrystal suspensions. Therefore, these two techniques, ITC and CAM, were tested, in this project, with respect to their potential to be used as screening techniques for shortcutting the stabiliser selection process.

4.4.2 Contact angle measurements

The interaction potential of a solid and a liquid (e.g. comprising a dissolved stabiliser) can be predicted by CAM. High CAs show, that an interaction is less likely. If the liquid and solid properties are similar, the CA can be low. Surfactants are one example for substances that increase interaction potential between solid surfaces and dispersion liquid. So that it was expected, for this thesis that higher stabiliser concentrations lead to more wetting of the drug surface. Generally, one can say that a reduction in CA stands for interaction of the dissolved stabiliser with water and/or the drug compact. As the drugs for nanosuspension production have a hydrophobic nature and the stabilisers are rather hydrophilic, the CAM can display this hydrophobic-hydrophilic interactions as well as the influence of the stabilisers on the surface tension of the water droplet applied to the drug.

For CUR, a trend of more wetting with higher stabiliser concentrations could be seen (Figure 45). The CAs of the stabiliser solutions on the drug compact were related to the CA of water on the drug compact on each experimental day. Hence, a negative number stands for a smaller CA related to the one of water and a positive number indicates a higher CA. CAs for water on GLI were mostly just below and on CUR just above 50°. When increasing the PS80 concentration, the wetting of CUR increased until 12.5 % PS80. This concentration led to an almost direct ingress of the water droplet in the CUR compact, so that a maximum reduction of CA was achieved.

Consequently, every concentration above 12.5 % could not reduce the CA any further. No significant change in CAs could be observed for different HPMC concentrations. Just a slight trend could be seen to higher CA reduction for higher concentrations. At higher concentrations of HPMC and PS80 mixtures, the CAs were slightly lower related to water than the average of the single substances. Only at the lowest concentrations, the combination of PS80 and HPMC seems to have a benefit on the wetting behaviour compared to PS80 alone.

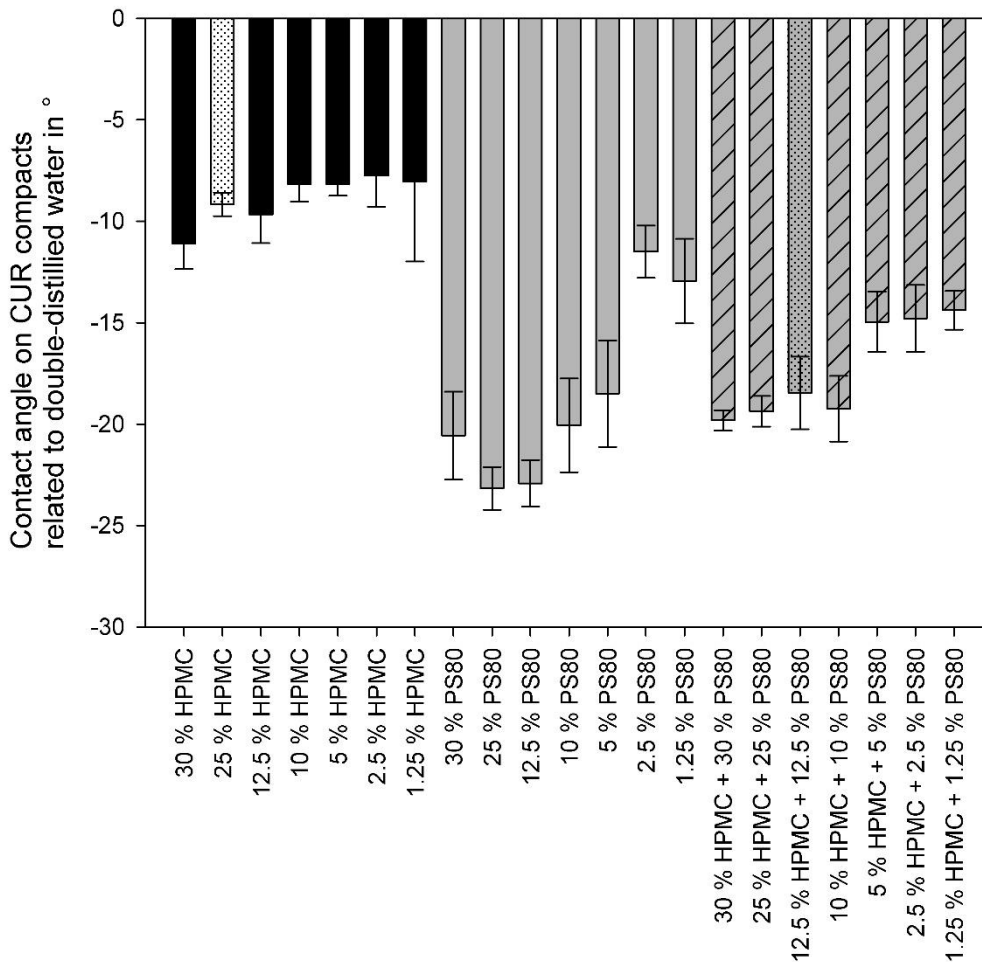


Figure 45: CAs of stabiliser solutions in double-distilled water on CUR compacts. Dotted columns represent minimal stabilising concentrations. n = 5. error bars = SD.

For GLI, the CA determination with the same stabiliser solutions that were tested with CUR, gave a different picture (Figure 46). PS80 addition to water at lowest concentrations led to comparably lower wetting of the GLI compact compared to CUR, e.g. at a concentration of 1.25 % PS80, the CA reduction on GLI was $-3.2^\circ \pm 0^\circ$ and on

CUR $-12.95^\circ \pm 2,08^\circ$, respectively. Still, the trend of decreasing CAs for higher concentrations could be seen.

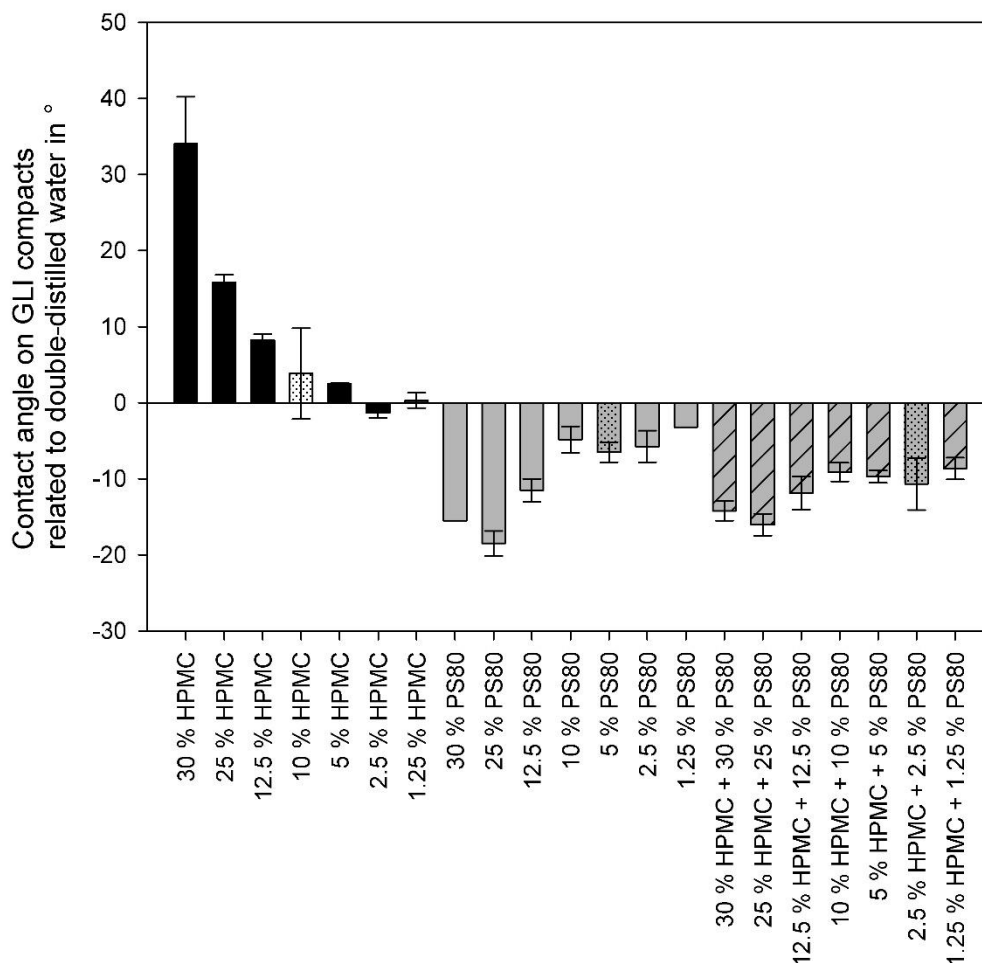


Figure 46: CAs of stabiliser solutions in double-distilled water on GLI compacts. Dotted columns represent minimal stabilising concentration. n = 5. error bars = SD.

The maximum wetting was up to $-18.5^\circ \pm 1.64^\circ$ for GLI and $-23.2^\circ \pm 1.05^\circ$ for CUR. In contrary, an increase in HPMC concentration led to less wetting on the GLI compact compared to CUR. For GLI, the values of PS80 alone and the combination of HPMC and PS80 seemed to have the same impact on the CA for the two highest stabiliser concentrations (30 % and 25 %) as for CUR. So here, HPMC did just lightly hinder the wetting effect of PS80. With less concentrated combinations, there was a decrease in contact angle to be seen like in the lowest combinations (1.25 % + 1.25 % and 2.5 % + 2.5 %) for CUR. Hence, the combination of the two stabilisers led, for these concentrations, to a better wetting than the substances alone.

The different behaviour of these two drugs, when exposed to the same amount of stabiliser, shows that stabiliser-drug interactions cannot be generalised. Each drug has its own optimal stabiliser and stabilising concentrations. For CUR and GLI, the difference was most prominent for HPMC interaction. GLI did not seem to interact with HPMC solutions. It is known that HPMC interacts with water while building up structures that lead to increased viscosity of the system. The interaction with the GLI compact seemed to be negligible compared to this self-interaction, as for the highest concentration, the CA increase compared to water was $34.03^\circ \pm 6.19^\circ$ so that the total CA was found around 84° , which nearly indicated no wetting at all, as defined in the European Pharmacopoeia [8th edition monography 2.9.45]. In contrast, HPMC had an influence on the wetting behaviour of water on CUR. With higher concentrations, the wetting increased slightly from $-8.04^\circ \pm 3.95^\circ$ for a concentration of 1.25 % HPMC to $-11.09^\circ \pm 1.26^\circ$ for the 30 % HPMC solution. The interaction between the HPMC molecules in solution might have been reduced with the effect that some HPMC molecules could interact with the CUR surface. This indicates that CUR seems to be a stronger interaction partner for HPMC than GLI. Unfortunately, this does not explain the different stabilising concentrations of CUR and GLI for HPMC. CUR had with 25 % even a 2.5 higher stabilising concentration than GLI with 10 %. There must be a more prominent factor influencing stabilising concentration during and after milling for CUR than the wetting alone. PS80 had similar interaction patterns with GLI and CUR just to another extent. One exception was the step when there was an abrupt rise in CA reduction. For CUR, it happened between 5 % and 10 % PS80 and for GLI between 10 % and 12.5 %. Again, CUR compact wetting was higher at medium stabiliser concentrations (10 % PS80) ($-20.06^\circ \pm 2.31^\circ$) compared to GLI ($-4.83^\circ \pm 1.73^\circ$).

Unfortunately, the course of the CAM values with various stabiliser concentrations could not give information about minimal stabilisation concentrations. Even though it is an often used method in literature for the prediction of stabilising potential, it is a method with just a small application window. In literature, a reduced CA of hydrophilic stabiliser solutions on hydrophobic drugs is claimed to lead to a higher chance in stabilisation possibility. Results from this project however suggest that this method might not be useful in general application. In this work, it could be seen that even though HPMC creates high contact angles, it is a suitable stabiliser for GLI. HPMC helps to produce stable and small-sized nanosuspensions. Therefore, CAM cannot be the only method to choose when wanting to predict stabilisation efficacy and/or

stabilising concentrations. Hence, in this thesis, a second method, ITC, was chosen to possibly display the interaction of stabiliser and drug on the molecular level in more detail.

4.4.3 Isothermal titration calorimetry

4.4.3.1 Analyses background and particle characteristics

ITC is rarely used until today for the study of interaction potential of stabilisers and drugs with regard to nanocrystal production. Just a few papers studied the interaction of different polymers on micron-sized calcite crystals [Dimova et al., 2003], polystyrene beads with a hydrophobic surface [Pinholt et al., 2011] and cationic silica nanoparticles [McFarlane et al., 2010] with ITC. Most of the measured interactions indicated an adsorption, which was expressed by large exothermic signals at the beginning of the titration with a decline until a plateau was reached. Normally, in ITC, enthalpy can be calculated out of the heat signal and the concentrations in the syringe and in the cell. As the interaction of stabiliser and drug is not a chemical reaction but physical interaction, the enthalpy was not selected as the evaluation value of choice for comparison of drug suspension and stabiliser solution interactions. The models that can be fitted to the enthalpy curves do not consider particle-molecule interaction but molecule-molecule interaction. For a comparison of different drug-stabiliser interactions, the peak length of the power amplitude for each injection was subtracted from the length in the control experiment, so that the extent of interaction could be compared between different drugs and different stabilisers. Thus, every experiment needed to have an additional control experiment. The calculated values do not display information about stoichiometry or other reaction characteristics but the relation to each other enables comparison of the systems. Positive values were received when the sample had higher amplitude (more exothermic) and negative values stand for smaller amplitude (less exothermic) than the control. Each dot in Table 19 and Table 20 does exhibit the amplitude of one injection of the sample with the amplitude of the control subtracted. Examples for more or less exothermic samples can be seen in Figure 47.

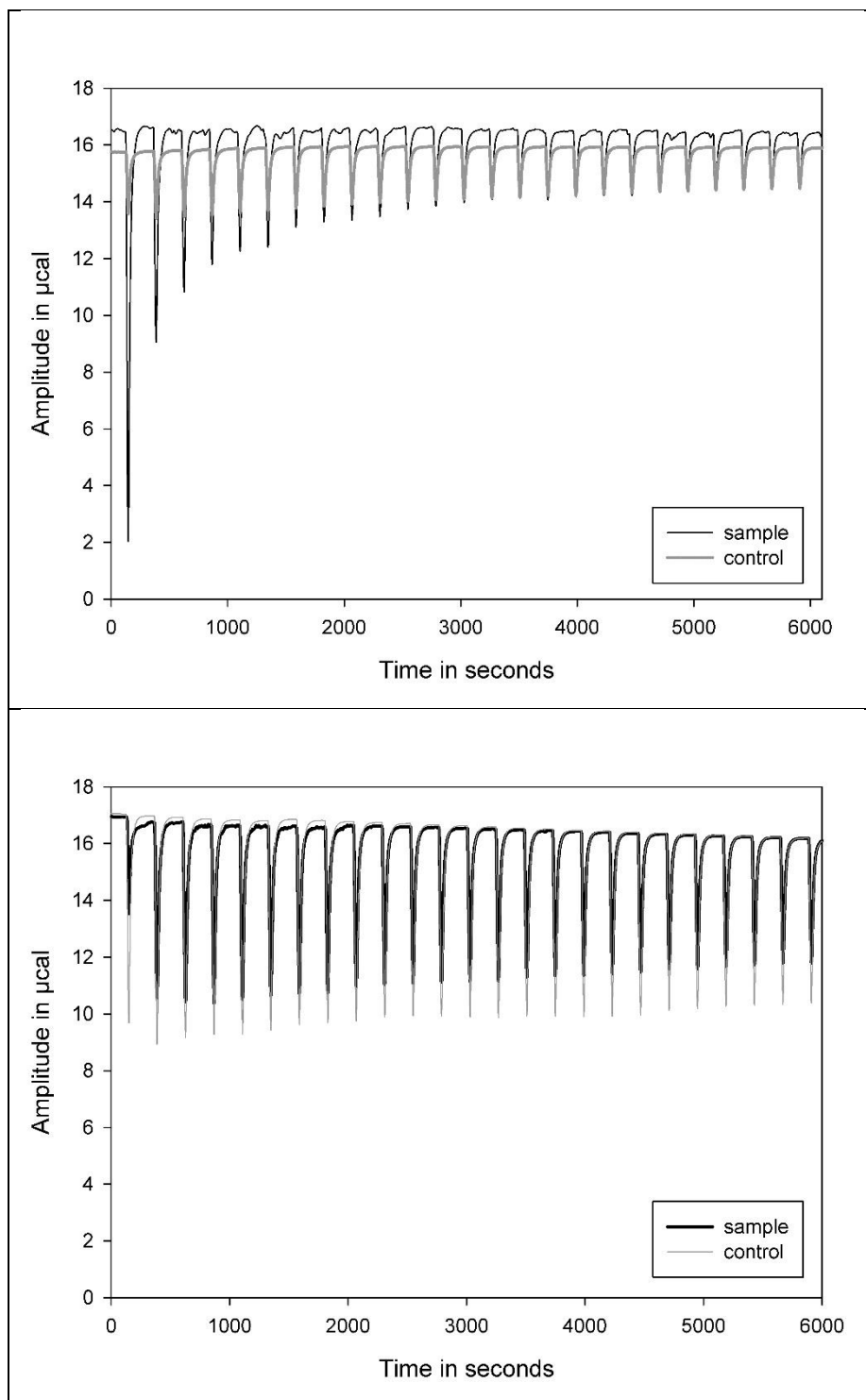


Figure 47: Raw data of injections of stabiliser solution in Milli Q water (control) and in a drug suspension (sample). Exemplary raw data, to show lower (top) or higher (bottom) heat generation of the control in relation to the sample (top: PS80 in CUR; bottom: HPMC in GLI).

The control experiment was chosen as a titration of stabiliser solution into water as this gave a higher signal than the titration of water into drug suspension and therefore had a higher impact on the setup. These phenomena can be explained by heat of dilution of the stabiliser solution into water which is much higher than the dilution of drug suspension by water as the drugs are poorly soluble in water. The titration of water into

drug suspension gave such a low signal that it was not put into calculation (raw data can be seen in chapter 9.4.4).

Unfortunately, it was not possible to investigate the interaction of the stabilisers with the nanocrystals as the nanocrystals agglomerated when the stabilisers were not present so that the coarse powder had to be used for interaction studies. As the coarse powder was used in suspension for ITC experiments, the knowledge of physico-chemical parameters of the coarse suspensions is of interest to interpret the results of the following ITC experiments. Inspection of Figure 48 indicates, that CUR coarse material has irregular shaped particles with a rough surface.

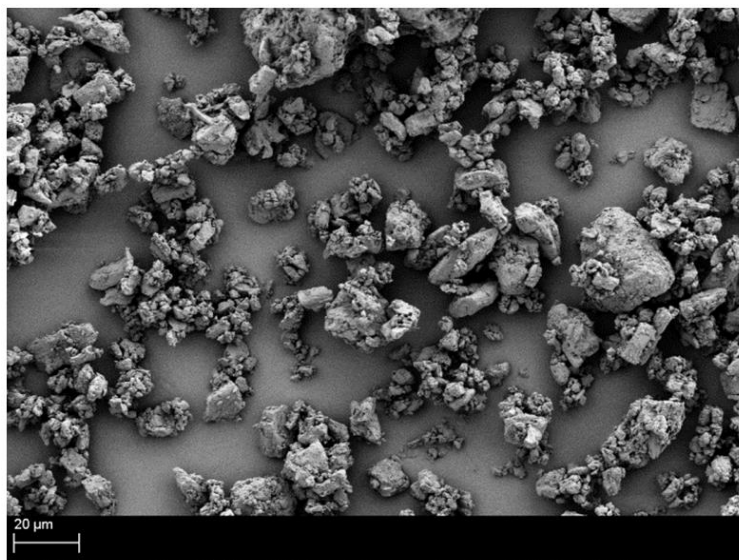


Figure 48: SEM image of CUR coarse material as received from supplier.

A broad particle size distribution could be imaged with some large and a high amount of small particles.

In comparison to CUR, GLI particles appeared more plate like and with a smooth surface (Figure 49). Furthermore, the size is differing, with GLI having larger particles than CUR. Particle size distribution seemed to be wide, with small particles being broken off larger crystals.

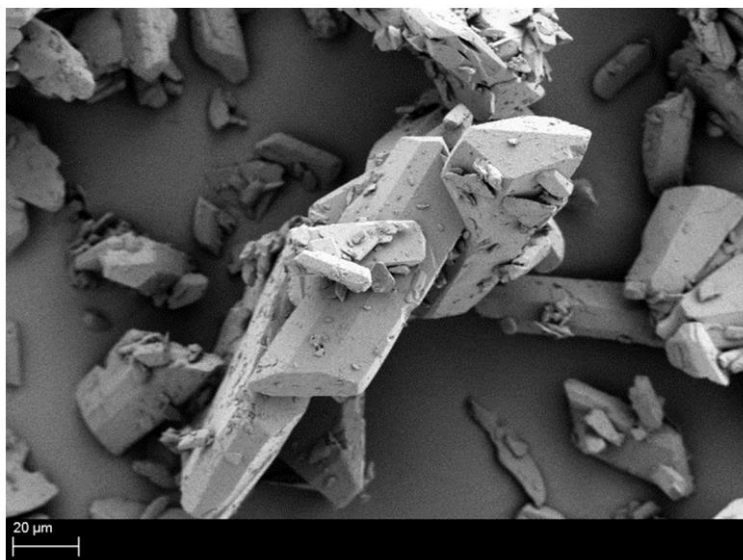


Figure 49: SEM image of GLI coarse material as received from supplier.

The difference in size, visualised in SEM, could also be reflected in particle size measurements by laser diffraction. CUR particle size distribution was slightly bimodal while GLI showed a broader but monomodal distribution (figures of particle size distribution can be seen in chapter 9.4.2). Table 18 shows that CUR had smaller particles and a narrower particle size distribution.

Table 18: Particle sizes of coarse powders measured with laser diffraction. n = 4. ± = SD.

sample	x ₁₀ in μm	x ₅₀ in μm	x ₉₀ in μm	Span value
Coarse powder GLI	8.35 ± 0.35	52.47 ± 4.60	135.21 ± 15.33	2.42
Coarse powder CUR	1.84 ± 0.04	8.70 ± 0.19	29.64 ± 0.83	3.20

Another interesting powder parameter is the surface area. The BET surface area of CUR was measured to be 1.38 m²/g ± 0.17 m²/g, whereas GLI had a five times smaller surface area with 0.27 m²/g ± 0.02 m²/g. This trend could complete the particle size data. The larger, monomodal distributed GLI has less surface area than the polydisperse, smaller CUR. These results indicate that there could be a higher chance of interaction of the stabilisers with CUR as it has a five times higher surface area.

4.4.3.2 ITC results

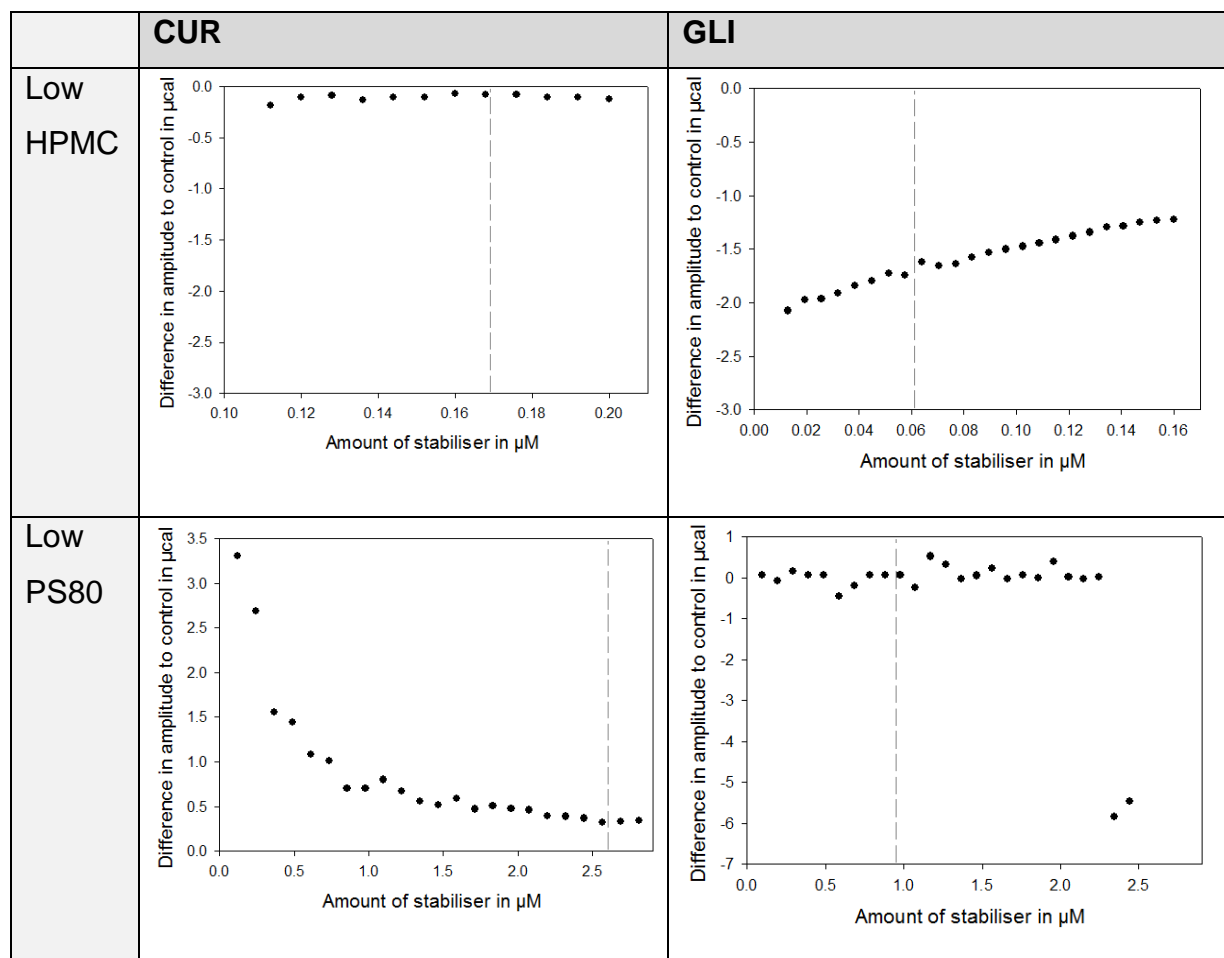
As shown above, already the two control experiments of PS80 and HPMC with the same concentration titrated into water were different (Figure 47). The amplitude for HPMC was with approximately 6 μcal in average three times higher than the 2 μcal amplitude average for PS80. This could mean that HPMC has a higher heat of dilution

than PS80. The heat of dilution got slightly smaller for HPMC and PS80 with increasing number of injections. A demicellisation could also have happened when the stabilisers were titrated into water which should be a process with loss in entropy as the micellisation is attributed to the disruption of the structure of water [Schicke, 2010]. Already these control experiments indicated that titration peaks can be a result of overlaying thermic interactions making a straightforward interpretation of the data challenging.

Usually, in ITC experiments, a concentration should be chosen at which the reaction is supposed to be ended, if a about half to two third of the volume to be injected is added to the cell. Accordingly, for the experiments within this project, the minimal stabilising concentration should be reached when half of the titration steps were performed. To highlight the trend of amplitude change, also higher concentrations were investigated, where the stabilising concentration was found in the beginning of titration.

First, the lower concentrated stabiliser solutions will be compared. In Table 19, the thermal profiles of HPMC and PS80 titrated into CUR and GLI suspensions are displayed. Three different thermal interaction profiles can be seen in this table. The first type is a profile that does not show a change in heat exchange over the whole titration and therefore increasing amount of stabiliser. This means that the drug does not have much effect on the stabilisers' thermometric measurable behaviour in water. Hence, the amplitude difference is fluctuating around 0 μcal . An explanation might be that no thermal interaction between the drug and the stabiliser takes place. Another interpretation approach could be that simultaneous thermal interactions in both endothermic and exothermic direction compensate each other. These thermal profiles were the case for HPMC - CUR and PS80 - GLI interactions. The latter had irregularities in the measurement at the end of the titration with the last two measurement points having a difference in amplitude around -6 μcal . As the titrations were done just once, these signals might be measurement errors. For HPMC - GLI interactions, even less heat was measured than for the control (negative values). With increasing HPMC concentrations the values of the control were approached slightly but not reached. An endothermic process did happen.

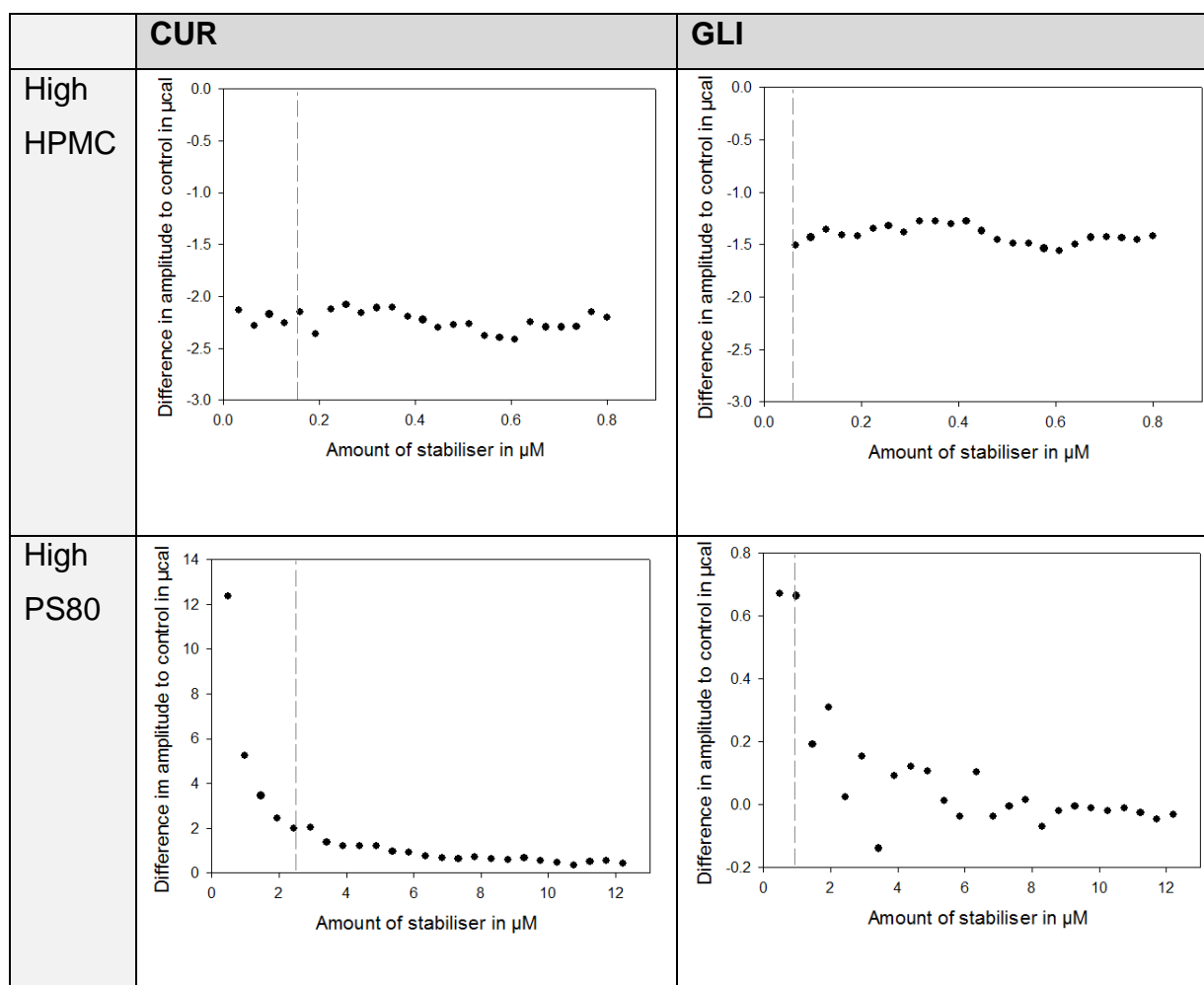
Table 19: Calculated heat interaction profiles of low HPMC (0.8 mM) and PS80 (12 mM) concentrations (16 mg/mL). dashed line indicates minimal stabilisation concentration. n = 1.



A complete different interaction profile was measured for PS80 - CUR. First titration steps showed an increase in amplitude compared to the control which was again approaching the values of the control with increasing stabiliser concentration in an exponential trend. This trend is typical for adsorption processes as first the stabiliser adsorbs onto the drug surface and interaction is decreasing with increasing adsorbed amount until nothing more is adsorbed and the state of the control is reached.

A second ITC setup utilising higher stabiliser concentrations was chosen to investigate whether the thermal interaction trends stays similar (Table 20). When increasing stabiliser concentrations, two thermal profiles changed. While HPMC - GLI interaction appeared to stay on the same level over increasing stabiliser amount, PS80 - GLI titration resulted in a profile that had a more exponential trend than with lower concentrations.

Table 20: Calculated heat interaction profiles of high HPMC (3.2 mM) and PS80 (49 mM) concentrations (64 mg/mL). dashed line indicates minimal stabilisation concentration. n = 1.



Except for HPMC - GLI titration, every magnitude of heat creation or consumption changed. HPMC - GLI and HPMC - CUR interactions both did not return to zero (to the values of the control). This drift from zero was also measured by other researchers in ITC experiments with high surfactant/polymer concentrations [Chiad et al., 2009; Wang et al., 2015]. One explanation proposed was that the temperature of the stabiliser solution and the drug suspension were not exactly the same and therefore a shift of baseline could be seen. As the thermic interactions were generally very low in the experiments for this work (compared to, for example, chemical interactions), this shift should not be over-interpreted but just the change in trend of the titration curves should be discussed.

HPMC did not show an adsorption with any drug or concentration. This could be due to several reasons. One reason could be a non-interaction of HPMC and CUR or GLI. As it is known that HPMC was able to stabilise CUR and GLI nanocrystals during and

after milling, non-interaction of drug and stabiliser is not likely. It is possible that the diffusion of HPMC in ITC experiments could be too slow to be measured while during hours of milling an interaction takes place.

Typical adsorption profiles were found for all PS80 interactions, except for low PS80 - GLI titration. An explanation therefore could be the above mentioned surface area of the two drugs. CUR has a higher surface area, so interaction could be more prominent and therefore, only at higher concentrations of PS80, a trend to an adsorption profile could be seen for GLI. Other approaches could be different surface properties of GLI, so that PS80 is less likely to adsorb compared to CUR. When producing nanocrystals via milling, the surface increases remarkably. Hence, it is likely that PS80 will also adsorb thermodynamically measurable on the new formed GLI surfaces. Unfortunately, the stabilisers could not be separated to full extent from the nanocrystals and also nanocrystals could not be produced without stabiliser as both causes highly agglomerated particles, so that the nano-surface-stabiliser interaction could not be measured with ITC but just the micro-surface-stabiliser interaction. For future experiments the particle sizes of both drugs should be brought to the same level to exclude this factor and just concentrate on the stabiliser interaction.

As this technique should also be investigated as a tool to predict minimal stabilising concentrations, the stabilising concentrations found in milling experiments were marked as dashed line in all figures. This experimental part showed as well that the determined absolute values cannot be used without the experimental frame to discuss interactions. As an example PS80 - CUR interaction shall be mentioned. For low starting concentrations of PS80 the stabilising concentration related to the difference of 0.4 μcal to the control while at high starting concentrations 2.0 μcal were measured. Depending on the starting concentrations, different values were determined but the thermal profile stayed similar. The plateau for the higher concentrations was achieved faster than for the lower concentrations, so that no direct correlation to the minimal stabilising concentrations could be drawn. Nevertheless, it could be shown for CUR, that a concentration of PS80, which is located on the exponential plateau, should always be sufficient enough for stabilisation.

4.4.4 Comparison of contact angle measurements and isothermal titration calorimetry

CAM and ITC display different interaction levels. While ITC measures interactions of stabiliser and drug surfaces, CAM deals with interaction of compressed drug surfaces and stabiliser solutions or the stabiliser self-interaction in water. CAM is detecting wettability where hydrophilic-hydrophobic interactions are most pronounced, while ITC displays interactions like hydrogen bonding or hydrophobic interactions. For nanocrystal stabilisation, hydrophobic interactions between the stabiliser and drug are most common because, typically, drugs are hydrophobic. Furthermore, other kinds of interactions, most importantly hydrogen bonding, can be found.

CAM and ITC results show a higher interaction potential of CUR with both stabilisers compared to GLI. Looking at the possibility of forming hydrogen bonds for the selected stabilisers and drugs, CUR and GLI were found to have similar hydrogen bond counts whereas HPMC has more possibilities to form hydrogen bonds than PS80. These counts for hydrogen bonds were found in a chemical data base (Pubchem) and are listed in Table 21.

It was shown in literature that the polyhydric alcohols of PS80 are capable of forming hydrogen bonds with the hydroxyl groups and hydrogen atoms present in CUR [Sharma et al., 2005] and also HPMC is known to form hydrogen bonds with CUR between the OH groups of HPMC and the CO group of CUR [Li et al., 2017].

Table 21: Calculated hydrogen donor and acceptor count of selected stabilisers and drugs taken from Pubchem.

substances	Hydrogen bond donor count	Hydrogen bond acceptor count
PS80	3	10
HPMC (estimated for a molecular weight of 20,000 g/mol)	126	475
CUR	2	6
GLI	3	5

Eudeng et al. calculated, with molecular dynamics simulations, that HPMC stabilises indapamide better than GLI, through a higher number of hydrogen bonds formed

[Edueng et al., 2017]. Indapamide can be found with 2 hydrogen bond donor counts and 5 acceptor counts, so that it has slightly less counts than GLI. These results indicate that not only the number of hydrogen acceptors and donators might play a role but also molecular dynamics and steric issues, regarding stabilisers and drugs. No direct correlation could be drawn from structural comparisons.

Both methods are fast and sample preparation is simple. Different interaction patterns of HPMC and PS80 with both drugs could be detected and differences between the two methods became obvious. Interaction patterns for HPMC with both drugs were similar in ITC measurements while in CAM they were different. Higher HPMC concentrations led to viscosity increase of the stabiliser solution and therefore, higher contact angles but the molecular interaction detected with ITC stayed similar over different HPMC concentrations because the heat of dilution, which increased at higher concentrations, was eliminated by subtracting the control experiment. CAM could be a useful method to select a certain range of stabiliser concentrations for milling experiments, while ITC experiments gave information about the feasibility of stabilisers in general.

4.4.5 Concluding remarks of stabiliser-drug interaction studies

CAM and ITC could not be used to forecast minimal stabilisation concentration. However, CAM could be utilised to imply 'maximum' stabiliser concentrations of PS80. The concentration that had CAs of approximately 0° were, in the frame of this thesis, mostly sufficient enough for stabilisation. Further, ITC experiments gave information about the feasibility of stabilisers in general and suitable stabiliser concentration, when an adsorption profile was detected. HPMC did not show an adsorption pattern, which could mean that it does not adsorb but just stabilises via viscosity change or that the adsorption is too slow to be measured with ITC. Also, a too low heat change, which could not be detected, could have been a reason. From these three theories, the middle one could be most likely. As the viscosity and concentrations for stabilising were different for GLI and CUR, only the stabilisation via viscosity seems not reasonable. HPMC is a comparably large molecule to PS80 and PS80 leads in most cases to an entropy change of the system, when adsorbing, which should also be the case for HPMC. That is why the theory of slow adsorbing HPMC molecules is plausible. In literature, it was described that the speed of adsorption also has an influence on stabilisation [Kumar Thakur and Kumar Thakur, 2015]. When the adsorption speed is

too slow, a stabilisation of nanosuspensions might not happen during milling, as the stabilisers cannot get fast enough to the newly formed surfaces and therefore aggregation can occur. Stabilisers with high molecular weight can have a decreased diffusion rate of the polymer chains but an increased physical adsorption. So, in the beginning of milling, stabilisers with low molecular weight might be favourable but most of the time this effect disappears upon prolonged milling [Choi et al., 2008]. For the millings in the Dispermat® SL-C 5, HPMC adsorption speed was fast enough but for other high energy millings it might not be sufficient enough. Then PS80 seems to be a better candidate as rapid adsorption patterns could be detected with ITC.

4.5 In-vitro dissolution of suspensions

A drug, which is in a solubilised state, often shows higher bioavailability than a non-dissolved drug. Therefore, dissolution studies can be one tool to predict bioavailability. Nowadays, they are more often used to compare different formulations than to predict bioavailability.

As stated by Noyes-Whitney, a beneficial dissolution can be found with drugs having a large surface area, like nanocrystals. Furthermore, drugs with a small molecular weight (large diffusion coefficient) [Hörter and Dressman, 2001], the right balance between H donors and acceptors as well as low melting points [Lipinski et al., 2001] are favourable for high bioavailability. As the molecular weights and melting points were similar comparing CUR and GLI different attributes of the structure of GLI and CUR lead to different solubility and dissolution profiles as discussed in this chapter.

4.5.1 Solubility in dissolution media

Creating a set-up for dissolution studies includes the investigation of saturation solubility of the drug in dissolution medium as the selected concentration can have an influence on the dissolution. For BCS class I and III drugs the concentration should be $\leq 10\%$ of the saturation concentration (perfect sink-conditions) to avoid an influence of the concentration on the dissolution rate but with poorly soluble drugs from BCS class II and IV the saturation concentration in bio-relevant media is already very low and even lower concentrations might not be detectable. As CUR and GLI face challenges with regard to aqueous solubility, a medium had to be found that provides detectability of the drugs even at short sampling time, meaning a medium in which the drug has sufficient saturation solubility.

The saturation concentration was therefore investigated for eleven different media with varying pH values, to find a suitable medium for each drug (data not shown). For GLI, boric acid buffer with pH 9.4 showed highest solubility while CUR was best soluble in acetic acid buffer at pH 4. Considering the bio-relevance of these media, a phosphate buffer (pH 8) was additionally investigated. A common practice to increase solubility in dissolution media is an addition of surfactants. In this study, the coarse powder of the respective drug was chosen as the reference for the produced nanosuspensions. As the nanosuspensions include stabilisers and the influence of these stabilisers should also be investigated throughout this thesis, an addition of external surfactants was avoided. Values for saturation solubility (ss) of the selected media and 'internal' stabilisers can be seen in Table 22.

Table 22: Saturation solubility (ss) of CUR in acetic acid buffer and GLI in boric acid buffer as well as phosphate buffer with and without the addition of stabilisers. n = 3. \pm = SD.

Acetic acid buffer	ss CUR in $\mu\text{g/mL}$	Boric acid buffer	ss GLI in mg/mL	Phosphate buffer	ss GLI in mg/mL
Without stabiliser addition	0.31 ± 0.00	Without stabiliser addition	0.54 ± 0.06	Without stabiliser addition	0.022 ± 0.0017
With 25 % HPMC	0.87 ± 0.12	With 10 % HPMC	0.55 ± 0.09	With 10 % HPMC	0.024 ± 0.0015
With 12.5 % HPMC + 12.5 % PS80	7.63 ± 0.83	With 2.5 % HPMC + 2.5 % PS80	0.59 ± 0.02	With 2.5 % HPMC + 2.5 % PS80	0.050 ± 0.0025

Depending on the drug, the solubility changes in dependency on the stabiliser. The increase in solubility is most pronounced for CUR with the addition of HPMC and PS80. A 24.6 times increase could be determined, while for GLI a rise of 2.3 in phosphate buffer was detected. When the solubility was already comparably high in the dissolution medium without the addition of stabiliser, like for GLI in boric acid buffer, the influence of the stabiliser was minimal. As dissolution rate is a function of saturation solubility, it

can be expected that the dissolution rate of the coarse drugs will be influenced by the stabilisers.

4.5.2 Dissolution of coarse suspension

CUR coarse powder dissolution was very poor as can be seen in Figure 50. Only $8.15\% \pm 1.93\%$ of saturation concentration did dissolve after 24 hours (1,440 min) even with the addition of stabilisers. After the experiment, non-dissolved powder could be seen floating on the dissolution medium. So, just approximate 0.023 mg of the roughly 1.4 mg CUR got dissolved (0.28 mg would be 100 % dissolved drug).

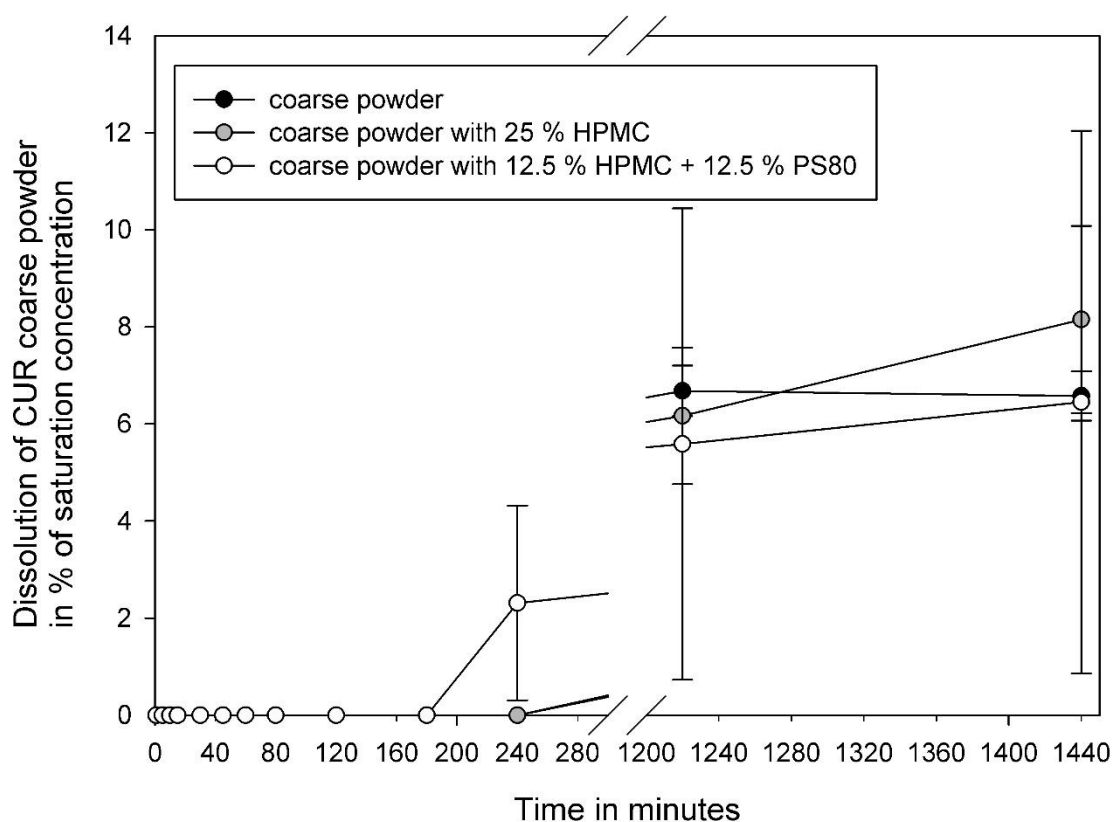


Figure 50: Dissolution of coarse CUR powder with and without the addition of stabilisers at 5 times saturation concentration in acetic acid buffer. n = 3. error bars = SD.

The coarse suspension of GLI showed a dissolution extent of $79.50\% \pm 2.11\%$ to $95.98\% \pm 1.27\%$ in boric acid buffer within 24 hours. So, approximate 25.9 mg were maximal dissolved from the applied 27 mg of GLI. When comparing the dissolution profiles in the first 200 minutes, HPMC and HPMC + PS80 addition changed the velocity and magnitude of dissolved drug which is plotted in Figure 51. In boric acid buffer pH 9.4, the stabilisers seemed to have a decelerating effect on the dissolution

rate of GLI. An addition of 2.5 % HPMC + 2.5 % PS80 to the dissolution medium decreased dissolution rate approximately by half at 200 minutes. 10 % HPMC addition lead to 17 % less solubilised amount of GLI after 200 minutes.

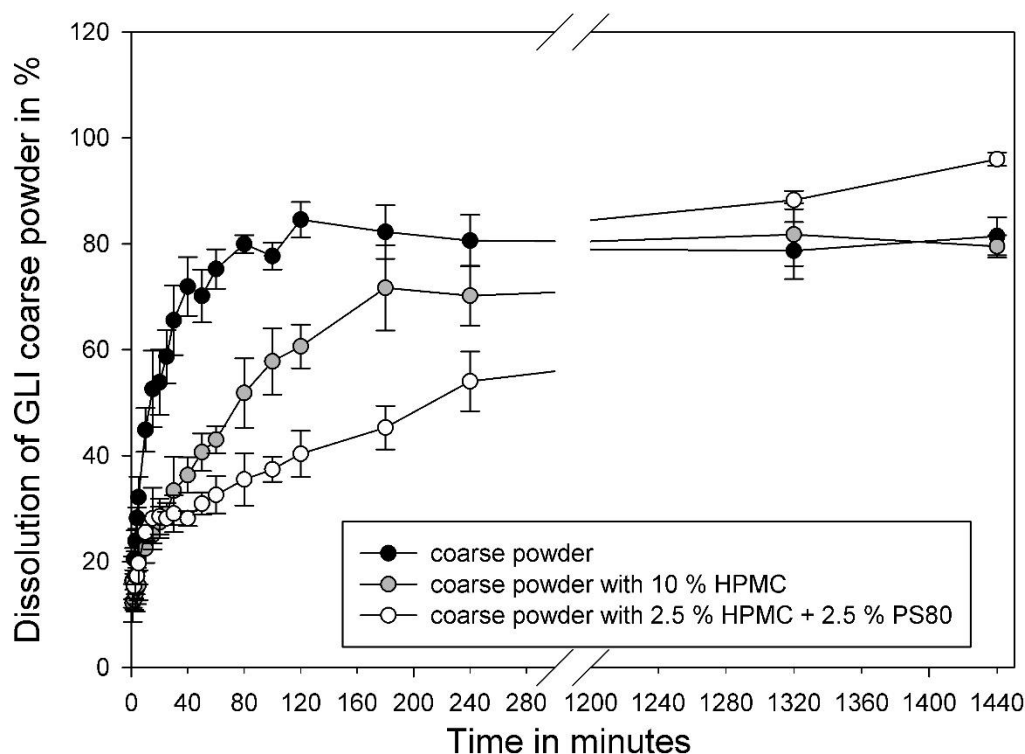


Figure 51: Dissolution of coarse GLI powder with and without the addition of stabilisers in boric acid buffer at perfect sink conditions. n = 3. error bars = SD.

After 24 hours, the dissolution of powder with 10 % HPMC was with 79.50 % \pm 2.11 % dissolved drug on a similar level as the coarse powder (81.45 % \pm 3.58 %) and the powder with 2.5 % HPMC and 2.5 % PS80 achieved 95.98 % \pm 1.27 % dissolution. This trend was not expected as surfactants or tensides are commonly used to increase solubility and wetting of drugs in dissolution media. For this purpose, usually SDS but also PS80 is used. Nevertheless, the phenomenon that stabilisers also lead to a decrease of dissolution was also found by a small number of other researchers. Chen et al. discovered that low PS80 concentrations slowed down the dissolution of their tested compound in 0.1 N HCl, while high concentrations led to an increase in dissolution [Chen et al., 2003]. Their proposal for the mechanism was that below CMC of PS80, there was an increase of the formation of insoluble chloride salt of their drug on the surface of their compound due to surface tension reduction, while for concentrations above CMC other factors played a more important role like adsorption

so that the dissolution was higher. These literature results raised the question of CMC values of the stabilisers in this thesis. Hence, the CMC of PS80 and HPMC was determined. Stabilisers, that form micelles, should have a long hydrophobic chain and a polar head group. This structure subdivision can be seen for PS80, while HPMC as polymer does not form typical micelles. From literature review it is expected that HPMC forms some kind of clusters or even fringed micelles [Müller, 2010]. In this work, the determined CMC of PS80 in water was 5 - 10 µg/mL and 2 - 10 µg/mL for HPMC. In general, the CMC of non-ionic surfactants should not be much affected by the presence of a buffer so that it can be assumed that HPMC and PS80 concentrations in dissolution studies (0.75 µg/mL for PS80 and 2.99 µg/mL for HPMC) were for PS80 below the CMC. This could be an influencing factor on dissolution. Contrariwise Li et al. experienced that an addition of PS80 (87.8 µg/mL) to their dissolution medium (water) decreased dissolution of carbamazepine. They suggested that PS80 formed an interfacial barrier which hindered the drug's dissolution and resulted in nucleation and growth of the applied crystals with the formation of carbamazepine dehydrate [Li et al., 2013]. Seedher et al. found, that PS80 lowered the dissolution rate of GLI in 0.1 M phosphate buffered solutions (pH 7.4) compared non-buffered solutions even though hydrogen bonds between water and PS80 should be decreased in the presence of a buffer so that PS80 should have higher interaction potential with the drug [Seedher and Kanojia, 2008]. All in all, PS80 was found in most publications as a dissolution rate enhancer. In this selected paper, the dissolution rate decreased when certain amount of PS80 was applied, like it was seen in this thesis. The buffer salt concentration might play a role and/or an interfacial barrier formation and nucleation of the drug.

A second dissolution medium was used to evaluate, if the influence of the stabilisers was the same and also to create a more bio-relevant condition than a boric acid buffer with a pH of 9.4. That is why a phosphate buffer with a pH of 8 was chosen for further investigations (see Figure 52). Phosphate buffers with even lower pH values, which would be more physiological, did lead to a drop in solubility so that the determination with HPLC was difficult. Therefore, a compromise between bio-relevant and precise content evaluation was chosen with the phosphate buffer of pH 8.

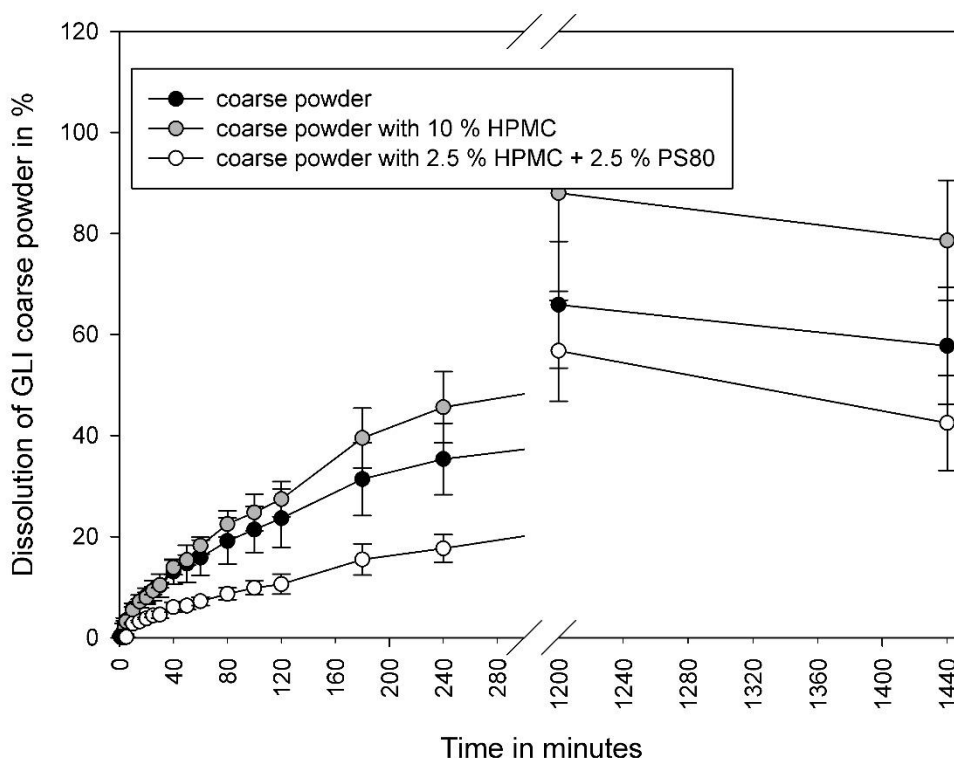


Figure 52: Dissolution of coarse GLI powder with and without the addition of stabilisers in phosphate buffer at perfect sink conditions. n = 3. error bars = SD.

With this dissolution medium, two differences could be detected. First of all, as the solubility was lower in this medium also the dissolution was slower than in boric acid buffer. Secondly, an addition of HPMC lead to fastest and highest dissolution followed by stabiliser free medium and phosphate buffer containing HPMC as well as PS80. Regarding HPMC, a formation of a gel layer around the GLI particles in boric acid might be possible and therefore an increase in diffusion layer. The salt concentration in phosphate buffer is different compared to boric acid buffer as the ionic strengths were calculated with 150 mM/L and 640 mM/L, respectively. Until today, the ion formation in boric acid buffer is not totally understood, so that an interaction with HPMC cannot be linked to one specific ion in the solution. Assuming that the buffer system has equal amounts of HB_4O_7^- and $\text{B}_4\text{O}_7^{2-}$ [Thorsten, 2013] an ionic strength can be calculated with 640 mM/L. Similarities with literature data could be found as Kavanagh et al. investigated the decrease in erosion rate of HPMC with a high molecular weight and explored an increase of erosion rate with high ionic strengths [Kavanagh and Corrigan, 2004]. They attributed this phenomenon to the ‘salting out’ of the polymer by the inorganic ions present in the dissolution media with the polymer’s molecular chains loosing water of hydration due to the ions competing for the available water of

hydration. This process could also have happened in this thesis even that different molecular weights for HPMC were used.

Consequently, it could be concluded that CUR has very low dissolution rate in acetic acid as well as low solubility in all tested media. As the dissolution rate was low, an addition of stabiliser did not change the dissolution pattern. For GLI, depending on the buffer, stabilisers had varying influences on solubility and dissolution.

4.5.3 Dissolution of nanosuspensions

CUR formulated as nanosuspension had an advantage in dissolution rate over the coarse powder as demonstrated in Figure 53.

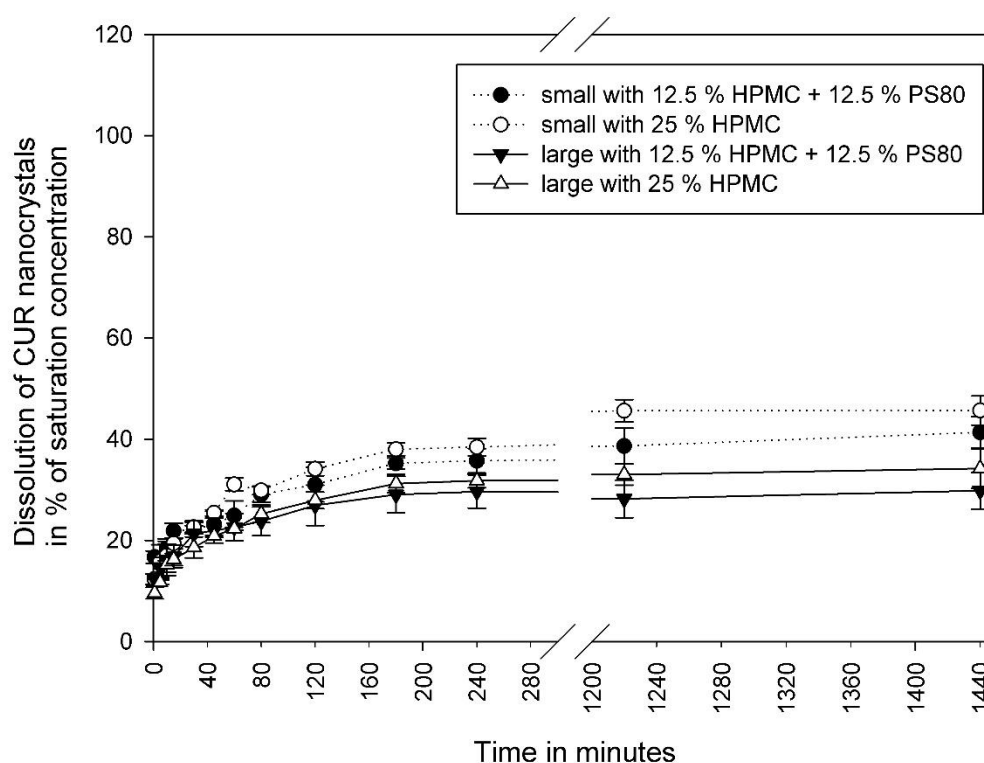


Figure 53: Dissolution of CUR nanosuspensions in acetic acid buffer at 5 times saturation concentration. n = 3. error bars = SD.

Compared to coarse powder, which did not show any dissolution in the first 4 hours, the nanosuspensions exceeded a value of approximate 29 % dissolution (with the saturation concentration being 100 %) after 4 hours. A trend for the influence particle size could be seen as smaller nanocrystals had faster and higher dissolution than larger nanocrystals. Furthermore, the influence of stabilisers was comparable between small and large nanocrystals. Nanocrystals stabilised with HPMC, led to slightly faster

and higher dissolution than a combination of HPMC and PS80 which can be linked to the saturation solubility of the drug which is with 0.00087 mg/mL in 25 % HPMC-acetic acid solution lightly higher than in 12.5 % HPMC + 12.5 % PS80-acetic acid solution (0.000763 mg/mL). The percentage is again related to the amount of drug which was used in the suspension. After 24 hours still just 29.82 % \pm 3.60 % to 45.66 % \pm 2.85 % were dissolved, so that no saturated solution could be achieved. So, from the applied 1.44 mg just 0.08 mg - 0.13 mg got dissolved (0.28 mg would be 100 % dissolved drug).

GLI dissolution was expected to be faster for the nanocrystals as even the coarse suspension had a comparably fast dissolution in boric acid and phosphate buffer. This expectation was met as can be seen in Figure 54 and Figure 55. All nanosuspensions exhibited dissolution of 76.61 % \pm 1.18 % to 80.78 % \pm 12.65 % after 5 minutes in boric acid buffer and 82.21 % to 91.90 % \pm 3.82 % in phosphate buffer. So, in boric acid buffer 20.7 mg - 21.8 mg from the applied 27 mg got dissolved, while in phosphate buffer it were 4.93 mg - 5.51 mg from 6 mg. In the first two hours no clear difference between different sizes or type of stabilisers could be seen.

At the end of the dissolution study in both media a slight difference between the types of stabiliser was measured, with HPMC + PS80 stabilised nanosuspensions showing a higher percentage in dissolution. This difference was more pronounced in boric acid buffer. Here, also a difference in particle size can be seen as small nanocrystals led to higher dissolution values.

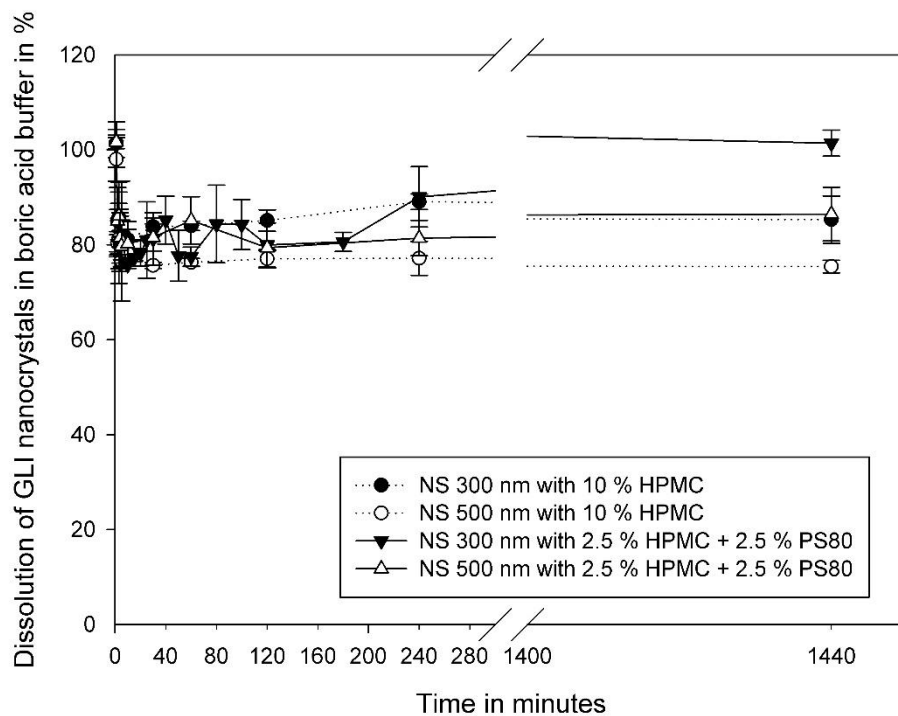


Figure 54: Dissolution of GLI nanosuspensions in boric acid buffer at perfect sink conditions. n = 3. error bars = SD.

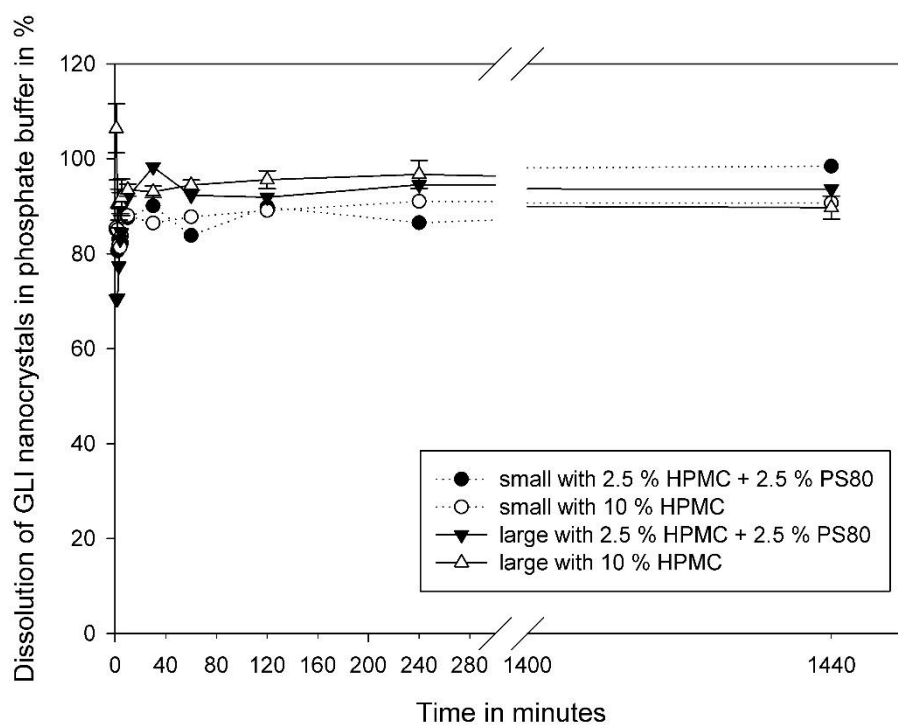


Figure 55: Dissolution of GLI nanosuspensions in phosphate buffer at perfect sink conditions. n = 3 for large nanocrystals stabilised with 10 % HPMC; all others n = 1. error bars = SD.

4.5.4 Concluding remarks of dissolution studies

All in all, the formulated nanosuspensions could increase dissolution rate to a higher level. Especially when the solubility in dissolution medium was low, the increase in dissolution rate was eminent when comparing nanocrystals and coarse powder. After 4 hours, the increase in dissolved amount from CUR coarse powder with HPMC and PS80 addition to small nanocrystals with the same amount of stabiliser was changing from 0 mg to 0.1 mg (of the applied approximate 1.4 mg). For GLI, these suspensions led to a 5 times increase in dissolved amount from 1.06 mg to 5.19 mg in phosphate buffer (of the applied approximate 6 mg).

For poorly soluble substances like CUR also the type of stabiliser plays a role in dissolution of nanosuspensions. The influence was, in this thesis, not as high as the particle size but it definitely has to be kept in mind in formulation development as most companies have their standard set of well investigated stabilisers. If there is no comparison done between different stabilisers, it could be the case of a non-fulfilment of the maximum benefit of nanosuspensions as a dosage form. For companies, it saves time to run a standard program but for promising drugs, which are known to be able to have a high value in therapy and which fail to get to clinical trials because of low bioavailability, the choice of stabiliser should be reconsidered.

Also, the stabiliser influence on the coarse powder should be explained. As CUR showed low dissolution rates, no influence could be detected. For GLI, different dissolution media had changing influence on the dissolution after stabiliser addition to the coarse powder. In boric acid buffer, addition of any stabiliser led to a decrease in dissolution rate while in phosphate buffer, HPMC addition did increase the dissolution rate and the extent of dissolution. Different pH values and salt concentrations could play a role.

Dissolution can usually not display/predict bioavailability but show a comparison of different kinds of formulations. Nevertheless, especially for BCS class III (and IV) sufficient dissolution profiles can be measured but permeation through tissues is low, so that dissolution as a forecast to bioavailability is limited. Hence, the investigation of the permeation of the two chosen model drugs through cellular barriers was examined for this thesis as well and results can be found in the next chapter.

4.6 Transport of drugs through epithelial cells

The assessment of transport of drugs through epithelial cells is one way to predict bioavailability of this drug from a formulation. In this work, the permeation of nanocrystals was investigated with a transwell system, in order to answer the question if the drug is transported in a dissolved state or even in a particulate form.

In the first step, the used transwell system had to be validated, followed by first experimental approaches to, in the end, investigate the influence of particle size, type of stabiliser and type of drug on the permeation.

4.6.1 Validation of the Caco-2 transwell model

Depending on the cell culture lab, the person who is handling the cells, the used equipment, the environment conditions and passage numbers of the cells, the outcome of cell experiments can be very different. That is why a validation is of major importance.

Three factors are commonly used in combination to create comparability between cell experiments with transwells. The transepithelial electrical resistance (TEER) displays integrity of the cell monolayer on the transwell membrane. When a monolayer is formed, the TEER should gradually increase until a plateau is reached at cell confluence. Two different pore sizes for the membranes were used in this work (1 μm and 3 μm pore sizes, respectively) which TEER values are presented in Figure 56.

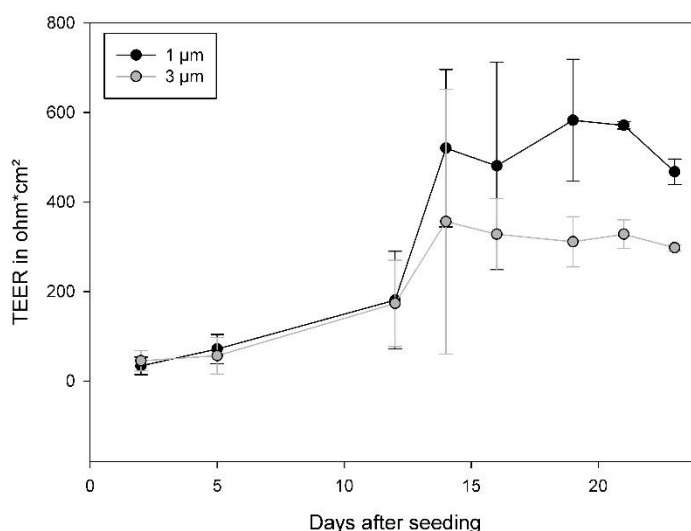


Figure 56: TEER value development over 23 days of cell growth on transwells; starting seeding density was 100,000 cells/cm² of Caco-2 cells. n = 3. error bars = SD.

For 3 μm transwells, all TEER values above 300 $\Omega\cdot\text{cm}^2$ indicated an intact monolayer while for 1 μm pore size transwells the minimum value was set to 500 $\Omega\cdot\text{cm}^2$. Below these values the experiment was not started. Further preliminary studies investigated the TEER value as a marker for integrity of the monolayer during the transport experiment (data not shown). The maximum specification border was set at a difference of 100 $\Omega\cdot\text{cm}^2$ regarding the TEER values before and after the experiment. Every well that showed higher negative difference was excluded from evaluation.

As drugs and stabilisers have an influence on the TEER value and the cells could not be totally cleaned from suspension that got stuck to the cell surface, another marker was included in the validation process. Lucifer yellow (LY) permeation is a better way to show a tight contact of cells after experiments: the lower the LY permeation the tighter the contact of the cells was. LY permeation results are displayed in Figure 57.

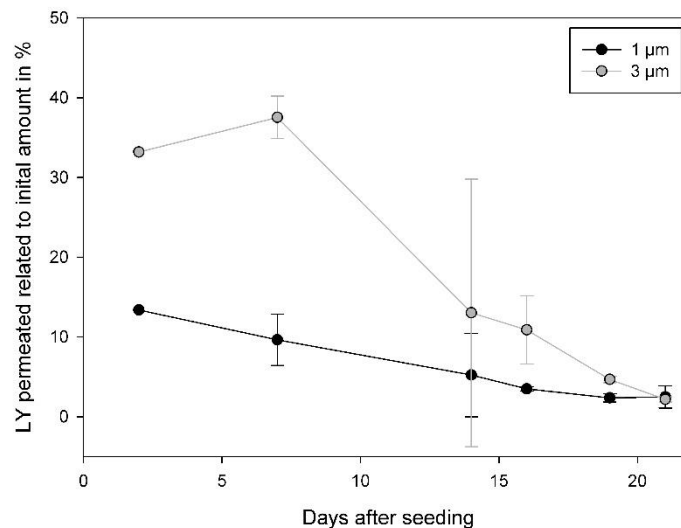


Figure 57: Paracellular permeation of lucifer yellow through Caco-2 cells during growing period of 21 days. starting seeding density was 100,000 cells/cm². n = 2. error bars = min/max. initial amount = 0.1 mg/mL.

As the cells grow, the connection to each other closes up. From the diagram above, the conclusion was drawn that if a LY permeation of 5 % or lower compared to the initial LY amount was determined, the monolayer could be considered as intact. All transwells that had a higher permeation of LY at the end of the experiment and did not show TEER values above the specified values were excluded from evaluation and the experiment was repeated. When the permeation of LY increased over 10 % the well was not evaluated even though the TEER value was in specification.

The next step for validation was the selection of a permeation marker. On every transwell plate one marker should be included in the experimental setup to exclude inter-day variability. Atenolol was selected as permeation marker. Atenolol is a poorly permeating substance through Caco-2 monolayers. Toxicity of atenolol (1.5 mM) was tested and no toxicity could be detected over 24 hours in transport buffer as well as in cell culture medium (data not shown).

As suspensions were investigated for permeation, the incubation time was extended to 24 hours because the uptake time for particles can be much higher than for molecules. This created a new problem. Normally, in transport experiments, a buffer is used as transport medium. Unfortunately, it was seen that an incubation of Caco-2 cells with transport buffer for 24 hours led to a complete disconnection of cells (TEER value on the same level than filter without cells and high LY permeation) and also a 15 % loss in viability was measured in MTT tests, so that another transport medium had to be found for 24 hour studies. For this purpose, full cell culture medium was tested. For medium, LY permeation was in specification and also the atenolol permeation was on the similar level at 3 hours and 24 hours incubation (data not shown). Nanocrystals sizes were measured to have similar sizes in transport buffer and cell culture medium as plotted in Figure 58.

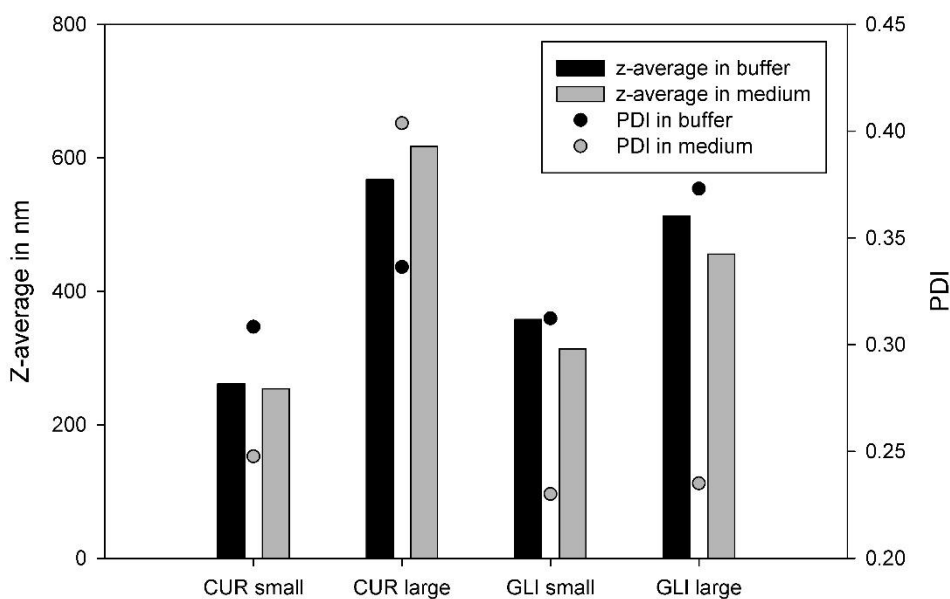


Figure 58: Particle size (bars) and particle size distribution (PDI; dots) of the same CUR and GLI nanosuspensions in buffer or medium. n = 1.

Differences could be observed for the particle size distribution as in buffer, PDI values were higher than in medium with the exception of the one selected example of large CUR nanocrystals.

4.6.2 Experimental approach for method set-up

The transport of GLI and CUR through different cell lines has already been investigated. Due to the low solubility of CUR some authors used organic solvents, heat or alkali solubilisation to prepare solutions that were investigated for their transport ability through Caco-2 cells [Zhen et al., 2017; Wahlang et al., 2011]. These preparations however do not mimic the in-vivo situation, thus physiological media should be utilised in this thesis.

For GLI, exemplary apparent permeability coefficients of 2.16×10^{-5} cm/sec [Zerrouk et al., 2006] and 2.6×10^{-5} cm/sec [Jiang et al., 2015] were found in literature. CUR has exemplary, with $1.13 (\pm 0.11) \times 10^{-6}$ cm/sec [Zhen et al., 2017] or $2.93 (\pm 0.94) \times 10^{-6}$ cm/sec [Wahlang et al., 2011] a slower permeability rate, which is why it is categorised into BCS class IV.

Data values in this and the following chapter will be plotted as permeation of the drug related to atenolol ($\frac{100}{P_{app\text{atenolol}}} \times P_{app\text{drug}}$).

First transport studies were conducted to test the range of permeation and feasibility of used concentrations and setup. The difference in permeation of the tested suspensions is visible in Figure 59 and Figure 60. CUR proved to be a drug with low permeability through intestinal barriers. No permeation could be seen in buffer even for the small nanocrystal suspension after 5 hours. Likewise, the coarse suspension in medium did not show any permeation. Just small nanocrystal formulations were able to permeate but still the permeation in medium was, after 24 hours, with $3.80 \% \pm 1.27 \%$ to $4.46 \% \pm 0.00 \%$ of atenolol permeation very low. As atenolol itself is categorised as low permeable and CUR nanocrystal formulations merely were able to reach 4.46 % of this permeation, the improvement from 0 % for coarse powder to 4.46 % for nanosuspension formulation might not be relevant for the pharmaceutical industry.

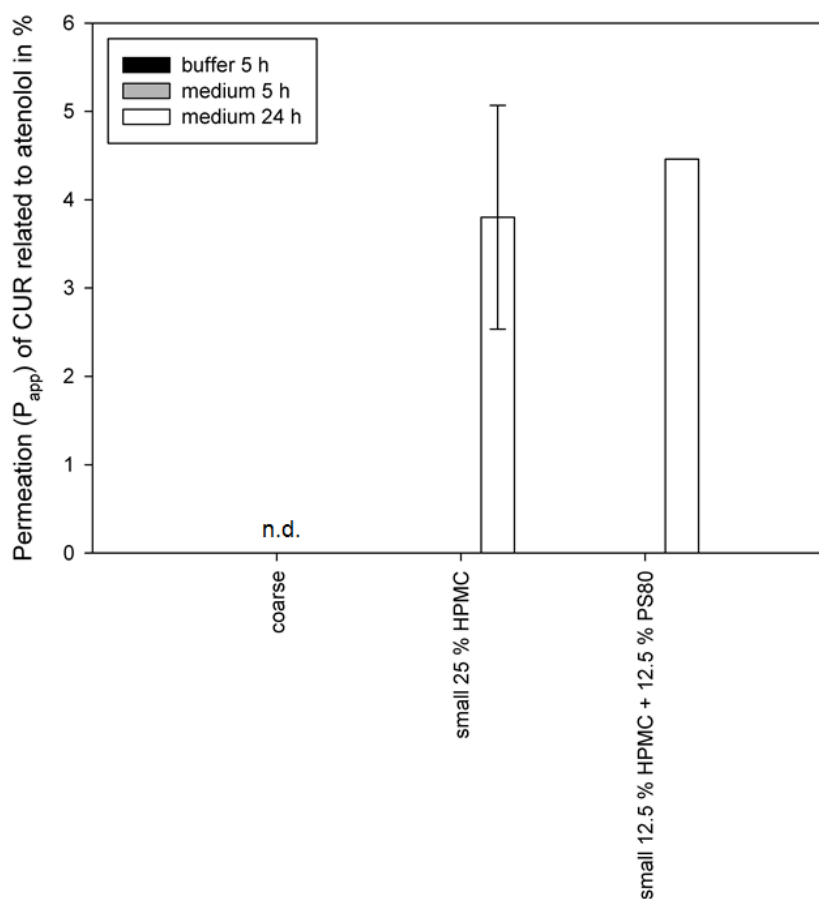


Figure 59: Permeation of CUR coarse suspension and small nanosuspensions in buffer and cell culture medium related to permeation of atenolol under the same conditions. The P_{app} of atenolol was set to 100 %. Pore sizes of 1 μm and different incubation times (5 h and 24 h) were investigated. $n = 2$. error bars = min/max

CUR is not a highly potent drug for which a small increase in permeation could improve treatment to a high extent. Furthermore, at this low value, a stabilisation with HPMC or HPMC + PS80 did not make a difference in permeation.

The permeation through 3 μm pore sized transwells was measured to be even lower than for 1 μm (data not shown). This could be due to different monolayer formation on the membrane. In microscopic images it could be seen that cells were growing within the pores of 3 μm diameter so that they were not free for particle/substance transport while for the 1 μm pore sized transwells a smooth monolayer growth was observed.

GLI was expected to have a different permeation pattern than CUR as it belongs to BCS class II and therefore, should be highly permeable. The values in Figure 60 confirmed this expectation.

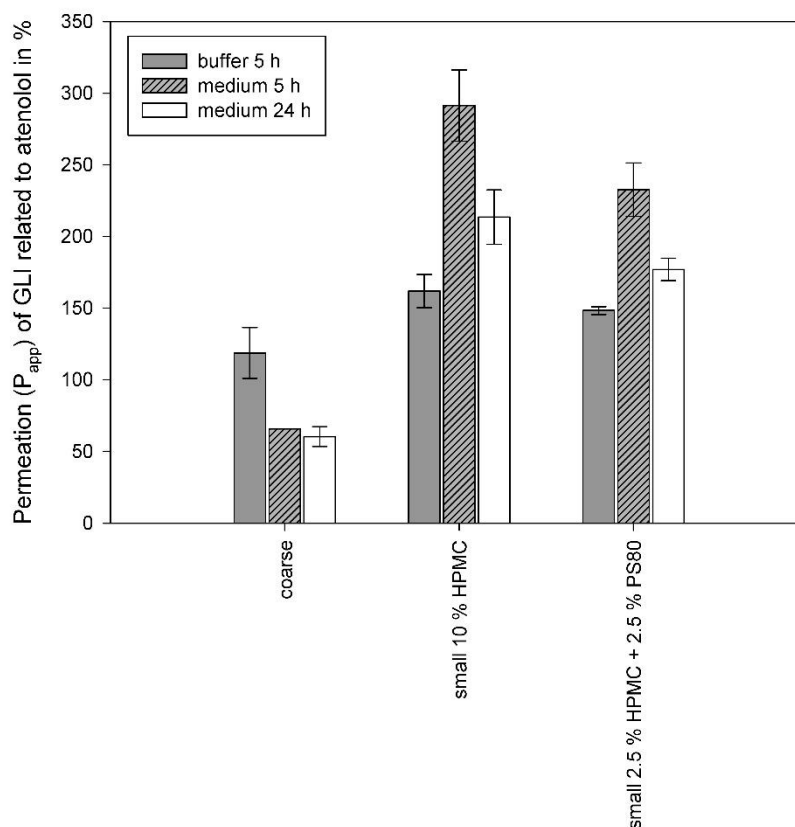


Figure 60: Permeation of GLI coarse suspension and small nanosuspensions in buffer and cell culture medium related to permeation of atenolol under the same conditions. The P_{app} of atenolol was set to 100 %. Pore sizes of 1 μm and different incubation times (5 h and 24 h) were investigated. $n = 2$. error bars = min/max

Again, the coarse suspension was lower in permeation than the nanocrystal formulations. In comparison to CUR, GLI achieved with 60.36 % \pm 6.83 % to 291.42 % \pm 24.89 % even a higher permeation than atenolol. The permeation through 3 μm pore sized transwells was again lower than through 1 μm pores.

As GLI is a good permeable substance, the achieved low values for coarse suspension permeation were taken as a hint that for GLI, the dissolution rate plays an important role for the amount of permeation. That is why the comparison of dissolution rate in buffer and medium for all tested suspensions and the corresponding permeation rate are described in chapter 4.6.4 in more detail.

As outcome of the preliminary studies, shown in this chapter, detailed permeation studies were planned. Therefore, for CUR, medium was taken as transport fluid and permeation over 24 hours was of interest. For GLI, buffer and medium were taken as transport fluids but buffer not for 24 hour studies.

4.6.3 Permeation comparison of coarse drug suspensions and nanosuspensions

Chapter 4.6.2 contains the findings for usable transwell setups, so that following experiments could be created to investigate the influence of stabiliser, drug, particle size and time on the permeation of drug being formulated as nanosuspension through Caco-2 cells.

For CUR, all these influences are depicted in Figure 61. Up to 5 hours, no CUR permeation could be detected. Thus, the permeation was not calculated from several values as a typical permeation rate but from the permeated amount after 24 hours. Furthermore, the size has a high impact. Particles in the micrometer range showed lowest permeation in average, followed by 300 nm nanocrystals and highest permeation was achieved with 500 nm sized nanocrystals.

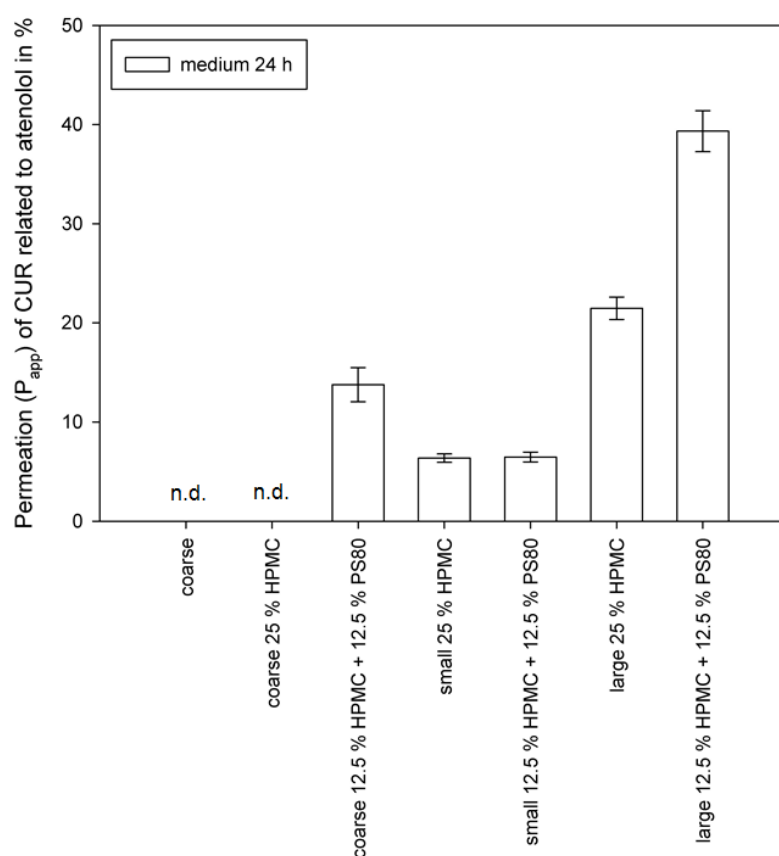


Figure 61: Permeation of CUR coarse suspension, small and large nanosuspensions in cell culture medium related to permeation of atenolol under the same conditions. The P_{app} of atenolol was set to 100 %. Filter pore size was 1 μm and permeation was measured over 24 h (sampling time points: 1 h, 3 h, 5 h and 24 h). $n = 2$. error bars = min/max.

The influence of the stabilisers was varying. For microcrystals and large nanocrystals HPMC - PS80 combination increased permeation while for small nanocrystals the combination was not benefiting compared to a stabilisation just with HPMC (6.47 % \pm 0.50 % and 6.36 % \pm 0.42 %, respectively).

For GLI, permeation was also detected between 1 and 5 hours of incubation, presented in Figure 62. The trend of particle size influence was similar to CUR. Permeation rate increased from coarse powder, over small nanocrystals to large nanocrystals.

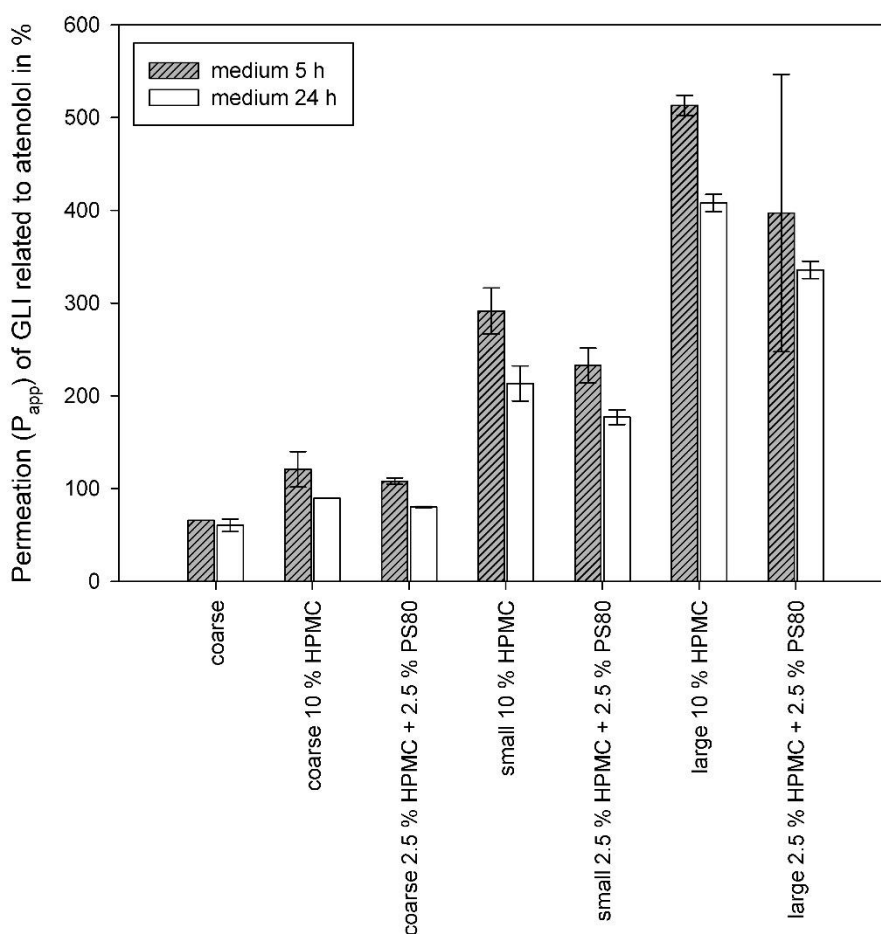


Figure 62: Permeation of GLI coarse suspension, small and large nanosuspensions in cell culture medium related to permeation of atenolol under the same conditions. The P_{app} of atenolol was set to 100 %. Filter pore size was 1 μ m and permeation was measured over 5 h and 24 h (sampling time points: 1 h, 3 h, 5 h and 24 h). n = 2. error bars =min/max.

The impact of stabilisers was opposed to CUR. HPMC, as a stabiliser, led to higher permeation rates. The difference does not appear to be high in this figure as permeation is much higher in general but when comparing, for example, the small

nanocrystals after 5 hours, stabilisation via HPMC (291.42 % \pm 24.89 %) led to 25 % higher permeation than stabilisation with HPMC and PS80 (232.68 % \pm 18.69 %).

The amount of stabiliser was not comparable between GLI and CUR as minimal stabilisation concentrations, as results from milling experiments did vary. Therefore, also GLI nanocrystals, stabilised with HPMC and PS80, with half of the HPMC stabilisation concentration were produced and tested for permeability to have a better comparison between CUR (25 % HPMC and 12.5 % PS80 + HPMC) and GLI (10 % HPMC and 5 % PS80 + HPMC). Results are plotted in Figure 63.

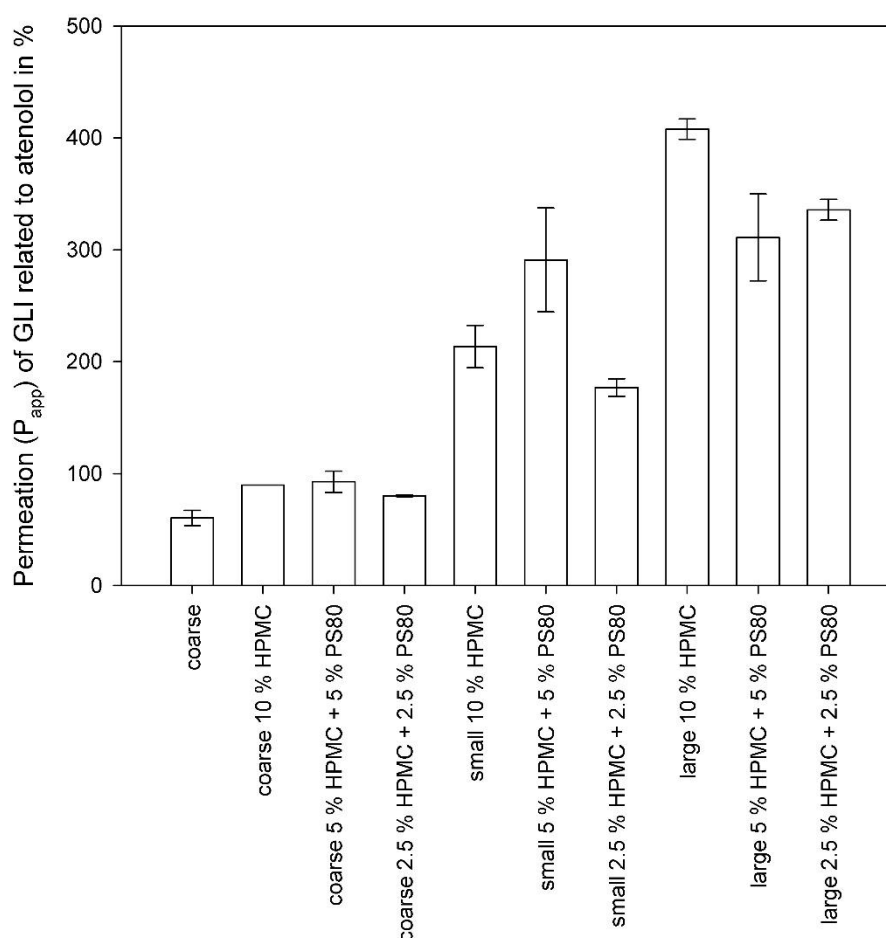


Figure 63: Permeation of GLI coarse suspension, small and large nanosuspensions in cell culture medium related to permeation of atenolol under the same conditions. The P_{app} of atenolol was set to 100 %. Filter pore size was 1 μ m and permeation was measured over 24 h (sampling time points: 1 h, 3 h, 5 h and 24 h). $n = 2$. error bars =min/max.

The permeation of the newly produced GLI suspensions was performed over 24 hours and in medium to have the same conditions as for CUR. Different trends regarding the influence of stabilisers could be seen comparing the coarse, small and large

suspensions. For the coarse suspensions, all stabiliser concentrations did increase the permeation rate but the influence of the stabilisers was marginal. For small nanocrystals stabilised with 5 % HPMC + 5 % PS80 mixture, the highest permeability could be detected (291.03 % ± 46.47 %) followed by the HPMC stabilised nanocrystals (213.51 % ± 18.93 %) and the 2.5 % HPMC + 2.5 % PS80 mixture (177.00 % ± 7.83 %). For the large nanocrystals, HPMC stabilised nanocrystals still showed, with 407.91 % ± 9.22 %, highest permeation and the added 5 % HPMC + 5 % PS80 mixture stabilised nanocrystals had similar permeation to the nanocrystals stabilised with the half concentrated mixture (311.23 % ± 38.80 % and 335.78 % ± 9.29 %, respectively). The nano-formulations created in this work could increase the permeation of GLI through intestinal barriers up to 7.8 times.

In comparison to CUR, the increase of the stabilising concentration mixture to half of the HPMC concentration led to similar permeation results regarding the small nanocrystals. The mixture showed highest permeation. For the large nanocrystals, HPMC alone stabilised nanocrystals showed highest permeation while for CUR the stabiliser mixture resulted in a higher permeation.

Additionally to 'normal' A-B transport studies also the transport from the basolateral to the apical compartment was measured. The ratio between the two permeability coefficients could then be used as a first indicator of possible involvement of an active transport process. For CUR, no permeation from B to A could be detected up to 24 hours in medium. GLI showed varying permeability coefficients. For the determination of the coefficient, every P_{app} value was again related to atenolol whereby the average of all conducted transport studies was chosen to calculate the average atenolol P_{app} for A-B (2.014×10^{-7} cm/sec) and B-A (1.897×10^{-7}), respectively. Results of the permeability coefficient are plotted in Figure 64. The value of 1 displays equal permeation values for A-B and B-A. Formulations with values above 1 have a higher permeation from A-B than from B-A and vice versa.

First of all it shall be mentioned that as for every experiment a 1 mM suspension was used, the solubility of GLI should be the same for A-B and B-A studies. Hence, the permeability coefficient should be also similar. It might be the case for the coarse suspension that the layer that was seen to settle on the cells at transport studies from A-B hindered the transport of solubilised drug. Hence, when the drug was settling on the bottom of the basolateral compartment at B-A studies, a higher transport could be

detected. 5 % HPMC + 5% PS80 stabilised nanosuspension display an exception. As the transport studies from B-A were just conducted once this could be a measurement error.

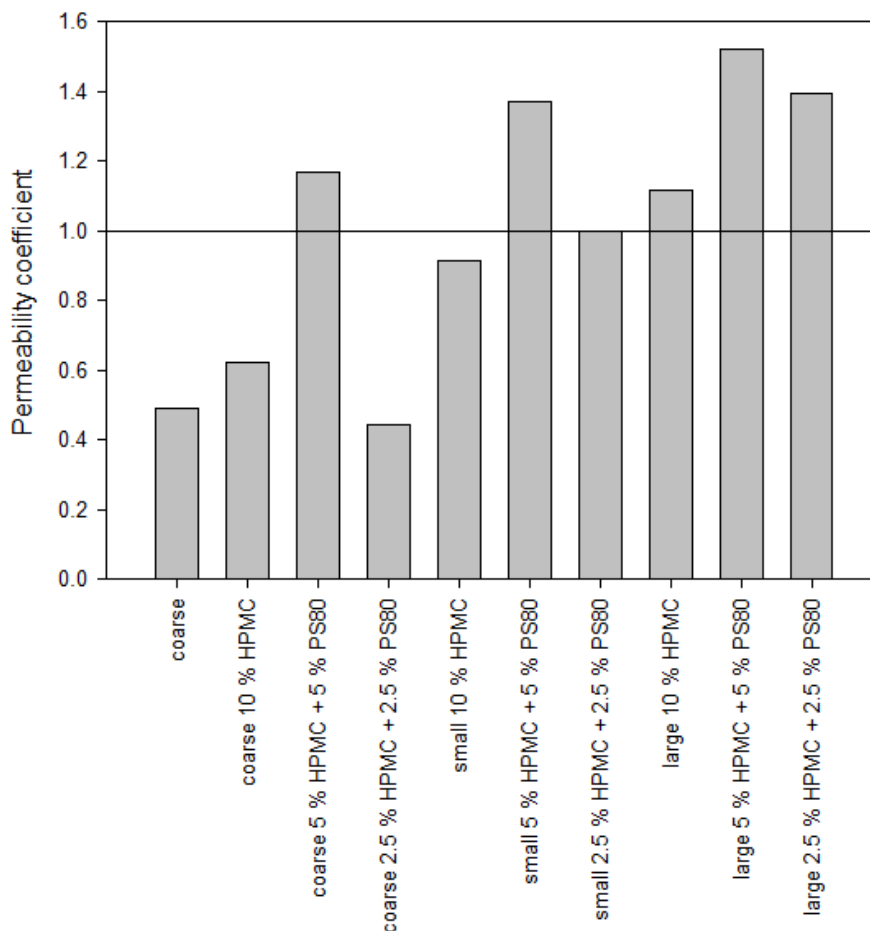


Figure 64: Permeability coefficients of 1 mM GLI suspensions. Permeation was measured from A–B and B-A for 24 hours in medium. P_{app} values of GLI were related to average atenolol P_{app} values before the coefficient was calculated. Filter pore size was 1 μm . $n = 1$.

All nanosuspensions show a coefficient above 0.9 so that most nanosuspensions (values above 1) have a higher permeation from A-B than from B-A. The 5 % HPMC + 5 % PS80 stabilised nanosuspension had enhanced transport from A-B compared to the other nanosuspensions. Larger nanosuspensions had a higher coefficient compared to small nanosuspensions. The differences in the coefficient can be explained by local changing concentration gradient around the Caco-2 monolayer. When particles are settling onto the membrane the concentration gradient in direct contact to the cell surface might be higher compared to equally distributed particles in the compartment. As just a small amount of large nanocrystals might be settling on the cells no repression of permeation could be seen like for the coarse suspensions.

4.6.4 Dissolution rate of drugs at transport study conditions and inclusion in permeation results

One possibility to investigate, whether particles or just molecules permeated through Caco-2 monolayers, is to compare the solubility at sampling time points and the permeation of the drug. If the permeation is above 100 % of the solubility at this time point, the permeation of particles is likely. Hence, the dissolution rate of coarse suspension with the addition of stabilisers and the solubility of large and small nanocrystals in medium and buffer were tested. In this chapter, the focus will be on the dissolution rate data of the suspensions and time points used in transport studies in the last chapter. For CUR, permeation could be seen in medium after 24 hours, so that this time point will be also plotted in the next Figure 65.

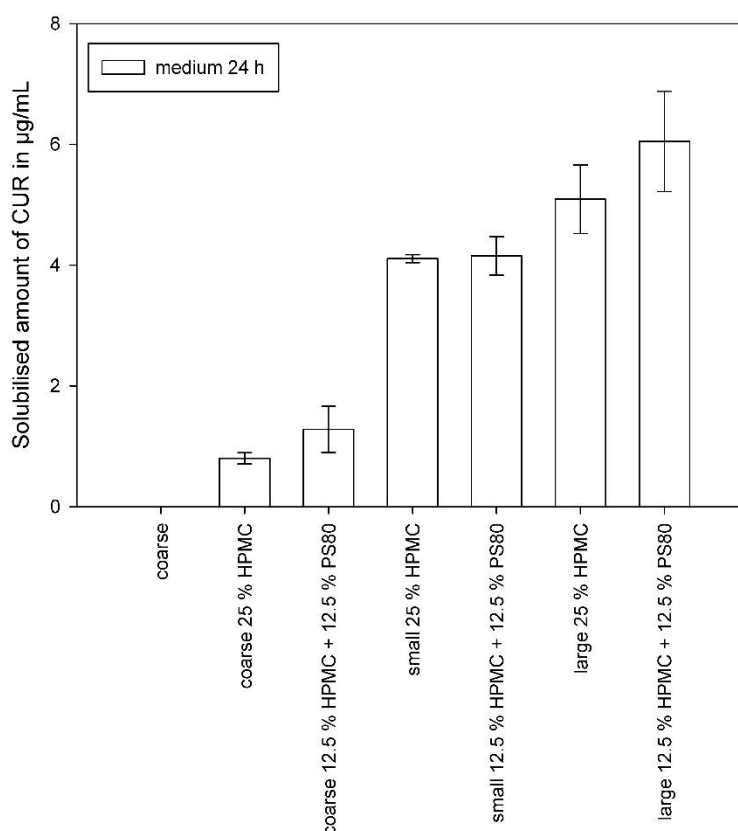


Figure 65: Solubilised amount of CUR suspensions in medium after 24 hours of a 1 mM suspension. n = 3. error bars = SD.

Coarse powder dissolution rate was not detectable while the large nanoparticles gave highest dissolution rates. A combination of HPMC and PS80 gave higher dissolution rates than just HPMC stabilised suspensions. The dissolution rate increases over

5 hours while at 24 hours, it decreases for almost all formulations (data not shown). This indicated that CUR undergoes degradation which is reasonable as it is known from literature [Wahlang, B. et al. 2011]. The degradation was more prominent in buffer than in medium so that it could be concluded that CUR is more stable in medium than in buffer. There is a chance that the small nanocrystals had a higher amount of dissolved drug so that also the degradation was faster and therefore a lower dissolution rate was measured as for the large nanocrystals. GLI had a different dissolution pattern than CUR (Figure 66).

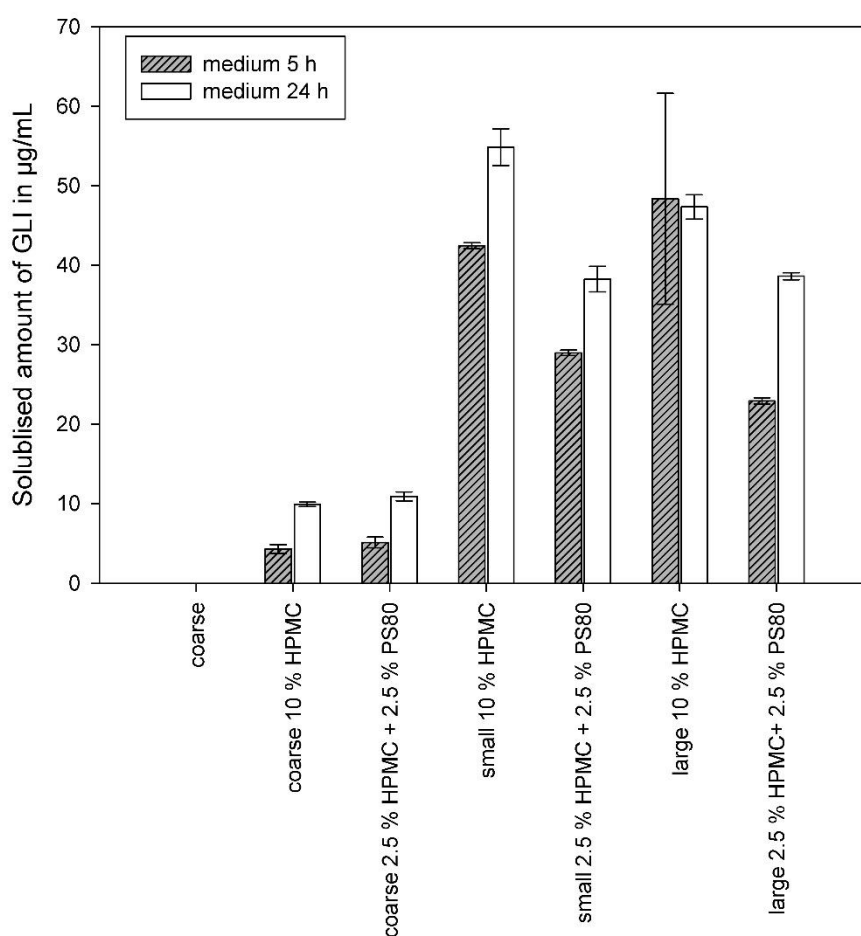


Figure 66: Solubilised amount of GLI suspensions in medium after 24 and 5 hours of a 1 mM suspension. n = 3. error bars= SD.

Similar to CUR were the low dissolution rates of the coarse powder compared to the nanosuspensions and the higher dissolution rate in medium compared to buffer (data not shown). A difference could be seen in the influence of the stabilisers. In most cases, a combination of HPMC and PS80 did not lead to higher dissolution rate but HPMC stabilised nanosuspensions showed highest dissolution rate. The results indicate that

larger nanosuspension formulations were not favourable compared to the small nanocrystal formulations which is in better agreement with the Noyes-Whitney equation as it was the case for CUR nanocrystals. The dissolution rate in buffer stayed more or less on the same level for all sampling time points (data not shown) while the dissolution rate in medium increased, in average, for all formulations over time. This indicated that no degradation was happening for GLI.

A lot of conclusions can be drawn from this experiment. Stabilisers can influence the dissolution from drug suspensions differently. While for CUR, a combination of HPMC and PS80 was most beneficial, GLI showed higher dissolution rates with just HPMC. With these solubility rate results, a connection to the transport studies can be drawn. As the solubility studies were done at similar conditions as the transport studies (37 °C, no shaking), the permeated amount of drug could be related to its dissolution at different time points. For CUR, permeation could just be seen at 24 hours incubation time in medium like described above. Therefore, in the next Figure 67, just the 24 hour data were put into relation.

For coarse CUR with addition of HPMC, no permeation could be seen, even though the solubilised amount was 0.56 µg in the apical compartment (700 µL). An addition of HPMC and PS80 to the coarse suspension led to an increase in permeation, even though the solubilised amount was with 0.89 µg just slightly higher. Of this solubilised amount 68.61 % ± 5.02 % permeated. For the large nanosuspension formulations, the permeability and the solubility were the highest but the percentage of permeation was on the same level as for the small nanocrystal suspensions. Just around 20 % (17.71 % ± 0.38 % and 20.47 % ± 1.50 %) of the solubilised amount permeated which indicated that probably no particles crossed the Caco-2 cells because not even the solubilised drug permeated completely.

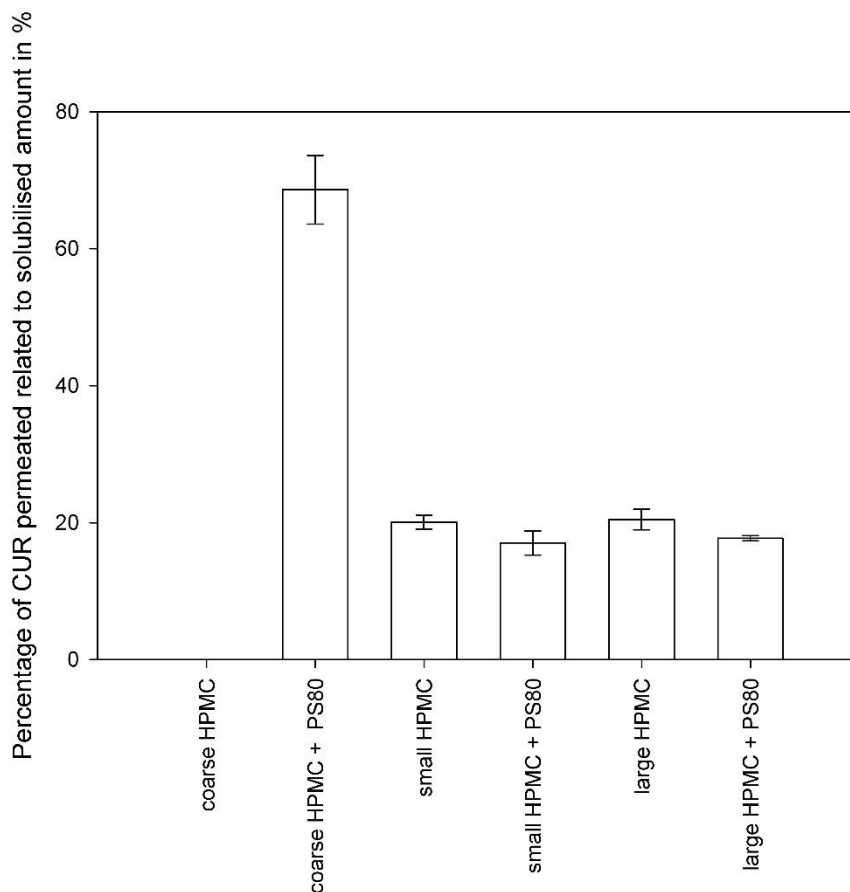


Figure 67: Relation of dissolution rate and permeation of formulations for CUR coarse suspension, small and large nanosuspensions. 100 % represents the solubilised amount determined at 24 h. Filter pore size was 1 μm and permeation was measured over 24 hours. $n = 2$. error bars = min/max.

For GLI, already after 3 hours permeation could be detected to that this time point and the following ones are plotted in Figure 68. Highest permeation, related to solubilised amount, could be detected for the coarse powder with HPMC addition. Of the $9.94 \mu\text{g} \pm 0.29 \mu\text{g}$ GLI dissolved after 24 hours, $79.76 \% \pm 0.16 \%$ could permeate. Large nanocrystals, stabilised with HPMC, showed highest permeation rates and with $47.34 \mu\text{g/mL} \pm 1.53 \mu\text{g/mL}$ second highest dissolution rate after 24 hours, so that their permeated percentage resulted in $46.37 \% \pm 0.51 \%$. Again, permeation seems to be governed by dissolved drug, so particulate transport is unlikely.

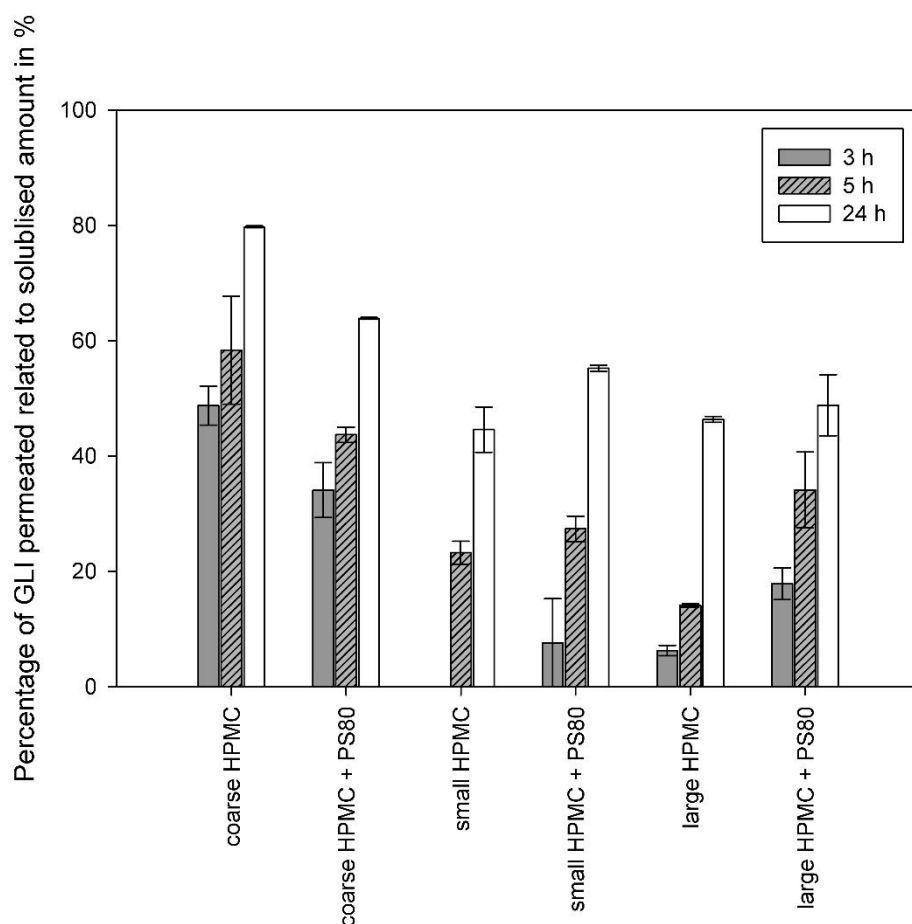


Figure 68: Relation of dissolution rate and permeation of formulations for GLI coarse suspension, small and large nanosuspensions. 100 % represents the solubilised amount determined at 24 h. Filter pore size was 1 μm and permeation was measured over 24 hours. $n=2$. error bars = min/max.

4.6.5 Concluding remarks of transport studies

A validated transwell model could be generated so that the influence of particle size, time and type of stabiliser on the permeation of nano-crystalline formulations could be investigated.

For the BCS class IV drug CUR, no permeation through epithelial cells could be seen within 5 hours. The solubility of this drug was very poor at all tested time points, so that the classification as BCS class IV drug could be confirmed. Addition of PS80 to all suspensions increased the solubility at all tested time points as well as the permeation rate for the coarse suspension. PS80 addition enhanced the permeation of large nanocrystals within 24 hours by approximately 100 % compared to large nanocrystals stabilised just with HPMC. It was mentioned in the material part (chapter 3.1.1.1) that CUR could possibly be a Pgp substrate and as PS80 is known to inhibit Pgp [Zhang et al., 2003] the increased permeation could be also due to the Pgp inhibition of PS80.

No influence of the type of stabiliser could be detected for the small nanocrystals. An explanation could again be related to Pgp. To be able to use the inhibitory effect of PS80, drug and stabiliser have to be at the same site at the same time. Possibly, smaller nanocrystals have a higher dissolution and high concentrations of PS80 are not at the same time with the solubilised CUR molecules in the cells. Larger particles could settle on the cells and be attached to the mucus layer of the cells, so that the local drug concentration and PS80 concentration might be higher and therefore, the Pgp inhibiting process can occur. Regarding the size, large nanocrystals led to higher permeation than small nanocrystals.

GLI, as a BCS II class drug, proved to show higher solubility and permeation rates than CUR. Addition of stabilisers changed the dissolution in dispersion media differently. In transport buffer, the dissolution was increased when adding HPMC compared to no stabiliser addition or mixtures of HPMC and PS80. For all tested suspensions, HPMC had a more positive effect on the permeation rate of GLI than a PS80-HPMC mixture (at lower concentrations) which might be due to solubility rate enhancement in the transport buffer. Only at higher concentrations of the mixture, a higher permeation could be detected for the small nanocrystals. The permeation rate within 5 hours was higher as within 24 hours.

Relating the dissolution to the permeation of the drugs, the coarse powders, for which permeation rates could be detected, exhibited the highest percentage of dissolved drug being transported. The reason might be again the settling of the particles on the monolayer creating a higher gradient. Amongst each other, GLI and CUR nanocrystals had similar percentages of permeated drug related to dissolution. Comparing the permeation and dissolution at 24 hours, CUR showed in average 18.8 % permeation of the dissolved amount and GLI 48.7 %. Still, looking at these numbers, a permeation of particles is not presumable.

It was mentioned above that for both, CUR and GLI, a higher permeation rate could be seen for the large nanocrystals compared to the small nanocrystals. This size dependence is inconsistent as small nanocrystals should lead to a faster dissolution and higher dissolved amount than the large nanocrystals (see Noyes-Whitney-equation chapter 2.3). Hence, it is an unexpected result as all other data suggest that the drug has to be dissolved before being transported through the cells and the better the dissolution/solubilisation, the higher the permeation rate. In literature, examined

size dependencies on the transport through Caco-2 cells were performed with non-dissolvable nano-objects [Awaad et al., 2012; Munger et al., 2014] or nano-objects that are taken up prior to getting dissolved [McClellan et al., 1998]. One very interesting publication showed the influence of the particle size of efavirenz solid drug nanoparticles on the permeation through Caco2 cells. With efavirenz solid drug nanoparticles, the expected trend could be seen with larger nanocrystals leading to a decrease in P_{app} [Siccardi et al., 2016]. A drawback of this study is that they produced the different particle sizes with different types of stabilisers, so that not only the influence of the particle size was tested. Therefore, this data cannot be used for just interpreting size dependencies. Anhalt explored in her dissertation that permeation was higher for 150 nm nanocrystals compared to 860 nm nanocrystals of a Merck Serono Compound [Anhalt, 2012]. Hence, the phenomenon, which was seen in this thesis, describes a poorly researched area of nanocrystals. Therefore, the following explanations for the large nanocrystals showing a higher permeation than the small nanocrystals are assumptions that need further investigations in the future. One reason could be that the large nanocrystals were more likely to settle on the Caco-2 cell monolayer and therefore increased the concentration gradient at the surface, so that the diffusion was more likely. Another reason for the higher permeation of large nanocrystals could be the supersaturation status of the nanocrystals in the apical compartment. Dissolution data in the last chapter suggest that a supersaturation is present as the solubility is tremendously higher for the nanocrystals compared to the coarse suspension. Literature data suggest that the saturation solubility increase is most pronounced with nanocrystal sizes below 200 nm [Anhalt, 2012], so that in this case a supersaturation, which is also caused by the stabilisers, is more likely than this high increase in saturation solubility. During permeation study, also stabiliser molecules would permeate, so that the possible higher supersaturation status of the small nanocrystals can lead to faster precipitation and therefore, less solubilised molecules would be there for transportation, so that a decrease in permeation would be possible. A third theory is related to the stabiliser-particle ratio. If an assumption is done, that all stabilisers adsorb on the surface of the nanocrystals, large nanocrystals have more stabiliser on the surface, as the weight percentage of stabiliser is the same for small and large nanocrystals but the particle number decreases when large nanocrystals are produced. A layer around the nanocrystals that composes of more stabiliser molecules can possibly interact with the Caco-2 monolayer in a way that

paracellular transport is more likely because it is known that stabilisers can make cells more penetrable [Tuomela et al. 2016].

Summarised, PS80 addition led to permeation and dissolution rate increase for CUR while for GLI just HPMC as a stabiliser was found to have a benefit. For both drugs larger nanocrystals lead to a higher permeation than smaller nanocrystals. Transport studies did indicate that a permeation of particles is not expectable. Consequently, further experiments would be needed to gain deeper inside into particle transport mechanisms with consequently smaller particle sizes. The signals expressed by cells or the adhesion to receptors can be different when a molecule or a particle permeates through the cell [Rauch et al., 2013] which is of major interest for fate and processing of nanocrystals in biological environments.

4.7 Uptake of nanocrystals in cells

The results of the uptake of nanocrystals in Caco-2 cells and RAW 264.7 cells will be explained in this chapter. Therefore, the cells were incubated with the selected nanosuspensions over different time periods and the amount of particles being taken up was calculated. Two microscopic methods were chosen: CARS and fluorescence microscopy.

4.7.1 Uptake studies with CARS microscopy

As CARS microscopy is not a standard technique in the field of uptake studies, some preliminary experiments for set-up arrangements had to be conducted.

4.7.1.1 Evaluation of CARS microscopy set-up

CARS microscopy is only chemically-specific when a wavenumber shift of the drug can be found that does not interfere to a high extent with the background. The backgrounds in these studies were cellular tissues. Therefore, CARS signals from the living and stained as well as fixed cells were collected. Both cell lines had high signals in the region between 2800 cm^{-1} and 2900 cm^{-1} . This is known as the 'lipid region' because the stretching of lipid C-H bonds can be related to this area. A CARS shift of the drugs had to be found aside from this 'lipid region' to be chemically-specific. Unfortunately, CUR did not show a suitable pattern, possibly due to its high fluorescent activity but GLI showed one maximum at 3074 cm^{-1} . Figure 69 shows the wavenumber shifts of

GLI, GLI nanocrystals and lipid droplets in cells. GLI could be clearly differentiated from the lipid droplet in the cells at 3074 cm^{-1} .

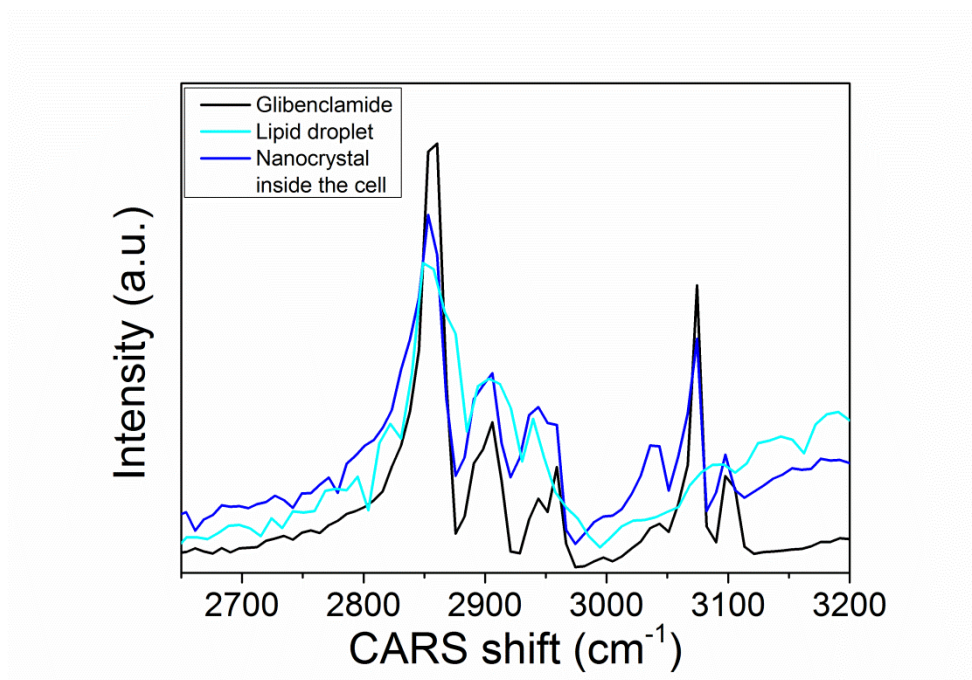


Figure 69: CARS spectra of GLI powder suspended in water, lipid droplets and GLI nanocrystals in RAW 264.7 cells.

In preliminary experiments also the CARS signals of buffer, medium, staining solution and fixation liquid were measured. They did not show interferences with the selected GLI peak. Furthermore, the stabilisers were tested and were also found not to interfere at the wavenumber of 3074 cm^{-1} .

CARS is claimed as a label-free technique but still, in this thesis, staining of the cell membranes had to be done and was detected with two-photon fluorescence excitation (TPFE). The staining had to be conducted because until today there is no specific membrane structure found that exhibits CARS signals aside from the 'lipid region'.

4.7.1.2 Uptake studies of epithelial cells

The uptake quantification of nanocrystals in cells was challenging. Caco-2 cells are building a connective cell structure, so that the localisation of nanocrystals was problematic to detect. To address this problem, the amount of stain was increased from $5\text{ }\mu\text{g/mL}$ to $7.5\text{ }\mu\text{g/mL}$. The connected Caco-2 cells could be visualised as can be seen in Figure 70.

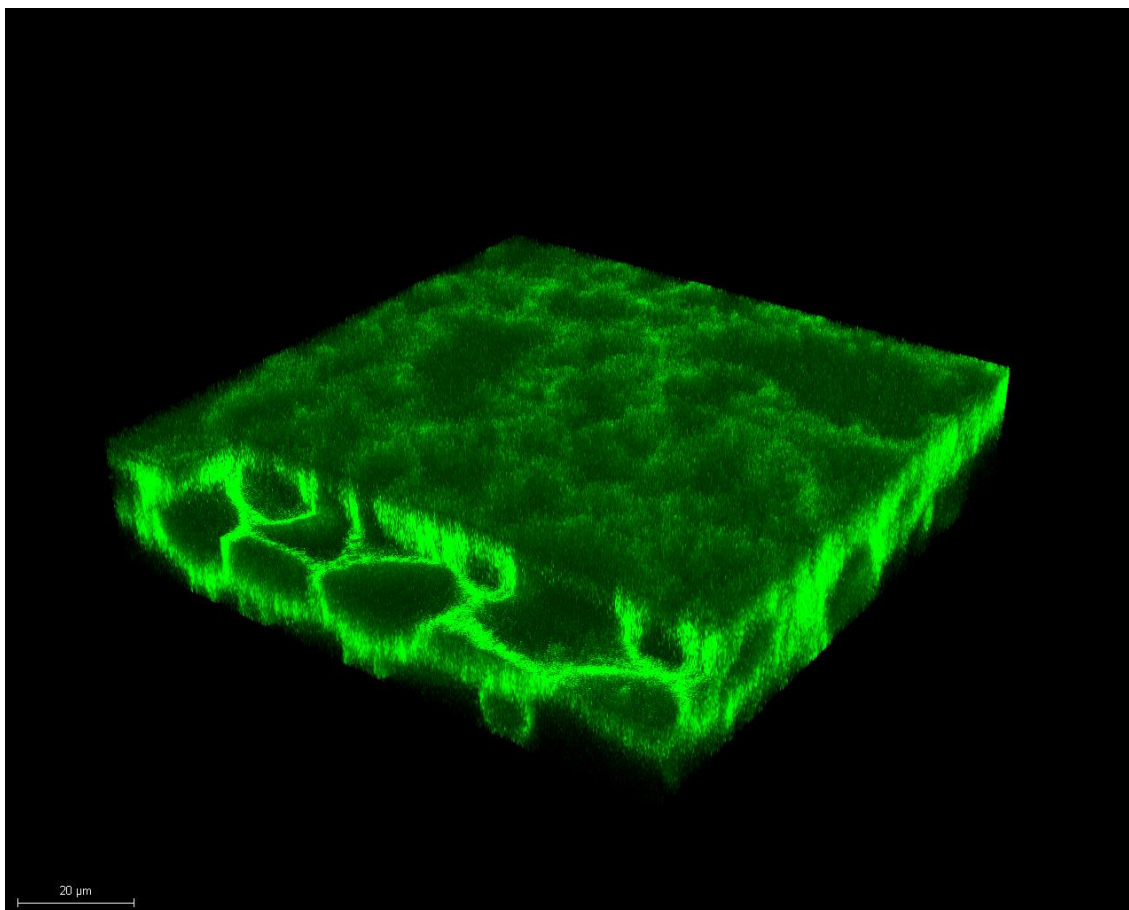


Figure 70: Z-stack of CellMask™ Orange stained Caco-2 cells at a concentration of 7.5 µg/ml.

Unfortunately, when adding nanocrystals, the visualisation of the membranes became blurry. Another problem was faced with the Caco-2 cells detaching from the bottom of the well when they were incubated for 6 hours with 500 µg/mL of API-nanocrystals stabilised with HPMC and PS80. Most of the cells of a lower concentration (250 µg/mL) were still attached. Hence, this concentration was chosen for all further experiments. Still some cells detached which is observable in Figure 71. When using cell culture medium as dilution medium for the nanocrystals, fewer cells detached so that for all further 24 hour incubations, medium was used as dilution liquid.

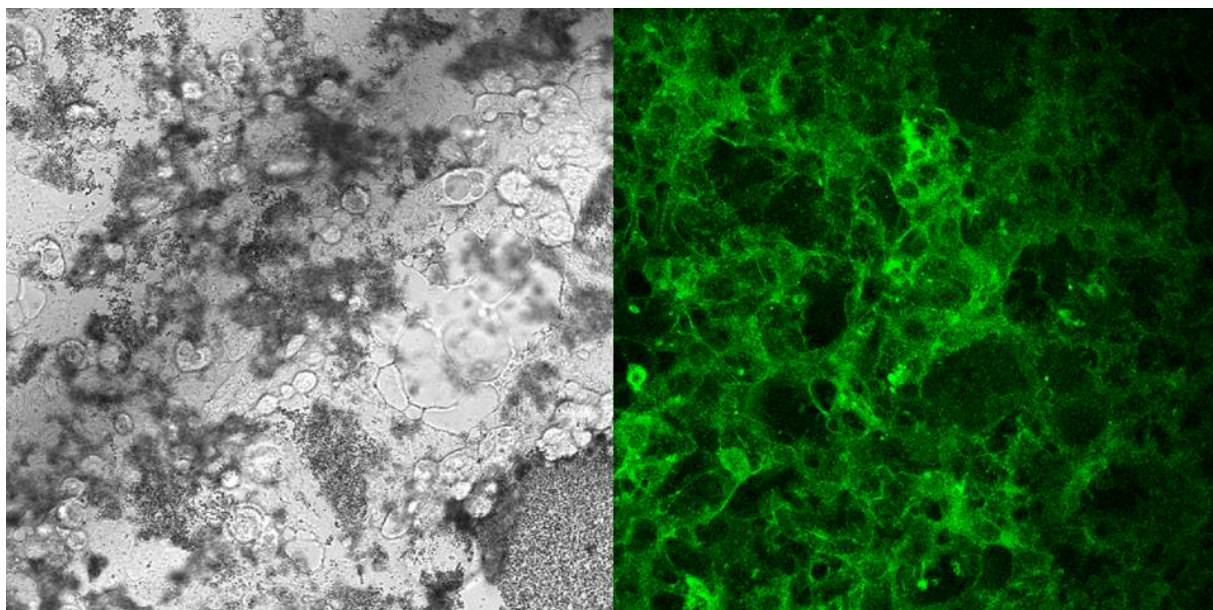


Figure 71: CellMask Orange™ stained and fixed Caco-2 cells incubated with small GLI nanocrystals (250 µg/mL) stabilised with HPMC + PS80 in buffer for 24 hours. Left: bright field image. Right: TPE detection of stain.

Still, at optimum experiment conditions for the cells, only a few images could be created, in which the uptake of nanocrystals into Caco-2 cells could be observed. An exemplary image can be seen in Figure 72.

As only a few areas of possible uptake of nanocrystals could be found in all experiments, quantification was not conducted. Just with incubation times of 24 hours, an uptake could be seen. This time period however is an artificial time for nanocrystal uptake in-vivo because most crystals will most likely be cleared by then. The Caco-2 cells were proven to be a barrier for particles as healthy intestinal cells should be in-vivo. Unfortunately, no influence of size and type of stabiliser could be measured as the uptake was this low. Therefore, another model was chosen: the RAW 264.7 macrophage cell line.

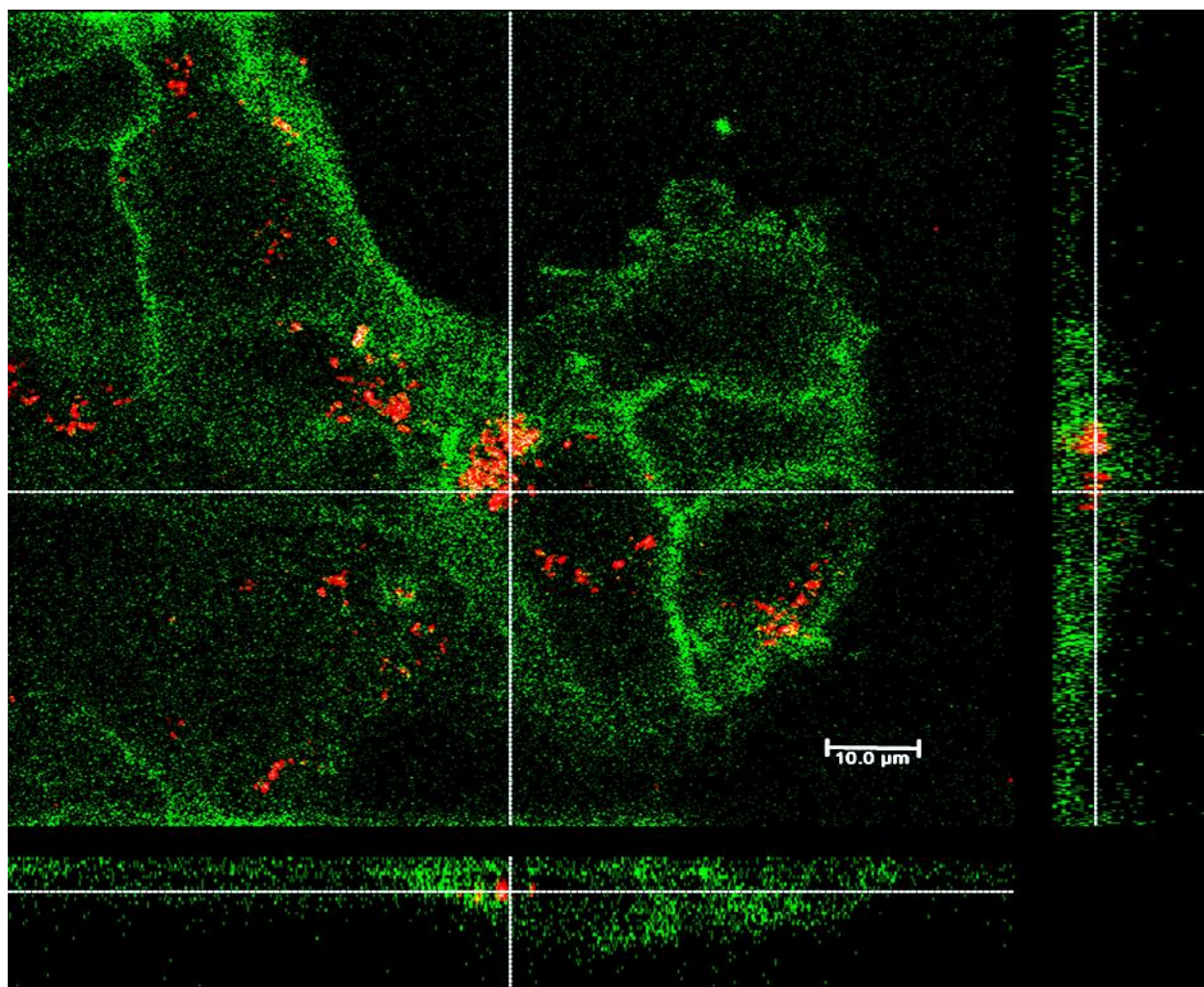


Figure 72: Orthogonal projection of Caco-2 cells incubated with small GLI nanocrystals stabilised with HPMC + PS80 over 24 hours. GLI (red) with a measured CARS shift at 3074 cm^{-1} . Cells were fixed and membrane was stained (green). Detection of the stain was accomplished with TPF.

Macrophages are more likely to take up particles in comparison to enterocytes, so that it was expected that a quantitative measurement of the uptake could be accomplished, showing a difference of the various nano-formulations.

4.7.1.3 Uptake studies in macrophages

Labelling and imaging conditions were the same as for the epithelial cells. Still, images were clearer for the macrophages. Furthermore, every experimental set-up showed a definite uptake of nanocrystals in the cells. An exemplary image is shown in Figure 73.

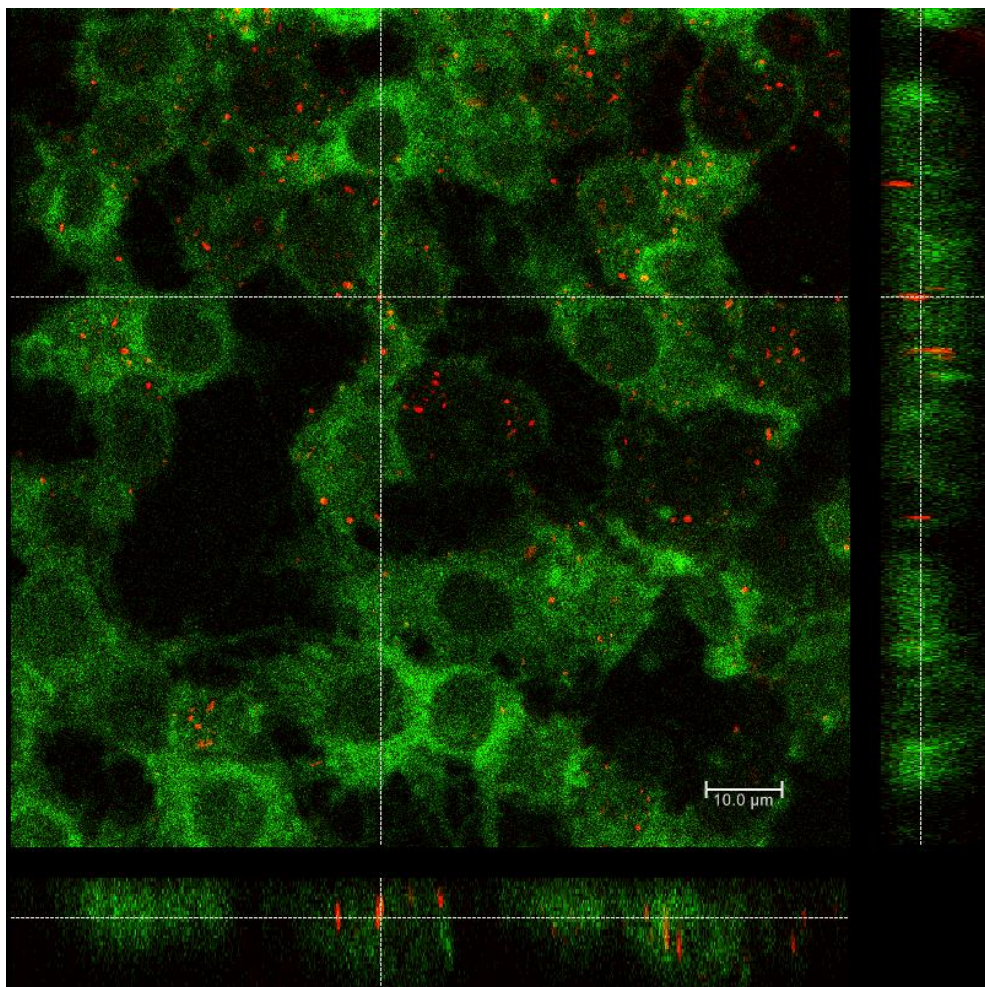


Figure 73: Orthogonal projection of RAW 264.7 cells incubated with small GLI nanocrystals stabilised with HPMC + PS80 over 2 hours. GLI (red) with a measured CARS shift at 3074 cm^{-1} . Cells were fixed and membrane was stained (green). Detection of the stain was accomplished with TPFE.

As imaging conditions were optimal and nanocrystal uptake could be imaged, the uptake could be quantified. The experimental setting is described in the method part (at the end of chapter 3.2.9.2). Here, the evaluation of the created images with the Imaris software should be explained. One set of images contained of one image done with TPFE, so that the cell membranes were plotted (green), and one image created with the CARS signals, where the particles are visualised (red). First, the threshold of the particle image was adapted manually so that the particles could still be seen but red in the background was minimalised. Afterwards the membrane image was loaded and the surface wizard was used for creating and adapting a surface on the cells. Furthermore, the spot wizard was utilised to mark the nanocrystals. The number of spots and the volume of the cells were given by the program so that just the spots (nanocrystals) had to be counted that were situated outside of the cells. This was done by manually counting the spots outside the cells and subtracting this number from the

total spot number. An exemplary image of the images after processing is shown in the appendix (chapter 9.4.5). These mentioned steps were done for each data set. To keep conformity in evaluation, all data sets were evaluated with Imaris within one week and from one person because the adaption of the cell surface and the adjustment of dots for the nanocrystals was still done manually and therefore, could cause bias in resulting values when evaluated with a time shift or from different persons. The following results are plotted as particles taken up per cell to achieve reasonable numbers for comparison. For this reason, a cell was defined as a cube with lengths of 15 μm .

The influences of particle size, time and type of stabiliser on the uptake of nanocrystals are manifold. For a better overview, the same data will be plotted in three different figures with one of the three parameters set into focus. Figure 74 shows the influence of the particle size on the uptake in macrophages.

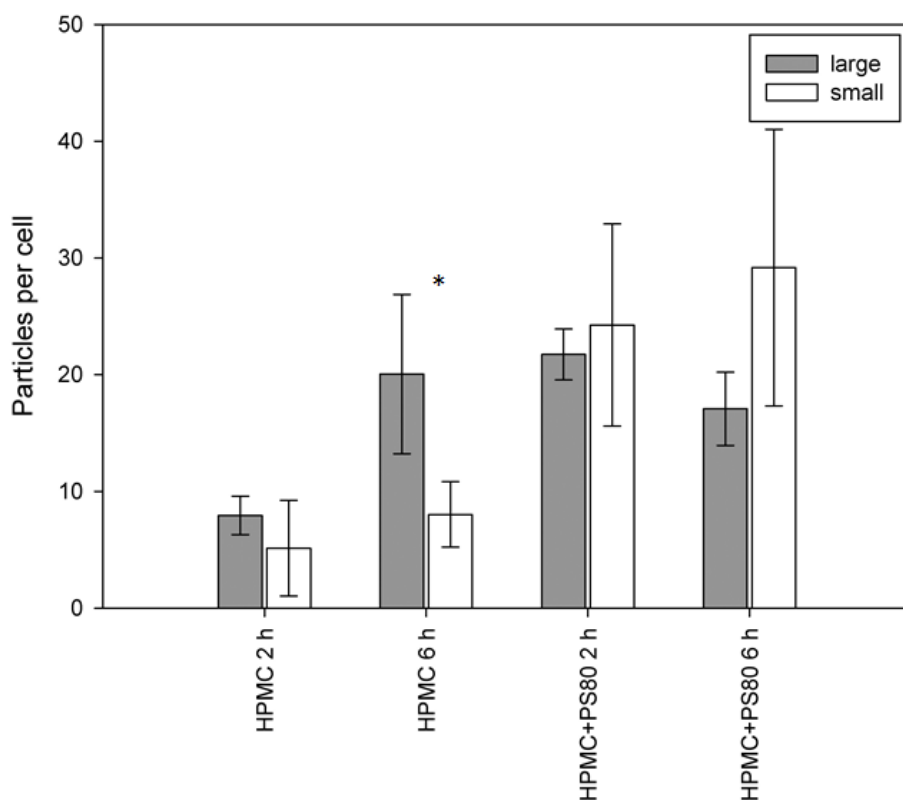


Figure 74: Influence of particle size, time and type of stabiliser on the uptake of GLI nanocrystals per cell with the focus set on the size. * = significant difference ($p = 0.01 - 0.05$). $n = 4$. error bars = SD.

Except for the HPMC stabilised nanocrystals after 6 hours of incubation, no stabiliser-time combination showed a significant difference in particle uptake due to its size.

Also different incubation times just led to one significant difference. Large, HPMC stabilised, nanocrystals are taken up in a larger number when incubated over 6 hours compared to 2 hours as shown in Figure 75.

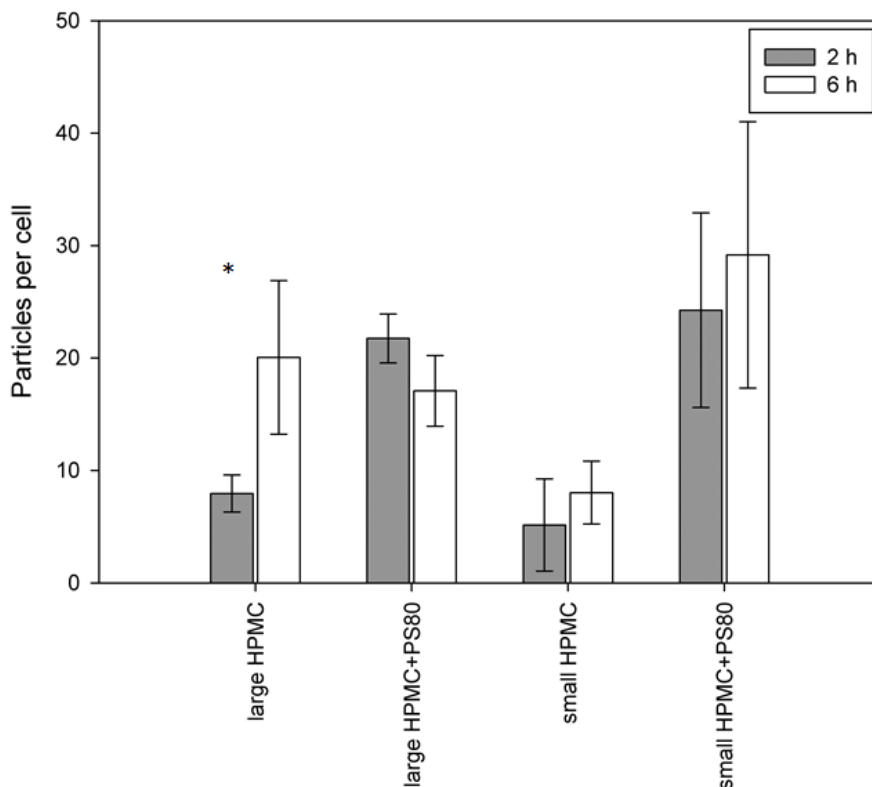


Figure 75: Influence of particle size, time and type of stabiliser on the uptake of GLI nanocrystals per cell with the focus set on the time. * = significant difference ($p = 0.01 - 0.05$). $n = 4$. error bars = SD.

Another picture is given by the influence of the stabilisers (Figure 76). Three time-size combinations showed a significantly higher uptake of the nanocrystals stabilised with HPMC and PS80 compared to HPMC alone. Just for large nanocrystals incubated over 6 hours, the stabiliser does not seem to influence uptake in macrophages. The highest uptake, calculated in average, could be seen for the small GLI nanocrystals incubated over 6 hours and stabilised with HPMC and PS80, followed by the small nanocrystals incubated over 2 hours and stabilised with HPMC and PS80.

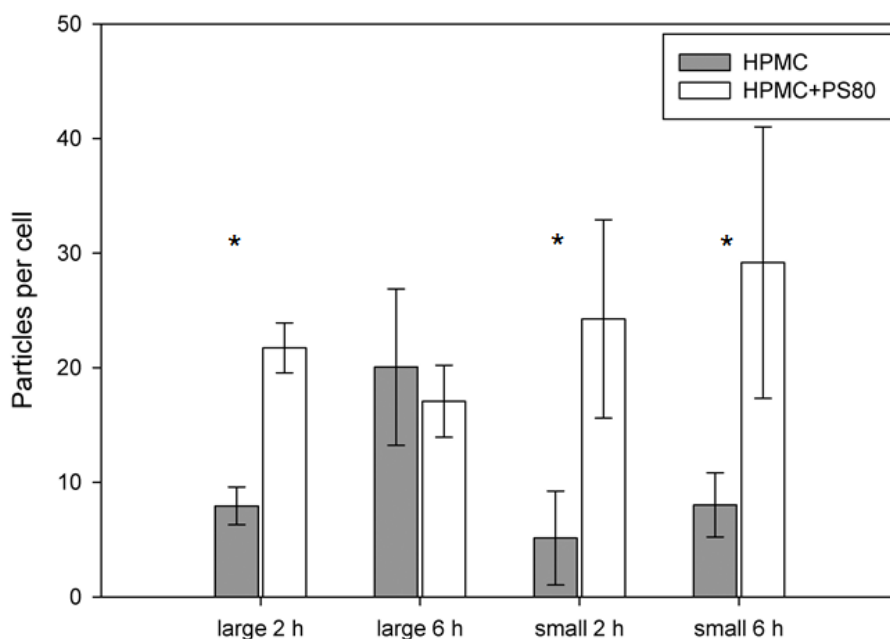


Figure 76: Influence of particle size, time and type of stabiliser on the uptake of GLI nanocrystals per cell with the focus set on the type of stabiliser. * = significant difference ($p = 0.01 - 0.05$). $n = 4$. error bars = SD

Comparing the lowest number of particle uptake with the highest, namely small nanocrystals after 2 hours of incubation stabilised with HPMC (5.1 ± 4.1) and small nanocrystals incubated over 6 hours and stabilised with HPMC and PS80 (29.2 ± 11.8), 5.7 times more GLI particles could be transported in the cell. Theoretical calculations with the estimation that the nanocrystals are perfect spheres, result in an increase in up-taken dose from 1.185×10^{-4} ng for 5.1 and 6.786×10^{-4} ng for 29.2 taken up particles, respectively for one macrophage. Detailed calculations can be found in the appendix (chapter 9.4.6).

CARS microscopy was successfully used to detect the influence of particle size, incubation time and type of stabiliser on the uptake of nanocrystals in macrophages. An important factor was that the fate of the nanocrystals could be measured even without labelling them, which can be beneficial for enhancing in-vitro in-vivo correlation compared to labelled particles or artificial metal particles. PS80-HPMC combinations were found to increase the uptake of nanocrystals of GLI compared to nanocrystals stabilised with HPMC alone. The type of stabiliser was the most prominent influencing factor on uptake compared to time and size.

4.7.1.4 Outlook on ex-vivo imaging with CARS

It was stated earlier, that in-vitro environments cannot mimic in-vivo conditions to a full extent. Therefore, also for this work, an intermediate state; a ex-vivo study was planned. The nanocrystals should be administered to the intestines of living rats and the intestinal cells should be visualised after incubation to either prove poor uptake as seen in-vitro in epithelial cells or to show that in-vivo, the uptake is enhanced. Also the location of the nanocrystals was of interest as different cell assemblies are present in the intestine like the Peyer's patches, which would naturally be more capable for particle uptake than epithelial cells. Unfortunately, the rat experiments could not be conducted but preliminary visualisation experiments could show that CARS microscopy is suitable to differentiate between different cellular structures in the intestine. To show this, different preparation and slicing of the intestine was investigated for an ideal sample preparation. It was found, that the best imaging results were conducted by freezing parts of the intestine, gluing them to a holder of a cryotom (Figure 77) and cutting them as a longitudinal section with a layer thickness of 40 μm .

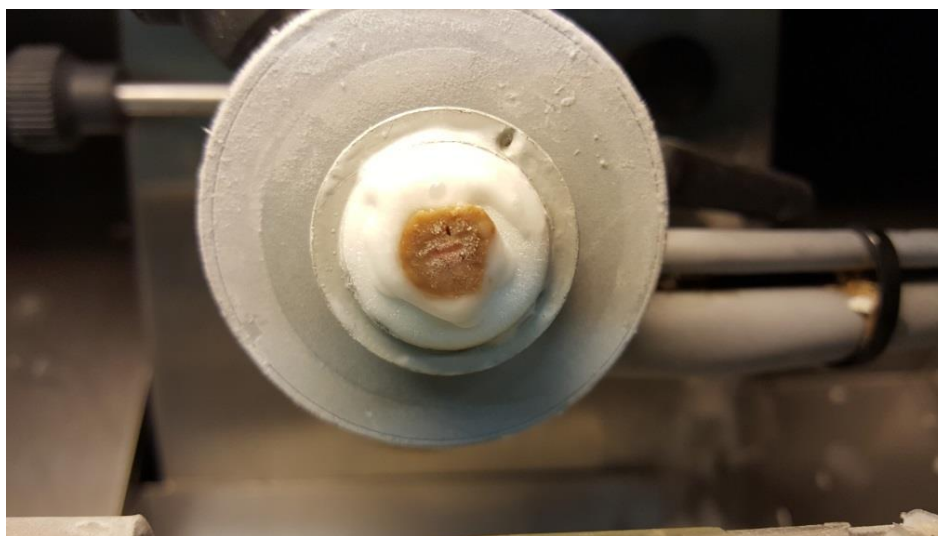


Figure 77: Plate holder of a cryotom. Frozen intestinal samples (brown) were glued (white) to the holder and a plate was used to cut the intestine in slices.

The cut samples were mounted between two object holders within a window of parafilm and a drop of buffer was added. These preparation methods gave the best images of the villi of the rat intestine as can be seen in Figure 78.

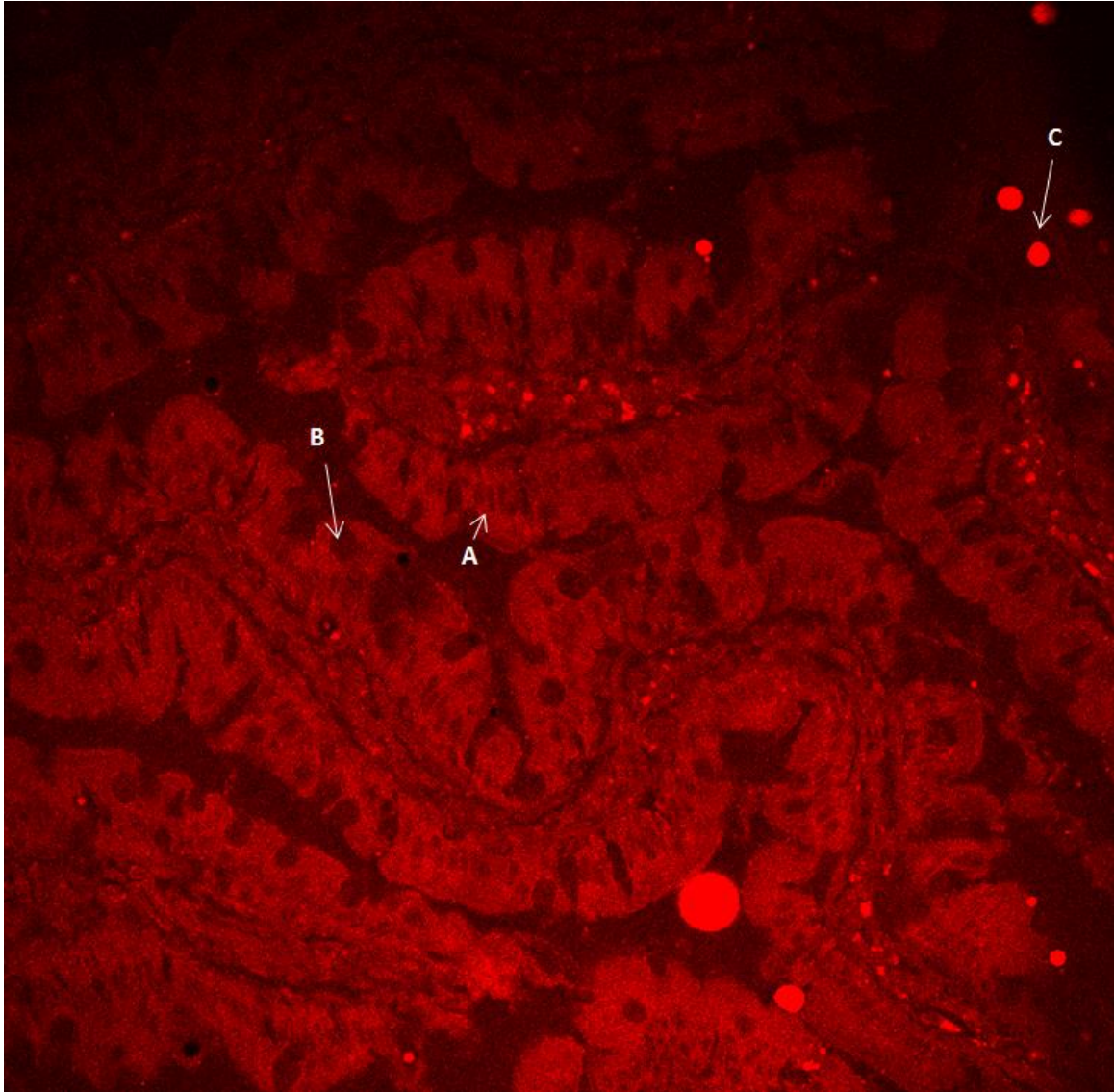


Figure 78: Villi of rat intestine. A was summed to be enterocytes, B goblet cells and C lipid droplets.

One feature of the used CARS microscope from Leica was of further advantage for the visualisation of rat intestines. Next to the TPFE detection for fluorescent materials, which was used in uptake experiments, also the second harmonic generation (SHG) was of use. SHG displays ordered crystalline structures. Therefore, the collagen layers, present in the intestine, could be imaged without further labelling which is observable in Figure 79.

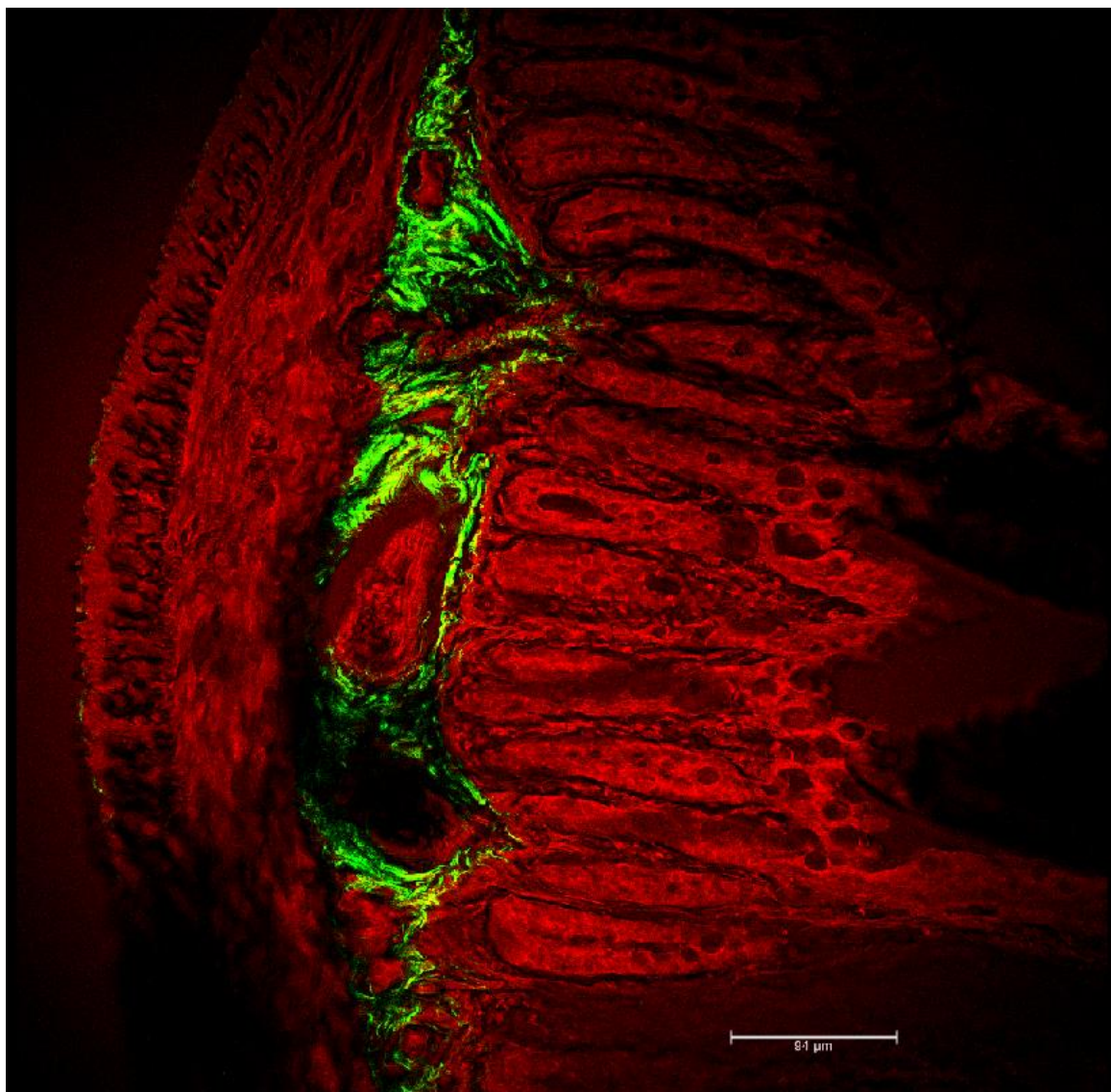


Figure 79: Parts of a rat intestine with following structures from left to right: intestinal outer wall, collagen layer (green) detected with SHG, Villi which were partly ripped apart.

Successful imaging of different structures and cell types in the rat intestine showed that, in future, the CARS microscope from Leica could be a good choice to investigate nanocrystal uptake ex-vivo.

4.7.2 Uptake studies with fluorescence microscopy

CUR, as a naturally fluorescent drug, could be imaged by fluorescence microscopy without labelling of the nanocrystals. GLI nanocrystals could not be detected with the fluorescence microscope as no laser for the excitation of GLI (302 nm) was available.

As the uptake studies for GLI nanocrystals in epithelial cells only showed a few particles being taken up in all the samples and CUR is known to even permeate less than GLI, uptake studies for CUR in epithelial cells were not conducted. Hence,

macrophage uptake studies should show the influence of time, size and type of stabiliser on the uptake of CUR nanocrystals in cells. This set of experiments was conducted to link CARS results and fluorescence microscopy results as these techniques could be used complementary.

4.7.2.1 Uptake studies in macrophages

The preparation of the cell line is explained in the method part (end of chapter 3.2.9.3). Evaluation of the quantitative uptake of the particles was the same than used for CARS images and can be found in chapter 4.7.1.3.

Again, the first parameter regarding its influence on the uptake to be investigated was the size of the nanocrystals as shown in Figure 80.

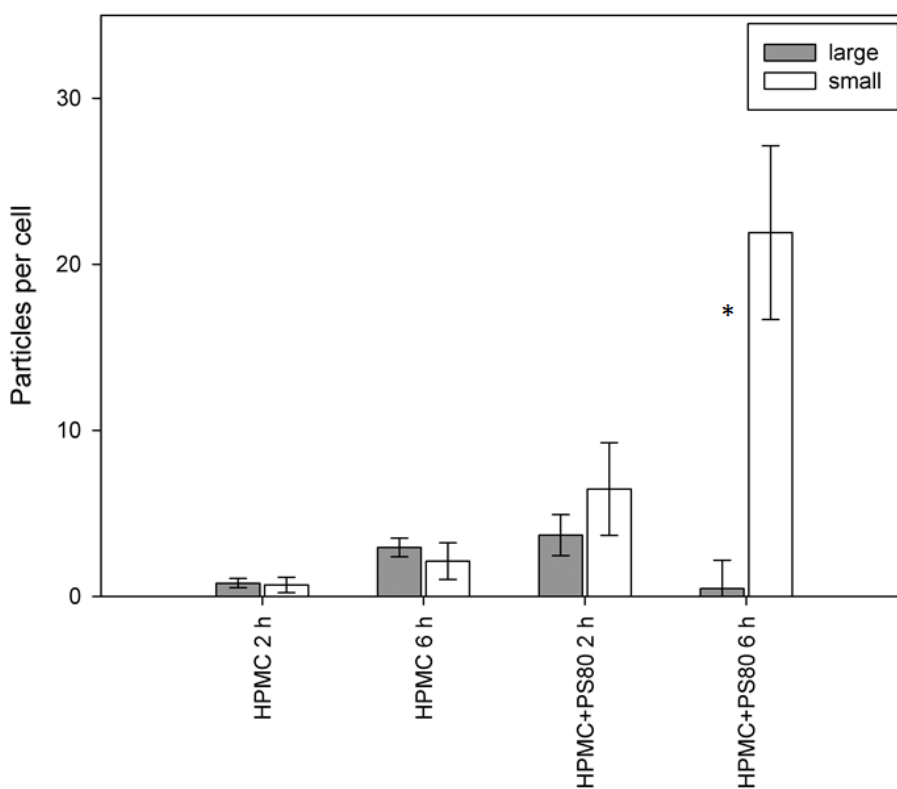


Figure 80: Influence of particle size, time and type of stabiliser on the uptake of CUR nanocrystals per cell with the focus set on the size. * = significant difference ($p = 0.01-0.05$). $n = 4$. error bars= SD

One statistical significant difference was calculated for HPMC and PS80 stabilised nanocrystals with an incubation time of 6 hours where the small crystals were taken up to higher extent than large nanocrystals.

More statistical differences of the influence on particle uptake were calculated for the time. Three significantly different stabiliser-size combinations showed a higher uptake for 6 hours as incubation time compared to 2 hours (Figure 81).

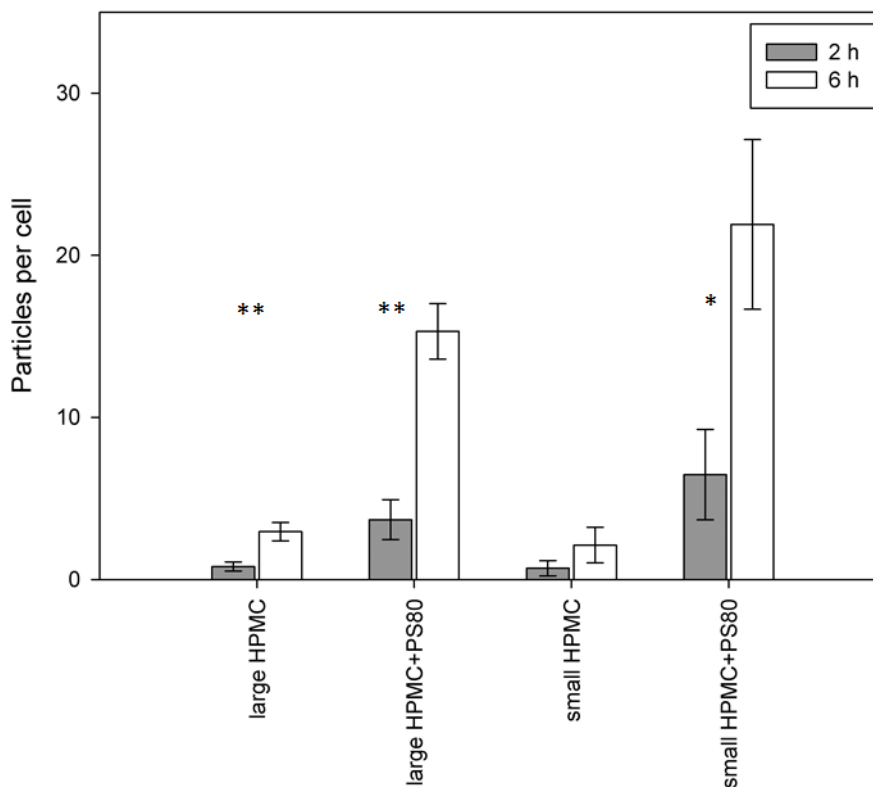


Figure 81: Influence of particle size, time and type of stabiliser on the uptake of CUR nanocrystals per cell with the focus set on the time. * = significant difference ($p = 0.01-0.05$). ** = highly significant ($p = <0.01$). $n = 4$. error bars = SD

Again, the highest influence was seen for the type of stabiliser as plotted in Figure 82. All size-time combinations showed a significant higher uptake for HPMC and PS80 stabilised nanocrystals compared to HPMC stabilised particles. The particle uptake per cell of the small nanocrystals with the fewest amounts of particles being taken up (0.69 ± 0.46) is 31.7 times lower uptake than the one with the highest uptake (21.90 ± 5.24). Here, the theoretical calculation leads to an up-taken dose of 1.826×10^{-5} ng and 5.794×10^{-5} ng, respectively for one macrophage. Details for the calculation can be again found in the appendix (chapter 9.4.6).

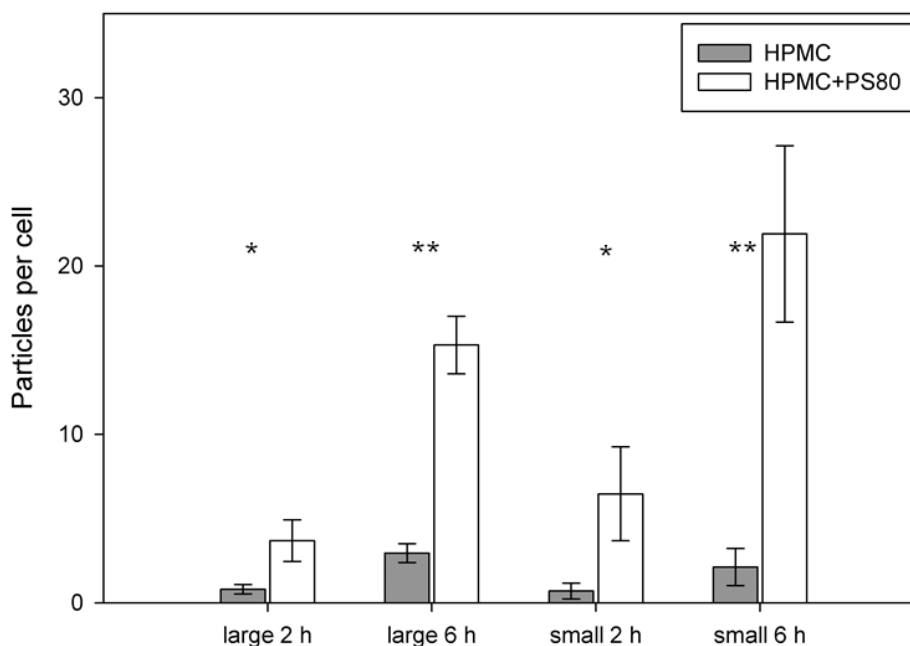


Figure 82: Influence of particle size, time and type of stabiliser on the uptake of CUR nanocrystals per cell with the focus set on the type of stabiliser. * = significant difference ($p = 0.01-0.05$). ** = highly significant ($p = <0.01$). $n = 4$. error bars = SD

4.7.3 Concluding remarks of fluorescence microscopy and CARS microscopy

The uptake of GLI nanocrystals in macrophages has been determined with CARS microscopy while CUR nanocrystals detection was done with fluorescence microscopy. GLI was not possible to image with standard fluorescence microscope as its autofluorescence is only visible at very short wavelengths, while the imaging of CUR causes problems in CARS microscopy possibly due to its high fluorescence. As these are two different techniques, the direct comparison between these two drugs is not without doubt. The direct comparison of GLI and CUR can be seen controversial as two different techniques were utilised. It might be that one method could show the uptake in more detail without becoming obvious to the operator and therefore, a higher number could have been calculated. One example can be given with the z-stack height difference. With the CARS microscope, every 500 nm an image could be taken, while the fluorescence microscope was able to go down to 100 nm. Therefore, small nanocrystals would have had a higher chance of being detected with the fluorescence microscope. Furthermore, the background-particle differentiation was more differentiated in the fluorescence microscope than in CARS microscopy. However, the trend of the influencing parts should be comparable. For both drugs, a stabiliser combination of HPMC and PS80 led to a higher extent in particle uptake compared to

just HPMC stabilised nanocrystals. This influence of the stabilisers was the most significant for both drugs compared to the size and incubation time. The difference of HPMC and HPMC + PS80 stabilised nanocrystals might be even higher for CUR as it has a 5 times higher concentration of PS80 in the nanosuspension than GLI, which is due to the different stabilisation concentrations. Nevertheless, the time had more influence on the uptake of CUR than GLI nanocrystals.

The usage of DMEM medium was possible for CARS but not for fluorescence microscopy (at least with phenol red). Consequently, incubations over 24 hours would have been challenging in fluorescence microscopy. Also, the knowledge about insert material is important. For CARS imaging, the image quality was better when the cells were imaged on polytetrafluoroethylene inserts rather than the poly ethylene and poly carbonate [Saarinen et al., 2017], while in fluorescence microscopy also poly ethylene filters could be used for imaging. Still, for both methods, glass bottom plates were most favourable. Fluorescence microscopy could have been used without labelling the membrane of the cells as CUR in its solubilised form did stain the membranes naturally whereas the solubilised amount of GLI could not be detected in CARS microscopy due to the high background signals in the cells. This background mainly comes from the lipids in the cells as CARS is highly sensitive to lipid structures. This can also be used as an advantage. Sometimes, granular structures could be seen in the cells which could have been confused with nanocrystals. These structures did not show a signal when tuning the laser to the 3047 cm^{-1} (GLI signal) but at the 'lipid-wavenumber' (2845 cm^{-1}) signals could be detected as plotted in Figure 83.

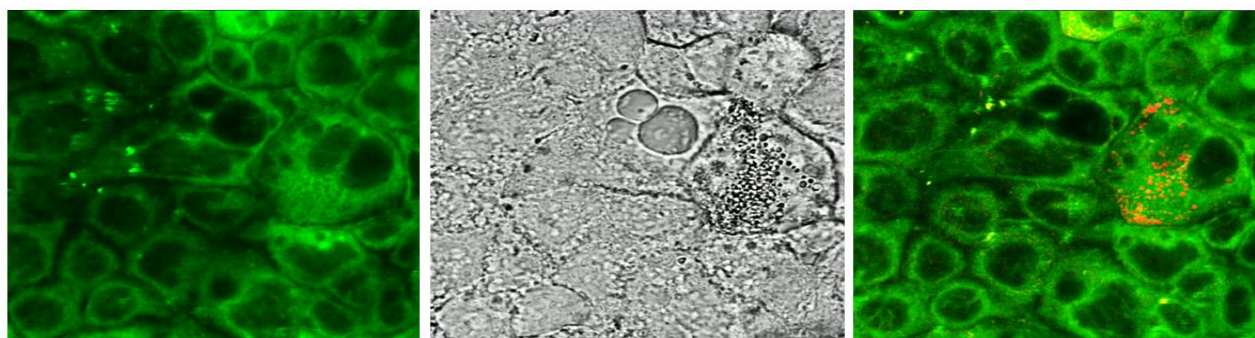


Figure 83: Caco-2 cells incubated with 330 nm GLI nanocrystals over 3 hours. Cells were fixed and the cell membrane was stained (green). Left: CARS signals at 3047 cm^{-1} . Middle: bright field image. Right: Lipid droplets (red) with a detected CARS shift at 2845 cm^{-1} .

In fluorescence microscopy the signals of solubilised drug-filled lipid droplets might be confused with nanocrystals. This was not the case for CUR as the nanocrystals were highly fluorescent compared to the solubilised drug but for less fluorescent drugs confusion might be possible. Still, CARS microscopy might nowadays not be that chemical-specific as it is claimed to be. At least the CARS microscope used for this thesis only had a small region of wavenumber shift detection. Some self-built equipment are able to visualise in the finger print region so that higher detection variability can be achieved. Broadband CARS microscopes can measure from 600 - 3,200 cm^{-1} while the narrowband microscopes, like the Leica microscopy, can just image from 1,400 - 3,300 cm^{-1} . The fingerprint region ($< 1,800 \text{ cm}^{-1}$) could be used to differentiate between different proteins or lipids, so that visualisation of cell compartments would perhaps be possible in detail and without labelling.

5 Concluding Remarks and Overall Discussion

This chapter will deal with the achieved results of this thesis in terms of drug-stabiliser interaction and their influence on cellular transport and uptake of GLI and CUR. The most important results from this thesis will be shortly summarised and the link to current research will be drawn. Furthermore, recommendations for formulation approaches and important factors for the pharmaceutical industry will be resumed. Therefore, three recently published review papers were chosen to identify challenges and opportunities in the field of nano-objects in pharmaceuticals. Yadollahi et al. stated in 2015 that future research directions in the field of nano-objects should include:

- i. Creation of an increase of in-vivo bioavailability and correlation to in-vitro experiments
- ii. Controlled and sustained drug release by incorporation of nano-objects in biocompatible matrix polymers
- iii. Development of stimuli-responsive systems
- iv. Increase in understanding of the behaviour of nanosuspensions in-vivo, including interactions with cells and biological barriers
- v. Surface engineering of nano-objects for active and passive targeting

[Yadollahi et al., 2015]

Jeevanandam et al. summarised in 2016 that improvement in uptake and efficiency of nano-formulations can be achieved by:

- i. Stable drugs in the formulation without self-aggregation
- ii. Knowledge of drug delivery and degradation mechanisms
- iii. Complying with FDA quality and related regulations while maintaining inexpensive production

[Jeevanandam et al., 2016]

Jain et al. named in 2017 that the understanding of the relationship between physico-chemical properties of nanoparticles and their biological interactions is still a challenge in nanotechnology [Jain et al., 2017].

All three review papers highlight the fact that there is still some work to do in the field on nano-bio-interactions. For Yadollahi et al. it is the "Increase in understanding of the behaviour of nanosuspensions in vivo, including interactions with cells and biological

barriers”, for Jeevanandam et al. the “Knowledge in drug delivery and degradation mechanism” and for Jain et al. the fact that “the relationship between physicochemical properties of nanoparticles and their biological interactions is still a challenge in nanotechnology”. In this work, regarding nano-bio-interactions, it could be shown that transport and uptake studies in the Caco-2 cell model indicate that a permeation of GLL and CUR nanocrystals with sizes of 300 nm and 500 nm is not supposable. The enterocytes were proven to be a healthy barrier for nanocrystals with sizes of 300 nm and above. Furthermore, PS80 was found to act as a permeation enhancer for CUR even in small concentrations, while HPMC addition led to a higher permeation of GLL. Still, the size of the nanocrystals was the most influencing factor on permeation. Large nanocrystals led to higher permeations than small nanocrystals. This unexpected results and following intensive literature review revealed that the influence of the size of nanocrystals on the permeation through Caco-2 cells is a poorly researched field in nanocrystal research. Three theories were developed to try to explain these results. The first explanation could be the settling of the large nanocrystals on the Caco-2 cell monolayer and therefore, increasing concentration gradient at the surface. Another reason could be the supersaturation status of the nanocrystals in the apical compartment. Higher dissolution of the small nanocrystals and permeation of the stabiliser molecules could lead to faster precipitation. A third theory is stabiliser-particle ratio related. Large nanocrystals could have more stabilisers on the surface, which can possibly interact to a higher extent with the Caco-2 monolayer. Regarding the uptake of nanocrystals in macrophages, the stabiliser was found as the most prominent factor in uptake enhancement whereby PS80-HPMC mixtures did increase the total uptake of nanocrystals.

Furthermore, stabilisers had different influences on dissolution rate and permeation rate on micro- and nanocrystals. In classical dissolution studies, HPMC stabilised CUR nanosuspensions led to a higher dissolution rate while in transport studies the stabilisation with HPMC and PS80 increased permeation rate. In dissolution studies that had similar conditions than the permeation studies, just large CUR nanocrystals that were stabilised with HPMC + PS80 showed a higher dissolution rate. As in the end, the permeation is necessary to achieve sufficient bioavailability, dissolution should, in this case, not be used to forecast the behaviour in biological environments. The transport through Caco-2 cells seemed to be highly dependent on the solubility of the drug in formulation while the influence on uptake in macrophages was dominated

by the stabiliser type which showed highest membrane interaction potential. The 5.7 times increase in uptake, which could be shown for small GLI nanocrystals, when just changing the stabiliser, is an alarming number for therapeutic treatments. The numbers both belong to small nanocrystals. Hence, it is not enough to just standardise size for nano-medicines, which is still the most investigated value in the field of nano-formulations. In transport studies, the size of the nanocrystals played an important role, while in uptake studies the size was the least influencing factor. One has to decide whether a transport through epithelial cells is of interest or the uptake in phagocytotic cells, to pick the best stabiliser for the purpose. The uptake data in macrophages could increase knowledge in drug delivery and degradation mechanism and can be used from different point of views. Either, one has an application aim for nanosuspensions where the macrophages serve as a clearance system, for example, for intra-venously administered drugs. Here, the results indicate that the addition of PS80 can lead to lower bioavailability compared to nanosuspensions just stabilised with HPMC. On the other hand, if the macrophages are aimed to be the therapeutic target, the loading might be more efficient with PS80 as a stabiliser. Prabhaker et al. suggested that PS80 enhances low density lipoprotein-mediated endocytosis and inhibits Pgp transport at the blood brain barrier [Prabhakar et al., 2013]. The enhanced endocytosis might be due to apolipoprotein E absorption on the PS80 surface [Kreuter, 2001]. Wang et al supported this data with gemcitabine nanoparticles [Wang et al., 2009]. Still, it has to be said that the uptake was measured in-vitro and with just two specific drugs, which cannot be transferred one to one to in-vivo environments and other drugs but gives an impression of what can happen if a change in formulation is not tested properly. If the drug is poorly soluble and permeable, like CUR, also the time plays an important role for uptake and transport of the drug. Here, formulations should be created which increase the time that the nanocrystals stay on the targeted cells with techniques like mucus adhesion/permeation for epithelial cells or PEG circulation enhancement, if the phagocytotic system is the aim. For good permeable substances, like GLI, the increase in solubilisation should be the major aim.

There is still a need in techniques that can measure and display nano-bio-interactions. In this work, CARS microscopy was shown to be a good alternative to usually used fluorescence microscopy (unless the material is fluorescent itself) as no labelling of the nano-objects has to be done. Also animal tissues could be imaged so that further ex-vivo studies are possible.

The interest in surface engineering of nano-objects for active and passive targeting shows that also methods are needed to evaluate the results of the surface engineering while even the addition of stabilisers to nanosuspensions can count as surface engineering. An understanding of the stabiliser-drug interaction is of major importance for the selection of an appropriate stabiliser. In the pharmaceutical industry, new drugs are developed frequently. If the formulation approach of a nanosuspension is chosen for a certain drug, a stabiliser has to be selected. Polymer adsorption on solid surfaces can be studied with several methods, such as solid-state NMR, Fourier transform infrared (FTIR), [Pawsey et al., 2002] Raman [Bjelopavlic et al., 2000], microcalorimetry [Pinholt et al., 2011], surface plasmon resonance (SPR) and atomic force microscopy (AFM). HPMC was shown to have high interaction potential with crystal surfaces [Verma et al., 2009a]. Literature review revealed following important facts:

- i. Surface hydrophobicity plays an important role. High hydrophobicity of the drug can lead to self-aggregation of the nanocrystals and therefore, lower the success rate of production [Eerdenbrugh et al., 2009] Furthermore, the hydrophobicity of the stabiliser should be high enough to increase the chance of interaction and the chance of a resulting stable nanosuspension [Lee. et al., 2005].
- ii. Non-ionic stabilisers were found to have a higher adsorption potential than polymers [Palla and Shah, 2002; Choi et al., 2008].
- iii. For surfactants, the CMC of the stabiliser might play a role. Clustered polymers can decrease stability of nanocrystals due to of possible micellar bridging [Liu et al., 2014]. Deng et al. found that they could achieve stable nanosuspensions of paclitaxel when they used Pol407 below CMC but not above CMC [Deng et al., 2010].

In this thesis, the findings about stabiliser-drug interaction revealed that:

- i. Zeta potential measurements can give an impression about the mechanism of the adsorption order of charged stabilisers, like SDS and TTAB with non-ionic

- stabilisers, like PS80. From this, stability of nanosuspensions can be forecasted and stabiliser selection can be optimised.
- ii. ITC can display the speed of interaction. As it is known that CUR and HPMC are interacting via hydrogen bonding but no signal could be detected in ITC, the speed of this formation process was possibly too slow. These results can improve the selection of stabilisers regarding the milling process as large polymers, like HPMC, might not be suitable for high energy millings. PS80 was found to be a fast adsorbing stabiliser.
 - iii. All used stabilising concentrations were above CMC but still, stable nanosuspensions could be created. Hence, the thesis of Deng et al. and other researcher could not be confirmed but must be a drug dependent phenomenon.

The above results were found for the used drugs and stabilisers but were not translated to other systems, so that no generalisation can be done. Further experiments with a higher variety of drugs and stabilisers should be conducted to gain more insight in interaction pathways and for the prediction of a suitable stabiliser for a certain drug.

Regarding pharmaceutical industry, maintaining inexpensive production is of great interest. Minimal stabilisation concentration is important for cost effective productions on a large scale. Also the stability of the nanosuspension is dependent on the minimal stabilisation concentration. A too high concentration can lead to Ostwald ripening while a too low concentration can lead to particle agglomeration or aggregation. Möschwitzer summarised with his review: "Drug nanocrystals in the commercial pharmaceutical development process" that nano-formulations are a well-established and proven formulation approach for poorly soluble drugs [Möschwitzer, 2013]. He concluded that the ongoing research should focus on the production of even smaller nanoparticles and that the bioavailability of oral administered nanocrystals can just be raised when the compounds show dissolution rate limited bioavailability. In this work, nano-formulation for the BCS II drug was confirmed to have a higher benefit than for the BCS IV drug, as CUR had an increase in permeation but the still very low values seem to be negligible for therapeutic issues. Still, these results could show that it should not be generalised that BCS IV drugs should not be formulated as nanosuspensions like Möschwitzer did. If a drug has a high potency, so that even a very small increase in permeation changes therapeutic responses, a nano-formulation might still be a promising approach. As described above, the aim of the industry is to

produce nanocrystals as small as possible. In this thesis it was found that milling conditions for small nanocrystals can be more or less independent of the drug. Following factors resulted in a decrease in size for both drugs: small milling beads, long milling times and high rotor speed. Even a continuous milling would be possible with the used mill so that large scale production could be possible.

Consequently, this work could increase the knowledge in production and nano-bio interaction of nanocrystals. Even though only 2 drugs and 2 to 6 stabilisers were tested, some results might be transferable to BCS classes II and IV, regarding drugs and stabiliser classes, like surfactants or polymers.

In the future, the already started work of ex-vivo and in-vivo studies should be continued as, generally, the reports on in-vivo in-vitro correlation are until today not consistent in the field of nanomedicines so that an increase in the knowledge of in-vivo in-vitro correlation would help to employ more safe and effective nano-medicines in the market.

6 Summary

Nowadays, the pharmaceutical formulation development faces various challenges. A high percentage of the newly developed active pharmaceutical ingredients (APIs) show poor aqueous solubility but high therapeutically efficacy. However, to be efficient, the API must reach its target. The oral administration is the most used type of application. Here, the API has to permeate from the intestine to the blood stream to get to the target location. The gastro intestinal tract displays a barrier for permeating substances. Usually, a solubilised API is desirable which can easily permeate via active or passive transport. When an API is poorly soluble in water, the absorption is usually low and therefore the therapeutic effect is decreased.

For this thesis, two poorly water soluble model APIs were selected: On the one hand, curcumin (CUR) which exhibits also low permeability and on the other hand, glibenclamide (GLI) which shows high permeability. In this work, a processing to nanocrystals (NCs) was performed. NCs have a large surface area due to the comminution to the nanometer area and therefore exhibit high solubility rates (SR). For the production of NCs, the API was suspended in a non-solvent (water) together with a stabiliser (ST) and grinded in a media mill. ST are essential as they hinder agglomeration of newly formed particles. Until today it is not fully explored which ST is most suitable for which API and how the stabilised NCs perform in-vivo. This is why in this work the focus was set on the influence of six different ST on the production and interaction with bio-relevant environments of NCs. With all stabilisers, nanosuspensions with particle sizes down to 300 nm could be produced. However, they had different efficacies. These nanosuspensions were tested for the applicability in bio-relevant environments. Hydroxylpropyl methylcellulose (HPMC) demonstrated to be stable in buffer and was also found to be non-toxic for epithelial cells even at high concentrations. Polysorbate 80 (PS80) exhibited relatively high toxicity, so that it was used in combination with HPMC for further studies. All other stabilisers were excluded from further cell studies as they exhibited high toxicity of instabilities in buffer.

To investigate interactions between ST and API and to possibly forecast minimal ST concentration, two methods were chosen: isothermal titration calorimetry (ITC) and contact angle measurements (CAM). ITC proved PS80 as being a fast adsorbing ST. HPMC showed a slow speed of diffusion. Therefore, HPMC might not be suitable for

high energy millings as it might not be able to stabilise newly formed surfaces fast enough. CAM could be used to forecast the PS80 concentration, which is most definitely suitable for stabilisation for GLI.

The influence of the ST on the permeation of CUR and GLI in bio-relevant environments was investigated in an epithelial cell model. Depending on the SR, different permeation rates were observed. GLI had higher SR for HPMC stabilised NCs and therefore also higher permeation compared to HPMC + PS80 stabilised NCs while CUR showed highest permeation rates for HPMC stabilised NCs as well as highest SR. Furthermore, the influence of the particle size was investigated. The larger NCs with 500 nm had higher permeation rates compared to 300 nm NCs. The influence of the particle size was even more pronounced than the influence of the stabiliser.

Fluorescence microscopy and coherent anti-Stokes Raman microscopy were utilised to investigate the uptake of NCs. No uptake of NCs after 24 hours of incubation could be seen for both substances in an epithelial cell line. The epithelial cells were proven to have a barrier function for GLI and CUR NCs in the tested size ranges. To further investigate the influence of the ST on the uptake of NCs, a macrophage cell line was employed. Next to the influence of the stabiliser also the influence of the particle size and incubation time were examined. The type of stabiliser had the most significant influence on uptake of NCs with HPMC + PS80 stabilised NCs giving the highest uptake rates.

In this thesis the substantial influence of the ST on every part of nanosuspension formulations could be highlighted. The production, absorption in enterocytes and elimination (through, for example, macrophages) of NCs are dependent on the type of ST. Therefore, the selection of ST must be of high priority in the development of nanosuspension systems.

7 Summary (German)

Die heutige pharmazeutische Entwicklung von Arzneiformen steht vor vielfältigen Herausforderungen. Ein großer Teil neu entwickelter Arzneistoffe (AS) weist eine schlechte Wasserlöslichkeit bei gleichzeitigem hohem Wirkungspotential auf. Davon kann jedoch nur dann profitiert werden, wenn die AS auch an den Zielort gelangen. Die orale Verabreichung ist die am häufigsten genutzte Applikationsart. Damit der AS zu seinem Zielort gelangen kann muss er vom Magen-Darm-Trakt in die Blutbahn gelangen. Der Magen-Darm-Trakt stellt allerdings eine Art Barriere für die Absorption von Stoffen dar. Meist muss die gelöste Form des AS vorliegen, da diese am einfachsten durch aktiven oder passiven Transport in den Körper aufgenommen werden kann. Weißt der AS jedoch eine schlechte Wasserlöslichkeit auf, kann er oft kaum absorbiert werden und somit auch keine systemische Wirkung entfalten. Um dem Körper diese schwer löslichen AS besser zugänglich zu machen wurden im Rahmen dieser Arbeit Nanosuspensionen entwickelt. Als Modelarzneistoffe wurde zum einen Curcumin (CUR) ausgewählt, das zusätzlich zu seiner schlechten Wasserlöslichkeit auch schlechte Permeationseigenschaften aufweist, zum anderen Glibenclamid (GLI), das über gute Permeationseigenschaften verfügt. Um die Lösungsgeschwindigkeit (LG) zu erhöhen, wurden diese Stoffe über einen Mahlprozess zu Nanokristallen (NK) verarbeitet. Dadurch kann von der in Folge der Zerkleinerung stark vergrößerte Oberfläche profitiert werden. Für die Herstellung von NK wurden die AS zusammen mit einem Nichtlösemittel (Wasser) und Stabilisatoren (ST) in einer Perlmühle zerkleinert. Letztere dienen dazu, die neu entstanden Partikel stabil zu halten. Sie sind also bei einem Nano-Mahlprozess essentiell. Es ist jedoch noch nicht vollständig geklärt, welche ST für welche AS am besten geeignet sind und wie die stabilisierten NK sich genau im Körper verhalten. Daher wurde in dieser Arbeit der Fokus auf die Frage gelegt, welchen Einfluss sechs verschiedenen ST auf die Produktion von NK und die Interaktion mit biorelevanten Umgebungen, wie Zellsysteme haben. Mit allen ST konnten für CUR und GLI bis zu 300 nm kleine NK hergestellt werden, jedoch waren die ST unterschiedlich effektiv. Weiterhin wurden die Nanosuspensionen auf die Applikationsfähigkeit in biorelevanter Umgebung untersucht. Durch Hydroxypropylmethylcellulose (HPMC) stabilisierte NK zeigten Stabilität in Puffer und entwickelten auch in hohen Konzentrationen keine Zelltoxizität. Polysorbat 80 (PS80) dagegen ließ eine relativ hohe Zelltoxizität erkennen, weshalb

es in Kombination mit HPMC für weitere Studien genutzt wurde. Alle anderen ST wurden für die Zellstudien ausgeschlossen, da sie entweder eine zu hohe Zelltoxizität oder Partikelgrößenwachstum in Puffer zeigten.

Um die Interaktion von AS und ST genauer zu untersuchen und eventuell die minimale Stabilisierungskonzentration vorausszusagen, wurden zwei Methoden herangezogen: Isothermale Titrationskalorimetrie (ITK) und Kontaktwinkelmessungen (KWM). ITK zeigte PS80 als schnell adsorbierenden ST. HPMC zeigte eine langsame Diffusionsgeschwindigkeit und könnte deswegen bei extrem schnellen Mahlprozessen nicht von Nutzen sein. KWM ließen eine Voraussage, der mit Sicherheit stabilisierenden Konzentrationen von PS80 für GLI zu.

Die ausgewählten ST zeigten einen Einfluss auf die Permeationseigenschaften der Nanoformulierungen durch Epithelzellen. Hierbei erwies sich die Messung der LG von CUR und GLI in den jeweiligen Nanosuspensionen als gute Methode zur Prognostizierung der Permeationsrate. GLI war, als HPMC stabilisierte NK, am schnellsten löslich und zeigte eine höhere Permeation im Vergleich zu den HPMC + PS80 stabilisierten NK. Die Permeationrate, sowie die LG, von CUR war bei den HPMC + PS80 stabilisierten NK höher. Der Einfluss der Partikelgröße auf die Permeationsrate war im Vergleich zu dem Einfluss der Stabilisierer größer, wobei die 500 nm NK gegenüber 300 nm NK eine höhere Permeationsrate zeigten.

Mit Hilfe der mikroskopischen Methoden Fluoreszenzmikroskopie und koherente anti-Stokes Raman Mikroskopie wurde die Aufnahme der NK in Zellen untersucht. Für die Darmepithelzelllinie ließen sich auch nach 24 Stunden Inkubation nur wenig Hinweise auf eine Aufnahme der NK finden. Die Enterozyten weisen also bei diesen Größenordnungen für die beiden Stoffe mit den ST eine Barrierefunktion auf. Um jedoch den Einfluss der ST auf die Aufnahme in Zellen zu untersuchen, wurde eine Makrophagenzelllinie herangezogen. Bei diesen Aufnahmestudien wurde auch der Einfluss der Inkubationszeit und der Partikelgröße untersucht. Es stellt sich heraus, dass der Einfluss der ST am höchsten ist, wobei bei CUR und GLI die HPMC + PS80 stabilisierte NK im Vergleich zu den HPMC stabilisierten NK die höchste Aufnahmequote zeigten.

In dieser Arbeit konnte nachgewiesen werden, dass die ST auf alle Teilschritte der Arzneiform Nanosuspension einen Einfluss haben. Die Produktion, die Absorption

durch Enterozyten und die Elimination der NK (durch z.B. Makrophagen) hängen von den jeweiligen ST ab. Die Auswahl der ST sollte also eine hohe Priorität bei der Entwicklung von Nanosuspensionen haben.

8 References

- Abhayraj, S. J., Avinash, G., Ashwani, K. T. (2016) Deciphering the mechanism and structural features of polysorbate 80 during adsorption on PLGA nanoparticles by attenuated total reflectance – Fourier transform infrared spectroscopy. *RSC Advances*. 6:108545-108557
- Anhalt, K. (2012) Oral nanocrystal formulations and their biopharmaceutical characterization. Dissertation. Heidelberg University, Heidelberg.
- Anuchapreeda, S., Leechanachai, P., Smith, M. M., Ambudkar, S. V., Limtrakul, P. (2002) Modulation of P-glycoprotein expression and function by curcumin in multidrug-resistant human KB cells. *Biochemical Pharmacology*. 64(4):573-582
- Anwar, M., Akhter, S., Mallick, N., Mohapatra, S., Zafar, S., Rizvi, M. M. A., Ali, A., Ahmad, F. J. (2016) Enhanced anti-tumor efficacy of paclitaxel with PEGylated lipidic nanocapsules in presence of curcumin and poloxamer: In vitro and in vivo studies. *Pharmacological Research*. 113, Part A:146-165
- Aprahamian, M., Michel, C., Humbert, W., Devissaguet, J. P., Damgé, C. (1987) Transmucosal passage of polyalkylcyanoacrylate nanocapsules as a new drug carrier in the small intestine. *Biol. Cell*. 61:69–76
- Araujo, L., Löbenberg, R., Kreuter, J. (1999) Influence of the Surfactant Concentration on the Body Distribution of Nanoparticles. *Journal of Drug Targeting*. 6(5):373-385
- Artursson, P. Palm, K. Luthman, K. (2012) Caco-2 monolayers in experimental and theoretical predictions of drug transport. *Advanced Drug Delivery Reviews*. 64:280-289
- Awaad, A., Nakamura, M., Ishimura, K. (2012) Imaging of size-dependent uptake and identification of novel pathways in mouse Peyer's patches using fluorescent organosilica particles. *Nanomedicine: Nanotechnology, Biology and Medicine*. 8(5):627-636
- Beinert, S., Fragnière, G., Schilde, C., Kwade, A. (2015) Analysis and modelling of bead contacts in wet-operating stirred media and planetary ball mills with CFD–DEM simulations. *Chemical Engineering Science*. 134:648-662

- Bjelopavlic, M., Singh, P. K., El-Shall, H., Moudgil, B. M. (2000) Role of Surface Molecular Architecture and Energetics of Hydrogen Bonding Sites in Adsorption of Polymers and Surfactants. *Journal of Colloid and Interface Science*. 226(1):159-165
- Blunk, T., Hochstrasser, D. F., Sanchez, J. C., Müller, B. W., Müller, R. H. (1993) Colloidal Carriers for Intravenous Drug Targeting: Plasma Protein Adsorption Patterns on Surface-Modified Latex Particles Evaluated by Two-Dimensional Polyacrylamide Gel Electrophoresis. *Electrophoresis*. 14(12):1382-1387
- Brandenberger, C., Clift, M. J. D., Vanhecke, D., Muhlfeld, C., Stone, V., Gehr, P., Rothen-Rutishauser, B. (2010) Intracellular imaging of nanoparticles: Is it an elemental mistake to believe what you see? *Particle and Fibre Toxicology*. 7(15):1-6
- Braun, A. C., Ilko, D., Merget, B., Gieseler, H., Germershaus, O., Holzgrabe, U., Meinel, L. (2015) Predicting critical micelle concentration and micelle molecular weight of polysorbate 80 using compendial methods. *European Journal of Pharmaceutics and Biopharmaceutics*. 94:559-568
- Braun, A., Hämmerle, S., Suda, K., Rothen-Rutishauser, B., Günthert, M., Krämer, S. D., Wunderli-Allenspach, H. (2000) Cell cultures as tools in biopharmacy. *European Journal of Pharmaceutical Sciences*. 11,Suppl 2:51-60
- Brockmeier, D., Grigoleit, H. G., Leonhardt, H. (1985) Absorption of glibenclamide from different sites of the gastro-intestinal tract. *European Journal of Clinical Pharmacology* 29(2):193-197
- Bruner, L. and Tolloczko, S. (1900) Über die Auflösungs geschwindigkeit fester Körper. *Zeitschrift für anorganische Chemie*. 28(1):314-330
- Butler, J. M. and Dressman, J. B. (2010). The Developability Classification System: Application of Biopharmaceutics Concepts to Formulation Development. *Journal of Pharmaceutical Sciences*. 99(12):4940-4954
- Camp, C. H., Lee, Y. J., Heddleston, J. M., Hartshorn, C. M., Hight Walker, A. R., Rich, J. N., Cicerone, M. T. (2014). High-Speed Coherent Raman Fingerprint Imaging of Biological Tissues. *Nature Photonics*. 8:627–634

- Cartiera, M. S., Johnson, K. M., Rajendran, V., Caplan, M. J., Saltzman, W. M. (2009) The uptake and intracellular fate of PLGA nanoparticles in epithelial cells. *Biomaterials*. 30(14):2790-2798
- Caster, J. M., Patel, A. N., Zhang, T., Wang, A. (2017) Investigational nanomedicines in 2016: a review of nanotherapeutics currently undergoing clinical trials. *WIREs Nanomedicine and Nanobiotechnol.* 9(1) e1416
- Cerdeira, A. M., Mazzotti, M., Gander, B. (2010) Miconazole nanosuspensions: Influence of formulation variables on particle size reduction and physical stability. *International Journal of Pharmaceutics*. 396(1–2):210-218
- Chainani-Wu, N. (2004) Safety and Anti-Inflammatory Activity of Curcumin: A Component of Tumeric (*Curcuma longa*). *The Journal of Alternative and Complementary Medicine*. 9(1):161-168
- Chearwae, W., Anuchapreeda, S., Nandigama, K., Ambudkar, S.V., Limtrakul, P. (2004) Biochemical mechanism of modulation of human P-glycoprotein (ABCB1) by curcumin I, II, and III purified from Turmeric powder. *Biochemical Pharmacology*. 68:2043–2052
- Chen, H., An, Y., Yan, X., McClements, D. J., Li, B., Li, Y. (2015) Designing self-nanoemulsifying delivery systems to enhance bioaccessibility of hydrophobic bioactives (nobiletin): Influence of hydroxypropyl methylcellulose and thermal processing. *Food Hydrocolloids*. 51:395-404
- Chen, L.R., Wesley, J.A., Bhattachar, S., Ruiz, B., Bahash, K., Babu, S.R. (2003) Dissolution behaviour of a poorly water soluble compound in the presence of Tween 80. *Pharmaceutical Research*. 20(5):797-801
- Chiad, K., Stelzig, S. H., Gropeanu, R. Weil, T., Klapper, M., Müllen, K. (2009) Isothermal Titration Calorimetry: A Powerful Technique To Quantify Interactions in Polymer Hybrid Systems. *Macromolecules*. 42:7545–7552
- Chin, W. W. L., Parmentier, J., Widzinski, M., Tan, E. H., Gokhale, R. (2014) A Brief Literature and Patent Review of Nanosuspensions to a Final Drug Product. *Journal of Pharmaceutical Sciences*. 103(10):2980-2999

- Choi, Y. J., Park, C. H., Lee, J. (2008) Effect of Polymer Molecular Weight on Nanocomminution of Poorly Soluble Drug. *Drug Delivery*. 15(5):347-353
- Ćirin, D., Krstonošić, V., Poša, M. (2017) Properties of poloxamer 407 and polysorbate mixed micelles: Influence of polysorbate hydrophobic chain. *Journal of Industrial and Engineering Chemistry*. 47:194-201
- Clemens, D. L., Lee, B.-Y., Xue, M., Thomas, C. R., Meng, H., Ferris, D., Nel, A. E., Zink, J. I., Horwitz, M. A. (2012) Targeted Intracellular Delivery of Antituberculosis Drugs to Mycobacterium tuberculosis-Infected Macrophages via Functionalized Mesoporous Silica Nanoparticles. *Antimicrobial Agents and Chemotherapy*. 56(5):2535-2545
- Costas, D. (2016) *Pharmaceutical Nanotechnology Fundamentals and Practical Applications*. 1st edition. Springer.
- D'Mello, S. R., Cruz, S. R., Chen, M.-L., Kapoor, M. Lee, S.L., Tyner, K. M. (2017) The evolving landscape of drug products containing nanomaterials in the United States. *Nature Nanotechnology*. 12:523–529
- Dalvi, S. V. and Yadav, M. D. (2015) Effect of ultrasound and stabilizers on nucleation kinetics of curcumin during liquid antisolvent precipitation. *Ultrasonics Sonochemistry*. 24:114-122
- Darville, N., Saarinen, J., Isomäki, A., Khriachtchev, L., Cleeren, D., Sterkens, P., Van Heerden, M., Annaert, P., Peltonen, L., Santos, H. A. , Strachan, C. J., Van den Mooter, G. (2015) Multimodal non-linear optical imaging for the investigation of drug nano-/microcrystal–cell interactions. *European Journal of Pharmaceutics and Biopharmaceutics*. 96:338-348
- De Waard, H., Hinrichs, W. L. J., Frijlink, H. W. (2008) A novel bottom-up process to produce drug nanocrystals: Controlled crystallization during freeze-drying. *Journal of Controlled Release*. 128(2):179-183
- Deng, J., Huang, L., Liu, F. (2010) Understanding the structure and stability of paclitaxel nanocrystals. *International Journal of Pharmaceutics*. 390:242-249

-
- Des Rieux, A., Fievez, V., Garinot, M., Schneider, Y. J., Preat, V. (2006) Nanoparticles as potential oral delivery systems of proteins and vaccines: a mechanistic approach. *Journal of Controlled Release*. 116(1):1–27
- Descamps, M. and Willart, J. F. (2016) Perspectives on the amorphisation/milling relationship in pharmaceutical materials. *Advanced Drug Delivery Reviews*.100:51-66
- Dhar, N., Au, D., Berry, R. C., Tam, K. C. (2012) Interactions of nanocrystalline cellulose with an oppositely charged surfactant in aqueous medium. *Colloids and Surfaces A: Physicochemical and Engineering Aspects*. 415:310-319
- Di Folco, U., De Falco, D., Marcucci, F., Nobili, G., Moretti, V., Gioventù, G., Tubili, C. (2012) Stability of Three Different Galenic Liquid Formulations Compounded from Tablet Containing Glibenclamide . *Journal of Nutritional Therapeutics*. 1:152-160
- DiMarco, R. L., Hunt, D. R., Dewi, R. E., Heilshorn, S. C. (2017) Improvement of paracellular transport in the Caco-2 drug screening model using protein-engineered substrates. *Biomaterials*. 129:152-162
- Dimova, R., Lipowsky, R., Mastai, Y., and Antonietti, M. (2003) Binding of Polymers to Calcite Crystals in Water: Characterization by Isothermal Titration Calorimetry. *Langmuir*. 19(15): 6097–6103
- Dou, H., Destache, J. C., Morehead, J. R., Mosley, R. L., Boska, M. D., Kingsley, J., Gorantla, S., Poluektova, L., Nelson, J. A., Chaubal, M., Werling, J., Kipp, J., Rabinow, B. E., Gendelman, H. E. (2006) Development of a macrophage-based nanoparticle platform for antiretroviral drug delivery. *Blood*.108:2827–2835
- Duncan, R. and Richardson, S. C. W. (2012) Endocytosis and Intracellular Trafficking as Gateways for Nanomedicine Delivery: Opportunities and Challenges. *U.K. Molecular Pharmaceutics*. 9(9):2380–2402
- Dunn, S. E., Coombes, A. G. A., Garnett, M. C., Davis, S. S., Davies, M. C., Illum, L. (1997) In vitro cell interaction and in vivo biodistribution of poly(lactide-co-glycolide) nanospheres surface modified by poloxamer and poloxamine copolymers. *Journal of Controlled Release*. 44:65–76
-

- Dutta, T., Garg, M., Jain, N. K. (2008) Targeting of efavirenz loaded tuftsin conjugated poly(propyleneimine) dendrimers to HIV infected macrophages in vitro. *European Journal of Pharmaceutical Sciences*. 34(2–3):181-189
- Dutta, A. K., Rösger, J., Rajarathnam, K. (2015) Using Isothermal Titration Calorimetry to Determine Thermodynamic Parameters of Protein–Glycosaminoglycan Interactions. *Methods in molecular biology* (Clifton, NJ).1229:315-324
- Duveneck, G. L., Bopp, M. A., Ehrat, M., Balet, L. P, Haiml, M., Keller U, Marowsky G, Soria S. (2003) Two-photon fluorescence excitation of macroscopic areas on planar waveguides. *Biosensors and Bioelectronics*. 18(5):503-510
- Edueng, K., Mahlin, D., Larsson, P., Bergström, C. A. S. (2017) Mechanism-based selection of stabilization strategy for amorphous formulations: Insights into crystallization pathways. *Journal of Controlled Release*. 256:193–202
- Eerdenbrugh, B. V., Vermant, J., Martens, J. A., Froyen, L., Humbeeck, J. V., Augustijns, P., Mooter, G. V. D. (2009) A screening study of surface stabilization during the production of drug nanocrystal. *Journal of Pharmaceutical Science* 98(6):2091-103
- Eldridge, J. H., Hammond, C. J., Meulbroek, A. J., Staas, R. M., Gilley, J. K., Tice, T. R. (1990) Controlled vaccine release in the gut-associated lymphoid tissues. 1. Orally administered biodegradable microspheres target the Peyer's patches. *Journal of Controlled Release*. 11:205–214
- EMA/HMPC/456848/2008 European medicines agency Committee on herbal medicinal products (HMPC) assessment report on curcuma longa l. rhizoma 2009 Doc. Ref.: EMA/HMPC/456848/2008
- Etheridge, M. L., Campbell, S. A., Erdman, A. G., Haynes, C. L., Wolf, S. M., McCullough, J. (2013) The big picture on nanomedicine: the state of investigational and approved nanomedicine products. *Nanomedicine: Nanotechnology, Biology and Medicine*. 9(1):1-14

- Evans, C. L. and Xie, X. S. (2008) Coherent Anti-Stokes Raman Scattering Microscopy: Chemical Imaging for Biology and Medicine. *Annual Review of Analytical Chemistry*. 1(1):883-909
- Fahr, A. and Liu, X. (2007) Drug delivery strategies for poorly water-soluble drugs. *Expert Opinion on Drug Delivery*. 4(4):403-416
- Flach, F., Konnerth, C., Peppersack, C., Schmidt, J., Damm, C., Breitung-Faes, S., Peukert, W., Kwade, A. (2016) Impact of formulation and operating parameters on particle size and grinding media wear in wet media milling of organic compounds – A case study for pyrene. *Advanced Powder Technology*. 27(6):2507-2519
- Florence, A. T. (2012) “Targeting” nanoparticles: The constraints of physical laws and physical barriers. *Journal of Controlled Release*. 164(2):115-124
- Florence, A. T. and Attwood, D. (2016) *Physicochemical Principles of Pharmacy: In Manufacture, Formulation and clinical use*. 6th edition Pharmaceutical Press.
- Fu, Q., Ma, M., Li, M., Wang, G., Guo, M., Li, J., Hou, Y., Fang, M. (2017) Improvement of oral bioavailability for nisoldipine using nanocrystals. *Powder Technology*. 305:757-763
- Fuguet, E., Rafols, C., Roses, M., Bosch, E. (2005) Critical micelle concentration of surfactants in aqueous buffered and unbuffered systems. *Analytica Chimica Acta*. 548:95–100
- Fussel, A., Isomäkki, A., Strachan, C. J. (2013) Nonlinear Optical Imaging – Introduction and Pharmaceutical Applications. *American Pharmaceutical Review*. 16 (6):54-63
- Gao, L. and Chen, D. Z. M. (2008) Drug nanocrystals for the formulation of poorly soluble drugs and its application as a potential drug delivery system. *Journal of Nanoparticle Research*. 10(5):845–862
- Gao, L., Liu, G., Ma, J., Wang, X., Zhou, L., Li, X. (2012) Drug nanocrystals: In vivo performances. *Journal of Controlled Release*. 160(3):418-430
- Ghadi, R. and Dand, N. (2017) BCS class IV drugs: Highly notorious candidates for formulation development. *Journal of Controlled Release*. 248:71-95

- Golstein, P.E. Boom, A., van Geffel, J., Jacobs, P. Masereel, B., Beauwens, R. (1999) P-glycoprotein inhibition by glibenclamide and related compounds. 437(5):652-660
- Gupta, A. K. and Curtis, A. S. G. (2004) Lactoferrin and ceruloplasmin derivatized superparamagnetic iron oxide nanoparticles for targeting cell surface receptors. *Biomaterials*. 25(15):3029-3040
- Gustafson, H. H., Holt-Casper, D., Grainger, D. W., Ghandehari, H. (2015) Nanoparticle Uptake: The Phagocyte Problem. *Nano today*. 10(4):487-510
- Hafner, A., Lovrić, J., Lakoš, G. P., Pepić, I. (2014) Nanotherapeutics in the EU: an overview on current state and future directions. *International Journal of Nanomedicine*. 9:1005-1023
- Hao, L., Wang, X., Zhang, D., Xu, Q., Song, S., Wang, F., Li, C., Guo, H., Liu, Y. Zheng, D., Zhang, Q. (2012) Studies on the preparation, characterization and pharmacokinetics of Amoitone B nanocrystals. In *International Journal of Pharmaceutics*. 433(1–2):157-164
- Hassan, S., Prakasha, G., Ozturk, A.B., Saghadzadeh, S. Sohail, M. F., Seo, J., Dokmeci, M.R., Zhang, Y. S., Khademhosseini, A. (2017) Evolution and clinical translation of drug delivery nanomaterials. *Nano Today*. 15:91-106
- He, B., Lin, P., Jia, Z., Du, W., Qu, W., Yuan, L., Dai, W., Zhang, H., Wang, X., Wang, J., Zhang, X., Zhang, Q. (2013) The transport mechanisms of polymer nanoparticles in Caco-2 epithelial cells. *Biomaterials*. 34(25):6082-6098
- Hersh, D. S., Simard J. M. and Eisenberg, H.M. (2017) Chapter 6 - The Application of Glibenclamide in Traumatic Brain Injury. *New Therapeutics for Traumatic Brain Injury*. Edited by Kim A. Heidenreich,, Academic Press, San Diego, Pages 95-107
- Hidalgo, I. J. (2001) Assessing the Absorption of New Pharmaceuticals. *Current Topics in Medicinal Chemistry*. 1:385-401
- Hillery, A. M. and Florence, A. T. (1996) The effect of adsorbed poloxamer 188 and 407 surfactants on the intestinal uptake of 60-nm polystyrene particles after oral administration in the rat. *International Journal of Pharmaceutics*. 132(1):123-130

- Hofmann-Antenbrink, M., Grainger, D. W., Hofmann, H. (2015) Nanoparticles in medicine: Current challenges facing inorganic nanoparticle toxicity assessments and standardizations. *Nanomedicine: Nanotechnology, Biology and Medicine*. 11:1689-1694
- Hörter, D. and Dressman, J.B. (2001) Influence of physicochemical properties on dissolution of drugs in the gastrointestinal tract. *Advanced Drug Delivery Reviews*. 46(1):75-87
- How, C. W., Abdullah, R., Abbasalipourkabir, R. (2011) Physicochemical properties of nanostructured lipid carriers as colloidal carrier system stabilized with polysorbate 20 and polysorbate 80. *African Journal of Biotechnology*. 10(9):1684-1689
- Imai, S., Morishita, Y., Hata, T., Kondoh, M., Yagi, K., Gao, J.-Q., Nagano, K., Higashisaka, K., Yoshioka, Y., Tsutsumi, Y. (2017) Cellular internalization, transcellular transport, and cellular effects of silver nanoparticles in polarized Caco-2 cells following apical or basolateral exposure. *Biochemical and Biophysical Research Communications*. 484(3):543-549
- Jain, P., Pawar, R. S., Pandey, R. S., Madan, J., Pawar, S., Lakshmi, P. K., Sudheesh, M. S. (2017) In-vitro in-vivo correlation (IVIVC) in nanomedicine: Is protein corona the missing link?. *Biotechnology Advances*. 35(7):889-904
- Jeevanandam, J., Chan, Y. S., Danquah, M. K. (2016) Nano-formulations of drugs: Recent developments, impact and challenges. *Biochimie*. 128–129:99-112
- Jiang, S., Zhao, W., Chen, Y., Zhong, Z., Zhang, M., Li, F., Xu, P., Zhao, K., Li, Y., Liu, L., Liu, X. (2015) Paroxetine decreased plasma exposure of glyburide partly via inhibiting intestinal absorption in rats. *Drug Metabolism and Pharmacokinetics*. 30(3):240-246
- Jinno, J., Kamada, N., Miyake, M., Yamada, K., Mukai, T., Odomi, M., Toguchi, H., Liversidge, G. G., Higaki, K., Kimura, T. (2006) Effect of particle size reduction on dissolution and oral absorption of a poorly water-soluble drug, cilostazol, in beagle dogs. *Journal of Controlled Release*. 111(1–2):56-64

- Jovanovic, S. V., Steenken, S., Boone, C. W., Simic, M. G. (1999) H-Atom transfer is a preferred antioxidant mechanism of curcumin. *Journal of the American Chemical Society*. 121:9677–9681
- Junghanns, J.-U. A. H. and Müller, R. H. (2008). Nanocrystal technology, drug delivery and clinical applications. *International Journal of Nanomedicine*. 3(3):295–310
- Junyaprasert, V. B. and Morakul, B. (2015) Nanocrystals for enhancement of oral bioavailability of poorly water-soluble drugs. *Asian Journal of Pharmaceutical Sciences*. 10(1):13-23
- Jurna, M., Korterik, J. P., Otto, C., Herek, J. L., Offerhaus, H. L. (2009) Vibrational Phase Contrast Microscopy by Use of Coherent Anti-Stokes Raman Scattering. *Physical Review Letters* 103(4):043905
- Karashima, M., Kimoto, K., Yamamoto, K., Kojima, T., Ikeda, Y. (2016) A novel solubilization technique for poorly soluble drugs through the integration of nanocrystal and cocrystal technologies. *European Journal of Pharmaceutics and Biopharmaceutics*. 107:142-150
- Kavanagh, N. and Corrigan, O. I (2004) Swelling and erosion properties of hydroxypropylmethylcellulose (Hypromellose) matrices—influence of agitation rate and dissolution medium composition. *International Journal of Pharmaceutics*. 279(1-2):141-152
- Keck, C. M. and Müller, R. H. (2006) Drug nanocrystals of poorly soluble drugs produced by high pressure homogenisation. *European Journal of Pharmaceutics and Biopharmaceutics*. 62:3–16
- Khalaf, K. D. and Perween, A. (2012) Spectrofluorimetric method for the determination of glibenclamide in pharmaceutical formulations. *Hassen Baghdad Science Journal*. 9(2):296-301
- Khan, A. M. and Shah, S. S. (2008) Determination of critical micelle concentration (Cmc) of sodium dodecyl sulfate (SDS) and the effect of low concentration of pyrene on its Cmc using ORIGIN software. *Journal of the Chemical Society of Pakistan*. 30:186-191

- Kim, S. and Lee, J. (2011) Folate-targeted drug-delivery systems prepared by nanocomminution. *Drug Development and Industrial Pharmacy*. 37:131–138
- Klemm, D., Heublein, B., Fink, H. P., Bohn, A. (2005) Cellulose: fascinating biopolymer and sustainable raw material. *Angewandte Chemie International Edition in English*. 44(22):3358-93
- Kolakovic, R., Peltonen, L., Laukkanen, A., Hellman, M., Laaksonen, P., Linder, M. B., Hirvonen, J., Laaksonen, T. (2013) Evaluation of drug interactions with nanofibrillar cellulose. *European Journal of Pharmaceutics and Biopharmaceutics*. 85(3)Part B:1238-124.
- Krafft, C., Popp, J., Dietzek, B. (2009) Raman and CARS microspectroscopy of cells and tissues. *Royal Society of Chemistry*. 134:1046-1057
- Kreuter, J., Muller, U., Munz, K. (1989) Quantitative and microautoradiographic study on mouse intestinal distribution of polycyanoacrylate nanoparticles. *International Journal of Pharmaceutics* 55:39–45
- Kreuter, J. (2001) Nanoparticulate systems for brain delivery of drugs. *Advanced Drug Delivery Review* 47(1):65-81
- Kukan, M., Bezek, S., Koprda, V., Labsky, J., Kalal, J., Bauerova, K., Trovec, T. (1989) Fate of ¹⁴C-terpolymer ([¹⁴C]methylmethacrylate, 2-hydroxyethylmethacrylate, butylacrylate) nanoparticles after peroral administration to rats. *Pharmazie*. 44:339-340
- Kulicke, W.-M., Clasen, C., Lohman, C. (2005) Characterization of Water-Soluble Cellulose Derivatives in Terms of the Molar Mass and Particle Size as well as Their Distribution. *Macromolecular Symposia*. 223(1):151-174
- Kumar, S., Shen, J., Zolnik, B., Sadrieh, N., Burgess, D. J. (2015) Optimization and dissolution performance of spray-dried naproxen nano-crystals. *International Journal of Pharmaceutics*. 486(1–2):159-166
- Kumar Thakur, V. and Kumar Thakur, M. (2015) *Handbook of Polymers for Pharmaceutical Technologies. Volume 4: Bioactive and Compatible Synthetic/Hybrid Polymers*. John Wiley & Sons

-
- Ladbury, J. E. (2001) Isothermal titration calorimetry: application to structure-based drug design. *Thermochimica Acta*. 380:209-215
- Lamprecht, A., Yamamoto, H., Takeuchi, H., Kawashima, Y. (2005) Nanoparticles Enhance Therapeutic Efficiency by Selectively Increased Local Drug Dose in Experimental Colitis in Rats. *Journal of Pharmacology and Experimental Therapeutics*. 315(1):196-202
- Le Ray, A. M., Vert, M., Gautier, J. C., Benoit, J. P. (1994) Fate of [¹⁴C]poly(dl-lactide-co-glycolide) nanoparticles after intravenous and oral administration to mice. *International Journal of Pharmaceutics*. 106:201–211
- Lee, J., Lee, S. J., Choi, J. Y., Yoo, J. Y., Ahn, C. H. (2005) Amphiphilic amino acid copolymers as stabilizers for the preparation of nanocrystal dispersion. *European Journal of Pharmaceutical Science* 24(5):441-9
- Lee, J., Martic, P. A., Tan, J. S. (1989) Protein adsorption on pluronic copolymer-coated polystyrene particles. *Journal of Colloid and Interface Science*. 131(1):252-266
- Leno, J. J., Chocalingam, V., Wilson, B. (2014) Albumin Nanoparticles Coated with Polysorbate 80 as a Novel Drug Carrier for the Delivery of Antiretroviral drug—Efavirenz. *International Journal of Pharmaceutical Investigation*. 4(3):142–148
- Lesniak, A., Fenaroli, F., Monopoli, M. P., Åberg, C., Dawson, K. A., Salvati, A. (2012) Effects of the Presence or Absence of a Protein Corona on Silica Nanoparticle Uptake and Impact on Cells. *ACS Nano*. 6(7):5845–5857
- Lestari, M. L. A. D and Indrayanto, G. (2014) Profiles of Drug Substances, Excipients and Related Methodology. Chapter Three - Curcumin, Editor(s): Brittain, H. G.. Academic Press. 39:113-204
- Li, M. and Qiao, N. and Wang, K. (2013) Influence of Sodium Lauryl Sulfate and Tween 80 on Carbamazepine–Nicotinamide Cocrystal Solubility and Dissolution Behaviour. *Pharmaceutics*. 5(4):508--524
- Li, W., Quan, P., Zhang, Y., Cheng, J., Liu, J., Cun, D., Xiang, R., Fang, L. (2014) Influence of drug physicochemical properties on absorption of water insoluble drug nanosuspensions. *International Journal of Pharmaceutics*. 460:13–23
-

- Li, X.-S., Wang, J. X., Shen, Z. G., Zhang, P. Y., Chen, J. F., Yun, J. (2007) Preparation of uniform prednisolone microcrystals by a controlled microprecipitation method. *International Journal of Pharmaceutics*. 342(1-2):26-32
- Liang, X.-J. (2012) *Nanopharmaceutics: The Potential Application of Nanomaterials*. 1st edition. Singapore: World Scientific Publishing Co. Pte. Ltd.
- Limtrakul, P., Chearwae, W., Shukla, S., Phisalpong, C., Ambudkar, S. V. (2007) Modulation of function of three ABC drug transporters, P-glycoprotein (ABCB1), mitoxantrone resistance protein (ABCG2) and multidrug resistance protein 1 (ABCC1) by tetrahydrocurcumin, a major metabolite of curcumin. *Molecular and Cellular Biochemistry*. 296(1–2):85–95
- Lindenberg, M., Kopp, S., Dressman, J. B. (2004) Classification of orally administered drugs on the World Health Organization model list of essential medicines according to the biopharmaceutics classification system. *European Journal of Pharmaceutics and Biopharmaceutics*. 58:265–78
- Lipinski, C. A., Lombardo, F., Dominy, B. W., Feeney, P. J. (2001) Experimental and computational approaches to estimate solubility and permeability in drug discovery and development settings. *Advanced Drug Delivery Reviews*. 46(1-3):3-26
- Liu, P. (2013) *Nanocrystal formulation for poorly soluble drugs [Dissertation]* Helsinki, Finland:University of Helsinki
- Liu, P., Viitala, T., Kartal-Hodzic, A., Liang, H., Laaksonen, T., Hirvonen, J., Peltonen, L. (2014) Interaction studies between indomethacin nanocrystals and PEO/PPO copolymer stabilizers. *Pharmaceutical Research*. 32(2):628-39
- Loebenberga, R. and Amidon, G. L. (2000) Modern bioavailability, bioequivalence and biopharmaceutics classification system. New scientific approaches to international regulatory standards. *European Journal of Pharmaceutics and Biopharmaceutics*. 50(1):3-12

- Loftsson, T. and Brewster, M. E. (2010) Pharmaceutical applications of cyclodextrins: basic science and product development. *Journal of Pharmacy and Pharmacology*. 62:1607–1621
- Lundquist, P. and Artursson, P. (2016) Oral absorption of peptides and nanoparticles across the human intestine: Opportunities, limitations and studies in human tissues. *Advanced Drug Delivery Reviews*. 106, Part B: 256-276
- Lyklema, J., Van Leeuwen, H. P., Minor, M. (1999) DLVO-theory, a dynamic re-interpretation. *Advances in Colloid and Interface Science*. 83(1–3):33-69
- Madelung, P., Østergaard, J., Bertelsen, P., Jørgensen, E. V., Jacobsen, J., Müllertz, A. (2014) Impact of sodium dodecyl sulphate on the dissolution of poorly soluble drug into biorelevant medium from drug-surfactant discs. *International Journal of Pharmaceutics*. 467(1–2):1-8
- Mah, P. T., Laaksonen, T., Rades, T., Aaltonen, J., Peltonen, L., Strachan, C. J. (2013) Unravelling the Relationship between Degree of Disorder and the Dissolution Behavior of Milled Glibenclamide. *Molecular Pharmaceutics*. 11(1):234-242
- Mathiowitz, E., Jacob, J. S., Jong, Y. S., Carino, G. P., Chickering, D. E., Chaturvedi, P., Santos, C. A., Vijayaraghavan, K., Montgomery, S., Bassett, M., Morrell, C. (1997) Biologically erodable microspheres as potential oral drug delivery systems. *Nature*. 386:410–414
- McCarty, M. (2011) FDA's new nanoscale materials guidance sets bar at 1,000 nm. *Medical Device Daily*. 15 (119):1-9
- McClellan, S., Prosser, E., Meehan, E., O'Malley, D., Clarke, N., Ramtoola, Z., Brayden, D. (1998) Binding and uptake of biodegradable poly-dl-lactide micro- and nanoparticles in intestinal epithelia. *European Journal of Pharmaceutical Sciences*. 6(2):153-163
- McFarlane, N. L., Wagner, N. J., Kaler, E. W., and Lynch, M. L. (2010) Calorimetric study of the adsorption of poly(ethylene oxide) and poly(vinyl pyrrolidone) onto cationic nanoparticles. *Langmuir*. 26:6262–6267
- Mendonça, D. V. C., Lage, L. M. R., Lage, P. P., Chávez-Fumagalli, M. A., Ludolf, F., Roatt, B. M., Menezes-Souza, D., Faraco, A. A. G., Castilho, R. O., Tavares, C. A.

- P., Barichello, J. M., Duarte, M. C., Coelho, E. A. F. (2016) Poloxamer 407 (Pluronic® F127)-based polymeric micelles for amphotericin B: In vitro biological activity, toxicity and in vivo therapeutic efficacy against murine tegumentary leishmaniasis. *Experimental Parasitology*. 169:34-42
- Merisko-Liversidge, E. and Liversidge, G. G. (2011) Nanosizing for oral and parenteral drug delivery: A perspective on formulating poorly-water soluble compounds using wet media milling technology. *Advanced Drug Delivery Reviews*. 63(6):427-440
- Metz, G. (2000) Nicht nur würzig, sondern ausgesprochen gesund. *Pharmazeutische Zeitung*. Ausgabe 19
- Moghimi, S. M. and Hunter, A. C. (2000) Poloxamers and poloxamines in nanoparticle engineering and experimental medicine. *Trends in Biotechnology*. 18(10):412-420
- Moon, J. J., Irvine, D. J., Huang, B. (2012) Engineering nano-and micro-particles to tune immunity. *Advanced materials*. 24(28):3724–3746
- Möschwitzer, J., Achleitner, G., Pomper, H., Müller, R. H. (2004). Development of an intravenously injectable chemically stable aqueous omeprazole formulation using nanosuspension technology. *European Journal of Pharmaceutics and Biopharmaceutics*. 58(3): 615-619
- Möschwitzer. J. P. (2013) Drug nanocrystals in the commercial pharmaceutical development process. *International Journal of Pharmaceutics*. 453(1):142-156
- Mouras, R., Rischitor, G., Downes, A., Salter, D., Elfick, A. (2010) Nonlinear optical microscopy for drug delivery monitoring and cancer tissue imaging. *Journal of Raman Spectroscopy*. 41(8):848-852
- Müller, B.-K. (2010) Suprastrukturen modifizierter Polysaccharide durch hydrophobe Wechselwirkungen in Wasser [Dissertation] Düsseldorf:Heinrich-Heine-Universität
- Müller, R. H. and Peters, K. (1998) Nanosuspensions for the formulation of poorly soluble drugs: I. Preparation by a size-reduction technique. *International Journal of Pharmaceutics*. 160(2): 229-237

- Müller, R. H. and Keck, C. M. (2012) Twenty years of drug nanocrystals: Where are we, and where do we go? *European Journal of Pharmaceutics and Biopharmaceutics*. 80(1):1-3
- Müller, R. H., Jacobs, C., Kayser, O. (2001) Nanosuspensions as particulate drug formulations in therapy: rationale for development and what we can expect for the future. *Advanced Drug Delivery Review*. 47:3–19
- Müllertz, A., Perrie, Y., Rades, T. (2016) *Analytical Techniques in the Pharmaceutical Sciences*. 1st edition. Springer
- Munger, M. A., Radwanski, P., Hadlock, G. C., Stoddard, G., Shaaban, A., Falconer, J., Grainger, D. W., Deering-Rice, C. E. (2014) In vivo human time-exposure study of orally dosed commercial silver nanoparticles. *Nanomedicine*. 10(1):1-9
- Nadai, T., Kondo, R., Tatematsu, A., Sezaki, H. (1972) Drug-induced histological changes and its consequences on the permeability of the small intestinal mucosa. I. EDTA, tetracycline, and sodium laurylsulfate. *Chemical and Pharmaceutical Bulletin (Tokyo)*. 20(6):1139-1144
- Nakach, M., Authelin, J.-R., Tadros, T., Galet, L., Chamayou, A. (2014) Engineering of nano-crystalline drug suspensions: Employing a physico-chemistry based stabilizer selection methodology or approach. *International Journal of Pharmaceutics*. 476(1-2):277-288
- Nativo, P., Prior, I. A., Brust, M. (2008) Uptake and Intracellular Fate of Surface-Modified Gold Nanoparticles. *ACS Nano*. 2(8):1639–1644
- Neal, J. C., Stolnik, S., Schacht, E., Kenawy, E. R., Garnett, M. C., Davis, S. S., Illum, L. (1998) In vitro displacement by rat serum of adsorbed radiolabeled poloxamer and poloxamine copolymers from model and biodegradable nanospheres. *Journal of Pharmaceutical Sciences*. 87(10):1242–1248
- Nuri, O. and Park, J.-H. (2014) Endocytosis and Exocytosis of Nanoparticles in Mammalian Cells. *International Journal of Nanomedicine*. 9,Suppl 1:51–63

- O'Hagan, D. T. (1990) Intestinal translocation of particulates -implications for drug and antigen delivery. *Advanced Drug Delivery Reviews*. 5:265-285
- Ornchuma, N., Okonogi, S., Schiffelers, R. M., Hennink, W. E. (2014) Curcumin nanoformulations: A review of pharmaceutical properties and preclinical studies and clinical data related to cancer treatment. *Biomaterials*. 35(10):3365-3383
- Owens, D. E. and Peppas, N. A. (2006) Opsonization, biodistribution, and pharmacokinetics of polymeric nanoparticles. *International Journal of Pharmaceutics*. 307(1):93-102
- Palla, B. J. and Shah, D. O. (2002) Stabilization of High Ionic Strength Slurries Using Surfactant Mixtures: Molecular Factors That Determine Optimal Stability. *Journal of Colloid and Interface Science*. 256:143–152
- Pardeike, J. and Müller, R. H. (2010) Nanosuspensions: A promising formulation for the new phospholipase A2 inhibitor PX-18. *International Journal of Pharmaceutics*. 391(1–2):322-329
- Pardeike, J., Strohmeier, D. M., Schrödl, N., Voura, C., Gruber, M., Khinast, J. G., Zimmer, A. (2011) Nanosuspensions as advanced printing ink for accurate dosing of poorly soluble drugs in personalized medicines. *International Journal of Pharmaceutics*. 420(1):93-100
- Pawsey, S., Yach, K., Reven, L. (2002) Self-Assembly of Carboxyalkylphosphonic Acids on Metal Oxide Powders. *Langmuir*. 18(13):5205-5212
- Peltonen, L. and Hirvonen, J. (2010) Pharmaceutical nanocrystals by nanomilling: critical process parameters, particle fracturing and stabilization methods. *Journal of Pharmacy and Pharmacology*. 62(11):1569–1579
- Pinholt, C., Hostrup, S., Bukrinsky, J. T., Frokjaer, S., and Jorgensen, L. (2011) Influence of acylation on the adsorption of insulin to hydrophobic surfaces. *Pharmaceutical Research*. 28:1031–1040
- Plakkot, S., De Matas, M., York, P., Saunders, M., Sulaiman, B. (2011) Comminution of ibuprofen to produce nano-particles for rapid dissolution. *International Journal of Pharmaceutics*. 415(1–2):307-314

- Powell, J. J., Thomas-McKay, E., Thoree, V., Robertson, J., Hewitt, R. E., Skepper, J. N., Brown, A., Hernandez-Garrido, J. C., Midgley, P. A., Gomez-Morilla, I., Grime, G. W., Kirkby, K. J., Mabbott, N. A., Donaldson, D. S., Williams, I. R., Rios, D., Girardin, S. E., Haas, C. T., Bruggraber, S. F. A., Laman, J. D., Tanriver, Y., Lombardi, G., Lechler, R., Thompson, R. P. H., Pele, L. C. (2015) An endogenous nanomineral chaperones luminal antigen and peptidoglycan to intestinal immune cells. *Nature Nanotechnology*. 10:361–369
- Prabhakar, K., Afzal, S. M., Surender, G., Kishan, V. (2013) Tween 80 containing lipid nanoemulsions for delivery of indinavir to brain. *Acta Pharmaceutica Sinica B*. 3(5):345-353
- Rabinow, B. (2005) Pharmacokinetics of drugs administered in nanosuspension. *Discovery Medicine*. 5:74–79
- Rabinow, B. E. (2006) Nanosuspensions in drug delivery. *Nature Reviews*. 3:785-796
- Rahman, A. and Brown, C. W. (1983) Effect of pH on the critical micelle concentration of sodium dodecyl sulphate. *Journal of Applied Polymer Science*. 28(4):1331–1334
- Ramawat (2009) *Herbal Drugs: Ethnomedicine to Modern Medicine*, Editors: Ramawat, Kishan Gopal. Springer p. 94-104
- Rauch, J., Kolch, W., Laurent, S., Mahmoudi, M. (2013) Big Signals from Small Particles: Regulation of Cell Signaling Pathways by Nanoparticles. *Chemical Reviews*. 113 (5):3391–3406
- Rejman, J., Oberle, V., Zuhorn, I. S., Hoekstra, D. (2004) Size-dependent internalization of particles via the pathways of clathrin and caveolae-mediated endocytosis. *Biochemical Journal*. 377:159–169
- Rixiang, H. and Lau, B. L. T. (2016) Biomolecule–nanoparticle interactions: Elucidation of the thermodynamics by isothermal titration calorimetry. *Biochimica et Biophysica Acta (BBA) - General Subjects*. 1860(5):945-956
- Rowe, E. S., Zhang, F., Leung, T. W., Parr, J. S., Guy, P. T. (1998) Thermodynamics of membrane partitioning for a series of n-alcohols determined by titration calorimetry: role of hydrophobic effects. *Biochemistry*. 37:2430–2440

- Roy, A., Ghosh, A., Datta, S., Das, S., Mohanraj, P., Deb, J., Bhanoji Rao, M. E. (2009) Effects of plasticizers and surfactants on the film forming properties of hydroxypropyl methylcellulose for the coating of diclofenac sodium tablets. *Saudi Pharmaceutical Journal*. 17(3):233-241.
- Ruge, C. A., Schaefer, U. F., Herrmann, J., Kirch, J., Cañadas, O., Echaide, M., Pérez-Gil, J., Casals, C., Müller, R., Lehr, C. M. (2012) The Interplay of Lung Surfactant Proteins and Lipids Assimilates the Macrophage Clearance of Nanoparticles. *PLOS ONE*. 7(7): e40775
- Saarinen, J., Sözeri, E., Fraser-Miller, S. J., Peltonen, L., Santos, H. A., Isomäki, A., Strachan, C. J. (2017) Insights into Caco-2 cell culture structure using coherent anti-Stokes Raman scattering (CARS) microscopy. *International Journal of Pharmaceutics*. 523(1):270-280
- Saleki-Gerhardt, A. Ahlneck, C., Zograf, G. (1994) Assessment of disorder in crystalline solids. *International Journal of Pharmaceutics*. 101(3): 237-247
- Sangalli, M. E., Maroni, A., Foppoli, A., Zema, L., Giordano, F., Gazzaniga, A. (2004) Different HPMC viscosity grades as coating agents for an oral time and/or site-controlled delivery system: a study on process parameters and in vitro performances. *European Journal of Pharmaceutical Sciences*. 22(5):469-476
- Sanphui, P., Goud, N. R., Khandavilli. U. B. R., Bhanoth, S., Nangia, A. (2011) New polymorphs of curcumin. *Chemical Communications*. 47(17):5013–5015
- Sarkar, N. (1979) Thermal gelation properties of methyl and hydroxypropyl methylcellulose. *Journal of Applied Polymer Science*. 24:1073
- Schärtl, W. (2007) *Light Scattering from Polymer Solutions and Nanoparticle Dispersions*. 1st edition. Springer
- Scherließ, H. (2008) *Wässrige Nanosuspensionen zur pulmonalen Applikation*. Dissertation. Kiel, Kiel University
- Schicke, B. C. (2010) *Anwendung der isothermalen Mikrokolorimetrie zur physikochemischen Charakterisierung molekularer Interaktionen in pharmazeutischen Formulierungen*. Dissertation. Braunschweig. TU-Braunschweig.

- Seedher, N. and Kanojia, M. (2008) Micellar Solubilization of Some Poorly Soluble Antidiabetic Drugs: A Technical Note. *AAPS PharmSciTech.* 9(2):431–436.
- Seedher, N. and Kanojia, M. (2009) Co-solvent solubilization of some poorly soluble antidiabetic drugs. *Pharmaceutical Development and Technology.* 14(2):185–92
- Shah, P., Jogani, V., Bagchi, T., Misra, A. (2006) Role of Caco-2 cell monolayers in prediction of intestinal drug absorption. *Biotechnology Progress.* 22:186–198
- Sharma, R. A., Gescher, A. J., Steward, W. P.(2005) Curcumin: The story so far. *European Journal of Cancer.*41(13):1955-1968
- Siccardi, M., Martin, P., Smith, D., Curley, P., McDonald, T., Giardiello, M., Owen, A. (2016) Towards a rational design of solid drug nanoparticles with optimised pharmacological properties. *Journal of Interdisciplinary Nanomedicine.* 1(3): 110-123
- Skoog, D. A., Holler, F. J., Crouch, S. R. (2013). *Instrumentelle Analytik.* 6nd edition. Editor: Nießner, R., Springer Spektrum
- Smith, K. C. A. and Oatley, C.W. (1955) The scanning electron microscope and its fields of application. *British Journal of Applied Physics.* 6(11):391-399
- Söderholm, J. D, (2015) Gut immunology: Nanoparticles ferry gut antigens. *Nature Nanotechnology.* 10:298–299
- Staedtke, V., Bräler, M., Müller, A., Georgieva, R., Bauer, S., Sternberg, N., Voigt, A., Lemke, A., Keck, C., Möschwitzer, J., Bäuml, H. (2010) In vitro inhibition of fungal activity by macrophage-mediated sequestration and release of encapsulated amphotericin B nanosuspension in red blood cells. *Small.* 6:96–103
- Strachan, C. J., Windbergs, M., Offerhaus, H. L. (2011) Pharmaceutical applications of non-linear imaging. *International Journal of Pharmaceutics.* 417:163–72
- Suleiman, M. S., Najib, N. M. (1989) Isolation and physicochemical characterization of solid forms of glibenclamide. *International Journal of Pharmaceutics.* 50:103-109
- Swarbrick, J. (2007) *Encyclopedia of PHARMACEUTICAL TECHNOLOGY.* 3rd edition. Volume 5. Informa healthcare USA

- Tenzer, S., Docter, D., Kuharev, J., Stauber, R. H. (2013) Rapid formation of plasma protein corona critically affects nanoparticle pathophysiology. *Nature Nanotechnology*. 8:772–781
- Thorsten, C. (2013) Chemistry of the Borate Boric Acid Buffer System. CR Scientific LLC (<http://www.crscientific.com/experiment4.html>) access 23.11.2017
- Timmins, P., Samuel, R. P., Colin, D. M. (2014) Hydrophilic Matrix Tablets for Oral Controlled Release. AAPS Advances in the Pharmaceutical Sciences Series 16. Springer.
- Tønnesen, H. H. , Karlsen, J., van Henegouwen, G. B.(1986) Studies on curcumin and curcuminoids. VIII. Photochemical stability of curcumin. *Zeitschrift für Lebensmittel-Untersuchung und -Forschung*. 183(2):116-122
- Toziopoulou, F., Malamataris, M., Nikolakakis, I., Kachrimanis, K. (2017) Production of aprepitant nanocrystals by wet media milling and subsequent solidification. *International Journal of Pharmaceutics*. 533(2):324-334
- Trows, S. and Scherließ, R. (2016) Carrier-based dry powder formulation for nasal delivery of vaccines utilizing BSA as model drug. *Powder Technology*. 292:223-231
- Tuomela, A., Hirvonen, J., Peltonen, L. (2016) Stabilizing Agents for Drug Nanocrystals: Effect on Bioavailability. *Pharmaceutics*. 8(2):16
- Tyrer, P. C., Foxwell, A. R., Kyd, J. M., Otczyk, D. C., Cripps, A. W. (2007) Receptor mediated targeting of M-cells. *Vaccine*. 25:3204–3209
- Uchegbu, I. F., Schätzlein, A. G., Cheng, W. P., Lalatsa, A. (2013) Fundamentals of pharmaceutical nanoscience. 1st edition. Springer.
- U. S. Food and Drug Administration. Drug Database. Dissolution methods. https://www.accessdata.fda.gov/scripts/cder/dissolution/dsp_getallData.cfm accessed 14.11.2016
- Vaynberg, K. A, Wagner, N. J., Sharma, R., Martic, P. (1998) Structure and Extent of Adsorbed Gelatin on Acrylic Latex and Polystyrene Colloidal Particles. *Journal of Colloid and Interface Science*. 205(1):131-140

- Verma, S., Huey, B. D., Burgess, D. J. (2009a) Scanning Probe Microscopy Method for Nanosuspension Stabilizer Selection. *Langmuir*. 25(21):12481–12487
- Verma, S., Lan, Y., Gokhale, R., Burgess, D. J. (2009b) Quality by design approach to understand the process of nanosuspension preparation. *International Journal of Pharmaceutics*. 377(1–2):185-198
- Wahlang, B., Pawar, Y. B., Bansal, A. K. (2011) Identification of permeability-related hurdles in oral delivery of curcumin using the Caco-2 cell model. *European Journal of Pharmaceutics and Biopharmaceutics*. 77(2):275-282
- Wang, C. X., Huang, L. S., Hou, L. B., Jiang, L., Yan, Z. T., Wang, Y. L., Chen, Z. L. (2009) Antitumor effects of polysorbate-80 coated gemcitabine polybutylcyanoacrylate nanoparticles in vitro and its pharmacodynamics in vivo on C6 glioma cells of a brain tumor model. *Brain Research*. 1261:91–99
- Wang, L., Du, J., Zhou, Y., Wang, Y. (2017b) Safety of nanosuspensions in drug delivery. *Nanomedicine: Nanotechnology, Biology and Medicine*. 13 (2):455-469
- Wang, Y., Zheng, Y., Zhang, L., Wang, Q., Zhang, D. (2013) Stability of nanosuspensions in drug delivery. *Journal of Controlled Release*. 172(3):1126-1141
- Wang, Y. (2014) Preparation of nano- and microemulsions using phase inversion and emulsion titration methods [Masterthesis] Auckland, New Zealand: Massey University
- Wang, Y.-H., Ke, X.-M., Zhang, C.-H., Yang, R.-P. (2017a) Absorption mechanism of three curcumin constituents through in situ intestinal perfusion method. *Brazilian Journal of Medical and Biological Research*. 50(11)
- Wang, Y.-L. and Taylor, D. L. (1990) *Fluorescence Microscopy of Living Cells in Culture, Part A: Fluorescent Analogs, Labeling Cells and Basic Microscopy*. Academic Press.
- Wang, Y. J., Pan, M. H., Cheng, A. L. (1997) Stability of curcumin in buffer solutions and characterization of its degradation products. *Journal of Pharmaceutical and Biomedical Analysis*. 15:1867–1876

- Wang, Z., Xu, S., Acosta, E. (2015) Heat of adsorption of surfactants and its role on nanoparticle Stabilization. *The Journal of Chemical Thermodynamics*. 91:256-266
- Windbergs, M., Jurna, M., Offerhaus, H. L., Herek, J. L. , Kleinebudde, P., Strachan, C. J. (2009) Chemical Imaging of Oral Solid Dosage Forms and Changes upon Dissolution Using Coherent Anti-Stokes Raman Scattering Microscopy. *Analytical Chemistry*. 81(6):2085–2091
- Wu, C.-P., Ohnuma, S., Ambudkar, S. V. (2011) Discovering Natural Product Modulators to Overcome Multidrug Resistance in Cancer Chemotherapy. *Current Pharmaceutical Biotechnology*. 12(4):609-620
- Wu, L., Zhang, J., Watanabe, W. (2011) Physical and chemical stability of drug nanoparticles. *Advanced Drug Delivery Reviews*. 63(6):456-469
- Wunderli-Allenspach, H., Van de Waterbeemd, H., Folkers, G., Guy, R. (Eds.) 2000 Methodologies in cell culture. In: Testa, B., , Pharmacokinetic Optimization in Drug Research: Biological, Physicochemical and Computational Strategies. Zurich: Wiley–VHCA
- Wynn, T. A., Chawla, A., Pollard, J. W. (2013) Macrophage biology in development, homeostasis and disease. *Nature*. 496:445–455
- Xu, H., Zhang, H., Wang, D., Wu, L., Liu, X., Jiao, Z. (2015) A facile route for rapid synthesis of hollow mesoporous silica nanoparticles as pH-responsive delivery carrier. *Journal of Colloid and Interface Science*. 451:101-107
- Xu, P. S., Gullotti, E., Tong, L., Highley, C. B., Errabelli, D. R., Hasan, T., Cheng, J. X., Kohane, D. S., Yeo, Y. (2009) Intracellular Drug Delivery by Poly(lactic-co-glycolic acid) Nanoparticles, Revisited. *Molecular Pharmaceutics*. 6(1):190-201
- Yadollahi, R., Vasilev, K., Simovic, S. (2015) Nanosuspension Technologies for Delivery of Poorly Soluble Drugs. *Journal of Nanomaterials*. 2015:1-13
- Yavuz, A. E., Masalci, Ö., Kazanci, N. (2014) Phase diagram of tetradecyltrimethylammonium bromide (TTAB) + water + octanol system with application of mechanical deformation. *Applied Surface Science*. 318:251-255

- Yu, B., Langer, R., Blankschtein, D., Kim, K. H., Peter, T. C. (2003) Visualization of oleic acid-induced transdermal diffusion pathways using two-photon fluorescence microscopy. *Journal of Investigative Dermatology*. 120(3):448-455
- Yu, S., Zhang, X., Tan, G., Tian, L., Liu, D., Liu, Y., Yang, X., Pan, W. (2017) A novel pH-induced thermosensitive hydrogel composed of carboxymethyl chitosan and poloxamer cross-linked by glutaraldehyde for ophthalmic drug delivery. *Carbohydrate Polymers*. 155:208-217
- Zakeri-Milani, P., Islambulchilar, Z., Majidpour, F., Jannatabadi, E., Lotfipour, F., Valizadeh, H. (2014) A study on enhanced intestinal permeability of clarithromycin nanoparticles. *Brazilian Journal of Pharmaceutical Sciences*. 50(1):121-129
- Zerrouk, N., Corti, G., Ancillotti, S., Maestrelli, F., Cirri, M., Mura, P. (2006) Influence of cyclodextrins and chitosan, separately or in combination, on glyburide solubility and permeability. *European Journal of Pharmaceutics and Biopharmaceutics* 62:241-246
- Zhang, H., Yao, M., Morrison, R. A. and Chong, S. (2003) Commonly used surfactant, Tween 80, improves absorption of P-glycoprotein substrate, digoxin, in rats. *Archives of pharmacal research*. 26:768-772
- Zhen, Z., Shen, Z. L., Zhai, S., Xu, J. L., Liang, H., Shen, Q., Li, Q. Y. (2017) Transport of curcumin derivatives in Caco-2 cell monolayers. *European Journal of Pharmaceutics and Biopharmaceutics*. 117:123-131
- Zhu, S., Niu, M., O'Mary, H., Cui, Z. (2013) Targeting of tumor-associated macrophages made possible by PEG-sheddable, mannose-modified nanoparticles. *Molecular Pharmaceutics*. 10(9):3525-3530

9 Appendix

9.1 List of abbreviations

A	Apical
API	Active pharmaceutical ingredient
B	Basolateral
BCS	Biopharmaceutics Classification System
CA	Contact angle
CAM	Contact angle measurements
CARS	Coherent anti-Stokes Raman spectroscopy
CMC	Critical micelle concentration
CUR	Curcumin
DLS	Dynamic light scattering
DMEM	Dulbecco's modified medium
DMSO	Dimethyl sulfoxide
DSC	Dynamic scanning calorimetry
EDTA	Ethylene diamine tetra acetic acid
EMA	European medicines agency
FBS	Fetal bovine serum
FDA	Food and drug administration
GLI	Glibenclamide
h	Hour/s
HEPES	Hydroxyethyl-piperazineethane-sulfonic acid buffer
HPLC	High performance liquid chromatography

HPMC	Hydroxypropyl methylcellulose
ISO	International organisation for standardisation
ITC	Isothermal titration calorimetry
LD	Laser diffraction
LY	Lucifer yellow
min	Minut/es
MLN	Mesenteric lymph nodes
mM	Millimole
PBS	Phosphate buffered saline
PDI	Polydispersity index
Pol124	Poloxamer 124
Pol407	Poloxamer 407
PP	Peyer's patches
PS	Polysorbates
PS80	Polysorbate 80
rcf	Relative centrifugal forces
SD	Standard deviation
SDS	Sodium dodecyl sulfate
SEM	Scanning electron microscopy
SHG	Second harmonic generation
Ss	Saturation solubility
TEER	Transepithelial electrical resistance
TPFE	Two-photon fluorescence excitation

TTAB Tetra decyl trimethyl ammonium bromide

UV Ultraviolet

XRPD X-ray powder diffraction

9.2 Materials

9.2.1 APIs, stabilisers and dispersion medium

Table 23 holds information about the utilised APIs, stabilisers and the used type of water.

Table 23: Used materials.

Substance name	CAS number	Supplier	LOT	Additional information
Curcumin	458-37-7	Alpha Aesar (Germany)	10165835	95 % total curcuminoid content extracted from turmeric rhizome
Glibenclamide (glybencyclamide)	10238-21-8	Alpha Aesar (Germany)	10197956 10190555 10147611	99 %
Polysorbate 80	9050-57-1	Croda GmbH (Germany)	1007PC0045	Kindly donated
Hydroxy propyl methyl cellulose	9004-65-3	Colorcon GmbH (Germany)	OL02012402	Methocel E5 Premium LV A 2 % solution at 20 °C has viscosity of 5 mPa*s Kindly donated
Poloxamer 124	9003-11-6	BASF SE (Germany)	WPNI564B	Kindly donated

Substance name	CAS number	Supplier	LOT	Additional information
Poloxamer 407	9003-11-6	BASF SE (Germany)	WPMI563B	Kindly donated
Myristyltrimethylammonium bromide (Tetradecyltrimethylammonium bromide)	1119-97-7	Sigma Aldrich Chemie GmbH (Steinheim, Germany)	SLBG3708V	99 %
Sodium dodecyl sulfate	151-21-3	Sigma Aldrich Chemie GmbH (Steinheim, Germany)	several	
Double-distilled water	-	produced in house with Finn Aqua 75, San-Asalo Sohlberg Corp., Finland	-	

9.2.2 Surface area measurements

Table 24 lists the supplier and quality information about the gases used.

Table 24: Information on gases used in BET measurements.

Gas	Quality	Supplier
Helium	5.0	Linde Gas, Germany
Nitrogen	5.0	Linde Gas, Germany

9.2.3 Buffer in dissolution studies

Boric acid buffer pH 9.4

A 0.2 M boric acid + 0.2 M KCl solution as well as a 0.2 M NaOH solution were prepared in demineralised water.

802.5 mL of NaOH solution and 1250 mL of boric acid/KCl solution were transferred to a 5000 mL volumetric flask and filled up with demineralised water to 5 L.

Phosphate buffer pH 8

0.2 M KH_2PO_4 solution as well as 0.2 M NaOH solution in demineralised water were prepared.

1250 mL of KH_2PO_4 solution and 1152.5 mL 0.2 M NaOH were transferred to a 5000 mL volumetric flask and filled up with demineralised water to 5 L.

Acetic acid buffer pH 4

A solution of 50 % (m/V) NaOH in demineralised water was prepared. 50 mL of this solution were added to 143 mL acetic acid and filled up to 5000 mL with demineralised water.

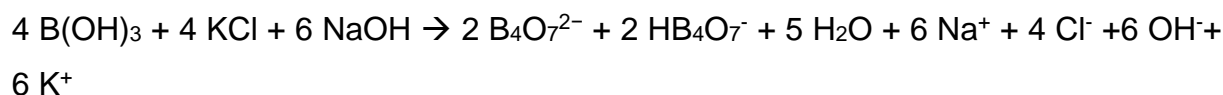
9.2.3.1 Ionic strength of buffers

Following dissociation reactions in buffered solutions were assumed for the calculation of ionic strength:

Phosphate buffer:



Boric acid buffer:



Ionic strength was calculated as $\frac{1}{2}$ sum of (concentration of salt in mol \times number of ions \times charge of ion²)

So that the ionic strength was calculated for phosphate buffer with $\frac{1}{2} \times (0.05 \text{ M} \times 1 \times 2^2 + 0.05 \text{ M} \times 1 \times 1^2 + 0.05 \text{ M} \times 1 \times 1^2) = 0.15 \text{ M/L}$ and boric acid buffer with $\frac{1}{2} \times (0.05$

$M \times 2 \times 2^2 + 0.05 M \times 2 \times 1^2 + 0.032 M \times 6 \times 1^2 + 0.05 M \times 4 \times 1^2 + 0.032 M \times 6 \times 1^2 + 0.05 M \times 4 \times 1^2 = 0.64 M/L$.

9.2.4 Cell culture

Caco-2 cells were acquired from the European collection of cell cultures, Salisbury, Great Britain. RAW 264.7 were purchased from ATCC® with a passage number of 8. DMSO was acquired from Sigma Aldrich Chemie GmbH (Germany). Trypsin/EDTA solution 0.25 %/0.02 %, penicillin/streptomycin solution (10.000 U/mL/10.000 µg/mL and non-essential amino acids (100x) were ordered from Biochrom GmbH (Germany).

Hanks' Salt solution (HBSS), Phosphate buffered saline (PBS) and Duplecco's MEM (DMEM) were ordered from Biochrom GmbH (Germany) with following composition (Table 25):

Table 25: Composition of buffers and cell culture medium.

Substance	Dulbecco's Phosphate buffered saline (PBS) (mg/L)	Hanks' Salt solution (HBSS) (mg/L)	Duplecco's MEM (DMEM) (mg/L)
NaCl	8000	8000	6400
KCl	200	400	400
Na ₂ HPO ₄	1150	48	124
KH ₂ PO ₄	200	60	-
MgCl ₂ *6H ₂ O	100	-	-
MgSO ₄ *7H ₂ O	-	200	200
CaCl ₂	100	140	200
glucose	-	1000	4500
NaHCO ₃	-	350	3700
Fe(NO ₃) ₃ *9H ₂ O	-	-	0.1
Phenol red	-	-	15

DMEM with 3.7 g/L NaHCO₃, 4.5 g/L D-Glucose and stable) containing additionally the substances listed in Table 26.

Table 26: Composition of DMEM as received from the supplier.

Substance	Concentration in mg/L
L-cystine	48
L-glutamine	580
L-histidine-HCl*H ₂ O	42
L-isoleucine	106
L-leucine	106
L-methionine	30
L-lysine-HCl	146
L-arginine-HCl	84
L-phenylalanine	66
L-threonine	95
L-tryptophan	16
L-tyrosine	72
L-valine	94
Glycine	30
L-serine	42
Choline chloride	4
Folic acid	4
Myo-inositole	7.2
nicotinamide	4
D-Ca-pantothenate	4
Pyridoxine-HCl	4
Riboflavin	0.05
Thiamine-HCl	4

9.2.4.1 Materials for toxicity tests

SDS was used as listed in chapter 9.2.1. MTT (Thiazolyl Blue Tetrazolium Bromide) supplied from Sigma Aldrich Chemie GmbH (Germany) with a purity of >97.5 %. Dimethyl formamid ordered as N, N-Dimethylformamid pro analysi from Merck GmbH (Germany)

9.2.4.2 Materials for transport studies

Transport buffer consisting of the substances displayed in Table 27. The pH was adjusted with sodium hydroxide before filling up 1 L with double-distilled water.

Table 27: Composition of transport buffer used in transport studies.

Substances	Concentration/Volume
Hydroxyethyl- piperazineethane-sulfonic acid (HEPES)	2380 in mg/L
Glucose	4500 in mg/L
HBSS	500 mL

Atenolol with a purity of ≤ 98 % and Lucifer yellow CH dilithium salt were purchased from Sigma Aldrich Chemie GmbH (Germany).

9.3 Methods

9.3.1 HPLC

Table 28, Table 29 and Table 30 display information about the utilised HPLC methods.

Table 28: HPLC method for CUR.

HPLC system	Waters HPLC system (Waters Materials and Methods Corporation, Milford, USA)
Software	Empower [®] Pro 2 software (Waters Corporation, Milford, USA)
Column	LiChroCart [®] 125-4, LiChrospher [®] 100 RP18-5 (Merck KGaA, Germany) with precolumn
Mobile phase	Acetonitrile to citric acid (Carl Roth GmbH+ Co. KG, Germany) (1 % m/v to pH 3 with NaOH) in a ratio of 60:40
Injection volume	100 μ L
Flow rate	1 mL/min
Retention time	3 minutes
Detection wavelength	425 nm
Temperature	Room temperature

Table 29: HPLC method for GLI.

HPLC system	Agilent 1100 Series LC with diode array detector (Agilent Technologies Inc., United States of America)
Software	HPChemstation (Agilent Technologies Inc.)
Column	LiChroCart® 125-4, LiChrospher® 100 RP18-5 (Merck KGaA, Germany) with precolumn
Mobile phase	A: 50 % of 20 mL triethylamine adjusted to pH 3 + 50 mL acetonitrile ad 1000 mL with double-distilled water B: 50 % of 20 mL mobile phase A + 65 mL double-distilled water + 915 mL acetonitrile
Injection volume	10 µL
Flow rate	1 mL/min
Retention time	6 minutes
Detection wavelength	230 nm
Temperature	35 °C

Table 30: HPLC method for atenolol.

HPLC system	Agilent 1100 Series LC with diode array detector (Agilent Technologies Inc., United States of America)
Software	HPChemstation (Agilent Technologies Inc.)
Column	LiChroCart® 125-4, LiChrospher® 100 RP18-5 (Merck KGaA, Germany) with precolumn
Mobile phase	Potassium dihydrogen phosphate buffer (0.067 M adjusted to pH 3) with 0.2 % triethylamine to acetonitrile in a ratio of 90:10
Injection volume	100 µL
Flow rate	0.8 mL/min
Retention time	4 minutes
Detection wavelength	225 nm
Temperature	21 °C

Phosphate buffer was production with 9.1188 g KH_2PO_4 , solubilised in approximately 950 mL double-distilled water. 2 mL of triethylamine were added and the pH was adjusted to 3.0 with orthophosphoric acid 85 %.

Acetonitrile and triethylamine were purchased from Sigma-Aldrich Chemie GmbH (Germany) while KH_2PO_4 and citric acid were ordered from Carl Roth GmbH+ Co. KG (Germany)

9.3.2 Fluorimetry

LY content was analysed with the following parameters (Table 31).

Table 31: Set-up of fluometric measurements.

Excitation wavelength	480 nm
Emission wavelength	520 - 550 nm
Width of slit Excitation	10 nm
Width of slit Emission	15 nm

9.4 Additions to results

9.4.1 Particle sizes and conductivity of zeta-potential measurements

In Table 32 and Table 33, additional information to the suspensions, that were investigated with zeta-potential measurements, are shown.

Table 32: Z-average and conductivity of CUR suspensions.

Stabiliser	Concentration in %	Z-average in nm	Conductivity in mS/cm
PS80	50	170	0.0268
SDS	1	609	0.01
TTAB	1	153	0.00217
PS80 + SDS	50 + 1	152	0.00574
PS80 + TTAB	50 + 1	161	0.00206

Table 33: Z-average and conductivity of GLI suspensions.

Stabiliser	Concentration in %	Z-average in nm	Conductivity in mS/cm
PS80	5	272	0.0109
SDS	1	1135	0.00598
TTAB	1	1643	0.0113
PS80 + SDS	5 + 1	261	0.00756
PS80 + TTAB	5 + 1	2519	0.0132

9.4.2 Particle size distributions

Figure 84 displays particle size distributions of CUR and GLI.

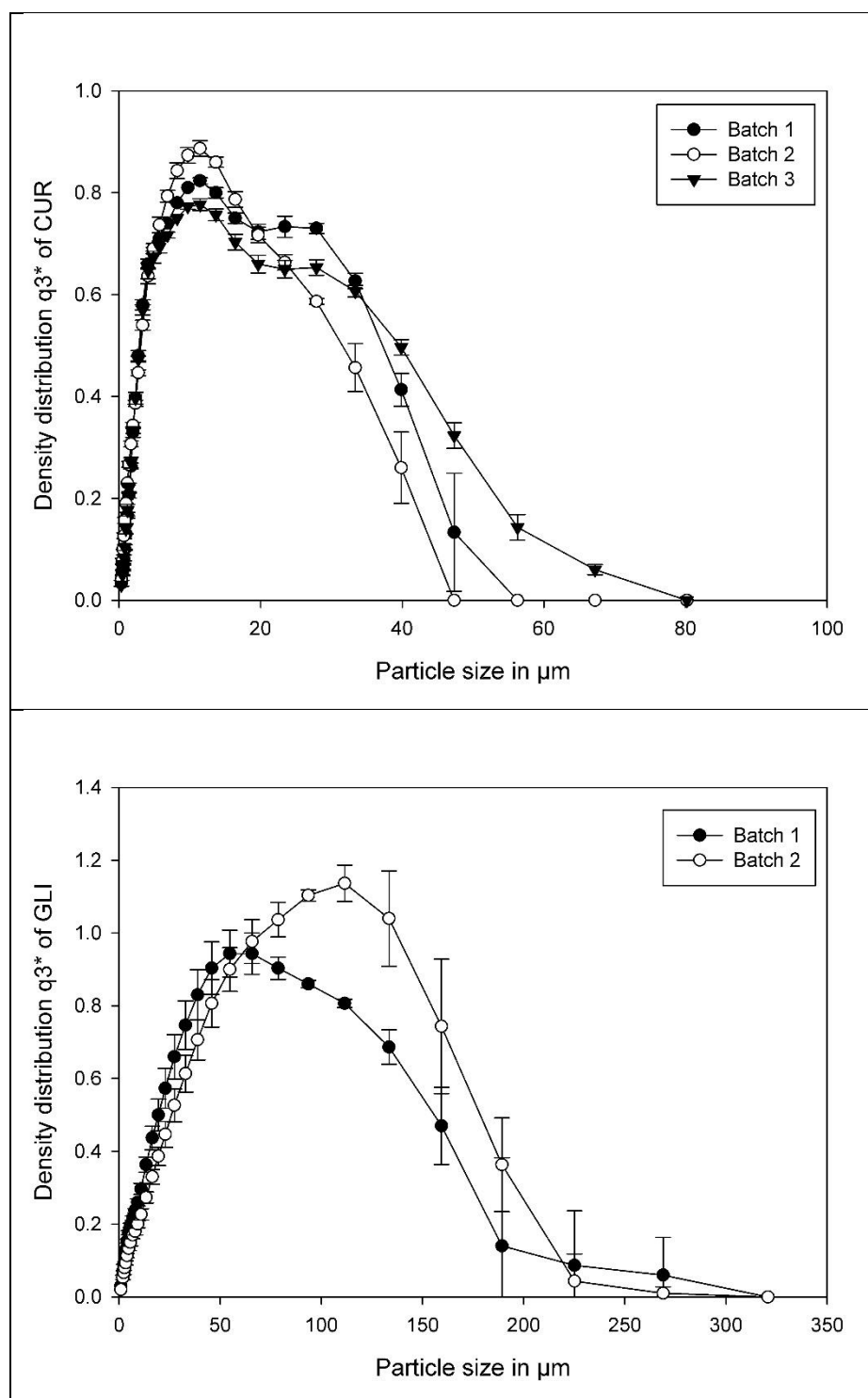


Figure 84: Particle size distributions acquired from laser diffraction measurements for CUR (top) and GLI (bottom).

9.4.3 Solid state of nanosuspensions

Additions to DSC measurements are listed in Table 34.

Table 34: Onset and Peak temperatures of GLI and CUR nanosuspensions.

Freeze dried suspension	Onset in °C	Peak in °C
GLI 500 nm 10 % HPMC	165.51	171.90
GLI 500 nm 2.5 % HPMC + 2.5 % PS80	161.59	170.50
GLI 300 nm 10 % HPMC	161.29	168.13
GLI 300 nm 2.5 % HPMC + 2.5 % PS80	162.48	168.10
CUR 500 nm 25 % HPMC	163.23	171.10
CUR 500 nm 12.5 % HPMC + 12.5 % PS80	161.20	170.35
CUR 300 nm 10 % HPMC	161.82	173.53
CUR 300 nm 12.5 % HPMC + 12.5 % PS80	164.72	172.03

9.4.4 Isothermal titration calorimetry

Figure 85 and Figure 86 hold information about the heat change in ITC experiments for the titration of water into CUR and GLI drug suspensions.

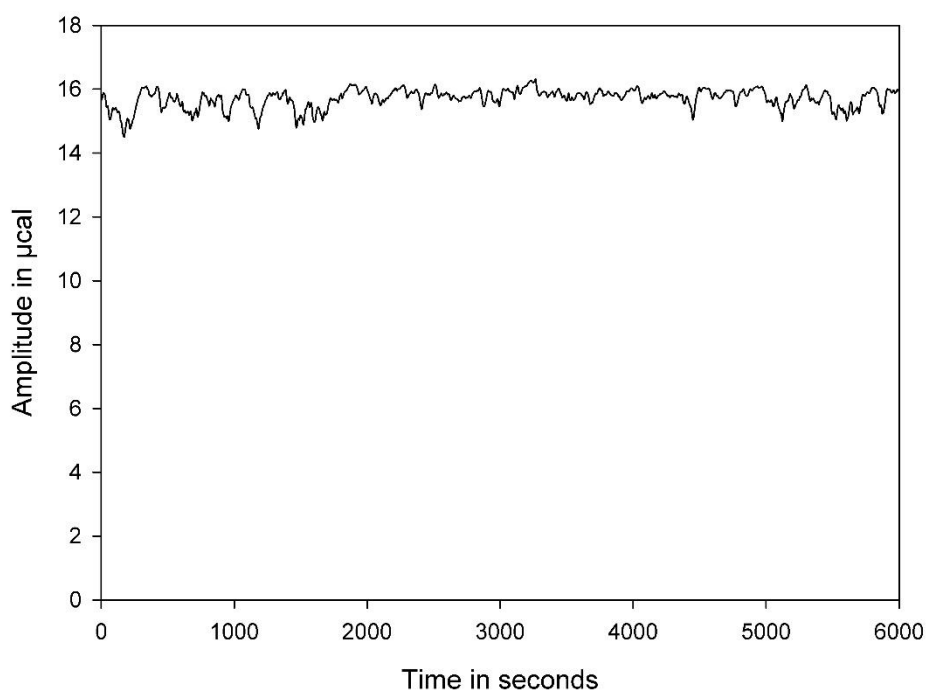


Figure 85: Control experiment of CUR. Titration of milli q water in a CUR suspension.

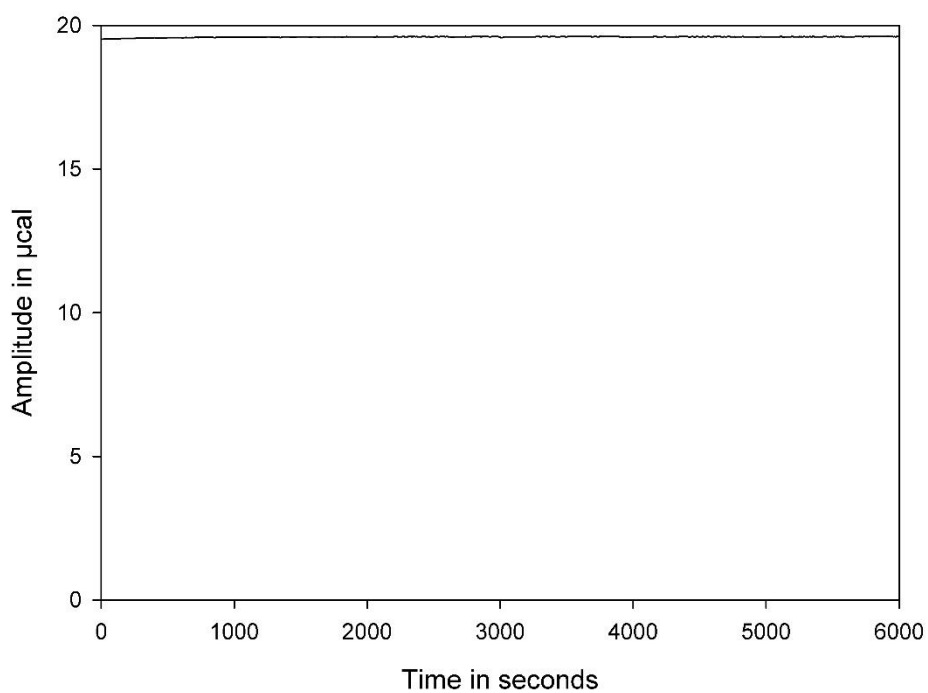


Figure 86: Control experiment for GLI. Titration of milli q water in a GLI suspension.

9.4.5 Quantification of particle uptake in cells with Imaris

An exemplary image of one data set with two channels (membrane and nanocrystals) is shown in Figure 87.

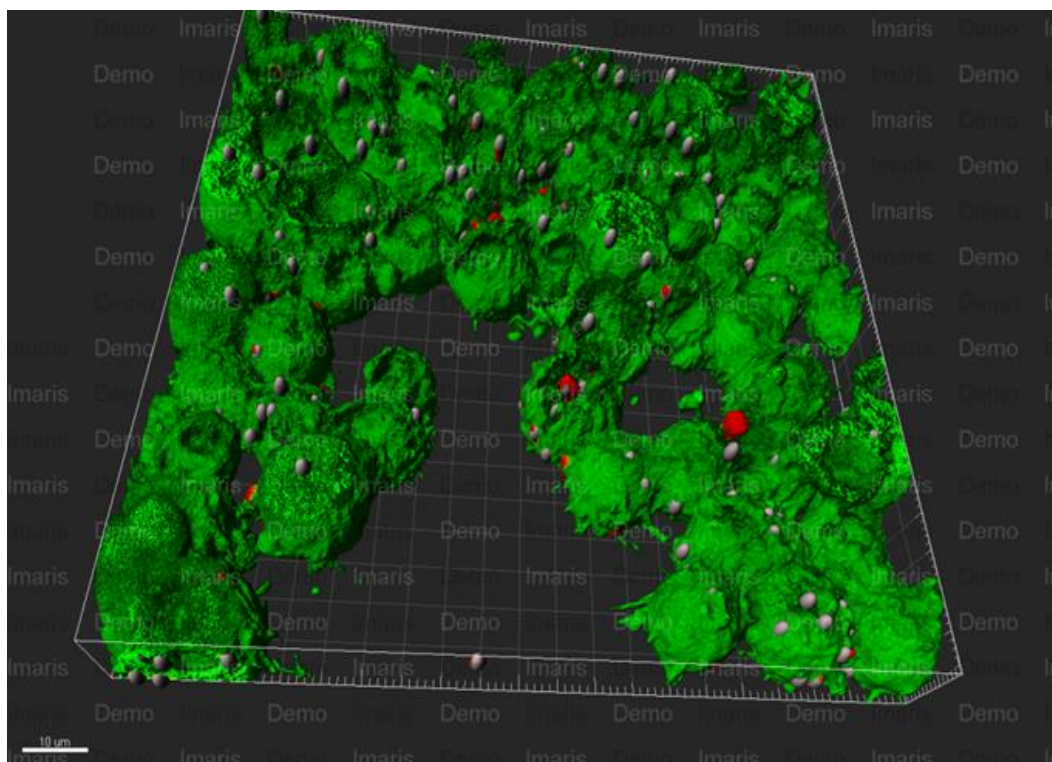


Figure 87: Image of RAW 264.7 cells (green) and nanocrystals (red) after application of the dot and surface wizard of Imaris demo software. The nanocrystals are marked with grey dots.

9.4.6 Calculation of dose per macrophage

A 300 nm nanocrystal which is a perfect sphere has a volume of $\frac{4}{3} * \pi * 0.150 \mu\text{m}^3 = 0.015 \mu\text{m}^3$. The density of GLI was measured with a helium pycnometer (Pycnomatic ATC, Porotec GmbH, Germany) at 1.66 g/mL. So, the mass of one particle is $1.4 \times 10^{-14} \text{ mL} * 1.66 \text{ g/mL} = 2.324 \times 10^{-5} \text{ ng}$.

CUR had a measured density (with the helium pycnometer Pycnomatic ATC, Porotec GmbH, Germany) of 1.89 g/mL so that the resulting mass of one particle is $2.646 \times 10^{-5} \text{ ng}$.

Erklärung nach § 8 der Promotionsordnung

Hiermit erkläre ich gemäß § 8 der Promotionsordnung der Mathematisch-Naturwissenschaftlichen Fakultät der Christian-Albrechts-Universität zu Kiel, dass ich die vorliegende Arbeit, abgesehen von der Beratung durch meinen Betreuer, selbstständig und ohne fremde Hilfe verfasst habe. Weiterhin habe ich keine anderen als die angegebenen Quellen oder Hilfsmittel benutzt und die den benutzten Werken wörtlich oder inhaltlich entnommenen Stellen als solche kenntlich gemacht. Die vorliegende Arbeit ist unter Einhaltung der Regeln guter wissenschaftlicher Praxis entstanden und wurde bei keiner anderen Universität zur Begutachtung eingereicht.

Friederike Gütter

Acknowledgments

Nun ist die Arbeit vollbracht. Dass die Arbeit so geworden ist, wie sie jetzt hier steht, habe ich vielen Personen zu verdanken.

First of all I would like to thank my supervisor Prof. Regina Scherließ. Thank you for adopting me and my nanocrystals. It is because of you that I considered to come to Kiel in the first place even that I did not think back then in New Zealand that you would be my supervisor one day. Thank you for your support and help; especially while building up the cooperation with the pharmaceutical technology in Helsinki.

I would also like to thank Prof. Hartwig Steckel for giving me the opportunity to start my doctoral thesis in Kiel and for the idea of my topic as well as for the guidance in the first time of my thesis. You also made it possible that I could accomplish a very exciting but sometimes scary project before I started my thesis.

As I already mentioned the cooperation with Helsinki I would also like to thank all my short term supervisors there. Especially Prof. Clare Strachan who already was a very welcoming person in New Zealand as my supervisor, for her continuous support while working together on my doctoral thesis. Furthermore, Docent Leena Peltonen and Prof. Hélder A. Santos, who were always there with scientific input and help. Tuomas Niemi-Aro made it possible that I could use the isothermal titration microcalorimetry as a technique in my thesis. Most of the time in Helsinki I spend together with *Dr. Jukka Saarinen* and the CARS microscope. Thank you so much for the nice time we had together and your CARS expertise. Even though we are both a little bit confused from time to time we managed to put together some nice data. Thanks to all your colleagues for letting me feel very welcome in Finland. Vielen Dank an dieser Stelle an den Internationalisierungsfond der CAU Kiel, der es mir finanziell ermöglicht hat, meine Arbeit in Helsinki durchzuführen.

Auch in Kiel hatte ich viel direkte und indirekte Hilfe. Ohne Hanna, Regina und Maren wär ich bei meinen HPLC Analysen aufgeschmissen gewesen. Danke für eure Hilfe bei so vielen Dingen und für ein immer offenes Ohr. Auch Rüdi hatte immer ein offenes Ohr und hat mir sehr in meiner Anfangszeit geholfen. Zusammen haben wir gelernt,

was es heißt, KOH und O₂ um sich zu haben. Doch auch in Bezug auf meine Doktorarbeit hast du mir bei vielen Fragestellungen geholfen und das, was immer bleiben wird, sind deine Zeichnungen. Vielen Dank. Mein Dank gilt auch meinen HiWis, die mich während meiner Zeit hier unterstützt haben.

Sehr wichtig war mir ein gutes persönliches Umfeld neben dem Arbeiten. Das habe ich in Kiel gefunden. Vielen Dank an meine ganzen Kollegen, die mich unterstützt haben oder manchmal einfach nur abgelenkt haben. Den ‚neuen‘ Kollegen wünsche ich viel Erfolg. Maire, erhalte dir deine offene und herzliche Art. Danke an Andrea und Phillip. Zu euch konnte ich immer und mit allem kommen. Auch Mathias hat mich immer wieder aufgenommen und sich vorrangig um meine gute Laune gekümmert. Judith und Annika: mit euch habe ich angefangen und wir haben sehr viel Zeit im fachlichen Rahmen und privat miteinander verbracht. Auch wenn wir alle drei sehr unterschiedlich sind hat das sehr gut gepasst. Danke Judith für alles. Also wirklich einfach alles. Ich weiß nicht, wo du mir nicht geholfen haben könntest. Annika, du warst immer für mich da. Du hast mich rausgeholt, mich unterstützt, mich aufgemuntert und kennst mich in und auswendig. Danke.

Als Betreuer team haben mich vor allem Eric, Thea, Nancy, Annika, Judith und Ann-Kathrin länger begleitet. Danke für die Unterstützung und das gegenseitig füreinander einspringen. Danke an Volkmar, Detlef und Dirk.

Joe, Leena, Verena, Mama, Judith, Annika: vielen Dank fürs Korrekturlesen. Ohne euch wäre es definitiv nicht so geworden, wie es jetzt ist.

Danke, dass du es mit mir aushältst, Sven. Das war in letzter Zeit nicht immer einfach. Ich danke dir für so vieles. Bei dir kann ich 100 % so sein, wie ich bin.

Danke an meine Familie. Mama, Papa: ihr glaubt immer an mich und habt mir all das ermöglicht.